School of Civil and Mechanical Engineering

Rest Period Healing Effect on Viscoelastic Continuum Damage Behaviour of Asphalt Mixture: Experimental Quantification and Numerical Verification of a New Approach

Yang Su

This thesis is presented for the Degree of
Doctor of Philosophy
of
Curtin University

January 2019

Table of Contents

Acknowledgement

Firstly, I am grateful of Professor Hamid Nikraz for his generous offer of opportunities, academic guidance, administrative support and encouragement for me to pursue the research topic on pavement engineering. I would also like to express genuine gratitude to Dr. Hossein Asadi for providing his sound technical opinions, patient review/editing and various academic support to lead me into the resourceful pavement engineering world and finally complete a PhD thesis on it.

It is highly appreciated that Department of Civil Engineering in Curtin University provides laboratory facilities and software to enable this research. In particular, I would like to thank Mr. Darren Issac for his generous guidance of all laboratory related works.

Else, my gratitude to my parents in China is beyond expression. Their care, belief and hope are inner motivation for me to achieve a doctorate degree in Australia.

Financially, I would like to acknowledge the contribution of an Australian Government Research Training Program Scholarship in supporting this research.

Paper Publications

Following is a list of academic papers produced from the original contents of this thesis:

1. "VECD Investigation and Quantification of Rest Period Healing within Pulse-Rest Loading" in *International Journal of Pavement Engineering* (accepted)

2. "Methods Development and Modelling Verification of Rest Period Damage Function using 4PB Tests" (subjects to possible wording change) in *International Journal of Pavement Engineering* (prepared to follow the above paper)
3. "Varied Specimen Geometry for Simplified VECD Test with Rest Period: Verification of a Small Specimen Size" in *2019 Transportation Research Board Annual Meeting* (accepted)
4. "Experimental Investigation of the Effect of Asphalt Healing under Rest Period on Stiffness Development and Damage Characteristic Curves" in *International Flexible Pavement Conference, Australia Asphalt Pavement Association 2017* (published)

Note: All technical contents of above listed papers are sourced from the original content of this thesis. All other contributors of the above publications, have involved in following contributions: concept recommendation, introduction, article presentation, grammar/sentencing and technical advice. All other contributors are correctly and consensually attributed as co-authors in relevant papers.

Abstract

With the prosperity of flexible pavement construction and maintenance around the world, there is an increasing demand to acquire a comprehensive and accurate asphalt mixture characterization method based on true physical principles. In past decades, viscoelastic continuum damage (VECD) has been developed as a mechanically rigorous and widely recognized approach for asphalt mixture's fatigue and crack damage response, with consideration of various conditional factors. However, the rest period healing effect on asphalt mixture's fatigue and damage behaviour is an area that has yet been fully addressed, especially with rest period after each load cycle. While most of test conditions are included in VECD model, a smeared continuum damage approach has also been developed to interpret the effect of rest periods within VECD model. In this research, a series of simplified VECD tests are conducted with various length of rest period (after each cycle) using Asphalt Mixture Performance Tester (AMPT). The test results lead into stiffness development curves and damage characteristic curves of certain asphalt mixture at each test condition. The test contains varied conditions such as different temperatures, length of rest periods, strain amplitudes, specimen geometries and specimen supplies. Also, a series of four point bending (4PB) beam tests are conducted on the same mixture, again with various length of rest periods at two temperature levels and under different strain amplitudes.

Based on experimental results, firstly, the effect of rest period healing is qualitatively investigated. Longer rest periods produce higher lying stiffness development curves and damage characteristic curves, demonstrating improved healing effect. Else, the relationship between rest period length and healing effect is specifically studied. Regarding the interaction between asphalt healing and temperature, one supply of mixture indicates increasing healing capability with rising temperature under certain rest period. However, the second supply of mixture has demonstrated an opposite trend of improved healing effect at same rest period when temperature is lower (12^{o}C). This effect has been demonstrated by both AMPT and 4PB beam fatigue tests.

Significantly, it is established the equational relationship between length of rest period and damage characteristic curves fitting coefficients. Based on this, novel equations termed as “rest period damage functions” have been developed. The current rest period damage functions are able to predict damage characteristic curves with any rest period after each load cycle for certain mixture under certain temperature. The new equations are used to generate damage characteristic curves, which clearly and accurately capture the effect of rest period. The application of rest period damage functions can significantly save laboratory time, and provides an approach to evaluate and improve VECD with rest period tests results. Else, standard procedures are suggested to obtain rest period damage functions based on AMPT tests and smeared VECD approach, with technical notices explained.

For verification, the obtained rest period damage functions are written as a constitutive model within numerical modelling software ABAQUS. Four point bending (4PB) beam model is built in ABAQUS with rest period damage functions as its constitutive model. The new model is able to produce pseudostiffness values and damage status for each number of load cycle. To realize correct modelling, there is theoretical study on the mechanism of the bending beam subjects to repetitive destructive loading, with explanation of relevant assumptions used by traditional flexural stiffness calculation. Accordingly, a new block method and relevant equations have been developed to convert the simulation results into the equivalent flexural stiffness output by the 4PB test software. Thus, the simulation and experimental results are directly comparable with each other. It is found that the proposed damage with healing model is capable of producing reasonably accurate results compared to real beam tests within the viscoelastic range. It is also verified that the model also has the capability to directly produce the stiffness development at the bottom section of the beam, and thus to identify the true fatigue failure point of beam’s critical bottom section.

In the meanwhile, a study on AMPT specimen’s geometry effect is conducted. The results have demonstrated that a reduced specimen size is capable of both dynamic modulus and VECD tests with rest period between consecutive load cycles at lower to medium temperature level (12 and 20^{o}C tested). The reduced specimen size has

significant advantage of saving time and material, while producing similar and reasonable results compared to standard size specimen.

Chapter 1. Introduction

1.1. Asphalt Mixture Characterization Methods

Flexible pavement is mainly made of hot mixed asphalt, which is commonly a mixture of bitumen and granular components. Traditionally, flexible pavement design and analysis are conducted through empirical methods. For instance, California Bearing Ratio (CBR) test is able to define the subgrade penetration resistance, which is then used to determine pavement thickness. However, the empirical method lacks a physical soundness considering the complexity involved in pavement response under changing loading and environmental conditions (H.Huang, 2004). Another widely used practical approach for asphalt pavement is mechanistic-empirical method, which combines mechanical approach, such as stress and strain response, with field data (H.Huang, 2004). Later on, with the fast development of experimental facilities and computational tools, more accurate analytical theories and tools have emerged, and they are capable of interpreting asphalt mixture behaviour from rigorously derived theories of mechanical or energy laws, while taking into account various influential factors such as temperature, aging, strain/stress amplitude etc. Thus it is highly valuable to have a systematic damage model for asphalt mixture that is based on basic physics laws and with the flexibility to include most of the influential factors. As a result, well supported characterization theories and methods for asphalt mixture and relevant amendments remains a highly interested topic for road engineers and researchers.

Asphalt mixture possesses a special feature of viscoelasticity, which means a changing stiffness modulus with loading time. One of the major and inherent distresses for asphalt mixture material are fatigue caused by repetitive traffic loadings. To better understand and interpret the fatigue failure mechanism, it is important to characterize both viscoelastic and crack damage behaviours of asphalt mixtures. Currently, one of the major constitutive models for asphalt mixture' fatigue damage is VECD model, which utilizes continuum damage and viscoelastic theories to define asphalt mixture's crack damage behaviour under various conditions. It combines viscoelasticity and damage mechanics, and has the capability to include the effect of various conditional parameters by quantification

of such effect to VECD. The VECD method can be realized through uniaxial cyclic tests using facilities such as Asphalt Mixture Performance Tester (AMPT). The VECD test finally produces a material unique damage characteristic curve, which is applicable for various strain, frequency and temperature levels. The current standard VECD test is developed by a number of significant theoretical and experimental research introduced in Literature Review chapter, with the current standardized procedures described in AASHTO TP 107-14.

The damage characteristic curve for a mixture can be transferred into stiffness development curves at various strain levels and temperatures, thus can be used to simulate real asphalt pavement's fatigue response under vehicle loadings as well as various forms of laboratory tests. With criterion of fatigue failure, the damage characteristic curves can also be used to calculate the number of cycles to fatigue failure, in the aid of a number of developed solutions (Lee et al., 2000, Christensen and Bonaquist, 2005, Kutay et al., 2008). Thus the damage characteristic curves have wide application in pavement engineering including prediction of fatigue life, simulating fatigue tests and damage tests, estimating the remaining life of pavement road etc.

1.2. Rest Period Healing of Asphalt and VECD Healing Model

As a bituminous material, asphalt mixture possesses self-healing capability, by which the material recovers its strength, resume its stiffness and extends the fatigue life. Rest period defines a no-loading period between traffic loadings, such as the time between two consecutively passing vehicles or even between two axles for one vehicle. In fact, the asphalt mixture's healing is always occurring during loading, unloading and rest period, but the healing is most significant only during the rest periods (Qiu et al., 2012b). This is also due to the fact that healing during loadings are already included in most material characterization approaches under continuous loading, while rest period healing effect is often neglected. In reality, there are enormous number of rest periods of various length, the rest period and vehicle loadings can be simulated in laboratory in different forms (see Figure 1-1). Neglecting the effect of asphalt healing will enlarge, up to 10 times (Qiu et al., 2012b), the discrepancy between desktop or laboratory models and field response.

For VECD model, the current standard approach using AMPT as stated in AASHTO TP 107-14 is based on continuous loading conditions only. The previous rest period healing studies adopted various forms of rest period insertion (see Figure 1-1), while the current healing models are fundamentally derived only from group rest type of rest period (Ashouri, 2014, Lee and Kim, 1998b). The same damage characteristic curve is used for interpreting rest period healing effect, which is derived from group-rest type only. However, there is inconsistency between current rest period healing model and practical application (Roque et al., 2010b), since the real pavement subjects to rest period pattern more similar to pulse-rest type, and this will be described in more details in literature review. Later on, a smeared continuum damage has been developed by Underwood and Zeiada (2014) to specifically apply a simplified VECD model into pulse-rest loading case and produce damage characteristic curves.

Consequently, it is significant to both qualitatively and quantitatively evaluate the rest period healing effect (mainly pulse rest period pattern) using VECD model. In particular, equational relationship between the length of rest period (pulse-rest) and the form of damage characteristic curves would be a significant addition to the application of VECD model.

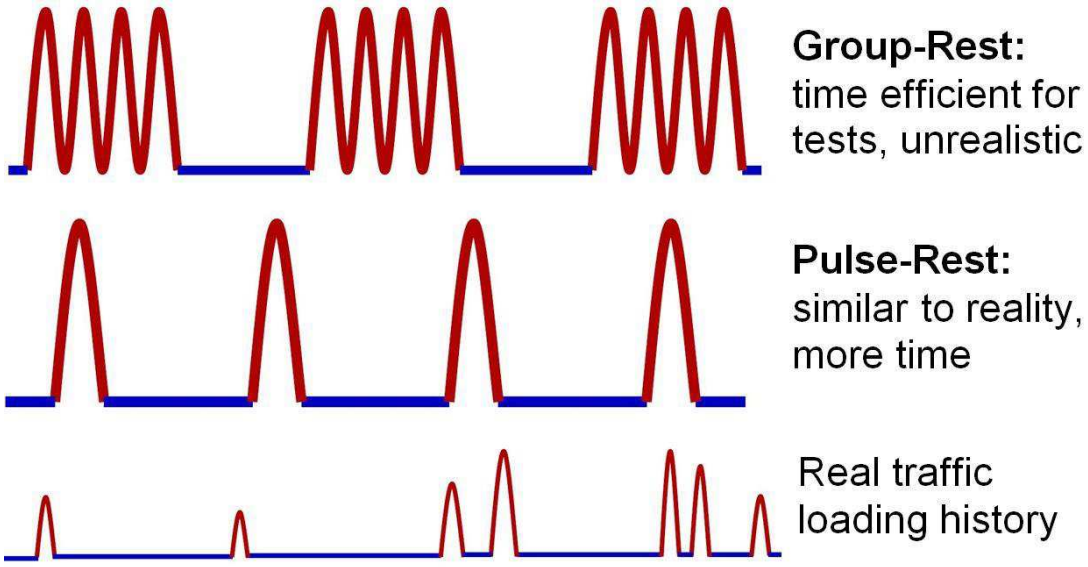

Figure 1-1: Different types of rest periods (Zeiada, 2012)

As an inherent and unique material property, the damage characteristic curves can be used to predict the stiffness development curves of the asphalt mixture under

various loading modes, loading frequencies and temperatures. One of the typical loading mode that is very similar to real road loading condition is from 4PB beam test, in which the bottom section of the beam subjects to fixed amplitude of cyclic tensile strain. As the controlling software to beam machine can also apply rest period after each load cycle, it is then available to verify the rest period healing effect with pulse rest pattern of rest period through bending beam test. As a result, beam fatigue tests provide a way to verify the VECD obtained rest period healing effect and its influence on mixture's damage characteristics.

The specimen geometry and loading mode used in VECD test are different to 4PB tests and real asphalt pavement. It is therefore important to provide a modelling tool that is able to transfer the VECD obtained constitutive model into other loading mode such as bending, thus to evaluate and verify the proposed model against real experimental results. ABAQUS as a powerful numerical modelling tool provides a comprehensive user programming function to define material behaviour, so it is used in this study to build realistic models using VECD derived asphalt constitutive models.

1.3. Various Specimen Geometry for VECD Tests

In the meanwhile, there is still a lack of investigation into the influence of AMPT specimen's geometry effect on its damage characteristic curves especially when rest period is present after each load cycle. It is therefore significant to provide an investigation into the geometric effect of AMPT specimen on rest period healing and VECD tests of asphalt mixture. In addition, the study on geometry of AMPT cylindrical samples are of particular interest to pavement engineers and researchers due to following reasons:

1. It will change the tendency of failure location for AMPT destructive tests, so geometry study may help selection of a most effective geometry in terms of desired failure locations
2. Smaller geometry will significantly reduce the amount of material and time spent on the testing procedures

3. Different specimen sizes may be used by different research, it is important to provide reference results for verification and comparison of tests results from various sources

1.4. Scope of Work

As a result, the scope of work for this research is summarized below:

1. Utilizing AMPT facility provided by Curtin University's Geomechanical Laboratory, conduct systematic VECD tests (including standard dynamic modulus tests) on one of the typical Western Australia mixtures, with various length of pulse rest period
2. Derive dynamic modulus master curves of the tested mixtures and obtain necessary parameters for VECD tests
3. Acquire stiffness development curves and damage characteristic curves of the mixture with various length of rest period under different conditions, thus to qualitatively investigate the interaction between damage, stiffness and rest period healing
4. From VECD tests results, develop a novel equational relationship between damage characteristic curve and length of rest period, so damage characteristic curves of various rest period length can be predicted by a single equation under certain condition
5. Propose procedures, including important technical notices, for the production of novel rest period included damage characteristic curves model equations from laboratory tests and spreadsheet data process
6. Carrying out a series of beam fatigue tests on the mixture with different rest period after each load cycle, investigate the effect of rest period healing on the stiffness development curves, and compare with AMPT findings
7. Write an ABAQUS subroutine that incorporates the obtained rest period healing and damage model, thus create a new user defined material constitutive model able to simulate asphalt's viscoelastic continuum damage behaviour with various rest periods
8. Using ABAQUS with the new constitutive model, build 4PB beam fatigue model subjects to various rest period corresponding to real 4PB tests

9. Based on damage progress and beam theory, develop a novel block method to convert modelling results obtained from ABAQUS simulation into equivalent flexural stiffness generated by 4PB beam fatigue tests
10. Critically evaluate the simulation results in comparison with 4PB beam fatigue tests results, verify the capability of the obtained VECD with rest period model
11. Conduct the VECD with rest period tests on different specimen geometries and identify the sample dimension effect on tests results, especially for the VECD with rest period tests, as well as to investigate the chance of different failure locations

Ultimately, this study develops a new approach to model the VECD based damage characteristics of asphalt mixture with various length of rest period (pulse-rest pattern). This new approach is critically evaluated and verified using numerical modelling technique with self-programmed constitutive model in ABAQUS, and comparison is made with real 4PB beam fatigue tests. The research especially contributes to the understanding of rest period healing effect of asphalt mixture on the basis of damage characteristic curves. The new damage characteristic with healing model provide a novel tool to predict VECD behaviour of asphalt mixture under any user defined rest period. The block method proposed provides an approach to analyze 4PB beam fatigue test results with consideration of true mechanism across the beam's cross section subjects to damage. The findings and methods proposed in this study contribute to future laboratory testing, asphalt mixture characterization and numerical modeling including rest period healing effect. It also provides a framework for 4PB beam fatigue tests results modelling using VECD model integrated into numerical software. Lastly, a parallel size effect study particularly provides useful information regarding the availability of different specimen sizes for VECD with rest period tests.

Chapter 2. Literature Review

The literature review firstly introduces the theoretical background of VECD theory, starting from its original mechanical form to the current simplified version used with AMPT facility. Also, significant research on asphalt healing is listed and briefly introduced, including the healing studies on both asphalt mixture and asphalt binder. It is followed by a specific review on current VECD based rest period healing model, with a detailed description regarding the current healing mechanism and methods proposed for VECD model plus relevant application in numerical modelling and experiments. As AMPT specimen's geometry is also studied in this research, relevant literatures on the size effect of AMPT specimen are also reviewed. Then, there is introduction on previous research including beam fatigue tests and relevant findings, especially the ones including rest period healing. Lastly, important research regarding the numerical modelling implementation of VECD and relevant methods are described and evaluated. The summary section concludes the literature review and briefly addresses the academic significance of current research in the context.

2.1. Development on VECD theories

The literature regarding the development of VECD theories and relevant applications are listed, including all important equations.

Utilizing thermodynamics of irreversible processes, Schapery (1990) established a theory to describe the damage growth of viscoelastic material with three fundamental equations:

1) Function of strain energy density:

$$W = W(\varepsilon, S_m) \tag{2.1}$$

2) Stress-strain relationship:

$$\sigma = \frac{dW}{d\varepsilon} \tag{2.2}$$

3) Damage evolution law:

$$-\frac{dW}{dS_m} = \frac{dW_s}{dS_m} \tag{2.3}$$

in which W is the dissipated energy due to structural change, S_m is the internal state variable, σ is stress tensor, ε is strain tensor.

Schapery (1984) introduced a correspondence principle that convert viscoelastic stress strain behaviour into a similar form to elastic relationship as shown in Eq. (2.4),

$$\sigma = E^R \varepsilon^R \tag{2.4}$$

ε^R is pseudostrain, E^R is a reference modulus that can be any constant (normally taken as 1); With introduction of E^R, the exact pseudostrain versus stress relationship with time can be expressed as:

$$\varepsilon^R = \frac{1}{E^R}\int_0^t E(t-\tau)\frac{\partial \varepsilon}{\partial \tau}d\tau \tag{2.5}$$

in which ε is true strain, $E(t-\tau)$ is relaxation modulus at a certain time. As a result, the pseudostiffness is defined as:

$$C = \frac{\sigma}{\varepsilon^R} = \frac{\sigma}{\frac{1}{E^R}\int E(t-\tau)\frac{\partial \varepsilon}{\partial \tau}d\tau} \tag{2.6}$$

in which C is the pseudostiffness used throughout this work.

With correspondence principal, the non-linear stress strain behaviour is transferred in a form similar to linear elastic equation, because of the introduction of pseudostiffness and pseudostrain parameters. The benefit of using pseudostiffness and pseudostrain is the elimination of viscoelastic effect from the equation, so any stiffness change can be attributed to damage of material only. This enables a direct damage quantification for asphalt material without the need to calculate the viscoelasticity part of stiffness change.

Based on Schapery's correspondence potential theory, a pseudostrain parameter is introduced by Kim and Little (1988) that successfully separate the viscoelastic

healing (or relaxation healing) from chemical healing. This separation then leads into a way to quantify chemical healing of damaged asphalt concrete. This study lays a foundation to the VECD modelling method for flexible pavement.

Kim and Little (1990) conducted uniaxial tensile testing using a specifically fabricated device that is able to provide a controlled horizontal movement to the base plate. It has the benefit of avoiding self-weight bending. The tested mixture is from California valley and includes a syenitic granite aggregate. The results from this laboratory tests contribute to a model for accumulated damage calculation under repetitive loading, which is also an earlier form of VECD method for asphalt mixture.

Lee and Kim (1998a) carried out uniaxial tension tests with a servo-hydraulic closed-loop testing machine. The tests use a gluing jig to make precise alignment of cylindrical specimen with respect to the loading axis so the possibility of eccentric stress can be prevented. The loading was input at 0.1 loading time (10Hz) in a haversine shape. Firstly, master creep compliance and master relaxation modulus are obtained through creep and relaxation tests conducted on a number of specimens. Secondly, pseudostrain (for controlled strain mode) is calculated based on tests results of relaxation modulus versus time and strain values versus time, so integration is then applied for estimation of pseudostrain history. The laboratory results in Lee and Kim (1998a)'s work also presents important information of controlled stress and controlled strain performances using Schapery's correspondence principle, as illustrated in Figure 2-1 and Figure 2-2.

Figure 2-1 and Figure 2-2, by Lee and Kim (1998a), demonstrate the stress-strain and stress-pseudostrain relationships under controlled stress (non-damage) and controlled strain (damaged) mode respectively. Regarding Figure 2-1, graph (a) demonstrates a shifting of stress cycle due to accumulative strain by viscoelastic behaviour, but from graph (b), an almost linear unchanged curve is present using pseudostrain. These two graphs clearly demonstrate the advantage of using pseudostrain as it provides a constant stress pseudostrain relationship when there is no damage. To illustrate the effect of damage on pseudostrain and stress relationship, Lee and Kim (1998a) conducted constant strain damaged tests with results shown in Figure 2-2: both graph (a) and (b) indicate a reduced stress strain or stress

pseudostrain ratio with number of cycles, and this is caused by damage. A secant pseudostiffness parameter was thus introduced to represent the degree of damage. A damage parameter against pseudostiffness relationship was established for controlled stress and controlled strain conditions respectively from this study.

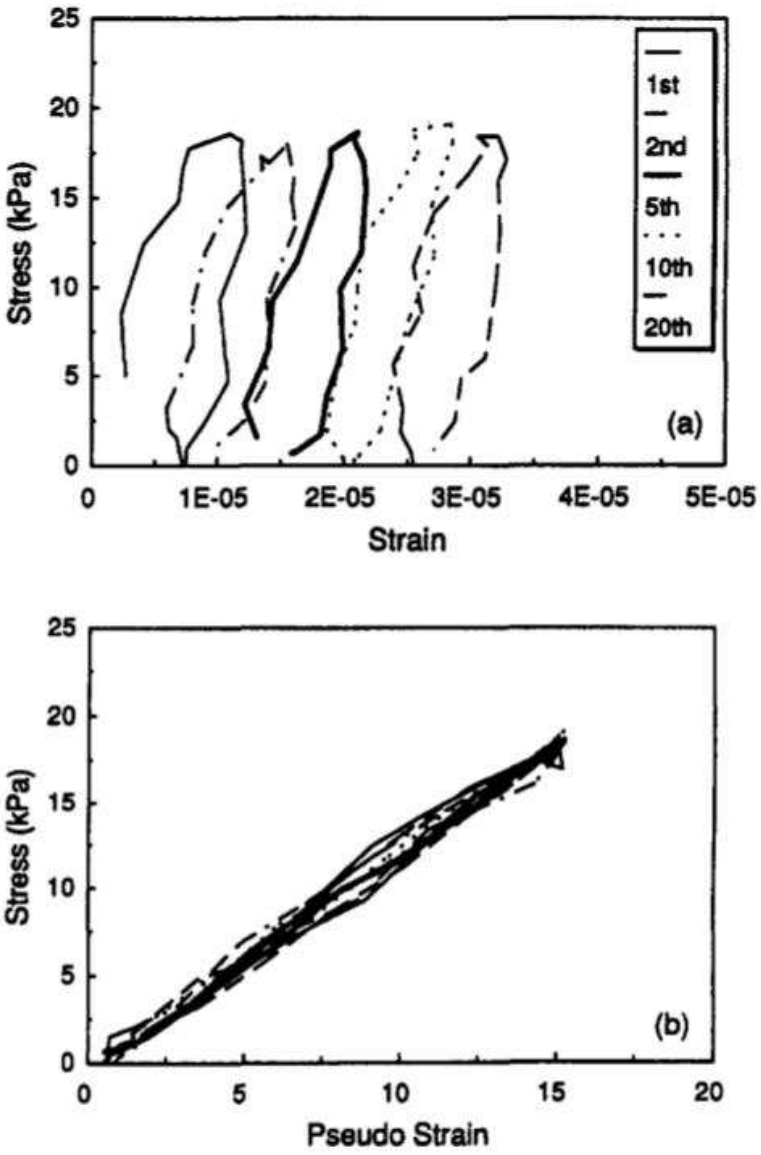

Figure 2-1: Stress-strain and Stress-Pseudostrain Behaviour from non-destructive controlled stress test (Lee and Kim, 1998a)

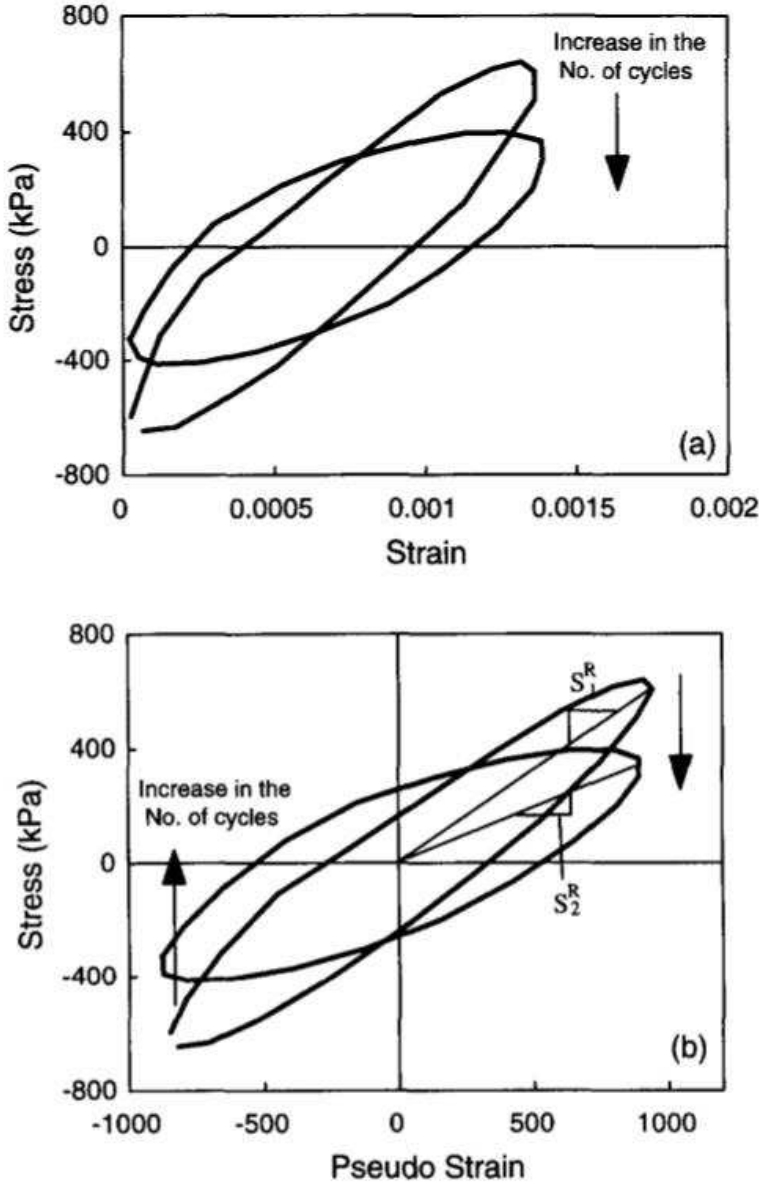

Figure 2-2: Stress-strain and Stress-Pseudostrain Behaviour from destructive controlled strain test (Lee and Kim, 1998a)

Lee and Kim (1998a) extended the above results by proposing a viscoelastic continuum damage model for asphalt mixtures, and this model can also be extended to account for micro-damage healing and calculation of damage parameter for asphalt mixture. Schapery (1990) further developed his work by combining continuum damage model for elastic material using the correspondence principle to establish a viscoelastic continuum damage model. Thus, an internal state variable (ISV) parameter is introduced based on rate type damage evolution law, while the fundamental equation is from Eq. (2.3).

Mainly based on above findings, researchers from North Carolina State University and Texas A&M University developed the ViscoElastic Continuum Damage (VECD) model specifically for asphalt mixture used in flexible pavement. This model has a major benefit of offering the flexibility of improvement by taking into account more influential factors, which might be obtained from more recent and future research on specific influential parameters and conditions. These influential factors may, but not limited to, include aging, temperature, confining conditions and length of rest period. A brief history of the establishment and amendment of VECD model catered for cyclic loading tests is described below. At the beginning, Lee and Kim (1998a) referred to results from uniaxial tensile cyclic loading tests and introduced a damage parameter S. In a time based model, the S parameter can be calculated by the damage development function listed below:

$$S = \sum_{i=1}^{N} \left[\frac{C_o}{2}(\varepsilon_t^R)^2(C_{i-1} - C_i)\right]^{\frac{a}{1+a}} (t_i - t_{i-1})^{1/(1+a)} \quad (2.7)$$

in which C_o is initial pseudostiffness from cyclic loading test, C_i represents the pseudostiffness of ith cycle of load, a is the continuum damage power term, t_i is the reduced pulse time of cycle i and $t_i - t_{i-1}$ can represent the change in the average reduced time between ith and (i-1)th cycles. However, this equation is only applicable on limited conditions, so the produced damage curve only applicable to viscoelastic response at certain temperature. Also, it requires the time increment to be very small and thus is computationally expensive considering the large amount of time included in a typical fatigue test. Thus the damage function has been further developed and simplified by studies listed below.

Chehab (2002) divide the mixture's response into two phases: viscoelasticity and viscoplasticity. The same continuum damage theories are applied for the viscoelastic behaviour of the mixture, while various methods have been studied for viscoplastic response of the mixture. These viscoplasticity methods originate from Uzan's strain hardening model. Chehab (2002) then developed a novel visco-elasto-plastic model that predicts reasonably accurate results to uniaxial repetitive creep and recovery tests, as well as uniaxial constant crosshead tests. While complex modulus test are also conducted to obtain necessary functions for mixture behaviour. It is proposed that the viscoplasticity theory should only be used when there is macro-cracks

formed within the specimen, while viscoelasticity continuum damage theories still applies to intact state and micro-cracks state.

Another remarkable contribution made by Chehab (2002) is the application of time-temperature superposition principals into viscoelastic continuum damage theories. Originally, the time-temperature superposition principal only applies to undamaged status of asphalt mixture so the complex modulus under various temperatures and loading frequencies can collapse into one unique master curve. Chehab (2002) conducted a series of uniaxial tension tests at different loading frequencies and temperatures on a mixture, which has also gone through complex modulus tests so obtained master curves. The time-temperature shift factor obtained from construction of dynamic modulus master curves is applied onto testing time and strain level for the calculation of damage characteristic curves. The original damage characteristic curves produced by Chehab (2002) with and without application of time temperature shift factor is shown in Figure 2-3 and Figure 2-4. The specimen label used by Chehab (2002) contains the temperature and strain amplitude information, for instance, "5-000025" indicates a specimen tested under 5°C and strain amplitude of 25 microstrain. From Figure 2-3, it is evident that damage curves under same temperatures almost collapsed into one unique curve regardless of strain amplitude. However, curves under different temperatures are away from each other before the application of time-temperature shift factor. Figure 2-4 demonstrates the curves after application of time-temperature shift factor, all damage curves nearly collapse into one single curve shape regardless of strain amplitude and temperature. The results verifies the ability of time-temperature shift factor to unify damaged status at different temperatures. Therefore, the use of time-temperature shift factor into production of damage characteristic curves can save a lot experimental effort and time since one single test can theoretically yield a unique damage curve that is shared by tests under various temperatures and strain amplitudes. In other words, the damage curve becomes a unique material based behaviour regardless of testing temperatures. (Chehab, 2002)

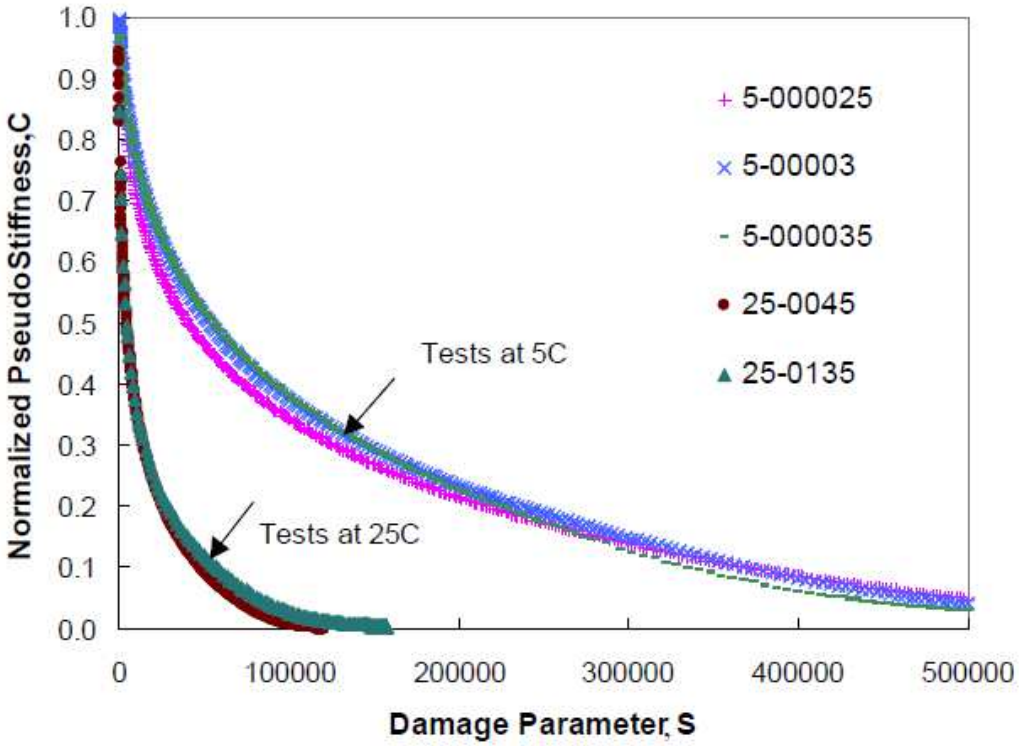

Figure 2-3: Damage Characteristic curves of specimen tested at different strain amplitudes and temperatures (before application of time temperatures shift factor)(Chehab, 2002)

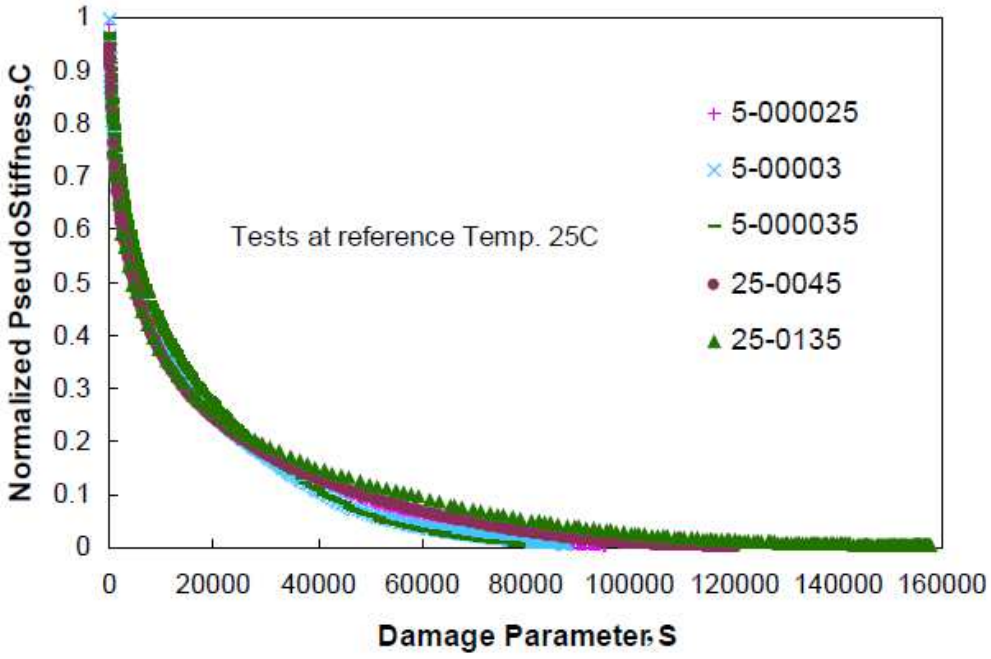

Figure 2-4: Damage Characteristic curves of specimen tested at different strain amplitudes and temperatures (after application of time temperatures shift factor) (Chehab, 2002)

In the meanwhile, there is still a need to develop an improved VECD model that can be utilized with AMPT tests results in a simple, reasonably accurate and efficient way. Daniel and Y.R.Kim (2002) proposed a simplified procedure for the calculation of damage characteristics using constant crosshead rate monotonic direct tension test. A few researches have been done trying to reach a simplified VECD model that is able to utilize AMPT test results. Underwood et al. (2006) presents a rigorous form of damage equation:

$$dS_i = \left[-\frac{1}{2}(\varepsilon_t^R)^2(\Delta C_i)\right]^{\frac{a}{1+a}}(\Delta t_i)^{1/(1+a)} \tag{2.8}$$

in which dS_i is the increase of damage parameter during time increment of Δt.

Underwood et al. (2010) suggested the original VECD method based on time is too complex for practical application, thus they made some significant improvements to rigorously simplify the VECD methods. Underwood et al. (2010) conducted a series of cyclic tensile fatigue tests on a 75mm diameter and 150mm height cylinder under both controlled stress and controlled cross-head mode. A servo-hydraulic loading frame was used to provide tensile loading, while linear variable differential transformer (LVDT) are installed to measure the displacement and strain on the specimen. The simplification procedures proposed by Underwood et al. (2010) utilizes cyclic based data such as cyclic time and peak to peak strain for calculation of damage parameter. The following simplification for pseudostrain computation is suggested:

$$\varepsilon_R = \begin{cases} \frac{1}{E^R}\int E(t-\tau)\frac{\partial \varepsilon}{\partial \tau}d\tau, \ for\ t \leq\ t_p \\ \frac{1}{E^R}\frac{\beta+1}{2}\ \varepsilon_{cyc}^R|E*|_{LVE}, \ for\ t > t_p \end{cases} \tag{2.9}$$

in which ε_{cyc}^R is the cyclic pseudostrain, and β represents the functional form factor. t_p is the cyclic time period. The first equation is the rigorous form the same as what Schapery has originally proposed in Eq.(2.5), while the second equation is the simplified version based on cyclic data. The effect of this simplification procedure is demonstrated in Figure 2-5, in which C_{bar} is the pseudostiffness using rigorous pseudostrain calculation, while F is the simplified pseudostiffness. The difference

between those two stiffness values are indicated to be small (Underwood et al., 2010).

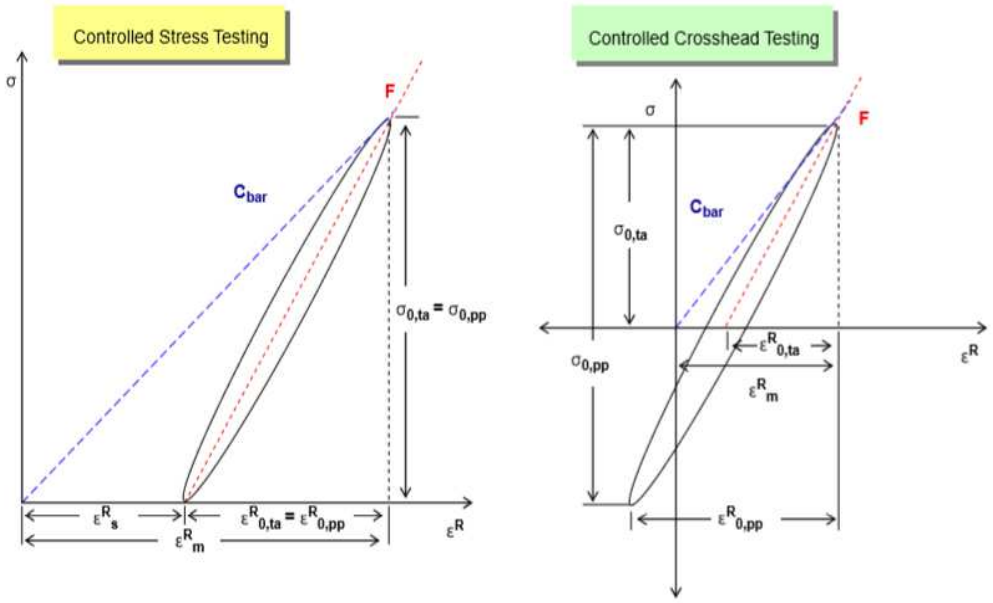

Figure 2-5: Graphic view of the stress, pseudostrain and pseudostiffness definitions used in both simplified and rigorous modelling approaches (Underwood et al., 2010)

Based on above simplification procedures, Underwood et al. (2010) then proposed a simplified calculation of damage parameter S as listed below:

$$\begin{cases} \mathrm{d}S_{transient} = \left[-\frac{I}{2}(\varepsilon^R)^2 dC^*\right]^{\frac{a}{1+a}} (\Delta t_r)^{1/(1+a)}, \quad for\ t \le t_p \\ \mathrm{d}S_{cyc} = \left[-\frac{I}{2}\left(\varepsilon^R_{cyc}\right)^2 (C^*_{i-1} - C^*_i)\right]^{\frac{a}{1+a}} (\Delta t_r)^{1/(1+a)} (K_1)^{1/(1+a)}, \quad or\ t > t_p \end{cases}$$

(2.10)

in which the first equation is time based rigorous calculation, while the second equation is cyclic based simplified calculation. $\varepsilon^R_{t,cyc}$ represents cyclic pseudostrain that is the distance between peak and valley strain amplitudes, Δt_r is the cyclic reduced time intervals, which can be obtained based on peak to peak time interval and application of time-temperature shift factor.

Similar to pseudostrain, Underwood et al. (2010) compare the difference between original and simplified solution for damage parameters S to investigate the error

caused by the simplification procedures, which are mainly using cyclic based pseudostiffness change. K1 factor is thus introduced to compensate for the error caused by simplification procedures.

The current simplified VECD test method adopted by American Association of State Highway and Transportation Officials standard (AASHTO TP107-14) is based on a simplified model that also takes into account the temperature effect. It is developed by Underwood et al. (2010) and listed below:

$$S_{cyc} = \left[-\frac{1}{2}\left(\varepsilon_{cyc}^{R}\right)^{2}\left(C^{*}{}_{i-1} - C^{*}{}_{i}\right)\right]^{\frac{a}{1+a}} (\Delta t_r)^{1/(1+a)} (K_1)^{1/(1+a)} \qquad (2.11)$$

However, as it is not the exact solution and used cyclic value instead of time based ones, certain error would occur, and the K_1 factor is used for error reduction (Kim et al., 2009). Both complete and simplified solutions as listed in Eq.(2.10) are suggested by AASHTO TP 107-14 standard. The complete version Eq. (2.8) is used to process first 5 cycles when dramatic reduction of stiffness thus damage is occurring, while simplified Eq. (2.11) is used for much quicker calculation for all remaining number of cycles.

The simplified VECD theory has been used for practical applications. Firstly, Christensen and Bonaquist (2005) have studied several practical applications of viscoelastic continuum damage theories including experimental data reduction and prediction of real asphalt pavement. They also produced a semi-empirical equation for the prediction of fatigue life, in the aid of tests data from beam fatigue tests. However, this method has certain requirements on mixture properties. (Christensen and Bonaquist, 2005, Christensen and Bonaquist, 2009).

Kutay and Lanotte (2018) in a recent study list several versions of commonly used VECD computation methods, with details and assumptions explained on different VECD models. It also summarizes the calibration procedures for commonly used VECD methods. In addition, uniaxial tension-compression fatigue tests were conducted on six types of different asphalt mixtures. The results are processed by different VECD computation methods, so the comparison are made on the produced

damage characteristic curves and fatigue life predictions between different methods. (Kutay and Lanotte, 2018)

2.2. Relevant Studies on Rest Period and Asphalt Healing

For material without self-healing capability, it degrades with damage that initially brings out micro-cracks which then coalesce and develop into macro-cracks, which is also a sign of fatigue failure for asphalt mixture. On the other hand, if a material has self-healing capability, it will recover those cracks by itself. For asphalt mixture, this mainly refers to recovery of stiffness and extension of fatigue life. At the beginning, asphalt modelling tests are conducted under continuous loading, while the shift factor between field and laboratory results are found to be in the order of 10 to 100, and this is caused by the rest period between load actuations for real traffic loadings on pavement (Ashouri, 2014). According to Qiu (2012), the research on asphalt healing can be dated back to 1960s using a fatigue with rest period test. There are two processes occurring when an asphalt concrete is removed from loadings: viscoelastic recovery and healing on micro-cracks, both of which recover the stiffness of the material and extend fatigue life (Qiu et al., 2012b).

For most research in asphalt healing, rest period is the main duration when healing is studied. Since, although asphalt mixture can heal at any time before failure, only during rest period it heals most. Traditionally, healing was studied by inserting one rest period after certain continuous application of loadings, or this is termed group rest period (see Figure 1-1). Later on with the advance of technology, there are more research using pulse-rate rest period (Zeiada, 2012, Ashouri, 2014)

According to Qiu (2012), a number of fatigue related healing tests using group rest period have been conducted during 1960s and 1980s, and the qualitative relationship between rest periods and fatigue life is investigated. Those initial healing studies also established a fundamental healing parameter: the ratio between fatigue life with inserted rest period and those without rest period (continuous loading).

According to Kim and Little (1988), polymer researchers have successfully identified the healing phenomenon by visually observing fracture surfaces after rest periods of certain lengths, and it is suggested that healing model must be able to

represent initial surface penetration and structural bonding development. Also, Kim and Little (1988) developed a quantitative method to predict chemical healing in a way of separating the viscoelastic part (relaxation part). The novel damage model is also established by Kim and Little (1988) based on Schapery's correspondence principle, and it is able to take into account different loading sequences as well as rest periods effect.

A number of previous studies are investigating healing effect on asphalt mixtures. Kim et al. (2003) conducted dynamic mechanical analysis on sand asphalt samples at 25°C and 10Hz. Change in dynamic modulus, change in pseudostiffness and change in dissipated strain energy are recorded as three parameters for damage. There are several rest periods (group rest) inserted during tests and they have proven ability to extend the fatigue life.

For a common asphalt mixture made of gravels and bitumen, the bitumen binder is the main reason that causes asphalt healing. Thus, there are also significant researches focusing on the binder property and healing. It has been suggested by previous findings that viscoelasticity is caused by rearrangement of molecules, while wetting at opened crack surfaces causes crack healing, which is followed by diffusion that further recovers formed micro-cracks so further healing (Ashouri, 2014, Qiu et al., 2012b, Philips, 1998). To quantify the effect of crack surface wetting and diffusion on asphalt healing, Wool and O'Connor (1981) developed an original equation that was later applied by various researchers to model healing of asphalt binders (Luo et al., 2015, Bhasin et al., 2008). However, the mechanical approach based on binders does not directly transfer to asphalt mixture which also contains gravels and voids, plus cracks that can be of microscopic scale.

Lu, Soenen et al. (2003) conducted dynamic shear rheometer (DSR) tests on various types of bitumen under different conditions including aging status, strain or stress controlled and with/without group rest periods. They have proved that bitumen type has a wide influence on the rest period healing capacity. Interestingly, Lu, Soenen et al. (2003) found rest period resumes stiffness to some degree for both controlled strain and controlled stress tests, however, only controlled stress tests indicate an increase of fatigue life, which also varies to a great degree between bitumen types. It

was also discovered that the significance of rest periods on fatigue life relies on the ratio between rest time and loading time (Lu et al., 2003).

Bhasin et al. (2008) established a novel framework that includes both the material and mechanical properties of the bitumen for estimating the binder's healing effect on asphalt mixture. The framework works on two healing mechanisms: instant cohesion of crack faces and molecules diffusion between separated surfaces. For wetting, the function is made up of the creep compliance properties of the target mixture, while measurement of surface free energy of bitumen can be sued to work out the healing caused by confusion. The benefit of this model is that it is theoretically based and thus can be integrated into any potential models based on crack damage and progression. To make the method applicable, Bhasin et al. (2008) proposed new experimental procedures using DSR, thus some necessary parameters for this novel analytical method can be obtained. Both the proposed theoretical method and laboratory procedures have been verified against tests results on selected asphalt mixtures, thus the hypothesis made is validated.

Van den Bergh and Van de Ven (2012) uses DMR to test the healing capability of mortar by suggesting a novel approach to conducte DSR with rest period, and the interaction between aging effect and healing. The paper also contains the configurations of the novel test. One issue with this new approach is it is not compatible with controlled strain test, instead controlled stress tests are used in the aid of a side program. They applied torque of various levels on five mortar samples at 15°C and 10Hz. The results indicates that artificial aging will boost the healing effect of binder.

Shen, Chiu et al. (2010) conducted constant load dynamic shear rheometer tests with specifically designed intermittent load sequence (resting period from 0-6 seconds) on asphalt binders to study the cohesive healing. A significant and novel dissipated energy approach was introduced and successfully applied into asphalt mixtures' healing effect estimation, by being used on binder. The ratio of the recovery of dissipated energy per unit of rest period is utilized as an indication of asphalt binder's healing capacity. The results identified that healing effect of asphalt mixture is influenced by the type of bitumen, strain amplitude and temperature. The

study proposed a special parameter of plateau value (see Figure 2-6) as an indication of fatigue failure, since it is proven to be an equal point for the number of cycles to reach 50% stiffness reduction in a fatigue tests on binder. The specific relation between ratio of dissipated energy curve in Figure 2-6 and the dissipated energy with number of cycles curve (Figure 2-7) is indicated by zone number of I, II and III. Thus, for asphalt mixture, zone III is the area where fatigue failure occurs. The test conducted by Shen et al. (2010) applied rest period insertions that are more similar to real road conditions. They have concluded that there is a quantitative relationship between healing effect of specific bitumen binder and healing rate, as well as the slope of the curve of plateau value drawn on a log – log scale. The binder type is found to have large effect on healing capacity, with certain type of bitumen demonstrating around 7 times extension of fatigue life. Another interesting finding made by Shen et al. (2010) is the influence of initial strain level on the healing ability, as an improved healing is found with a reduced reduction of initial strain amplitude. However, the amplitude of stress does not demonstrate evident relation to healing capacity. In addition, higher temperature is found to improve the asphalt healing in most cases. (Qiu et al., 2012b) carried out tests with beam on elastic foundation set-up and the results again proved the presence of cohesive healing behaviour in asphalt. Firstly, a clear and explanatory illustration of cracking mechanism is presented as shown in Figure 2-8.

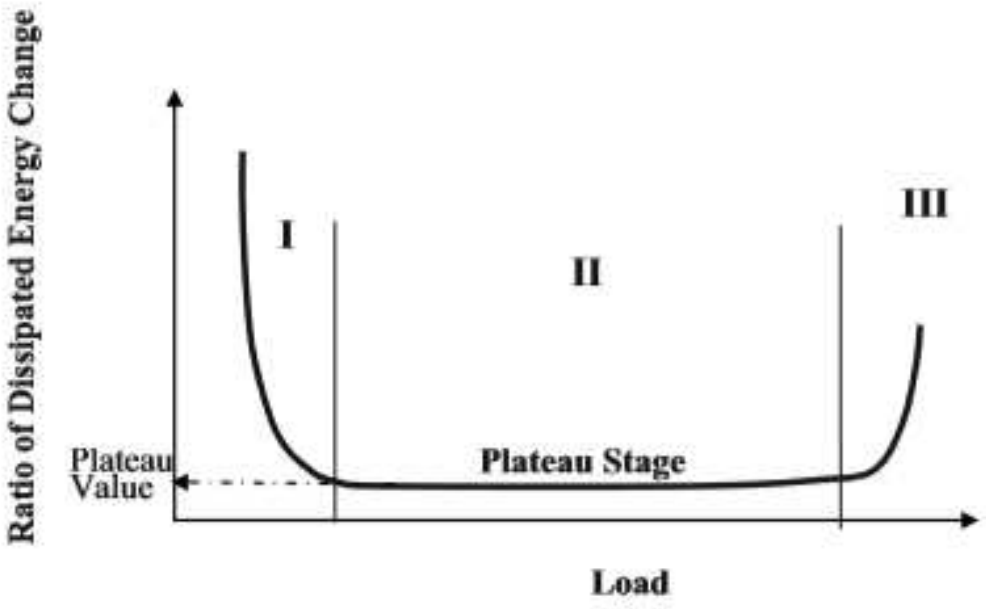

Figure 2-6: Demonstration of typical ratio of dissipated energy versus number of cycles plot with three response zones (Shen et al., 2010)

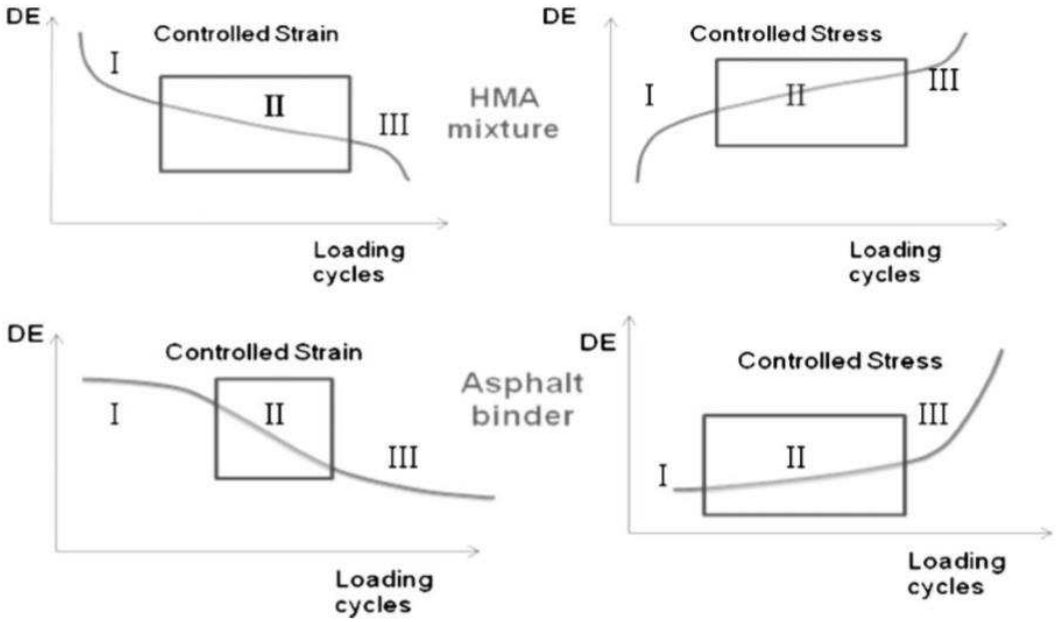

Figure 2-7: Dissipated energy (DE) versus number of cycle curves for both controlled strain and controlled stress tests on both asphalt mixture and binder (Shen et al., 2010)

(Qiu et al., 2012b) has also found that healing effect increases with longer healing time and higher temperatures. In addition, it is proposed that healing mechanism has two forms of effect: viscoelastic healing and viscosity healing (Qiu et al., 2012b). A

cohesive zone model was proposed (Qiu et al., 2012b) to simulate the crack damage of asphalt mixture. The mechanism of cohesive zone is that the zone can be activated once the applied stress is larger than the maximum traction force. These researchers then integrate a smeared crack typed cohesive zone model into finite element modelling software. The modelling results are then compared with experimental results of beam on elastic foundations set-up, the model predicts good results on crack development behaviour of asphalt concrete compared with lab results. Also, the healing effect during reloading procedures is observed and identified as very significant for these tests. Lastly, they proposed more research on asphalt damage and healing mechanisms will be valuable.

A number of bending beam tests have been conducted and prove that the insertion of rest period extends the fatigue life, while the extent of this extension is tightly related with the length of rest period (Raithby and Sterling, McElvaney and Pell, Verstraeten et al., cited in Zeiada, 2012).

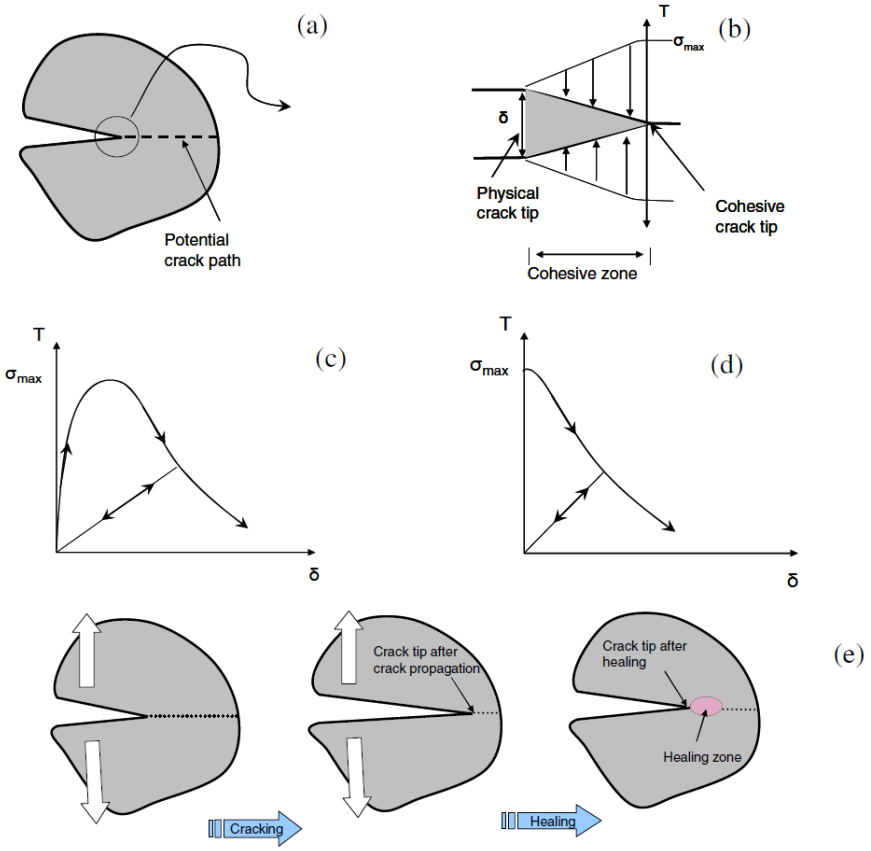

Figure 2-8: Graphical Illustration of cracking progress mechanism for asphalt mixture and crack healing (Qiu, 2012)

2.3. Current Healing Models for VECD

With VECD method, healing effect is mainly accounted for by interpreting the effect of rest period on pseudostiffness development or damage characteristics. As this study is for mechanical characterization and modelling of asphalt concrete's damage behaviour, a review regarding rest period healing and its development on VECD method is specifically listed below.

There are two types of healing mechanism identified during rest period: viscoelastic recovery (time dependent) of stiffness and chemical healing due to closure of cracks and molecule diffusion (Lee and Kim, 1998a). While viscoelasticity is an inherent property for asphalt mixture, the formation of cracks only exists in cases of destructive loadings that renders micro damage and cracks. Thus, two mechanisms of healing are working here and they need to be treated separately.

Lee and Kim (1998b) have studied the C vs S curve with rest period inserted after certain cycle, for example, a rest period of 32 mins was inserted between continuous load cycles in a cyclic uniaxial tensile loading test. The change of pseudostiffness with number of cycles is illustrated in Figure 2-9.

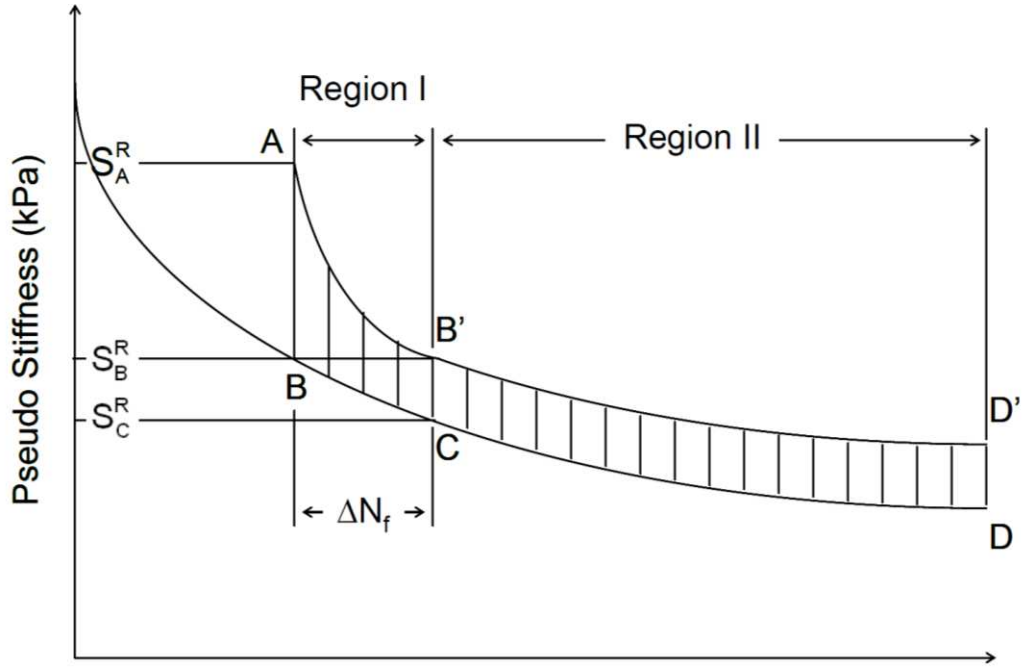

Figure 2-9: Change in PseudoStiffness caused by a Rest Period. Region I: redamaged material; Region II: damage of previously intact material (Lee and Kim, 1998b)

In Lee and Kim (1998b)'s research, additional parameters related to C and S are introduced to amend the original C vs S curve based on rest period length and healing effect. From Figure 2-9, region I represents response of healed material after rest period being inserted at cycle number 20, while region II is for intact material after the healed section is damaged again (Lee and Kim, 1998b). Based on the above material response, additional parameters of C2, S2, C3 and S3 were introduced and the damage characteristic curve is modified accordingly. A modified C(S) function was also proposed by Lee and Kim (1998) to represent the healing in terms of damage parameters S1, S2 and S3. And these relationships are shown in Eq. (2.12) for Region I and Eq. (2.13) for Region II as seen in Figure 2-9:

$$H = [C_B + C_2(S_2)]C_3(S_3) \tag{2.12}$$

$$H = (C_B - C_C) \tag{2.13}$$

Where:

$C_2(S_2)$	=	Function corresponding to the jump of C value right after the application of rest period (AB in Figure 2-9)
$C_3(S_3)$	=	Function corresponding to the change of slope BC to AB' after healing
H	=	Healing parameter to account for the difference between healed and unhealed material

Using the damage evolution laws the S2 and S3 parameters could be obtained by solving Eq. (2.14) and Eq. (2.15) accordingly:

$$S_2 = \int_0^{t_{rp}} [\frac{1}{2}(\varepsilon^R)^2 \frac{\partial C_2}{\partial S_2}]^{\alpha_2} dt \tag{2.14}$$

$$\dot{S}_3 = [-\frac{S_A^R}{2}(\varepsilon^R)^2 \frac{\partial C_3}{\partial S_3}]^{\alpha_3} \tag{2.15}$$

Eq. (2.16) and Eq. (2.17) then can be used for curve fitting purpose:

$$C_2(S_2) = C_{20} + C_{21}(S_2)^{C_{22}} \tag{2.16}$$

$$C_3(S_3) = C_{30} - C_{31}(S_3)^{C_{32}} \tag{2.17}$$

in which C_{xy} is curve fitting parameter. A modified C(S) function is therefore proposed by Lee and Kim (1998b) to include rest period healing in damage characteristics curves of asphalt mixture.

Using the above VECD based group rest period healing model, Lee et al. (2000) established a prediction model for asphalt mixture's fatigue behaviour with mathematical simplifications. A relationship is also established between the regression fitting parameters for a phenomenological fatigue model and the viscoelastic properties of the mixture. What's more, other factors such as damage behaviour and loading conditions are also related with curve fitting coefficients of damage characteristic curves. Also, the effect of healing is integrated into the model based on Lee and Kim (1998b)'s VECD model to simulate a fatigue with rest period test, and the modelling and test results of fatigue life compared favourably with each other. The benefit of such a VECD based healing model to predict the fatigue life of asphalt mixture is, firstly, it has a decent prediction accuracy due to the fact that VECD method is based on the true mechanical constitutive model. Secondly, a micro damage based healing mechanism is included in the model. Thridly, the model has the capability to account for various influencing factors such as rate of loading, stress/strain levels and rest period length. The simplification method provided in this study also serves as a foundation for the final simplified VECD theory.

However, this healing model has a drawback at dealing with repetitive rest period since the results are based on certain damage status while the healing effect at different damage status (different S value) varies (Roque et al., 2010b). For instance, the group-rest healing model. While for a real highway road, numerous rest periods are generated between vehicles as they are passing through one after another Figure 1-1). Ashouri (2014) distinguishes two rest period tests as "group-rest test", similar to Lee and Kim (1998b)'s, while "pulse rest test" that has certain rest period after each load pulse. For example, the test results demonstrated in Figure 2-9 are based on healing of intact material with a group-rest period, while the actual healing may occur again on previously healed material such as pulse rest test. As demonstrated in Figure 2-9, it is clearly against reality by applying results from group rest test to repetitive rest periods as the stiffness is impossible to recover to be stiffer than the

original state (Kim et al., 2009). Roque et al. (2009) incorporated the above mentioned healing model into VECD FEP++ software and used healing potential factors to counter the inherent inaccuracies of the model. However, it is still only a mathematical correction factor that is not based on factual data nor theoretical derivations.

Zeiada (2012) carried out a research to study the rest period healing effect on asphalt mixture and its relation to fatigue endurance limit under various conditions. This research involves systematic AMPT tests with repetitive rest periods (pulse rest period in Figure 1-1) between each load cycle, using the "VECD with rest period" software. The study applied pseudostiffness concept from VECD theory to study the stiffness development curves produced under various tests conditions, and fatigue endurance limit is defined as the strain level that reaches constant pseudostiffness without failure. Two pseudostiffness regression models are developed to capture the relationship between pseudostiffness and number of cycles. The regression models are worked out by regression analysis tools such as Excel, and statistical softwares such as Statistica, Minitab etc. A regression function is developed that is able to calculate pseudostiffness based on input number of cycles, temperature, percent air voids, tensile strain amplitude and rest period. Then, Zeiada (2012) compared the results obtained from regression models with tests results of beam fatigue tests, and good agreement between them is obtained. However, the curve fitting methods used in this study is only applicable for certain mixture, while the results are based on laboratory tests of endurance limit (normally low strain amplitude that incurs small damage) so no effect of rest period healing on asphalt's damage characteristics is directly presented.

To apply VECD model in the case of rest period after each loading cycle, Underwood and Zeiada (2014) develop a modified version of simplified VECD approach specifically for the case of rest period after each loading cycle. Displacement controlled tests were conducted with various length of pulse-rest period of 1, 5 and 10 seconds at 4.4, 21.1 and 38^{o}C. The tested asphalt mixture are made of same aggregate structure and constitution. The impact made by pulse-rest period is clearly demonstrated by test results. Significantly, they proposed a smeared continuum damage approach to interpret pulse-rest healing effect within the

framework of original simplified VECD model, by establishing a modified function to calculate pseudostrain after each loading and rest period. Thus, VECD tests with rest period of different lengths can be reflected by different forms damage characteristic curves. It has been pointed out that healing capacity increases with better asphalt concrete and lower air void content. The findings indicate varied healing mechanism between pulse-rest and block-rest loading cases. Remarkably, Underwood and Zeiada (2014) treat rest period healing as microcrack healing only, while also suggested that both viscoelasticity and microcrack healing contributes to stiffness recovery during pulse-rest period. Thus it is important to define the healing before to adjust smeared continuum damage approach.

Ashouri (2014) conducted a series of VECD with rest period tests to investigate and quantify the healing effect. The experiment adopted four rest periods of 10, 30, 90 and 270 seconds applied at different damage levels and temperatures. Similar to the time-temperature shift factor used for production of dynamic master curves, Ashouri (2014) introduced a parameter of reduced rest period, obtained from application of time-temperature superposition principle on cyclic time, into the production of damage characteristic curves using the VECD with healing model, which is proposed by Lee and Kim (1998b). This new healing model was obtained from VECD with group-rest healing but then was used to model VECD with pulse-rest tests through percent healing parameters. Thus, novel results of damage with healing master curves (C vs S curves) can be drawn to produce a unique master curve regardless of lengths of rest period inserted between each load cycle. It is followed by successful modelling of pulse-rest test using damage characteristic curves obtained from VECD tests with both group-rest rest period and continuous loading, and the results have shown good agreement with pulse-rate tests results. Although pulse rest period tests results are modelled with good agreement, the number of test as well as the length of rest period is limited in this study. For instance, only the specified rest period of 10, 30, 90 and 270 seconds are used for either group rest and pulse rest tests by Ashouri (2014), while for many other mixtures, healing capability already reaches its maximum at a much lower rest period. Considering most traffic load subjects to frequent rest period of 1s or even less (for higher speed highways etc.), original pulse rate rest period test results are still significant for healing model study for asphalt concrete especially a different mixture is used.

2.4. Specimen Geometry Considerations for AMPT

For asphalt specimen geometry used in laboratory, a representative volume element (RVE) concept is a mandatory requirement, this means the ratio of nominal maximum aggregate size (NMAS) to the specimen diameter should be within the range of 1/4 and 1/2 based on ASTM D3497-79 (Lee et al., 2017a). While for a direct tension cyclic tests like AMPT, a conservative ratio of 1 to 2 was suggested (Witzcak et al., 2002).

Normally, dynamic modulus tests are more lenient on sample geometry than destructive tests since it is a linear elastic range non-destructive test. For the diameter, both 100mm and 75mm are proposed by previous research. Kim, Guddati et al. (2009) adopted 100mm sample for compression test while 75mm for tension with height of 150mm fixed. Zeiada (2012) used 100mm diameter for dynamic modulus test and 75mm for AMPT tension-compression fatigue test. Later on, a standard size of 100x150mm cut from a compacted 170mm long sample is adopted by AASHTO TP 79-13. However, a recent research by Castorena et al. (2017) and Lee et al. (2017b) examined specimen of reduced geometry for dynamic modulus tests and verified the small size specimen for producing accurate damage characteristic curves at low or medium temperatures, but slightly increased dynamic modulus at higher temperature. For VECD tests, originally, the same dimension to Dynamic Modulus tests of 100x150mm is proposed. However, for many mixtures, this lead into a high propensity of end failure, thus a reduced cylindrical sample length of 130mm after a compaction height of around 178mm is adopted (Lee et al., 2017a). On the other hand, almost all research found different specimen geometries, even regardless of either end failure and middle failure (see Figure 3-10), can capture damage characteristics sufficiently (Hou et al., 2010, Lee et al., 2017a). The latest AASHTO standard adopted Lee et al. (2017a)'s suggestion and proposes a 130mm x 100mm specimen size for AMPT destructive tests, and this should be the case especially when the behaviour up until fatigue failure is required. In the meanwhile, AASHTO TP 107-14 also recommends that the compaction and cutting length are both adjustable based on specific equipment and material type. In reality, various specimen geometries may be adopted by different research.

From an email communication with Industrial Process Controls (IPC) Global, a 54x110mm geometry, which can be produced in Curtin's Pavement laboratory, could be a small size option for AMPT tests. This specimen size will offer the following advantages:

1. Save of mixture components, since the volume of mixture used for 54x110mm sample is just 40 percent of 100x130mm diameter samples
2. Largely save time and physical effort required in procedures of mixing, compaction and cutting involved in the making of AMPT specimens
3. 54x110mm specimen has much smaller cross section area, thus it can withstand larger strain level not exceeding the machine limit, this will increase the types of tests available, such as future study on plastic response that requires larger specimen strain
4. (potential) smaller specimen has less scope for void ratio variation along the sample length and this will increase the chance of middle failure

What's more, as the influence of asphalt mixture's healing capability has risen as a concern for experimental tests on asphalt mixtures, which normally use continuous loadings. While some healing models are being developed for VECD, there is still a lack of study on availability of different specimen geometry on VECD tests with the presence of rest period healing.

2.5. Beam Fatigue Tests

Beam fatigue tests, or flexure tests, are one of the most popular test approaches for asphalt mixture's fatigue, master curve and stiffness. Three and four point bending beam tests are two widely used test types, in particular, the stress strain and deformation status of such beam tests is a close simulation to real field asphalt layer. A variety of asphalt research are produced based on these tests results.

Daniel and Kim (2001) carried out three point beam fatigue tests to investigate the influence of various factors to asphalt mixture's stiffness change including fatigue damage, rest period healing and temperature. An impact resonance method was applied to investigate the asphalt mixture's stiffness behaviour during loading and rest period cycles. The advantage of this method is to separate the damage caused

stiffness change from viscoelasticity nature (relaxation) of the mixture. The rest period used in this study is intermittent ones after certain cycles of continuous loadings (group rest period in Figure 1-1). Three rest period lengths are tested, and relevant dynamic modulus of elasticity versus number of cycle curves are drawn as shown in Figure 2-10. From the figure, a rise of flexural stiffness is seen from tests with rest period and it is caused by healing of microcracks during the rest period (Daniel and Kim, 2001). Also, higher temperature indicated improved healing effect, thus larger stiffness rise. However, interestingly, Figure 2-10 seems to demonstrate higher initial stiffness at 60^{o}C compared to 20^{o}C, the reason could be a previous three point beam fatigue tests configuration as well as the type of mixture used.

Christensen and Bonaquist (2005) developed a method to correlate the stiffness values produced by beam tests to the stiffness prediction made by VECD methods. In their method, a representative damage status of middle third of the beam is used for the whole cross section of the beam, which is divided by 10 blocks of equivalent height. Each block is assigned a virtual length based on its damage and stiffness reduction. The results have indicated that, during destructive fatigue test, the critical bottom surface of the beam has a damage ratio that can be quantitatively related to the ratio of flexural stiffness produced by the software no matter what type of the material is. Thus, damage status at the beam's bottom surface can be calculated based on the proposed quantitative relationship and the flexural stiffness values produced by beam fatigue tests.

Castro and Sánchez (2006) conducted 3 point bending beam controlled strain test on an asphalt mixture with 10Hz loading cycle. One set of test is under continuous loading, while another set, invented by Castro and Sánchez (2006), has 1 second rest period after each load cycle. The results are compared between tests with and without rest period in terms of fatigue life: strain level versus failure number of cycles. A statistical tool called descriptive discrimination is utilized to distinguish the failure results between with and without rest period test. Finally, as demonstrated in Figure 2-12, it is illustrated that the presence of rest period has evidently improved the fatigue life, while the degree of improvement is decreasing with strain amplitude.

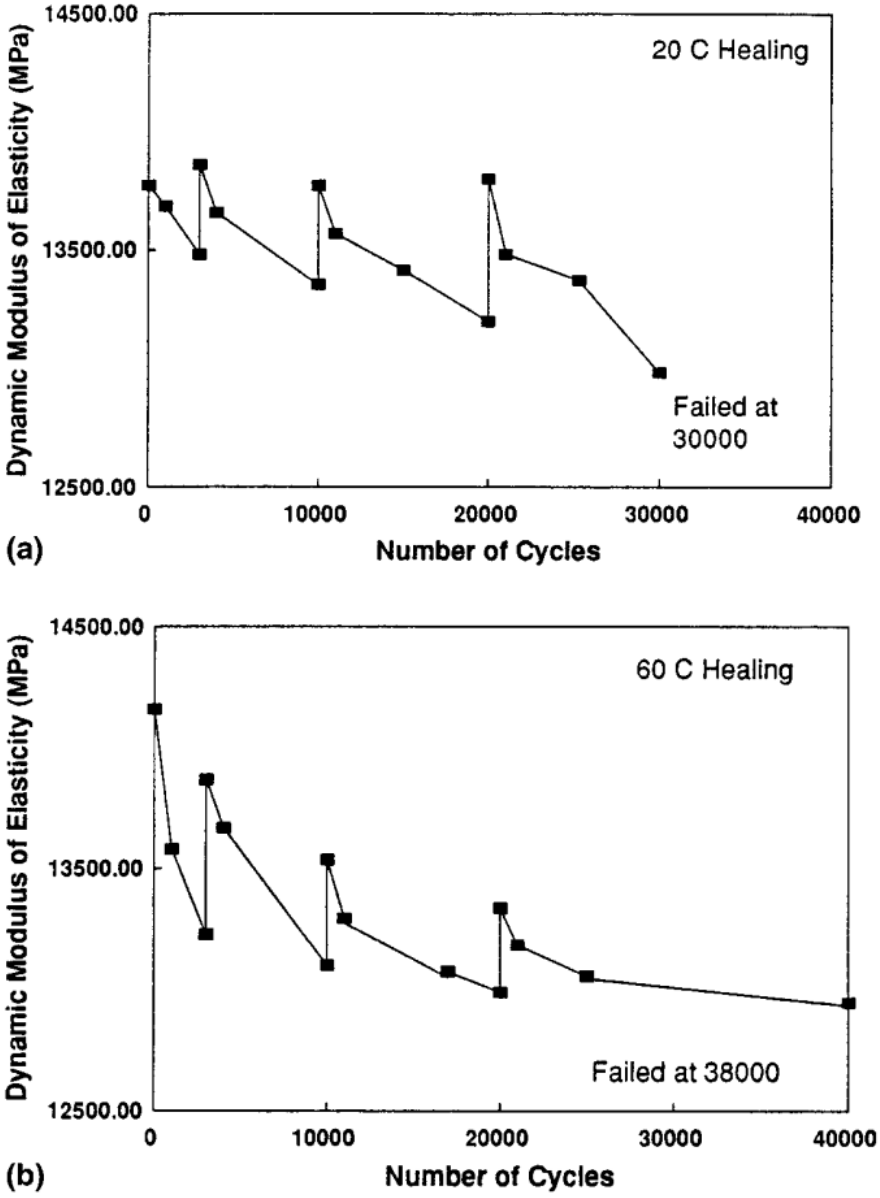

Figure 2-10: Stiffness development curve with rest period at two temperatures (Daniel and Kim, 2001)

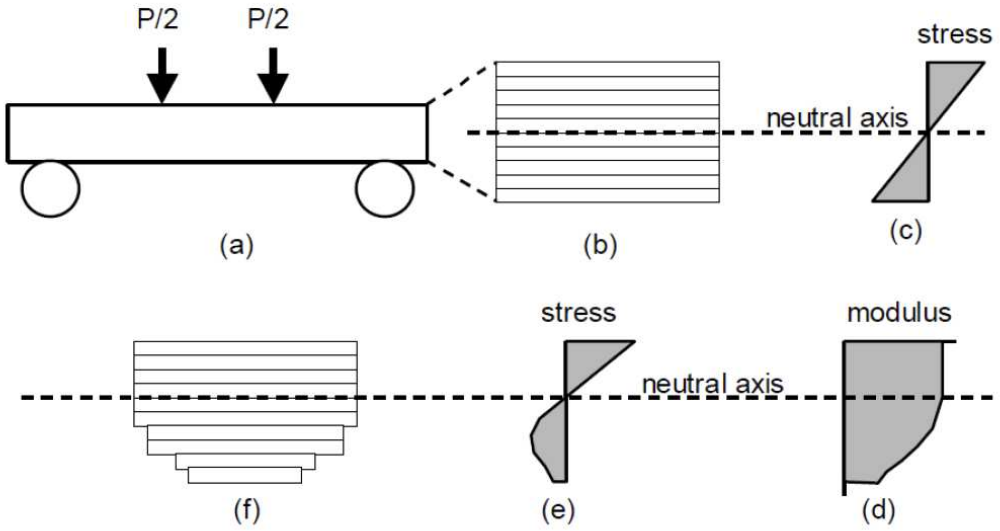

Figure 2-11: Illustration of the block method proposed by Christensen and Bonaquist (2005), cited in Zeiada (2012)

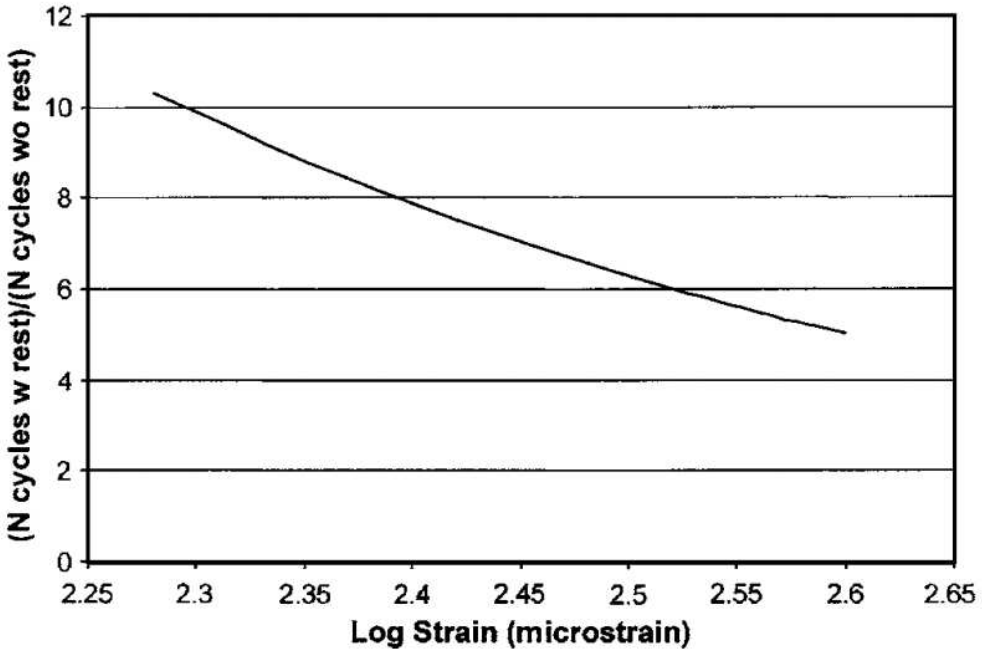

Figure 2-12: Beam Fatigue results comparison between tests without and with 1s pulse rest period (Castro and Sánchez, 2006)

Pramesti et al. (2013) conducted a series of 4PB bending beam fatigue tests on gravel asphalt concrete (GAC) specimens, and produced stiffness development, master curve and fatigue failure. Firstly, temperature and frequency sweeping tests are conducted to obtain master curves for the GAC mixture. The, fatigue tests were

conducted on constant displacement mode and at temperatures of 5, 20 and 30^{o}C, under load frequency of 3 and 8Hz. With the same mixture, model pavement lanes have been built using the accelerated pavement testing facility, and results have been produced for stiffness development, fatigue failure and master curves. Comparing 4PB to accelerated pavement tests results, it has a higher stiffness level at the same reduced loading time than accelerated tests results. Significantly, the fatigue life predicted by accelerated pavement tests are generally longer, from 1.5 to 13.5 times, than the 4PB tests results. Pramesti et al. (2013) suggested that rest period healing could be a one of the main contributors to the results deviation.

Haddadi et al. (2015) utilized data from 4PB beam fatigue tests to simplify the calculation of damage parameters used in VECD model. The peak-to-peak stress and strain values from beam fatigue tests are used to determine damage parameter S, which is calculated from uniaxial tests in standard VECD method. A particular damage power term α, used in damage parameter calculation equation such as Eq.(2.11), is defined so the damage curves obtained from beam fatigue tests can collapse into one unique curve. The α is suggested to be 1/m, in which m is found to be central slope of the relaxation modulus versus time curve, obtained from dynamic modulus tests using 4PB beam tests.

2.6. Numerical Modelling for VECD Methods

For VECD methods, the main use of numerical modelling is to implement the VECD model, thus damage characteristic curves, as a material constitutive model. However, as VECD theories directly produce damage parameters “S” and pseudostiffness “C” by its damage characteristic curves, a pure mathematical simulation without the need of a geometrical model is another feasible solution as long as the strain amplitude is known. For instance, if it is known the bottom asphalt strain at a road is 100 microstrain plus all necessary properties of the mixture as well as environmental conditions, it is possible to directly use a mathematical analysis software like MatLab to calculate the pseudostiffness at the asphalt bottom layer at each number of cycles based on VECD model. However, a numerical tool with geometrical building up can provide the damage status and stiffness values for the

whole geometry that subjects to different strain levels, such as the cross section of a bending beam.

Mun et al. (2005) incorporated VECD model for monotonic cracking mechanism into a finite element module using ABAQUS. The VECD model is realized through programming of stress strain relationship into ABAQUS user subroutine according to viscoelastic continuum damage theories, which were complete time based solution at that time. The model requires linear viscoelasticity parameters obtained from complex modulus tests and damage properties from monotonic tensile strength test. The capability of the model is verified by comparing simulation results with experimental results of monotonic loading tests with different strain rate, and close agreement is demonstrated. However, the numerical modelling technique utilized is a time domain simulation thus computationally expensive, also the model is based on monotonic tests results as constitutive parameters thus not applicable for cyclic fatigue damage mechanism, while no rest period healing effect is included.

Roque et al. (2010b) produced a top-down cracking model for asphalt mixture using relatively complete VECD model that includes a number of conditions such as temperature, aging, rest period healing, viscoplasticity and thermal stress etc. The model is used for prediction of asphalt mixture's behaviour before fatigue damage or major cracking. The model's ability to simulate the asphalt mixture's fatigue behaviour is proven by a parametric study.

For the healing part of Roque et al. (2010b)'s model, it still uses the healing model proposed by Lee and Kim (1998b) to predict the healing and damage. While this healing model is applied on predicting pulse rate rest period test, the concept scheme of the model is illustrated in Figure 2-13. From the figure, the damage status and pseudostiffness after each number of cycle is calculated so the status point moves up and down along a unique damage characteristic curve. One important thing about this model is that, regardless the length of rest period, one single damage characteristic curve, obtained from continuous loading VECD test is used. So the healing is calculated based on recovery of both S and C. However, Figure 2-14 demonstrates the unrealistic prediction of stiffness recovery that may be encountered by using group rest healing model proposed by Lee and Kim (1998b),

when it subjects to real road rest period healing effect. Although Roque et al. (2010b) applied a factor to solve this problem (see Figure 2-15), it is only a mathematical adjustment that still lacks of theoretical or factual support. In other words, the accuracy of this healing model is doubtful at dealing with numerous rest periods between each consecutive load cycles.

Ashouri (2014) used MatLab to compute the stiffness and damage status of asphalt mixture from the proposed VECD with healing models by Lee and Kim (1998b). Although the healing model is obtained from tests with group-rest rest periods, the MatLab program is written to predict the pulse-rate rest period healing and the results are compared favourably with real fatigue tests with rest periods in between each consecutive load cycle. However, relatively long length (no less than 10s) insertion and limited number of pulse rest period tests are presented, while the real road sometimes subject to rest period of much smaller duration such as less than 1s.

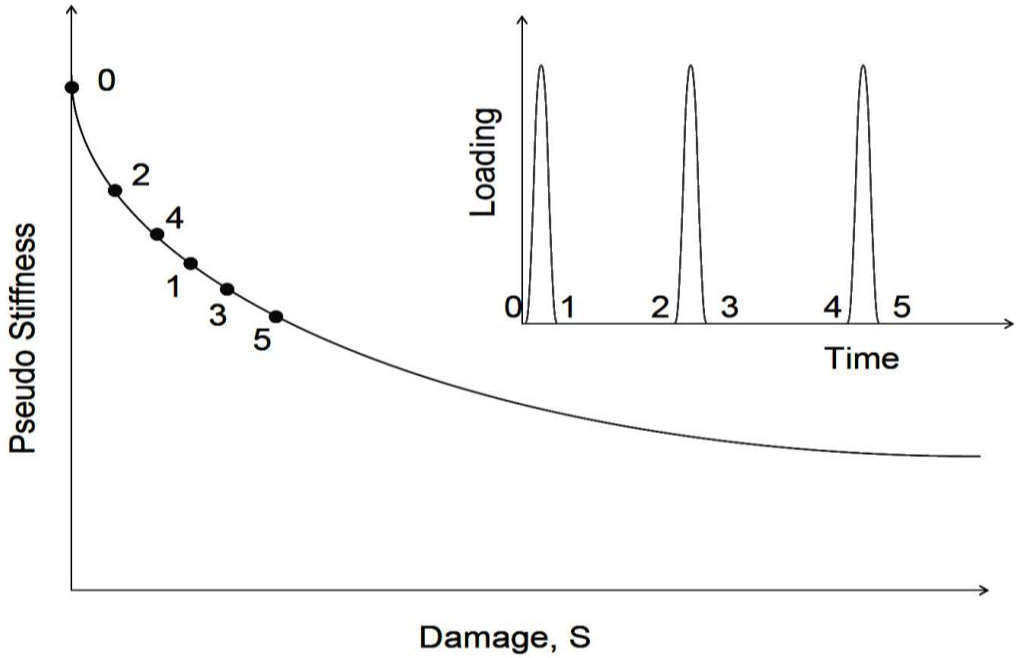

Figure 2-13: Demonstration of Lee and Kim (1998b)'s Healing Model concept used to predict pulse-rate rest period (Roque et al., 2010b)

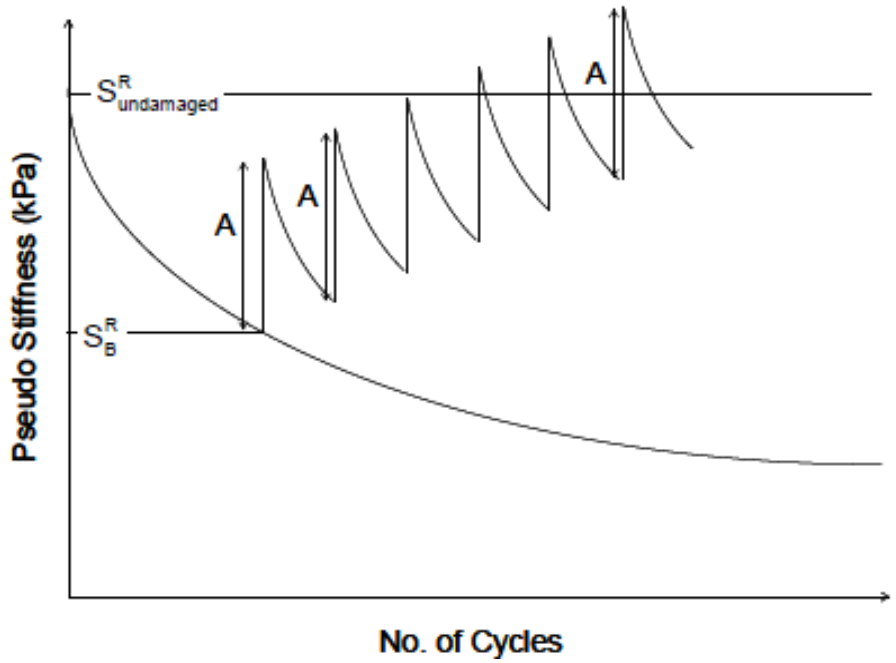

Figure 2-14: Illustration of unreasonable increase of pseudostiffness after healing (Roque et al., 2010b)

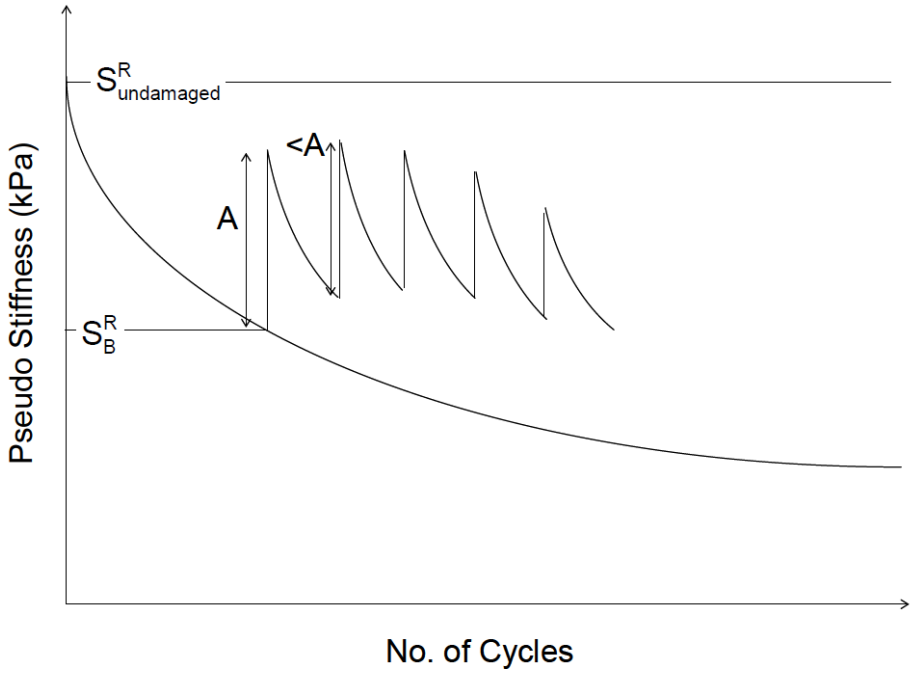

Figure 2-15: Illustration of group rest Rest Period Healing effect after applying adjustment factor (Roque et al., 2010b)

A widely used asphalt pavement prediction tool called layered viscoelastic continuum damage (LVECD) program is developed by Eslaminia et al. (2012). The fundamental theory of the program is time-scale separation and Fourier transform-based layered analysis, in combination with VECD constitutive model for asphalt mixture. The benefit of the program is its capability to run stress analysis for asphalt pavement at a much reduced analysis runs, while the application of Fourier transform based analysis greatly reduced the computational cost of stress analysis. The program is able to interpret the effect of temperature as well as the loading condition caused by moving traffics. By application of Fourier transforms, the computational cost for solving moving vehicle is significantly reduced compared to normal 3D finite element softwares. However, there is currently no direct rest period input into the program, thus in most cases, the effect of rest period healing on asphalt pavement performance has to be solved by certain results adjustments.

Nascimento (2015) used the LVECD program to simulate 27 asphalt road sections from Fundao project with real vehicle loading conditions, the input parameters included asphalt mixture properties, loading conditions, climate temperature and structure of pavement. The simulation results on road distresses are compared with field observations, and good agreement are discovered. They also established an adjustment factor, from the damage shift approach to obtain a unique relationship between LVECD modelling results and field-identified areas of cracks.

At present, VECD FEP++ software, originally developed by Hinterhoelzl and Schapery (Baek, 2010), is still the main finite element tool for VECD relevant models. The capability of the software is based on material isotropy at intact state and local transverse isotropy when damaged. The main benefit of VECD FEP++ is that it combines the VECD constitutive model and finite element method thus enables the calculation of stress redistribution when the pavements are damaged (Roque et al., 2010b). Also, quite a number of exemplary simulations have been conducted by various researchers using VECD FEP++, thus it has a proven capability at predicting pavement damage subject to numerous cycles of loadings (Ashouri, 2014, Roque et al., 2010b, Baek, 2010).

2.7. Summary

Based on the literature review, the VECD theory has been systematically developed by various research and is able to predict the fatigue and damage behaviour of asphalt concrete under various conditions including temperature, load magnitude, frequencies, length of rest period, loading conditions etc. Nevertheless, there is still a lack of systematic investigation and quantification of pulse rest period healing effect on VECD model and damage characteristic curves. While for the real flexible pavement road, it subjects to repetitive rest period between vehicles, so is more similar to pulse-rest fatigue test. In addition, little research has been done with respect to the changing form of damage curves caused by varied length of rest periods between each load cycles using VECD tests. Therefore, it is significant to experimentally investigate the rest period healing effect on the stiffness development and damage characteristic curves of certain asphalt mixture, as well as the interaction of healing with other factors like strain level, temperature etc.

In the meanwhile, relevant numerical studies have demonstrated the power of numerical tools to implement VECD models for the analysis and prediction of asphalt pavement's behaviour. However, the current VECD healing models used in VECD FEP++ has certain degree of limitations as discussed in Section 2.3, mainly because it is obtained from VECD tests with group-rest type of rest period. Regarding LVECD program, it has great benefit at analysing layered asphalt system but it also lacks consideration of healing effect. Thus it is meaningful to conduct phenomenological study on the rest period healing effect on the VECD produced fatigue performance and damage characteristic curves. This could lead into a quantitative relationship between the form of damage curves and length of rest period (pulse-rate type) to form a novel rest period damage functions based constitutive model that can be used in numerical tools.

Remarkably, it is valuable to develop a mechanics based solution to model beam fatigue tests results from certain constitutive models obtained from damage characteristic curves, especially when rest period exists between each consecutive load cycles so rest period healing effect is also included. Such method will not only enable modelling of beam fatigue tests from VECD based constitutive model, but

also provide an approach to verify the ability of the constitutive model when compared with real beam fatigue tests results.

In this study, AMPT was used to test a Western Australia based asphalt mixture using VECD method under various pulse rest period between each load cycles, thus to investigate the relevant rest period healing effect on damage characteristic curves and stiffness development curves. As ABAQUS is a general tool used in engineering numerical modelling, it is used to integrate the newly developed rest period damage functions from this study using user subroutine and Fortran programming. According to mechanics based beam theories, solutions need to be developed to convert the modelling results of pseudostiffness to experimental results. In the meanwhile, a series of beam fatigue tests are conducted with various rest periods, the results are compared between ABAQUS beam model and real 4PB beam fatigue tests result so to evaluate the capability of proposed rest period included damage characteristic solutions for asphalt mixture.

Chapter 3. AMPT Tests Configuration

For this research, AMPT test consists of dynamic modulus test and VECD test. Dynamic modulus master curves are produced by dynamic modulus test while damage characteristic curves are results of VECD tests. This chapter contains detailed description regarding the experimental configurations for all tests conducted using AMPT. The chapter firstly introduces the details of the materials used for making the asphalt mixture for AMPT tests, then detailed introduction on the facilities, procedures, fundamental parameter derivation etc. for both dynamic modulus and VECD tests. Since different specimen sizes are adopted for AMPT tests, the chapter also introduces relevant information for tests on geometry effect.

3.1. Tested Materials/Specimen

The single material being used for this study is AC10 75 aggregates (supplied by local supplier organization BGC) mixed with C320 bitumen. The aggregates have maximum size of 10mm, and are compacted by 75 Marshall blows. The Particle Size Distribution (PSD) chart for design purpose is demonstrated in Figure 3-1. The C320 bitumen is defined as with 320Pa.s of viscosity at 60^{o}C and 0.5 Pa.s at 135^{o}C. The target air void ratio is 5%. Table 3-1 contains the mass percent of mixture's components. The gravel and bitumen proportion are obtained from trial and error based on AS 2150: Hot mix asphalt—A guide to good practice. This asphalt mixture is made of gravel and binder that are widely used in industry, laboratory testing and research in Western Australia., so these results may provide valuable source of reference for future study.

Table 3-1: Components percentage and basic mechanical properties of tested AC10 C320 asphalt mixture

Material Component	Mass Percentage
Bitumen C320	4.9%
10/7mm (Max) Gravel	43.7%
5mm (Max) Gravel	11.4%
2.36mm (Max) Dust	39.9%
Mechanical Properties	
Maximum Density (t/m3)	2.471
Target Void Ratio (% in volume)	5%

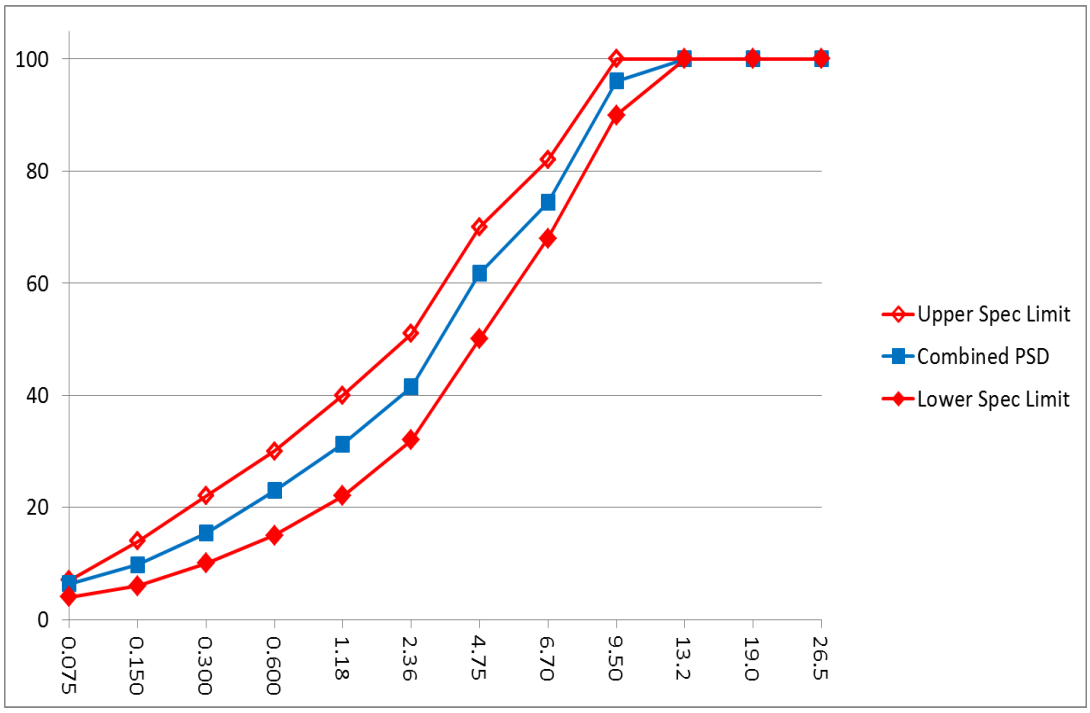

Figure 3-1: Particle size distribution for the gravel components based on AS 2150 (Issac, 2014)

3.2. Different Batches of Gravel and Bitumen Supply

There are different supply of gravel and bitumen that makes the mixture property such as stiffness change, it is also possible that healing ability is also changed.

Using different batch of material supply is inevitable since the first batch of gravel and bitumen were used out before the project finishes, then the laboratory purchased more from BGC as aggregates provider and Sami as bitumen supplier. Although the gravel and bitumen types are identical as AC10 (gravel) and C320 (bitumen) respectively, the specific mixture stiffness are found to be altered to a small extent (the extent of difference is described in results presentation of Chapter 6). The type of tests conducted on both batches of mixtures are marked in relevant tables and figures. Thus, in comparison study, different batch of materials are treated separately with each other, however, certain graphs collect both batches together to investigate the difference between them.

3.3. Laboratory Procedures

3.3.1. Mixing

The asphalt mixing procedures strictly follow *AS/NZS 2891.2.1: Methods of sampling and testing asphalt - Method 2.1: Sample preparation - Mixing, quartering and conditioning of asphalt in the laboratory*. The below section describes the mixing procedures specifically carried out in Curtin University's pavement laboratory.

The dried gravel component mixture was weighed and left in 180^{o}C oven for overnight. It is then mixed with bitumen, which is heated up for 4 hours in a 150 ^{o}C oven. The oven conditioned bitumen and gravels are then poured into mixing bowl and get mixed using a mechanical mixer, which is shown in Figure 3-2. The mixed samples are then put into 150^{o}C oven (as specified in AS/NZS 2891.2.1*)* for temperature conditioning for around 1 hour. Then the mixtures are transferred into compaction moulds of 150mm diameter as demonstrated in Figure 3-3. The required amount of mixture into the compaction mould is able to achieve the desired 5% void ratio and 2.34 tone/m^3 of bulk density (maximum density is in Table 3-1). The mixture in compaction mould is then put back to oven to heat up to around 150^{o}C to reach the required compaction temperature, but this duration should not exceed one hour.

Figure 3-2: Mechanical mixer used for mixing in this study

Figure 3-3: 150mm diameter compaction mould for asphalt mixture

3.3.2. Compaction

After reaching specified compaction temperature of 150^{o}C (with 3^{o}C allowable variance), the compaction mould is then transferred into the gyratory compactor. The specific settings for compaction follow AS/NZS 2891.2.2, and are based on the nominal size of mix and the diameter of specimen in the compaction mould. A picture illustration of the gyratory compactor in Curtin University's pavement laboratory is in Figure 3-4. For standard size of AMPT tests, the required compaction settings for the cylindrical specimen used in dynamic modulus and VECD tests are listed in Table 3-2. The machine takes 17-25 cycles to reach the desired compaction height for a 150mm diameter mould (for 100mm diameter specimen), and 30-50 cycles for 100mm diameter mould (for 54mm diameter reduced size specimen). The user then recorded the compaction temperature and number of compaction cycles for future reference. After compaction, the specimen moulds are transferred to a safe location to cool down, in preparation for cutting and coring.

Figure 3-4: Gyratory Compactor made by IPC Global

Table 3-2: Compaction Input Parameters for different types of tests

Specimen and equipment details	Dynamic Modulus Tests	VECD test
Diameter of Compaction Specimen (mm)	~150	~150
Compacted Specimen Height (mm)	~170	~178
Gyratory angle (^{o})	3	3
Vertical loading stress (kPa)	240	240

3.3.3. Cutting/Coring

The purpose of cutting/coring procedure is to extract AMPT specimen cylinders of required dimensions from the compacted mixture. Figure 3-5 shows a 100mm diameter corer in operation, while Figure 3-6 shows cored out specimen.

The cutting procedure uses an electric powered Autosaw, so the specimen is cut into required height of 150 and 130mm for dynamic modulus and VECD specimens respectively. Figure 3-7 demonstrates sawing procedure in progress.

Figure 3-5: Electric powered corer in operation

Figure 3-6: Cored specimen before cutting

Figure 3-7: saw cutting of cored specimen into required length

3.3.4. Determination of Bulk Density and Air Void Ratio

The next step is to measure the bulk density and air void ratio of each specimen based on AS 2891.9.2 and AS 2891.8. Maximum density (ρ_{max}) of the asphalt mixture is measured based on water displacement method according to AS 2891.7.1. With known maximum density for this mixture as tested previously, the mass of

block in water (m1), mass in air of saturated surface dry sample (m2) and final dry mass (m3) are then measured for each specimen, so the bulk density (ρ_{bulk}) and void ratio can be calculated as below:

$$\rho_{bulk}=m1*\rho_{water}/(m2-m3) \quad (3.1)$$

$$Void\ Ratio = (\rho_{max}-\rho_{bulk})/\ \rho_{max}\ ) \quad (3.2)$$

and specimen out of this range are discarded. An example record of Bulk Density and Air Void Ratio calculation is listed in Table 3-3. The desired air void ratio is 5% as mixture design requirement; it is achieved by controlling the amount mass of asphalt mixture into the compaction mould. Such amount is a fixed number for certain mixture and can be obtained based on trial and error when a different mixture or compaction size is used.

3.3.5. Determination of Specimen Dimension

Although the target specimen dimensions are fixed, experimental procedures will cause slight variation on each sample. The height and diameter of each specimen are measured using laboratory calibrated calliper: four measurements are made for height, each measurement is 90 degree apart on circular cross section; two orthogonal measurements of diameter on bottom and top faces respectively, plus another two on the cross section plane at middle height. All measurements are averaged to obtain representative height and diameter values for the specimen. An example of sample dimension measurement for one 150mm sample and one 130mm sample is shown in Table 3-4.

Table 3-3: Example of relevant parameters of specimen's bulk density and void ratio

Maximum Density for the Mixture (t/m^3)	2.472
Final Mass of Block in Air (g)	2419.72
Mass of Block in Water (g)	1396.95
Mass of Block in air SSD (g)	2422.96
Bulk Density (t/m^3)	2.351
Air Voids (%)	4.9

Table 3-4: Example of specimen dimension measurements

100 x 150mm (Diameter x Length) Specimen								
Dimensions	***Point 1***	***Point 2***	***Point 3***	***Point 4***	***Point 5***	***Point 6***	***Average***	***Std Dev.***
Diameter (mm)	100.4	100.3	100.5	100.4	100.4	100.4	100.4	0.064
Length (mm)	149.3	149.3	149.3	149.2	-	-	149.3	0.076
100 x 130mm (Diameter x Length) Specimen								
Dimensions	***Point 1***	***Point 2***	***Point 3***	***Point 4***	***Point 5***	***Point 6***	***Average***	***Std Dev.***
Diameter (mm)	100.4	100.6	100.4	100.4	100.5	100.5	100.5	0.091
Length (mm)	130.1	130.1	129.9	129.9	-	-	130	0.156

3.3.6. Gluing and Glue Conditioning

After above procedures, the cylinder specimen are ready to be assembled with gauging knots, and gluing of platen (VECD tests only), which all require strong glue. The strength of the glue should be able to avoid interruption to tests, since inappropriate glue may cause local failures in contact areas. For instance, the specimen may fail around the gauging knots and the test is disrupted, especially at relatively higher temperatures when mixture is soft and fragile.

Firstly, gauging knots glue are required for both dynamic modulus and VECD tests since measuring of strain deformation via LVDT is a must for both, while gauging knots provide fixing points for LVDT to be mounted onto the specimen. The locations of six gauging knots (for 3 LVDTs) have to be very accurate to achieve 70mm between vertical knots, when set up in the temperature cube, and 120 degree apart along the circular cross section. The accurate location can be achieved in the aid of mechanical gauging knots fixer (see Figure 3-8), which is specifically designed for AMPT tests by IPC Global. Otherwise, careful manual fixing is required, mostly by highly experienced technicians. Gauging knots glue is achieved

by using Sellys Araldite Epoxy Hardner with strength level of “5 minutes everyday”, which, by its name, just requires conditioning time of around 5-10 minutes.

Figure 3-8: Mechanical gauging knots fixer used in this research

Platen gluing is required for any tests that involve tension pull on the specimen in AMPT, and this includes VECD tests. However, dynamic modulus tests is non-destructive compression based so no platen glue is needed. The platens are precisely manufactured according to lab standards by IPC Global. Two important points for platen gluing are: 1. the glue needs to be strong enough to prevent glue failure during the tests, since the glue failure will make results incorrect; 2. the top and bottom platens should be glued right at the centre of the platen to prevent stress deviation and eccentricity on top and bottom surfaces. A specifically manufactured platen fixer is used to help positioning specimen correctly between platens while glue conditioning is in process (see Figure 3-9). The glue used for platens is Sellys Araldite Epoxy Hardener with strength level of “super strength”, which requires a recommended 72 hours (as indicated in the glue package) of conditioning time.

Figure 3-9: Platen fixer for glue conditioning

3.4. Failure Location of VECD Tests

Before proceeding to next section, it is important to discuss about the propensity of failure location, which applies to all destructive tests using AMPT (including VECD). As the AMPT uses LVDT to measure on-specimen strain, it is important to control the failure location when the specimen forms a major crack, since a failure can be formed either within the LVDT range or outside of the LVDT range as seen in Figure 3-10. Generally, most researchers suggest that middle failure is necessary when fatigue performance of the tested sample is required, since once fracture coalesce to form a crack outside of the gauging length, the machine will try to stretch excessively to reach the specified constant strain level, which is measured by LVDT gauging sets. Although in this study, damage performance and stiffness variation results from end failure specimen are still used due to following reasons:

1. The current standard specimen size, compaction size, specimen making procedures and mixture type etc. determine that there is certain chance of

encountering end failure, and it is time consuming to only select tests subject to middle failure since much more tests are required then

2. The end failed specimen is still able to capture correct damage behaviour before major crack appears, although it gives an incorrect and normally underestimated fatigue failure (Hou et al., 2010); else, the stiffness development following end failure can still be predicted based on curve fitting and extrapolation
3. As demonstrated in the results chapters, the stiffness development curve follows certain trend that can be easily interpolated until a common failure criteria such as 0.5 stiffness ratio at 20^{o}C; for damage characteristic curves, it is common practice to present the regression curve so interpolation is automatic and reliable
4. Due to an earlier version of AASHTO 107 standard (proposes 150 mm long specimen) was used at the beginning of this research, many specimen used are large specimen (100 x 150 mm) that has high possibility of end failure, it is a waste to discard those results since the damage characteristic curves obtained are still correct before end failure occurs, since the whole damage characteristics can still be extrapolated until the failure

Figure 3-10: Demonstration of sample subjects to: (a) end failure (150 mm specimen), (b) end failure (130 mm specimen), and (c) middle failure (130 mm)

However, it is still a research interest to bring the failure location within the LVDT range since only in this case the LVDT captures the response of the asphalt mixture

correctly throughout the true fatigue life. Actually, one of the main reasons for trying different compaction height and final specimen length of asphalt mixture is also to investigate the chance of different failure locations. For instance, with VECD tests' 178mm compaction height and 130mm specimen height suggested by latest version of AASHTO TP 107-14, it has a higher chance of middle failure, than 100 x150 mm geometry. Although as mentioned earlier, many other factors are in play such as mixture type so the tester need to evaluate and try out their best options of specimen geometry.

3.5. Main Testing Facility

Originally, many cyclic tension compression testing facilities can be used for dynamic modulus as well as VECD tests on asphalt mixtures. Later on, National Cooperative Highway Research Program (NCHRP) conducted a series of studies on the feasibility of various facilities used for asphalt mixtures testings (Bonaquist et al., 2003, Bonaquist, 2008a, Bonaquist, 2008b, Bonaquist, 2011). Considering its feasibility, efficiency and accuracy, Asphalt Mixture Performance Tester (AMPT) is selected as a standard test facility for asphalt mixture's fatigue, stiffness, flow number etc. Based on this background, later on, the simplified Visco Elastic Continuum Damage (S-VECD) is also developed based on AMPT since it provides relatively stable and controllable axial tensile test. There is proprietary and continuously updated software for S-VECD tests such as those produced by IPC Global, while the necessary parameters used in S-VECD can be directly collected from frequency and temperature sweeping (dynamic modulus) tests on the same mixture. As a result, AMPT is the most widely used facility for VECD tests by researchers around the world, although other options may also have be trialled and developed based on different purposes of research.

The servo-hydraulic Asphalt Mixture Performance Tester (AMPT) in Curtin University's Pavement Laboratory is being used for this research. This facility is one of the standard testing facilities manufactured by IPC Global. This AMPT facility can provide both tension and compression repetitive load with a limit of 15kN. The machine is equipped with LVDT that has a gauging length of 70mm, and is capable of controlling the strain level endured by LVDT for repetitive load cycles.

Therefore, on-specimen controlled strain test can be conducted. Figure 3-11 illustrates a prepared set up of AMPT VECD test with important parts marked out in graph.

Figure 3-11: Demonstration of AMPT set-up in Curtin University's pavement laboratory

3.6. Testing Softwares

"SPT Dynamic Modulus" version 2.21 software provided by IPC Global is used for dynamic modulus tests.

There are two software used in this study for VECD tests. The first one is a commonly used VECD tests software for continuous loading: S-VECD version 3 supplied by IPC Global. Although the software also has a function to provide one rest period after certain cycles (group-rest), it can not provide rest period between each cycle (pulse-rate rest). A query was initiated to IPC Global regarding their capability at providing a software capable of inserting rest period after each load cycle, like the one used in Zeiada (2012)'s research. As a result, such software is courteously provided by IPC Global. The software, as a beta version at this stage, is then set up and verified for its capability at conducing VECD with pulse-rate rest period tests using AMPT facilities in Curtin University.

3.7. Laboratory Standards

The testing procedures and data processing methods are following the below listed standards:

1. *AS/NZS 2891.2.1: Methods of sampling and testing asphalt - Method 2.1: Sample preparation - Mixing, quartering and conditioning of asphalt in the laboratory*
2. *AS/NZS 2891.2.2: Methods of sampling and testing asphalt - Method 2.2: Sample preparation - Compaction of asphalt test specimens using a gyratory compactor*
3. *AS 2891.9.2-2014 Bulk Density – Presaturation*
4. *AS 2891.8 – 2014 Voids and Volumetric Properties*
5. *AASHTO TP 79-13: Determining the Dynamic Modulus and Flow Number for Asphalt Mixtures Using the Asphalt Mixture Performance Tester*
6. *AASHTO TP 107-14: Standard Method of Test for Determining the Damage Characteristic Curve of Asphalt Concrete from Direct Tension Cyclic Fatigue Tests*

These standards serve as a main reference for test procedures, while the specific procedures used could subject to reasonable adjustments based on facility availability, material conditions and previous experience such as available mixture design results, specific dimensions of cylindrical specimen etc., however, highly experienced asphalt technicians in laboratory is consulted to validate all adjustments.

3.8. Dynamic Modulus Test

As a frequency and temperature sweeping test, the experimental configurations for dynamic modulus tests are listed in Table 3-5. Set-up parameters for both standard size and reduced size specimen are demonstrated.

Figure 3-12 demonstrates an AMPT set-up of dynamic modulus test. Different to VECD tests, the platens are not glued to the surfaces of the specimen since there is no tension pull required as the loads are compression only and be within non-destructive range to the mixture. Based on current standard, the specimen for master

curve tests should be of 150mm long. Also, a reduced specimen is tested for the purpose of specimen geometry study (both listed in Table 3-5). As a non-destructive test, the post-dynamic modulus test specimen can directly be used for following VECD tests after the gluing procedure for platens on top and bottom surfaces of the specimen, as described in the Section 3.3.6.

Table 3-5: Dynamic modulus tests configurations

Standard Specimen Size (100 mm x 150 mm, both batches)		
Temperature (C)	***Frequency (HZ)***	***Number of Tested Specimen***
4	0.1	3
4	1	3
4	10	3
12	0.1	3
12	1	3
12	10	3
20	0.1	3
20	1	3
20	10	3
38	0.1	3
38	1	3
38	10	3
Reduced Specimen Size (54mm x 100mm, batch 1)		
Temperature (C)	***Frequency (HZ)***	***Number of Tested Specimen***
4	0.1	1
4	1	1
4	10	1
12	0.1	1
12	1	1
12	10	1
20	0.1	1
20	1	1
20	10	1
38	0.1	1
38	1	1
38	10	1

Figure 3-12: Dynamic modulus test set-up in AMPT cube

3.9. VECD Test

For VECD test, the current software offers functions to have user input parameters like strain/stress level, testing mode (controlled strain only), temperature, rest period, frequency etc. Like most experimental studies, there are several considerations regarding the choice of tests configurations: accuracy, efficiency, machine capacity and test stability etc. Also, previous studies related to VECD method as listed in the literature review sections provide experiences and insights into experimental settings for VECD. However, the selection of VECD test set-up also depends on the research purpose, target asphalt mixture, representative environmental conditions, local laboratory conditions and user preference/technique etc.

For this research, the experimental parameters selected for VECD tests are listed in Table 3-6, and detailed description of tests for both batches is provided in below sections.

Table 3-6: Experimental settings adopted for S-VECD tests

Batch 1 Mixture		
Temperature (^{o}C)	**20**	**12**
Strain Level (Microstrain)	200, 300, 400	200
Frequency (Hz)	10	10
Rest Periods (s)	0, 0.1, 0.2, 0.3, 0.5, 0.7, 1, 1.5	0, 0.05, 0.1, 0.2, 0.3, 0.5, 1
Testing Mode	Tension-Compression	Tension-Compression
Control Mode	Constant Strain	Constant Strain
Batch 2 Mixture		
Temperature (^{o}C)	**20**	**12**
Strain Level (Microstrain)	200, 250, 300	200
Frequency (Hz)	10	10
Rest Periods (s)	0, 0.1, 0.3, 0.7	0, 0.05, 0.1, 0.2, 0.3, 0.5, 1
Testing Mode	Tension-Compression	Tension-Compression
Control Mode	Constant Strain	Constant Strain

3.9.1. Temperature

As discussed in literature review, temperature is an important factor to asphalt mixture, as it can not only change the stiffness of the mixture but also its healing capacity. Although influence of temperature is already included inside dynamic modulus master curves using time-temperature shift factor, the temperature level should be adequate for VECD tests since either too high or too low temperature will incur potential problems. Since VECD is a destructive test that in essence requires the specimen to deteriorate fast enough for an accurate interpretation of its damage characteristics. Normally, larger strain/stress level is required when the temperature is higher thus the material damages fast enough and the damage characteristic curve can be produced clearly. Based on simplified VECD theories, larger strain/stress

level at high temperature or longer rest period also tends to finish the test in a timely manner, so save experimental time. Too low strain/stress amplitude can lead into excessively low damage progress rate, or even no fatigue limit if it reaches endurance limit of asphalt mixture. Else, another issue with too high temperature is that after some trial tests under 38^{o}C, there is too high chance of unexpected gauge point failure. What's more, plasticity is a potential issue due to the large strain level required at high temperature especially when the rest period is also long, while the complex interaction between temperature and plasticity is out of current scope of study. Plastic behaviour violate the principles of VECD approach that is based on viscoelastic status only. Due to these issues with high temperature, AASHTO TP 107-14 suggests the test temperature should not exceed 21 ^{o}C.

On the contrary, too low temperature will cause mixture to have frozen water in the voids and is also outside the scope of current study. Also the complex plasticity and strain level relationship needs to be addressed since a relatively low strain level is required for low temperature but the material may still get great damage. It is estimated that at two low temperature, the available strain range for VECD test is quite limited, it is a topic related with interaction between temperature and plasticity for asphalt mixture. As a result, 12 and 20 ^{o}C are chosen as temperatures for this project since they can provide reasonable test stability while temperature effect is obvious.

3.9.2. Constant Strain and Constant Stress

Previous AMPT facilities are capable of both controlled-strain and controlled-stress modes (CS), although the latest version of VECD testing software as well as AASHTO TP 107-14 only provides controlled strain mode. For controlled stress mode, the stress amplitude of each cycle is kept constant, while controlled-strain tests have a constant strain amplitude for each cycle. For practical pavement application, normally, constant stress tests are better at simulating pavement with larger asphalt thickness, while constant strain tests are more suitable for thin pavement as the strain level in thinner asphalt layer is influenced more by underlying layers rather than by repetitive loadings (H.Huang, 2004). A figurative demonstration of controlled stress and controlled strain modes of testings is

indicated in Figure 3-13, in which SR is pseudostiffness of relevant cycles, ε_S^R is permanent psdudostrain. As demonstrated in Figure 3-13, with accumulative permanent strain of asphalt under cyclic test, there is possibility of high permanent strain developed during tension only cyclic test.

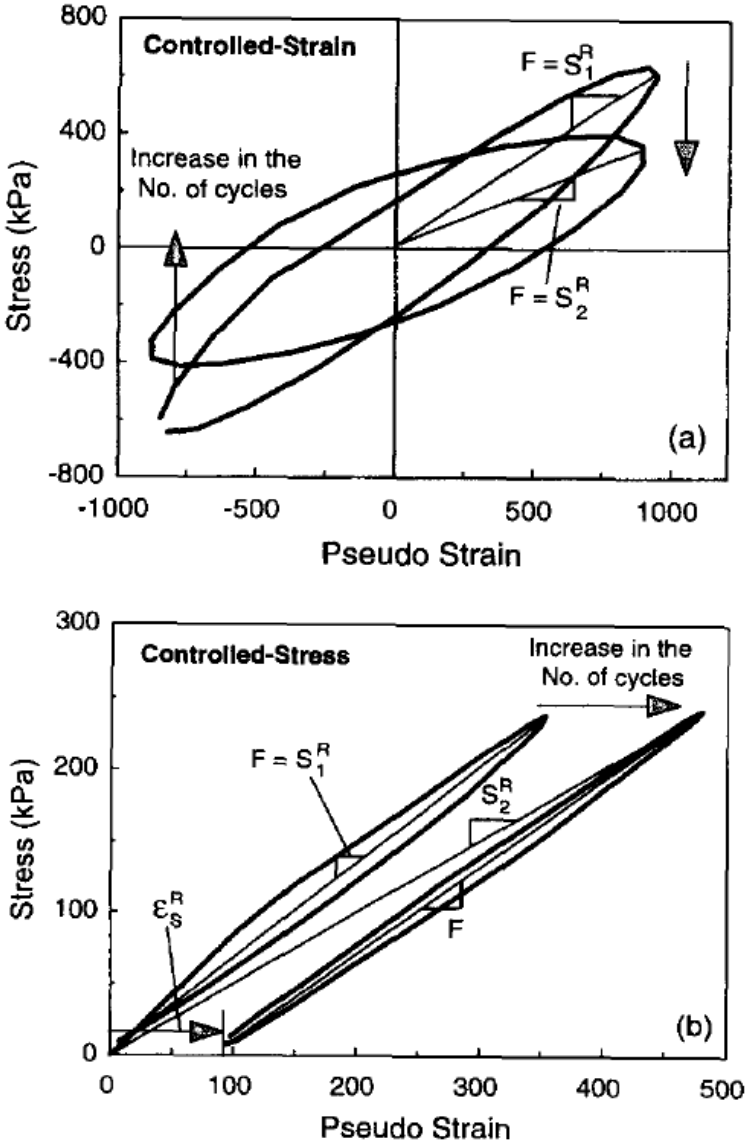

Figure 3-13: Stress and pseudostrain relationship from controlled stress and controlled strain uniaxial tests (Lee and Kim, 1998b)

What's more, previous research pointed out that there are inherent complexities in the interpretation of pseudostrain components under controlled stress test due to reasons such as difficult pseudostrain calculation (Lee and Kim, 1998b) and the high likelihood of plastic strain especially for soft material under high temperature

(Nascimento, 2015). On the other hand, the controlled strain test has the benefit of better capturing the change of material stiffness due to damage progression. As the stiffness of asphalt specimen declines with more loading cycles, there will be larger strain and much larger propensity to plastic behaviour in controlled stress tests compared to controlled strain tests. Furthermore, the aggressive nature of controlled stress tests could also damage the facility if it was not carefully monitored and adjusted (Nascimento, 2015). While controlled stress mode has the benefit of maintaining zero load magnitude during rest period, but the current AMPT machine has the capability to maintain very low stress level especially when tension compression mode is selected. A demonstration of stress history for a typical VECD with rest period of 0.1s test is shown in Figure 3-14 to verify the statement. From the figure, the stress reaches almost 0 during the rest period.

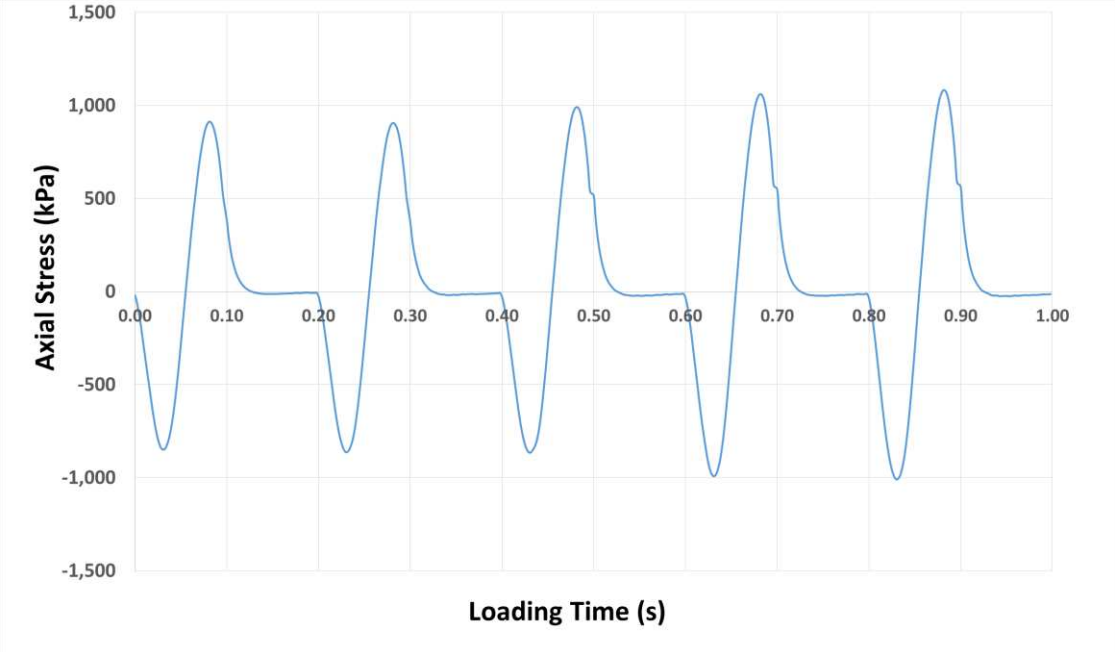

Figure 3-14: Stress history for an example VECD with 0.1s set rest period tests, first 5 cycles

Initially, the strain in a cyclic tension/compression tests is controlled by actuator displacement (CX). Later on, controlled on-specimen strain (CS) is developed and equipped onto AMPT, which is then able to control the strain measured by LVDT. Compared to CX test, CS test enables a direct control of on specimen strain by mainlining the level between gauging points. CS tests circumvent the need of applying machine compliance factors, which is inevitably with certain degree of

error, in CX tests. What's more, it is suggested CX test will be more likely to cause plastic strain, while CS test directly control the on-specimen strain and prevent plastic behaviour by controlling the strain between gauging points (Roque et al., 2010b). As a result, the AMPT facility used for this research has controlled on-specimen strain (CS) mode for VECD tests.

3.9.3. Selection between Tension and Tension-Compression tests

There are two strain application modes available: direct tension and tension-compression. In direct tension test, the specimen is only pulled in tension from its original state (harversian loading spectrum), while tension-compression test applies sinusoidal loadings to push and pull the sample, so both tension and compression occur at the same magnitude when constant strain is selected. Compared to tension compression test, it is believed that direct tension test causes earlier specimen failure thus it can be more time effective. On the other hand, the real asphalt on road does not necessarily fall into either direct tension or tension compression case, while some previous research indicate that the stress history for real asphalt road is sinusoidal (Zeiada, 2012).

The results from AMPT's simplified VECD tests carried out in this research contain peak to peak strains of each cycle. Based on previous cyclic direct tension tests as shown in Figure 3-15 by Daniel and Kim (Zeiada, 2012), tension only tests generate permanent strain that will be carried on for the whole fatigue test, and this will also incur problems of reaching plastic response due to strain accumulation. Thus to keep the constant strain requirement of each cycle, a compressive stress is necessary to push the specimen to counter the generated permanent strain, and this lead into erroneous modulus values calculated from peak to peak stress of each cycle. As a result, tension-compression mode is adopted for this study.

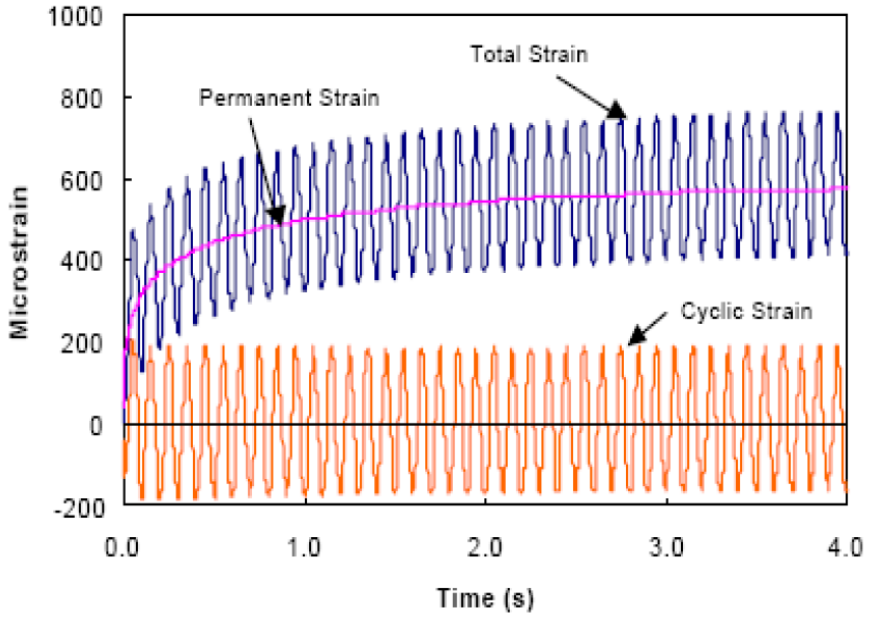

Figure 3-15: Cyclic, total and permanent strain results of direct tension test (Daniel and Kim, cited in Zeida 2012).

3.9.4. Strain Levels

The strain level is chosen to fall into a range that is overly highly to prevent plastic behaviour, while not too low so the damage can develop sufficiently to yield suitable stiffness changes for accurate construction of damage characteristic curve and to avoid reaching fatigue endurance limit level or non-destructive status. AASHTO TP 107-14 suggested an initial strain level of 300 microstrain, however, a more practical way to initially determine the strain level for a VECD test has to take into account temperature and rest period healing effect. Dynamic modulus test results on complex stiffness can be an indication to estimate the strain level input for the first trial of VECD test, and then adjust the strain level based on methods suggested in AASHTO TP 107-14. However, the standard just gives a suggested level, actually any elastic strain levels that make the specimen fail within a reasonable test time and produce proper damage progression are sufficient. Another factor that determines the strain level is research purpose, since stiffness development and healing effect will be investigated in this study, it is essential to test with different rest periods and temperatures under same strain level, since the stiffness results are strain dependent.

As the standard 300 microstrain suggested in AASHTO TP 107-14 is found to be too aggressive at 12^{o}C and may exceed machine limit, a lower strain level is required. While low strain amplitude such as 150 microstrain can incur lengthy test period especially when rest period is long at 20^{o}C. As a result, 200 microstrain is found to be an appropriate reference strain level for most VECD tests at both 12 and 20^{o}C, thus it is used as a strain level for investigation of stiffness development curves and temperature effect on healing. In the meanwhile, some 300 microstrain tests are also conducted at 20^{o}C as they are very time efficient and can produce more accurate damage curves without heavy filtering. As mentioned above, since damage characteristic is unique material behaviour regardless of strain/stress levels, so using different strain levels can lead into a study about damage curves under different strain levels when rest periods are present.

For tests under 12 ^{o}C, 200 microstrain was used as main strain level, since it has been found after first tests that the specimen usually fails earlier and damage accumulates more quickly (same strain) at lower temperature. Although damage characteristic curves are not influenced by strain level, it is a common sense that the reduction of stiffness is more drastic when the mixture is subject to larger strain or stress.

3.9.5. Frequency

A frequency of 10Hz is chosen as exactly suggested by AASHTO TP107-14 for all VECD tests in this study. Again, damage characteristic curves are not affected by frequency levels based on time-temperature superposition theory, although the stiffness level will be changed.

3.9.6. Length of Rest Period

The length of pulse rest period selected in this research is listed in Table 3-6. The length of rest period used for tests are selected to make the results of various rest periods distinguishable with each other. While the reasons for not including testing results of longer than 2s rest period are based on two considerations:

1. it takes around 117 hours for a test with 4s rest period between each loading cycle to reach 100,000 cycle.
2. A shorter rest period below 2s (at 20 ^{o}C) and even below 1s (at 12 ^{o}C) have already reached the optimum rest period, so further increase of rest period will make little different results. And this will be demonstrated in details in tests results section.

3.10. Experimental Configurations for Small Specimen

As discussed earlier, it is meaningful to test the VECD properties as well as healing effect on AMPT specimen of different dimensions, especially a smaller specimen that is able to save material and testing time. Alongside the main study, a parallel study is made on the ability of 54x110mm size specimen for VECD tests including rest periods. Table 3-7 lists the basic test configurations for small size specimen of VECD tests. Consistent with all other tests done in this research, it adopts tension-compression mode, and the used temperature and strain levels are also tested using standard sizes (label "L" and "M") specimen. Some of the tests results also contribute the main results presentation of this research, such as curves labelled as "S". The sample preparation procedures for smaller specimen VECD generally follow the same philosophy to the original size specimen, while some significant and novel experimental procedures to make smaller specimen are listed below.

Table 3-7: VECD tests configurations for Study of Specimen's Size Effect

Test Temperature (^{o}C)	Test Mode	Strain Amplitude (micro strain)	Load Frequency (hz)	Rest Period (ms)
12	Tension-Compression	125, 200	10	300
20	Tension-Compression	200, 300 and 400	10	300

3.10.1. Mixing and Compaction for Small Specimen

Different to standard size, a 100mm diameter mould is used for producing each 54x110mm specimen (see Figure 3-16). After trial and error, the amount of hot mixed asphalt in the mould is worked out to achieve 5 percent final void ratio, while

the compaction configuration is listed in Table 3-8. It needs to be mentioned that the amount of components required for each mould is significantly reduced, besides, the mixing and compaction all require much less labour compared to the making of standard size specimen.

Figure 3-16: 100mm diameter mould for producing 54x110mm specimen for AMPT

Table 3-8: Gyratory compactor configuration for 54x110mm specimen

Specimen and equipment details	**54x110mm Specimen**
Diameter of Compaction Specimen (mm)	~100
Compacted Specimen Height (mm)	~160
Gyratory angle (^{o})	3
Vertical loading stress (kPa)	240

3.10.2. Coring and Cutting for Small Specimen

The coring and cutting procedures for 54x110mm specimen is similar to that of standard size, with a smaller corer size of 54mm diameter corer (see Figure 3-17) being used.

Figure 3-17: 54mm diameter corer drilling

3.10.3. Gluing for small specimen

Exactly the same types of glue, to standard size specimen, are used to attach the gauging knots and platen onto the specimen. Since the mechanical gauging knots fixer available is designed for 100mm diameter specimen only (the 54mm fixer can also be acquired from IPC Global), some manual technique is used to attach the gauging knots as illustrated in Figure 3-18. This will enable the distance between LVDT to be exactly 70mm as required by the standard, while care needs to be taken trying to set each LVDT as close as around 120 degree apart from each other.

For platen gluing, care needs to be taken to position the specimen as close as possible to the centre of the platen to avoid eccentric loading and deviation during

the test. The platen fixer is still used to make sure the platens are installed horizontally aligned on the two faces of the specimen. An illustration of platen gluing set is Figure 3-19.

Figure 3-18: Gauging knots gluing for 54x110mm specimen

Figure 3-19: Platen gluing and conditioning for 54x110mm specimen

3.11. VECD Specimen Labelling Rules

Considering the amount of tests conducted under various rest periods, two temperatures and different strain amplitudes, it is helpful to label each specimen based on their test conditions. For instance; sample ID "S-12C-0.3R-200 (2)" represents a 54 mm × 110 mm specimen tested at 12^{o}C with the applied 0.3 second rest period between each loading cycles and subject to a strain amplitude of 200 microstrain, and it is a second sample of repeated test under same parameters. It should be noted that for dynamic modulus tests, only specimen geometry is a distinguishing factor between samples since it is a temperature and frequency sweeping test with machine controlled strain. Therefore, "L" and "S" only are sufficient to label samples for dynamic modulus tests based on geometry. The batch of material supply is denoted as "B1" or "B2" at the beginning of specimen label for batch 1 and batch 2 mixture respectively. The material batch is also mentioned in all tables and figures that are separated by batch. A summary of specimen label rules is listed in Table 5-9.

Chapter 4. Beam Fatigue Test Configurations

In this study, the purpose of running beam fatigue tests is to provide comparison and reference data for modelling results. Specifically, the damage characteristic with healing models obtained from VECD will be utilized to numerically simulate the beam fatigue tests, and the simulation results will be compared with true beam fatigue tests, thus to verify the capability of the proposed damage characteristics with rest period model. This chapter contains laboratory configurations for 4PB beam fatigue test, and includes information on relevant mixture supply, test facilities, test procedures, tests configurations etc..

4.1. Beam Specimen Labelling Rules

Considering the amount of tests conducted under various rest periods, two temperatures and different strain amplitudes, it is helpful to label each specimen based on their test conditions. For instance; sample ID "B1-12C-0.3R-200 (2)" represents a 54 mm × 110 mm specimen tested at 12^{o}C with the applied 0.3 second rest period between each loading cycles and subject to a strain amplitude of 200 microstrain, and it is a second sample of repeated test under same parameters. It should be noted that for dynamic modulus tests, only specimen geometry is a distinguishing factor between samples since it is a temperature and frequency sweeping test with machine controlled strain. Therefore, "L" and "S" only are sufficient to label samples for dynamic modulus tests based on geometry. The batch of material supply is denoted as "B1" or "B2" at the beginning of specimen label for batch 1 and batch 2 mixture respectively. The material batch is also mentioned in all tables and figures that are separated by batch. A summary of specimen label rules is listed in Table 5-9.

4.2. Different Batches of Gravel and Bitumen Supply

Similar to VECD tests as described in Section 3.2, beam fatigue tests are influenced by different batches of material supply that caused slight but not negligible change of material properties. Table 4-1 and Table 4-2 list the type of beam fatigue tests conducted on both batches of material supply.

Table 4-1: Summary of tested specimen for beam fatigue tests (Batch 1 mixture)

	Specimen ID	Finger Print Stiffness (MPa)
Beam Fatigue Test at 20°C	B1-20C-0.7R-400	6320
	B1-20C-0.3R-400 (1)	6380
	B1-20C-0.3R-400 (2)	6150
	B1-20C-0.1R-400	7090

Table 4-2: Summary of tested specimen for beam fatigue tests (Batch 2 mixture)

	Specimen ID	Finger Print Stiffness (MPa)
Beam Fatigue Test at 20°C	B2-20C-0.0R-400	7982
	B2-20C-0.1R-400 (1)	8450
	B2-20C-0.1R-400 (2)	6770
	B2-20C-0.3R-400	7090
Beam Fatigue Test at 12°C	B2-12C-0.0R-300	10920
	B2-12C-0.5R-300	11972
	B2-12C-0.3R-300 (1)	11500
	B2-12C-0.3R-300 (2)	12600
	B2-12C-0.1R-300 (1)	12743
	B2-12C-0.1R-300 (2)	13400
	B2-12C-0.1R-400	12500
	B2-12C-0.3R-400	12632
	B2-12C-0.5R-400	11300

4.3. Laboratory Procedures

4.3.1. Mixing/ Compaction of Beam Specimen

The mixing for the making of beam specimen is similar to that of AMPT tests so it basically follows AS/NZS 2891.2.1, while the quantity of mixture needed for each compaction is different to AMPT cylinders. The beam specimen reaches 5% void ratio and bulk density of 2.34 tones/m^3. The desired mixture properties of beam are identical to VECD mixture properties as listed in Table 3-1. One mixing run produce 20871g of mixture that will be transferred into the compaction mould (will be cut into three beams). This should be achieved by three sub-runs of mixing using mixing bowl and mechanical mixer (see Figure 3-2), the same as AMPT specimen mixing. The quantity of mixture in beam assembly is obtained after trial and error as being able to achieve a void ratio of around 5 percent for the final beams. It also

follows the same mixture conditioning process until the mixture is ready for compaction, which uses a compaction mould assembly of 400mm long, 305mm wide and 75mm deep.

Wheel track roller is utilized to compact the slab made of asphalt mixture sitting in the mould as demonstrated in Figure 4-1. It consists of two compaction runs to ensure the mixture is compacted consistently and to reach a same surface level of the inner mould edge.

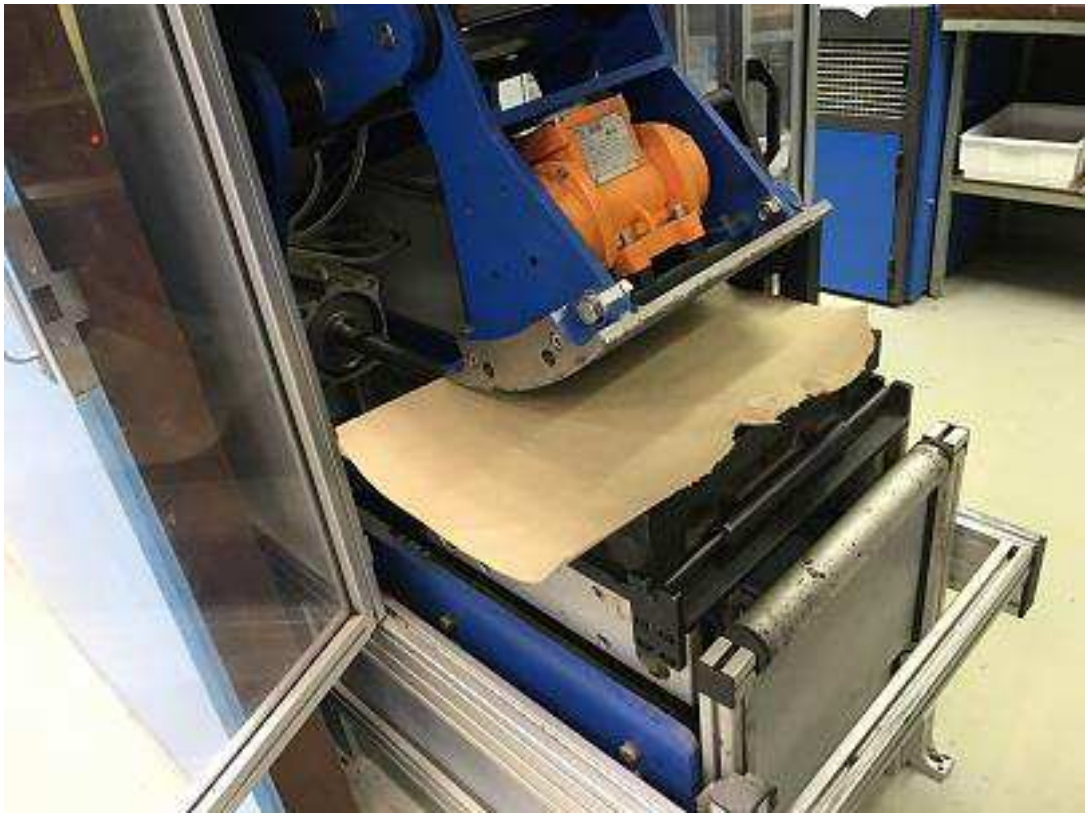

Figure 4-1: Beam specimen compaction in progress under wheel track roller

4.3.2. Beam Specimen Cutting

Three beam specimen are cut from each compacted mixture slab using Auto saw (see Figure 4-2). The target dimension of beam is 390 x 63.5 x 50mm, with individual specimen varies slightly in dimension.

4.3.3. Beam Specimen Bulk Density and Void Ratio measurement

Similar to AMPT specimen, the same water displacement procedures listed in AS 2891.9.2 and AS 2891.8 are used to work out the bulk density and air void ratio of beam specimen.

Figure 4-2: Demonstration of mixture slab being cut by mechanical saw (auto saw)

4.3.4. Dimension of Beam Specimen and Set Up Dimension

The width and height of each beam specimen are measured at following points: 1. within 20mm of each end; 2. within 10mm of centre; 3. two points 90mm either side of the centre. Average value of 5 measurements of width and height are taken as representative width and height for the specimen. Table 4-3 and Table 4-4 show an example record of measured bulk density, air void ratio and specimen dimension recorded during sample preparation.

When set up in the 4PB beam apparatus, the support span is 355.5mm, which is the distance between two clamps; while the loading span is 118.5mm, which is the

distance between two load actuators located at one third of support span each. Table 4-5 lists the summary of beam and apparatus dimensions.

Table 4-3: Example of relevant parameters of one beam specimen

Maximum Density for the Mixture (t/m^3)	2.472
Final Mass of Block in Air (g)	2964.08
Mass of Block in Water (g)	1707.85
Mass of Block in air SSD (g)	2967.12
Bulk Density (t/m^3)	2.347
Air Voids (%)	5.0

Table 4-4: Example spreadsheet of one beam specimen's dimension

4PB Beam Specimen						
Dimensions	***Point 1***	***Point 2***	***Point 3***	***Point 4***	***Point 5***	***Average***
Width (mm)	63.8	63.74	63.5	63.5	63.6	63.6
Height (mm)	52.8	53.0	53.2	53.1	53.4	53.1

Table 4-5: Idealized dimension of beam specimen and set-up spans

Beam Dimension	
Length (mm)	390
Width (mm)	63.5
Height (mm)	50
Beam Set-Up Spans	
Support Span (mm)	355.5
Loading Span (mm)	118.5

4.4. Testing Standards for Beam Fatigue

The beam tests adopted Austroad's technical report AP-T100/08 "Testing Asphalt in Accordance with the Austroads Mix Design Procedures (mainly in Chapter 8)". The specific procedures may subject to slight variations subjecting to research needs and laboratory conditions, but all under the instruction of highly experienced laboratory technicians.

Table 4-6: Experimental settings adopted for beam fatigue tests

Batch 1 Mixture		
Temperature (^{o}C)	**20**	
Strain Level (Microstrain)	400	
Frequency (Hz)	10	
Rest Periods (s)	0, 0.1, 0.3	
Testing Mode	Tension-Compression	
Batch 2 Mixture		
Temperature (^{o}C)	**20**	**12**
Strain Level (Microstrain)	400	300, 400
Frequency (Hz)	10	10
Rest Periods (s)	0, 0.1, 0.3	0, 0.1, 0.3, 0.5
Testing Mode	Tension-Compression	Tension-Compression

4.5. Testing Mode and Configurations for Beam Fatigue Test

Table 4-6 also lists a summary of adopted test parameters including temperature, strain amplitude, frequency, rest periods and testing modes used for beam fatigue tests in this study. Batch 1 mixture only undergoes 20^{o}C tests as insufficient material to cover both temperatures.

4.5.1. Main Facility

The facility used is IPC beam fatigue apparatus (see Figure 4-3), it is a 4 point bending facility with two end clamps, two loading frames and one measurement transducer at the centre.

Figure 4-3: IPC 4 point beam fatigue facility used in this research

4.5.2. Temperature

The same to VECD tests, the beam fatigue tests are conducted at temperature of 12^{o}C (for batch 2 only) and 20^{o}C respectively (both batch 1 and batch 2).

4.5.3. Loading Frequency

The same to VECD tests, 10Hz is the frequency for load/strain periodic loadings used for beam fatigue tests as specified in either Australia or European standard for beam tests.

4.5.4. Controlled strain or controlled stress

Similar to AMPT tests, there are two testing modes available for beam tests: controlled stress and controlled strain. The Austroad's technical report AP-T100/08 adopted controlled strain only for beam tests. Also, the available softwares are only available for controlled strain beam tests. This research follows the controlled strain tests due to the following two reasons. Firstly, controlled stress beam fatigue tests

normally works for pavement of larger thickness, while in Australia, most pavement's asphalt layer falls into thinner range so controlled strain tests can better simulate the real pavement situation (Hubner and Alderson, 2008). Secondly, although theoretically the damage behaviour should be applicable for both stress and strain controlled mode, controlled stress test subjects to issues such as permanent strain and aggressive failure. So both beam and AMPT tests adopted controlled strain mode.

4.5.5. Tension or Tension Compression

Tension compression mode is selected for beam tests, so the bottom section of the beam subjects to extension and contraction during each load cycle. The reason is to keep it in line with the tension compression mode used in AMPT tests as the results from beam will be verified against the results predicted by the novel damage characteristic with rest period healing models from VECD tests.

4.5.6. Strain Amplitude

An appropriate flexural strain amplitude is selected for beam tests. The strain amplitude here refers to the bottom section of the beam that is the most critical section in beam fatigue tests, since a harmonic sinusoidal loading is applied, a cyclic strain level of 400 tension-compression microstrain is the same as tensile strain level 200 microstrain.

The Ausroad Standard specifies a strain level of 400 microstrain for beam fatigue tests with a standard temperature of 20^{o}C. In this study, standard strain level of 400 microstrain is adopted for beam fatigue tests at 20 ^{o}C. While for 12 ^{o}C, both 300 and 400 cyclic microstrain are used, as it is stiffer material at 12 ^{o}C thus supposed to damage more quickly at same strain amplitude and same rest period compared to that of 20 ^{o}C.

4.5.7. Rest Period

Rest period is also inserted between load cycles for beam test to investigate the healing effect and compare with AMPT findings. However, due to time limitation

and the long testing time for beam fatigue tests with rest period, it is not viable to try all rest period length as same as AMPT, which has the task to produce a constitutive model. The selected rest periods length for beam fatigue tests under different conditions are listed in Table 4-6.

4.6. Testing Software

"UTS019 1.07b (Released on 17/06/2011) User Programmable Test" is the software used as testing controller for all beam fatigue tests with and without rest period. It is capable of inserting rest period of prescribed length between each load cycle (pulse rest period in Figure 1-1), so rest period healing effect can be investigated.

4.7. Finger Print Test

Similar to S-VECD tests, it is also important to obtain finger print stiffness for beam specimen. The stiffness produced by beam tests refers to flexural stiffness. This is realized by conducting a non-destructive tests with strain amplitude of 50 tensile microstrain before the actual destructive fatigue tests that will be conducted at a much higher strain amplitude. The finger print stiffness is taken as the stiffness at 50^{th} cycle of such test. The finger print stiffness will be used for calculating the stiffness ratio of each load cycle as below:

$$Stiffness\ Ratio = \frac{E_n}{E_{finger}} \tag{4.1}$$

in which E_n is the flexural stiffness at the nth cycle output by the controller software, Efinger is the fingerprint flexural stiffness. The fingerprint stiffness for all beam specimen has been listed in Table 4-1 and Table 4-2

Mathematically, the stiffness ratio is the same in form as pseudostiffness from cyclic based calculation as listed in AASHTO TP 107 - 14. The finger print stiffness also serves as an important reference parameter for material responses such as stiffness development and healing, as found by previous research (Roque et al., 2010b, Zeiada, 2012).

Chapter 5. Laboratory Data Process

For both VECD and 4PB beam fatigue tests, the laboratory data needs to be processed according to state of art solutions so accurate and comparable results can be produced. This chapter contains laboratory data processing theories, methods as well as results of some fundamental laboratory derived parameters for the production of dynamic modulus master curves, stiffness development curves and damage characteristic curves. Thus, it contains such information for all types of tests in this research such as dynamic modulus tests, VECD tests and 4PB beam fatigue tests.

5.1. Dynamic Modulus Results Data Process

As mentioned above, the construction of damage characteristic curves of an asphalt mixture relies on input parameters obtained from dynamic modulus master curves. Else, the frequency and temperature effect can be utilized in damage characteristic curves through time-temperature shift factor obtained from master curves (Chehab, 2002). Thus, it is necessary to conduct dynamic modulus master curve tests before VECD tests, the following parameters should be worked out:

1. long-time equilibrium modulus ($E\infty$)
2. average representative dynamic modulus (E_{lve}) at certain temperature and frequency
3. modulus of Prony term (E_m) (for complete solution)
4. time-temperature shift factor a_T
5. power model factor α

The production of master curves and relevant parameters using AMPT follows the methods developed through a series of projects initiated by NCHRP (Bonaquist, 2008a, Bonaquist, 2011, Roque et al., 2010a, Witzcak et al., 2002). The useful equations are listed in below. Firstly, the dynamic modulus calculation equation suggested by Bonaquist (2008a):

$$log|E^*| = log(Min) + \frac{log(Max)-log(Min)}{1+e^{\beta+\gamma log\omega_r}} \quad (5.1)$$

where E* is dynamic modulus, Max = limiting maximum modulus (Mpa), Min = limiting minimum modulus (Mpa), β and γ = fitting parameters, and ω_r = reduced frequency (Hz):

$$log\omega_r = log\omega + \frac{\Delta E_a}{19.14714}\left(\frac{1}{T} - \frac{1}{T_r}\right) \quad (5.2)$$

in which ω is loading frequency at the test temperature, T_r is reference temperature (°C), T is test temperature (°C) and ΔE_a is activation energy (obtained as a fitting parameter). The Maximum Dynamic Modulus can thus be obtained as:

$$|E^*|_{max} = P_c\left[4200000\left(1 - \frac{VMA}{100}\right) + 435000\left(\frac{VFA \times VMA}{10000}\right)\right] + \frac{1 - P_c}{\left[\frac{1 - \frac{VMA}{100}}{4200000} + \frac{VMA}{435000 \times VFA}\right]} \quad (5.3)$$

Where

$$P_c = \frac{\left(20 + \frac{435000 \times VFA}{VMA}\right)^{0.58}}{650 + \left(\frac{435000 \times VFA}{VMA}\right)^{0.58}}$$

in which VMA is "Voids in mineral aggregates, %", VFA is "Voids filled with asphalt, %" and $|E^*|_{max}$ stands for "Max" as stated above.

The time-temperature shift factor is calculated as:

$$log[a(T)] = \frac{\Delta E_a}{19.14714}\left(\frac{1}{T} - \frac{1}{T_r}\right) \quad (5.4)$$

in which a(T) is shift factor at a specific temperature , T_r is reference temperature (°C), T is test temperature (°C), ΔE_a is activation energy (treated as a fitting parameter).

Table 5-1 and Table 5-2 demonstrate the obtained dynamic modulus of the specimen at each temperature and frequency levels as listed in Table 3-5 for both batches of material supply. Based on procedures described in AASHTO 79-13, the time temperature shift factor for each temperature level is obtained using "Modified Mastersolver" spreadsheet (Bonaquist, 2009). The temperature shift factor results as

well as relevant reduced frequency values and calculated dynamic modulus values are listed in Table 5-3 and Table 5-4 for both batches of mixture. It should be noted that the reason of adding 12^{o}C tests is to have directly referable and accurate resulting parameters (such as E_{lve}) for S-VECD tests at this temperature, although it can also be back calculated based on time-temperature shift factor and master curves.

Table 5-1: Dynamic modulus tests results data collection for batch 1 material

		Specimen 1		Specimen 2		Specimen 3		Average	Modulus	Average	Std Dev	Fitted
Temp (oC)	Frequency (Hz)	Modulus Mpa	Phase Degree	Modulus Mpa	Phase Degree	Modulus Mpa	Phase Degree	Modulus Mpa	CV %	Phase (Deg)	Phase (Deg)	Modulus Mpa
4	0.1	9011.0	18.1	8790.0	17.9	8709.0	18.4	8836.7	1.8	18.1	0.3	8579.9
4	1	13006.0	13.1	12718.0	13.0	12711.0	13.4	12811.7	1.3	13.2	0.2	12455.4
4	10	17144.0	9.7	16798.0	9.7	16886.0	9.9	16942.7	1.1	9.7	0.1	15777.2
12	0.1	4639.0	27.1	4490.0	26.7	4414.0	27.4	4514.3	2.5	27.0	0.3	4432.8
12	1	7984.0	20.4	7691.0	20.2	7661.0	20.6	7778.7	2.3	20.4	0.2	8005.3
12	10	12065.0	14.9	11644.0	14.9	11707.0	15.1	11805.3	1.9	15.0	0.1	11907.6
20	0.1	1869.0	34.8	1820.0	34.6	1791.0	34.9	1826.7	2.2	34.8	0.2	1812.5
20	1	4114.0	29.0	3892.0	28.8	3867.0	29.2	3957.7	3.4	29.0	0.2	4174.9
20	10	7474.0	22.2	7047.0	22.1	7055.0	22.4	7192.0	3.4	22.2	0.2	7678.5
38	0.1	148.1	35.0	186.3	36.3	156.7	35.6	163.7	12.2	35.6	0.7	164.2
38	1	447.2	40.4	565.5	39.8	465.0	40.1	492.6	12.9	40.1	0.3	499.7
38	10	1452.0	39.5	1680.0	37.8	1435.0	39.0	1522.3	9.0	38.8	0.8	1443.4

Table 5-2: Dynamic modulus tests results data collection for batch 2 material

		Specimen 1		Specimen 2		Specimen 3		Average	Modulus	Average	Std Dev	Fitted
Temp C	Frequency Hz	Modulus Mpa	Phase Degree	Modulus Mpa	Phase Degree	Modulus Mpa	Phase Degree	Modulus Mpa	CV %	Phase (Deg)	Phase (Deg)	Modulus Mpa
4	0.1	8558.0	18.6	9541.0	17.6	7637.0	18.1	8578.7	11.1	18.1	0.5	8676.0
4	1	11961.0	13.0	13369.0	12.4	10737.0	12.7	12022.3	11.0	12.7	0.3	12331.5
4	10	15385.0	9.2	17121.0	8.9	13762.0	9.1	15422.7	10.9	9.1	0.1	15486.1
12	0.1	5197.0	27.9	5168.0	27.1	4435.0	27.9	4933.3	8.8	27.6	0.4	4711.9
12	1	8362.0	20.4	8643.0	19.8	7368.0	20.0	8124.3	8.2	20.0	0.3	8179.3
12	10	11810.0	14.3	12538.0	14.0	10672.0	14.0	11673.3	8.1	14.1	0.2	11862.2
20	0.1	2024.0	36.2	2154.0	35.5	1803.0	37.0	1993.7	8.9	36.2	0.7	2032.0
20	1	4736.0	29.9	4768.0	29.2	4010.0	30.2	4504.7	9.5	29.8	0.5	4492.1
20	10	8592.0	22.2	8321.0	21.7	7230.0	22.1	8047.7	9.0	22.0	0.3	7913.9
38	0.1	158.9	32.4	183.9	35.5	157.0	34.7	166.6	9.0	34.2	1.6	164.2
38	1	509.6	38.8	633.7	40.3	498.4	40.7	547.2	13.7	40.0	1.0	568.4
38	10	1606.0	40.4	2005.0	40.0	1520.0	41.7	1710.3	15.1	40.7	0.9	1668.0

Table 5-3: Useful parameters for master curve and damage characteristic curve production obtained from dynamic modulus tests results for Batch 1 mixture

Celcius Degree ^{o}C	Frequency (Hz)	Temperature Shift Factor (at)	Reduced Frequency w_r (Hz)
4	0.1	170.2539295	17.02539295
4	1	170.2539295	170.2539295
4	10	170.2539295	1702.539295
12	0.1	12.14106788	1.214106788
12	1	12.14106788	12.14106788
12	10	12.14106788	121.4106788
20	0.1	1	0.1
20	1	1	1
20	10	1	10
38	0.1	0.005810892	0.000581089
38	1	0.005810892	0.005810892
38	10	0.005810892	0.058108918

Table 5-4: Useful parameters for master curve and VECD obtained from dynamic modulus tests results for Batch 2 mixture

Celcius Degree ^{o}C	Frequency (Hz)	Temperature Shift Factor (at)	Reduced Frequency w_r (Hz)
4	0.1	160.4603763	16.04604
4	1	160.4603763	160.4604
4	10	160.4603763	1604.604
12	0.1	11.79649746	1.17965
12	1	11.79649746	11.7965
12	10	11.79649746	117.965
20	0.1	1	0.1
20	1	1	1
20	10	1	10
38	0.1	0.006166317	0.000617
38	1	0.006166317	0.006166
38	10	0.006166317	0.061663

5.2. S-VECD Parameters Derivation

As stated above, necessary parameters used for S-VECD tests are obtained from dynamic modulus tests results, and the procedures for derivation of these parameters are listed in AASHTO TP107-14. As for simplified VECD analysis, no pseudostrain

at specific time is required and relevant parameters/procedures used for time based rigorous solutions are not listed here.

5.2.1. Representative Dynamic Modulus

For simplified VECD method, firstly, E_{lve} is obtained as the representative dynamic modulus at a particular temperature and frequency level. So it can be directly read from dynamic modulus tests as the temperature and frequency for VECD tests in this study (see Table 3-6) are directly covered by dynamic modulus tests (see Table 3-5). As a result, at 10Hz, E_{lve} are 11805 and 7192 Mpa at 12 and 20^{o}C respectively for batch 1 mixture (see Table 5-1), and 11673 Mpa (12^{o}C) and 8047.7 Mpa (20^{o}C) for batch 2 mixture (see Table 5-2).

5.2.2. Time-Temperature Shift Factor

The time – temperature shift factor is a factor used to shift the stiffness curves at different temperatures into one unique curve, so a master curve can be obtained. The time-temperature shift factor is obtained through tests on asphalt mixture at different temperature and frequencies (temperature/frequency sweeping tests) and computed by curve fitting technique such as Eq. (5.4). Based on Table 5-3 and Table 5-4, the obtained time-temperature shift factor a_t for 12 and 20 ^{o}C for both batch 1 and batch 2 mixture are presented.

5.2.3. Long-Term Equilibrium Modulus and Relaxation Modulus Prony coefficients

The long-term equilibrium modulus E∞ and Relaxation Modulus Prony coefficients (ρ_m and E_m) are calculated following appendix X1. The results are presented in Table 5-5 and Table 5-6 for batch 1 and batch 2 mixture respectively. Prony coefficients are used to calculate the relaxation modulus of a material when the modulus is changing with time progression. AASHTO TP107-14 lists the procedures to process the data from dynamic modulus tests results and produce prony coefficients using Microsoft Office Excel spreadsheets with regression fitting functions, which is also the method used in study.

Table 5-5: Prony coefficients obtained from dynamic modulus tests results on Batch 1 mixture

E∞(kPa)	14015
Relaxation Time of Prony Term m: ρ_m	**Modulus of Prony Term m: E_m (kPa)**
200000000	1660.36028
20000000	1135.417127
2000000	2906.952211
200000	6199.07201
20000	15019.14439
2000	41684.85063
200	133568.8486
20	449645.9275
2	1285022.117
0.2	2545685.219
0.02	3284549.175
0.002	2960771.879
0.0002	2106241.295
0.00002	1307193.582
0.000002	752552.7565
0.0000002	415822.7985
0.00000002	231242.7063

Table 5-6: Prony coefficients obtained from dynamic modulus tests results on batch 2 mixture

E∞(kPa)	8712.825
Relaxation Time of Prony Term m: ρ_m	**Modulus of Prony Term m: E_m (kPa)**
200000000	1679.966484
20000000	1068.409777
2000000	2783.66434
200000	6010.96894
20000	15063.98996
2000	43762.42334
200	145882.6092
20	498704.5212
2	1425477.506
0.2	2862508.893
0.02	3848125.178
0.002	3686559.007
0.0002	2799330.564
0.00002	1846476.707
0.000002	1123132.55
0.0000002	652276.2599
0.00000002	380317.6817

5.2.4. Continuum Damage Power Term

The Appendix X3 in AASHTO TP107-14 lists procedures for the determination of continuum damage power term α, and this is a necessary parameter for the application of S-VECD theories. Before solving for damage power term α, Appendix X1 in AASHTO TP107-14 should be followed to calculate the Prony coefficients, which is listed in Table 5-5 and Table 5-6 for batch 1 and batch 2 mixture respectively. The relaxation modulus versus time plus the Gaussian fitting curves are obtained from spreadsheet operations and the results are demonstrated in Figure 5-1 and Figure 5-2 for batch 1 and batch 2 mixture respectively, while the values for continuum damage power term α are also calculated and indicated in the figures for both batches of mixture.

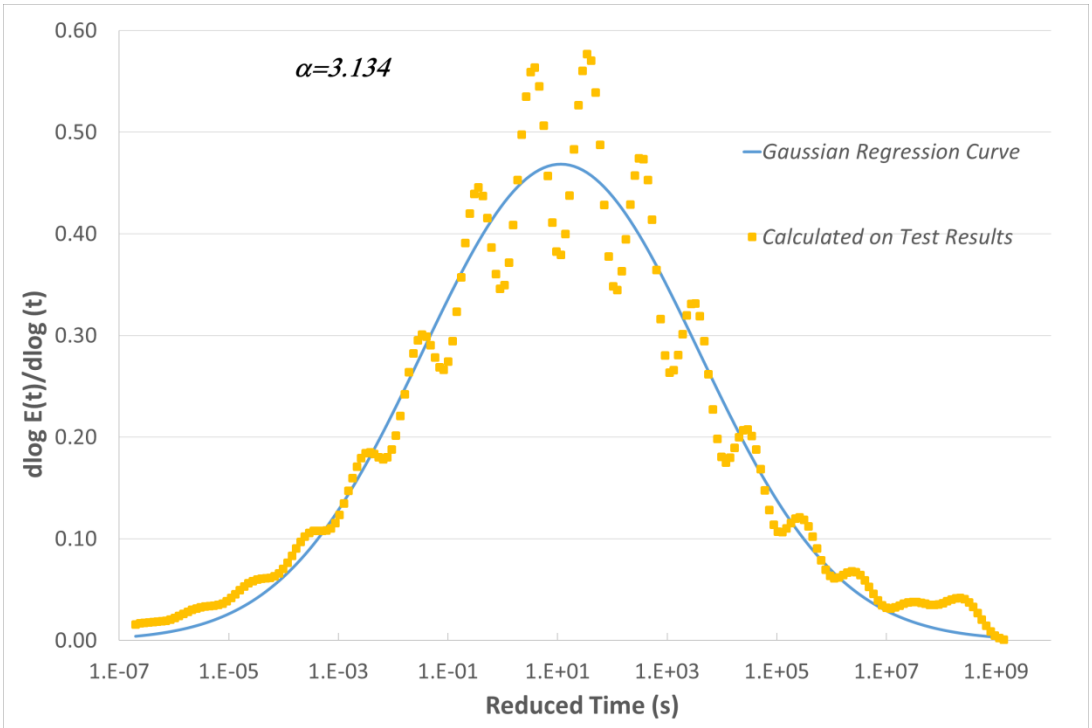

Figure 5-1: Plot of relaxation modulus versus time and Gaussian distribution regression curve for batch 1 mixture

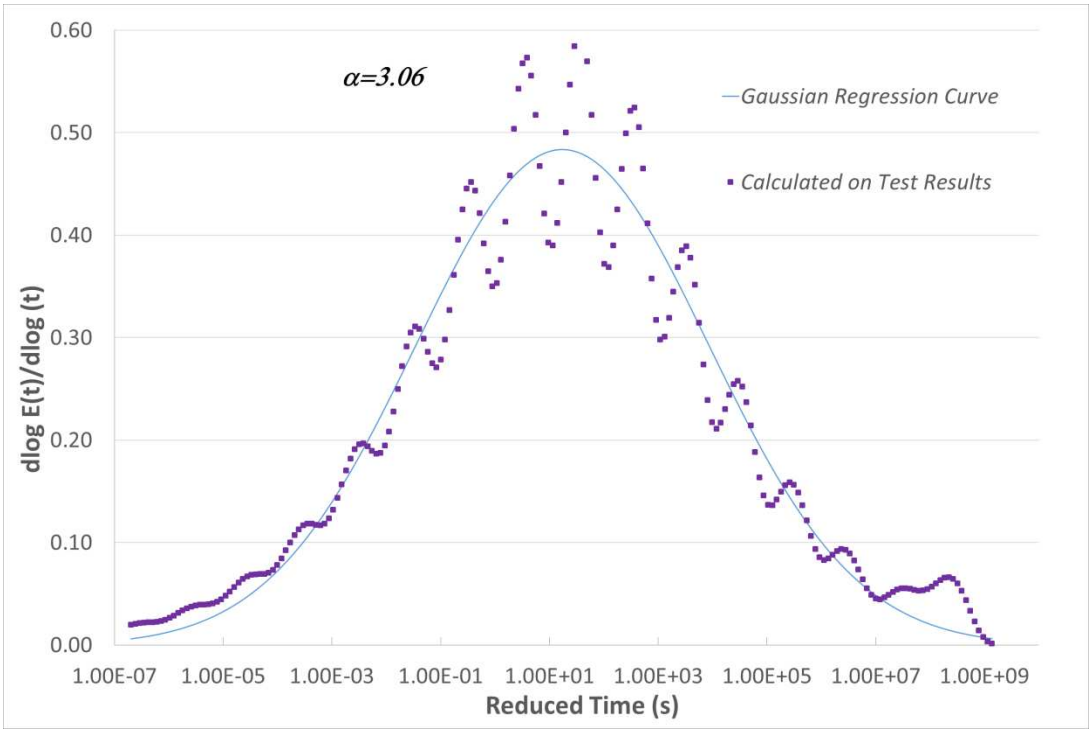

Figure 5-2: Plot of relaxation modulus versus time and Gaussian distribution regression curve for batch 2 mixture

5.3. S-VECD Results Data Process

Firstly, dynamic modulus finger print tests are conducted before each S-VECD tests on each specimen. The dynamic modulus finger print tests are to apply a load to generate a displacement level of 50 to 75 microstrain on the specimen, so to keep the mixture undamaged, thus the obtained stiffness of the intact mixture. The VECD test controller software worked out the magnitude of load for finger print tests automatically, with reference to the representative at relevant temperature and frequency dynamic modulus already obtained from time temperature sweeping tests. Although each specimen has unique stiffness property, the general range of stiffness should not vary too much. The finger print stiffness representing the tested specimen's unique undamaged stiffness as recorded at the 50th cycle of repetitive loadings.

After the finger print test, the dynamic modulus ratio, the specimen to specimen's stiffness normalization parameter, is calculated as:

$$DMR=\frac{|E_{finger}|}{E_{LVE}} \tag{5.5}$$

Application of DMR parameter in S-VECD tests eliminates the influence of specimen to specimen variance.

Then, main S-VECD tests are conducted based on configurations mentioned in Section 3.9. A typical example of raw data spreadsheet collected from an S-VECD test is listed in Table 5-7, which only lists the relevant parameters useful for the production of damage characteristic curves. Although Table 5-7 only lists first 10 cycles, all remaining cycles are in a similar format..

Table 5-7: Example results data from S-VECD test (only important data is presented)

Cycle	Dynamic Modulus (MPa)	Phase Angle (Degrees)	Peak to Peak Stress (kPa)	Maximum Stress (kPa)	Minimum Stress (kPa)	Peak to Peak Average Strain (microstrain)
1	6714.1	20.96941	2165.094	1162.721	-1002.373	322.469
2	6605.9	20.96941	2171.007	1151.358	-1019.649	328.645
3	6551.8	20.96941	2229.847	1210.199	-1019.649	340.344
4	6454.4	20.96941	2393.209	1307.996	-1085.214	370.789
5	6418.5	20.96941	2501.151	1343.068	-1158.083	389.68
6	6376.9	20.96941	2514.136	1352.981	-1161.155	394.258
7	6341.4	20.96941	2532.861	1363.01	-1169.851	399.417
8	6319.7	20.96941	2556.339	1375.879	-1180.46	404.503
9	6289.5	20.96941	2544.107	1366.024	-1178.083	404.503
10	6292.7	20.96941	2535.354	1363.01	-1172.344	402.905

5.3.1. Miscellaneous Results Parameters from VECD tests

The simplified equation for calculating damage parameter S is listed in Eq. (2.11). The following section will describe how these parameters are obtained from VECD tests results.

The time temperature shift factor α_t is collected from Table 5-3 for relevant temperatures, and it is from dynamic modulus master curve.

ε_{pp}^{R} is the cyclic peak to peak pseudostrain and calculated as:

$$\varepsilon_{pp}^{R} = \varepsilon_{pp} * E_{lve} \tag{5.6}$$

in which ε_{pp} is cyclic peak to peak strain level as directly read from test output such as those shown in Table 5-7.

As a result, the tensile amplitude pseudostrain is calculated:

$$\varepsilon_{ta}^{R} = \frac{\beta+1}{2} \varepsilon_{cyc}^{R} \tag{5.7}$$

with the functional form factor β calculated as:

$$\beta = \frac{F_{peak}+F_{valley}}{|F_{peak}|+|F_{valley}|} \tag{5.8}$$

5.3.2. Calculation of Pseudostiffness

For pseudostiffness, this study calculates cyclic pseudostiffness only, as the time based rigorous calculation for first cycles as suggested by AASHTO TP 107-14 is not necessary after some trial, also because the VECD with rest period test records all first 10 cycles. The cycle based pseudostiffness is computed as described in AASHTO TP107-14 as:

$$C = \frac{\sigma_{pp}}{\varepsilon_{PP}^{R} * DMR} \tag{5.9}$$

in which ε_{PP}^{R} is It is worth mentioning that tensile pseudostrain is used for pseudostif fness calculation, since the asphalt mixture is not regarded as damaged under this m agnitude of compression so damage is only caused by tensile strain pulling the speci men.

5.3.3. Calculation of reduced time factor

The reduced time used in simplified equation refers to the time difference between two cycles of consecutive harmonic loadings. Originally for the case of continuous loading, it was calculated as:

$$t_R = \frac{1}{\alpha_T}\left[\frac{t_{peak}+t_{valley}}{2}\right] \tag{5.10}$$

in which t_{peak} and t_{valley} are time at the peak and valley of a sinusoidal loading cycle.

5.3.4. Calculation of Form Adjustment Factor K

The form adjustment factor K accounts for the error made by VECD equation simplification so the value depends on the simplification method used to transfer original VECD solution as listed in Eq.(2.8) into simplified form Eq.(11) (Roque et al., 2010b). For the current standard S-VECD calculation as listed in AASHTO TP107-14, the K is calculated from an integration process that can be conducted with a spreadsheet. It should be noted that the calculation of K requires certain computer power since it generates large amount of columns. However, K value does have common value for certain mixture under certain test conditions. For the mixture and conditions used in this research, the K value is found to be around 0.465 and 0.455 for 20 and 12^{o}C respectively and the difference to end results of damage characteristic curves seems negligible, so 0.46 is selected for the whole mixture.

5.3.5. Calculation of Damage Parameter S

With all above parameters obtained, Eq. (2.11) is then used for the calculation of damage parameter S. It should be mentioned that S-VECD calculation should only be executed between cycles that has seen a damage progress, in other words, the

higher cycle number should demonstrate a lower pseudostiffness than the stiffness at a lower number of cycle. To include this logic, the following equation are demonstrated:

$$\begin{cases} S_{cyc} = \left[-\frac{1}{2}\left(\varepsilon_{cyc}^{R}\right)^2 (C^*{}_{i-1} - C^*{}_{i})\right]^{\frac{a}{1+a}} (\Delta t_r)^{1/(1+a)} (K_1)^{1/(1+a)}, & for\ C_{n-1} \le C_n \\ 0, & for\ C_n \le C_{n-1} \end{cases}$$

(5.11)

While the accumulated S at certain number of cycles is the sum of S_{cyc} of all damage caused by previous cycles:

$$Sn = \sum_1^N S_{cyc} \tag{5.12}$$

A demonstration of spreadsheet results of calculated values of pseudostiffness, damage parameter S etc. from S-VECD tests is listed in Table 5-8.

When smeared continuum damage approach is applied, Underwood and Zieadla suggested a modiflied pseudostrain calculation method for pulse-rest loading mode. However, it only applies to microcrack healing part of stiffness recovery. As there are both viscoelasticity and microcrack healing occurring simultaneously during rest period, an alternative way to define healing as the total stiffness recovery validates Eq.(5.9) for rest period loading.

Table 5-8: Example of data sheet for production of damage characteristic curve from an S-VECD test

Cycle	ε_{taR} (tensile pseudo microstrain)	PseudoStiffness	Form Factor (β)	K1	DS	S
0		1			0	0
1	1245.479	0.927363972	0.074060526	0.465452334	1912.026547	1912.026547
2	1253.504413	0.912421748	0.060667239	0.462358431	581.3144199	2493.340967
3	1328.462524	0.904937114	0.085454255	0.468096334	376.9957745	2870.336741
4	1457.478401	0.891487421	0.093089198	0.469874507	677.2242323	3547.560974
5	1504.928563	0.886529576	0.073959949	0.465429044	332.8562583	3880.417232
6	1525.924775	0.880784546	0.076298975	0.465970895	380.2067722	4260.624004
7	1545.837752	0.875883299	0.076261192	0.465962138	343.7617289	4604.385733
8	1565.788943	0.872887215	0.076444869	0.466004708	241.360659	4845.746392
9	1562.048026	0.868710478	0.073873072	0.465408928	309.2696852	5155.016077
10	1557.803845	0.869155301	0.075202911	0.465716926	0	5155.016077

5.3.6. Relationship between C and S

From numerous studies on damage characteristic curves (Lee and Kim, 1998a, Roque et al., 2010b), the form of damage curves for asphalt mixture can be curve fitted into regression equations:

$$C = 1 - C_1 S^{C_2} \tag{5.13}$$

$$C = e^{a{S_1}^b} \tag{5.14}$$

At present, it is a convention to present damage characteristic curves produced by regression equations, so is this study. It has benefit of accurately capturing the damage curve before macro-crack appears, while provide reasonable prediction of the curve when tests do not continue until failure.

5.3.7. Evaluation of the Damage Characteristic Curve Production Method

When a rest period is inserted between load cycles, the rest period itself is not included in the t_R calculation since there is no loading during this period thus no damage increment. However, damage parameter S does recovers to certain degree during each rest period due to healing. It is not within the current scope to interpret the damage and healing recovery after each load cycle mechanically. In stead, in this research, the damage parameter is directly calculated based on the pseudostiffness change between two consecutive load cycles, and the effect of healing is reflected by how fast the stiffness change with number of cycles. In other words, the healing effect is to be phenomenologically identified. Thus, damage characteristic curves produced under different rest period are different with this process method. However, it is not directly calculating the healing mechanism of each rest period. It is worth mentioning that this methodology is an alternative to Lee and Kim (1998b)'s method that tries to calculates the recovery of S for each rest period, in addition to damage made by loadings. A detailed description of Lee and Kim (1998b)'s healing mechanism and its limitations are presented in Section 2.3. So the present method has the advantage of directly and accurately capturing the influence of rest period healing effect by distinguishing it from different forms of damage

characteristic curves under various conditions. On the other hand, Lee and Kim (1998b)'s method is believed to be better at predicting fixed rest period insertion after continuous loadings (group rest), but producing larger error when there are a great amount of rest periods after each load cycle (see Section 2.6).

Applying this calculation of damage parameter, it is expected that VECD tests with various pulse-rate rest periods are similar to that of different asphalt mixtures thus producing different damage characteristic curves. The existence of rest period is like improving the material performance, so higher lying C vs S curve, caused by slower stiffness reduction (being recovered after each cycle). Thus, it is significant to firstly qualify the influence of rest periods on damage characteristics, and then the results will further lead into an equational relationship between rest period and damage characteristic curves.

5.4. Beam Fatigue Tests Data Process

The software used specified vertical displacement to control the strain amplitude at the bottom section using the following correlating equations:

$$\Delta_{vertical} = \frac{\in_t * (3 * L_{support}{}^2 - 4 * L_{loading}{}^2)}{12000000 * H^2} \tag{5.15}$$

in which $\Delta_{vertical}$ is the input vertical displacement at the centre of the beam, $\in_t$ is the desired strain amplitude at the bottom of the beam, $L_{support}$ and $L_{loading}$ are support and loading spans respectively; H is the height of the beam specimen. Actually, only the H is a specimen specific parameter, and other parameters are shared by all individual specimen. For example, B2-12C-0.1R-400 has an average height of 50.1mm, so based on Eq. (5.15), it requires an input vertical displacement of 0.0537mm.

Derived from common beam elasticity theory, the software computes tensile stress at the bottom of the beam as:

$$\sigma_t = \frac{L_{support} * \sigma_{cyc} * 1000000}{b * H^2} \tag{5.16}$$

in which σ_t is the tensile stress at the bottom of the beam, σ_{cyc} is the cyclic load that is an output from the software, b is the width of the beam specimen. However, it is important that this equation is derived based on non-destructive situations, where the stiffness of the beam material is intact. So is the flexural stiffness is derived as

$$E_{flexural} = \frac{\sigma_t}{\varepsilon_t} \tag{5.17}$$

Since σ_t is not true stress at the bottom, so $E_{flexural}$ is not the same as the stiffness at the bottom section, since there is damage induced stiffness reduction with number of cycles along the beam's cross section, and it is varying along the beam height (see Figure 8-3). The software assumes an undamaged section and uses Eq. (5.16) when calculating flexural stiffness. Since the current test facility has no capability to directly measure bottom strain and stress, yet the bending moment it provides is still correct. As a result, the true bottom stress can only be calculated as long as the stiffness change at the cross section is known and this will be realized by ABAQUS modelling in Chapter 8.

For 4PB beam fatigue tests, the details of machine setup and inner calculations are already described in Chapter 4. As the flexural stiffness is a direct output from the controlling program, there is no need to process the data. While VECD method only applies to AMPT tests at the moment, the availability of beam fatigue tests results for VECD analysis may remain as a future research topic, so are other analysis methods for asphalt mixture.

5.5. Tested Specimen Summary

All first batch AMPT (both dynamic modulus and VECD) specimen in this project are listed in Table 5-10, while second batch specimen is listed in Table 5-11. Table 5-10 and Table 5-11 also include the initial finger print stiffness and void ratio information for each specimen. When representative results for certain rest period is presented, they can be averaged values of different specimen geometries, so the size label is removed in such case.

Similarly, since there is no geometry variation for beam fatigue tests, sample label like "B1-20C-0.3R-200" is sufficient to describe a beam tested under 20^{o}C, 0.3s rest

period and 200 microstrain with batch 1 mixture. In certain specific graphic presentation, for instance when results from Beam Fatigue tests and AMPT tests are presented together, extra description is added in parentheses such as “B1-20C-0.3R-200 (Beam)”.

Table 5-9: Summary of specimen labelling rules

S-VECD TESTS				
Specimen Size	**Test Temperature**	**Applied Rest Periods**	**Strain Amplitude**	**Repetitions**
"L" for 100 mm ×150 mm cylinder (Large) "M" for 100 mm × 130 mm cylinder (Medium) "S" for 54 mm × 110 mm cylinder (Small)	"12C" for tests at 12 °C "20C" for tests at 20°C	"0.0R" for continuous tests "0.3R" for 0.3 second rest period and so forth	Value of Strain in unit of microstrain, e.g. 200 for 200 microstrain	Certain parameters for tests are repeated and marked as "(1)", "(2)" and "(3)"
Beam Fatigue Tests				
Specimen Size	**Test Temperature**	**Applied Rest Periods**	**Strain Amplitude**	**Repetitions**
Uniform Beam Size, so "B" is used throughout to mean "Beam"	"12C" for tests at 12 °C "20C" for tests at 20°C	"0.0R" for continuous tests "0.3R" for 0.3 second rest period and so forth	Value of strain in unit of microstrain, e.g. 200 for 200 microstrain	Tests of identical conditions are repeated and marked as "(1)", "(2)" and "(3)", label without repetition marks are non-repetitive or as described

Table 5-10: Summary of VECD Tested Specimen for Batch 1 Mixture

Dynamic Modulus Test	**Specimen ID**	**Testing Temperature (^{o}C)**
	L (average of 3 same size samples)	4, 12, 20 and 38
	S	4, 12, 20 and 38
S-VECD Test at 20^{o}C	**Specimen ID**	**Finger Print Stiffness**
	L-20C-0.0R-200 (1)	7214
	L-20C-0.0R-200 (2)	7065
	M-20C-0.0R-200	6996
	S-20C-0.0R-200	5976
	L-20C-0.1R-200 (1)	6753
	L-20C-0.1R-200 (2)	7031
	M-20C-0.1R-200	7545
	L-20C-0.2R-200 (1)	6784
	L-20C-0.2R-200 (2)	6815
	L-20C-0.3R-200 (1)	6443
	L-20C-0.3R-200 (2)	6772
	L-20C-0.3R-400	7240
	S-20C-0.3R-200	6482
	L-20C-0.5R-300	7178
	L-20C-0.5R-200	6895
	L-20C-0.7R-200 (1)	7188
	L-20C-0.7R-200 (2)	7159
	L-20C-1.0R-200 (1)	6822
	L-20C-1.0R-200 (2)	7538
	L-20C-1.0R-200 (3)	6364
	L-20C-1.5R-200	7192
S-VECD Test at 12^{o}C	M-12C-0.0R-200	11655
	S-12C-0.0R-200	11338
	M-12C-0.1R-200 (1)	11132
	M-12C-0.1R-200 (2)	11649
	L-12C-0.1R-200	10976
	S-12C-0.2R-200	10980
	L-12C-0.2R-200	10968
	L-12C-0.3R-200	11441
	M-12C-0.3R-200 (1)	11269
	M-12C-0.3R-200 (2)	11267
	M-12C-0.5R-200	11554
	L-12C-0.5R-200	11805
	M-12C-1.0R-200	10937
	L-12C-1.0R-200	11289

Table 5-11: Summary of VECD Tested Specimen for Batch 2 Mixture

Dynamic Modulus Test	**Specimen ID**	**Testing Temperature (^{o}C)**
	L (average of 3 same size samples)	4, 12, 20 and 38
S-VECD Test at 20^{o}C	**Specimen ID**	**Finger Print Stiffness (MPa)**
	M-20C-0.0R-300	8519
	M-20C-0.0R-250	9100
	M-20C-0.1R-300	8250
	M-20C-0.1R-250	8350
	M-20C-0.1R-200	8079
	M-20C-0.3R-250	8227
	M-20C-0.3R-300	8519
	M-20C-0.7R-250	8380
S-VECD Test at 12^{o}C	M-12C-0.0R-200	13238
	M-12C-0.05R-200	13738
	M-12C-0.1R-200(1)	13762
	M-12C-0.1R-200(2)	14144
	M-12C-0.2R-200(1)	13569
	M-12C-0.2R-200(2)	12708
	M-12C-0.3R-200(1)	14053
	M-12C-0.3R-200(2)	13238
	M-12C-0.5R-200	13798
	M-12C-1.0R-200	13120

Chapter 6. AMPT Tests Results

This chapter presents main laboratory findings of this research from AMPT tests. It firstly demonstrates dynamic modulus test results by listing master curves for both batches of mixture. Next, it presents the stiffness development curves under various rest periods and test conditions, including detailed evaluation of rest period healing effect. Then, the damage characteristic curves of various rest periods are presented, and both qualitative and quantitative findings are described with regard to rest period healing effect on mixture's damage properties. It is followed by the derivation of a novel rest period damage function that incorporates rest period length into damage characteristic functions. Also, the proposed procedures to obtain such novel function are suggested.

6.1. Dynamic Modulus Master Curve

As mentioned, it is necessary to acquire dynamic modulus master curve of the mixture to provide necessary parameters for the production of damage characteristic curves from simplified VECD tests. Based on the results in Table 5-1 to Table 5-2, the dynamic modulus master curve for first batch of AC10 C320 asphalt mixture is drawn in Figure 6-1. Similarly, batch 2 material results are drawn in Figure 6-2.

In this project, the rest period healing effect is studied through two ways, firstly, compare the stiffness development with number of cycles curves produced under various rest periods; secondly, evaluate the damage characteristic curves produced with various rest periods. Focus is on the damage characteristic curves due to its nature as an inherent material property that has much wider applicability than other curve.

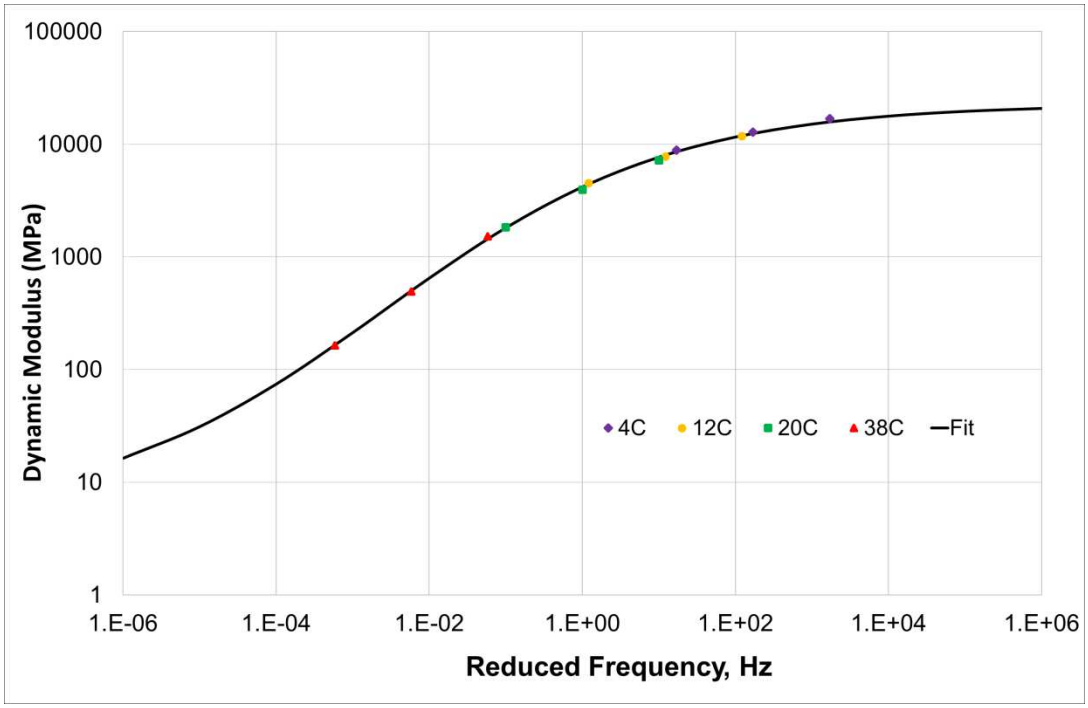

Figure 6-1: Dynamic modulus master curve of batch 1 mixture

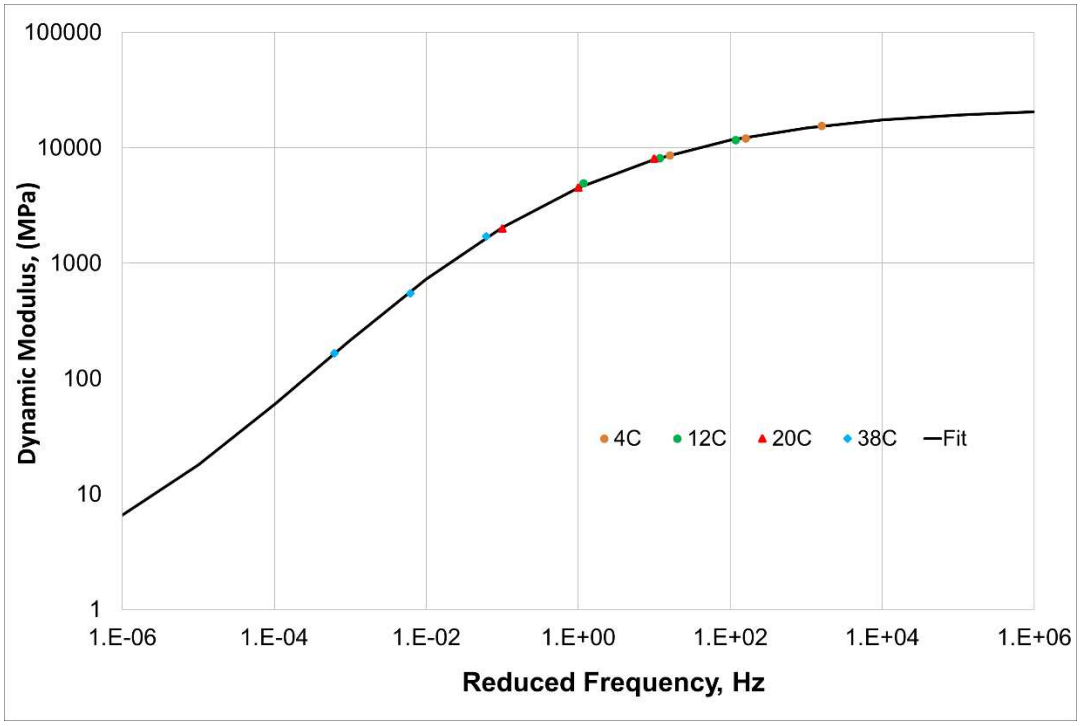

Figure 6-2: Dynamic modulus master curve of batch 2 mixture

6.2. Stiffness Development from VECD Tests with Rest Period

As mentioned in Section 3.9.4, the pseudostiffness versus number of cycles curves under same strain amplitude are plotted together so the effect of rest period healing can be correctly evaluated. The stiffness development curves with various length of rest periods are demonstrated from Figure 6-3 to Figure 6-6 under two temperatures of 12 and 20^{o}C respectively. As described earlier, the stiffness values in these curves take the form of pseudostiffness, since the true stiffness is not effective to specimen to specimen variations. What's more, by separating the damage from the effect of viscoelasticity, pseudostiffness versus number of cycle curves can indicate the degree of material deterioration due to strain/stress caused damage at every cycle. From Figure 6-3 to Figure 6-6, the showcased curves can be averaged results from more than one repeated test with the same rest period. While variation between curves under same condition does occur, only the representative stiffness development curves (reasonable average excluding obviously abnormal curves) are demonstrated since this improves the reliability of results.

6.2.1. General Trend of Rest Period Healing

Regarding the findings from the stiffness development curves, firstly, it is obvious that longer rest periods demonstrate higher lying curves at both 12 and 20^{o}C, regardless of material batches. In other words, all 4 graphs (Figure 6-3 to Figure 6-6) indicate the same trend of rest period related recovery of pseudostiffness. This phenomenon is in line with the fact that longer rest period gives the material more time to recover its micro-cracks (by wetting and diffusion) and thus the material stiffness bounces back to certain extent, then the material performance improves in comparison to continuous loading cases. However, once optimum rest period is reached, any longer rest period barely change the position of curves, e.g. the 1.0s curve in Figure 6-6. Higher lying curves lower the rate of stiffness reduction with number of cycles, while the material at longer rest period indicates a less material deterioration at certain number of loading cycles.

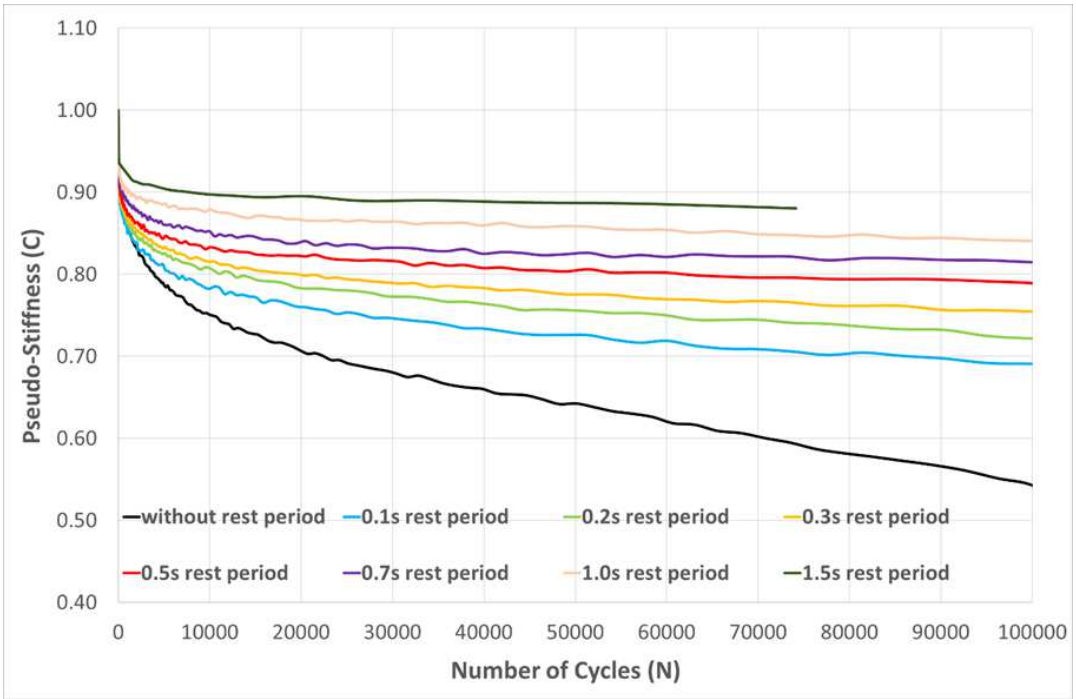

Figure 6-3: Pseudostiffness development with Number of Cycles at 20^{o}C, 200 cyclic microstrain (1st Batch)

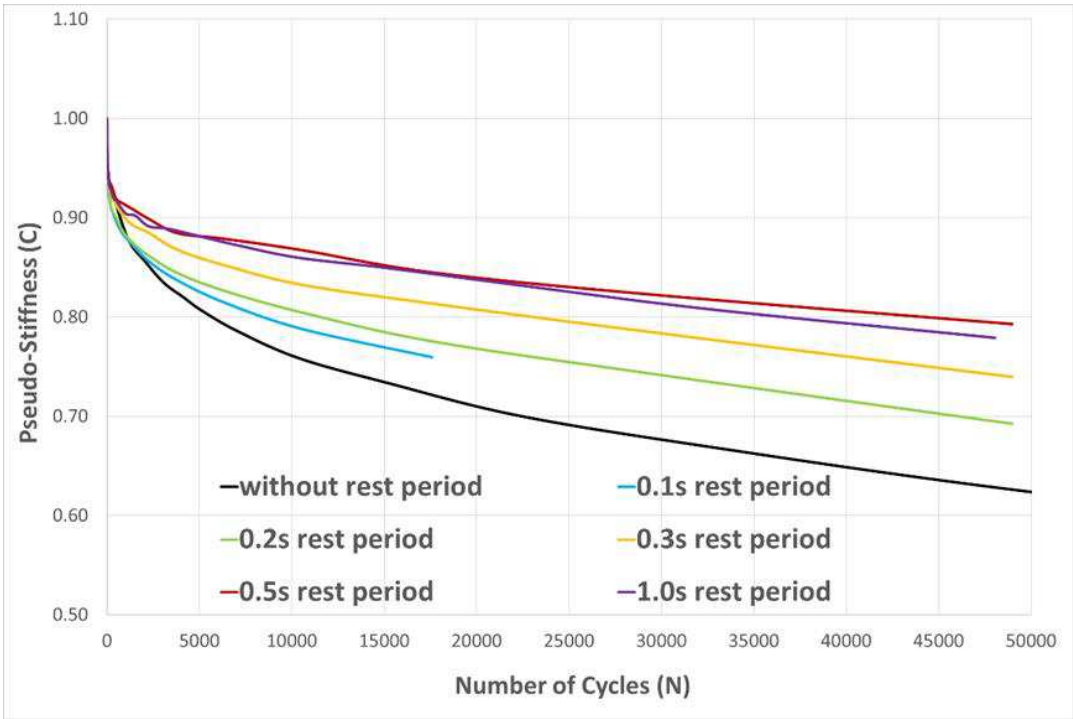

Figure 6-4: Pseudostiffness development with Number of Cycles at 12^{o}C, 200 cyclic microstrain (1st Batch)

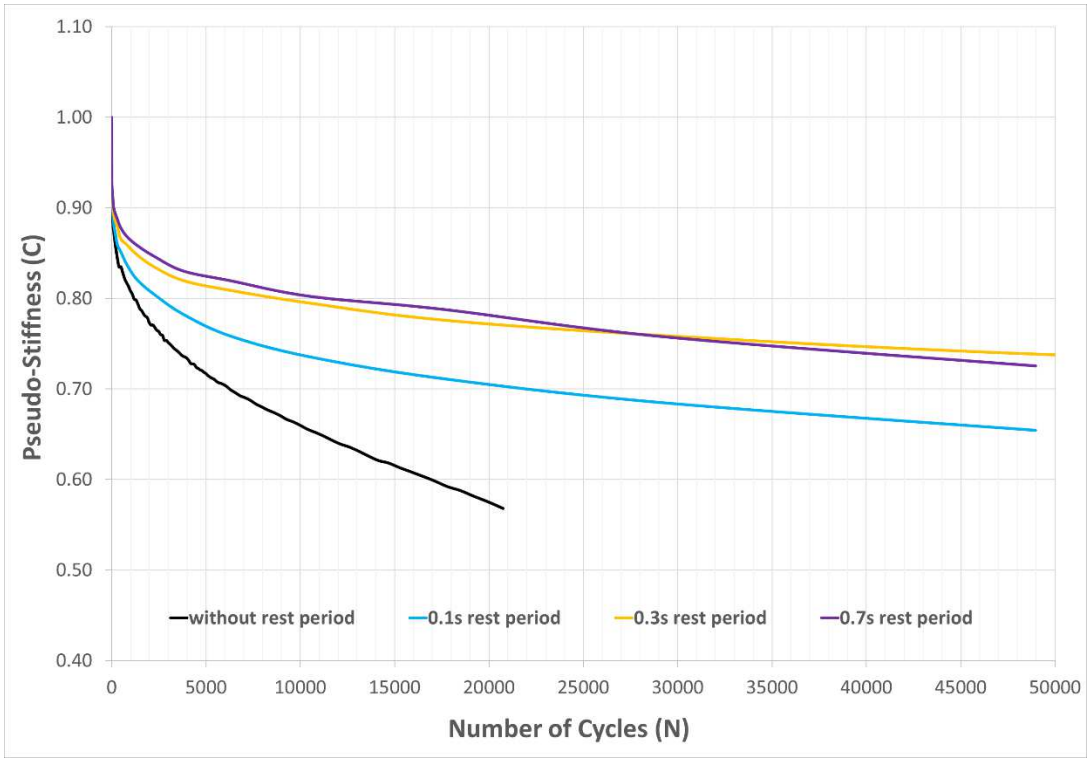

Figure 6-5: Pseudostiffness development with Number of Cycles at 20^{o}C, 250 cyclic microstrain (2nd Batch)

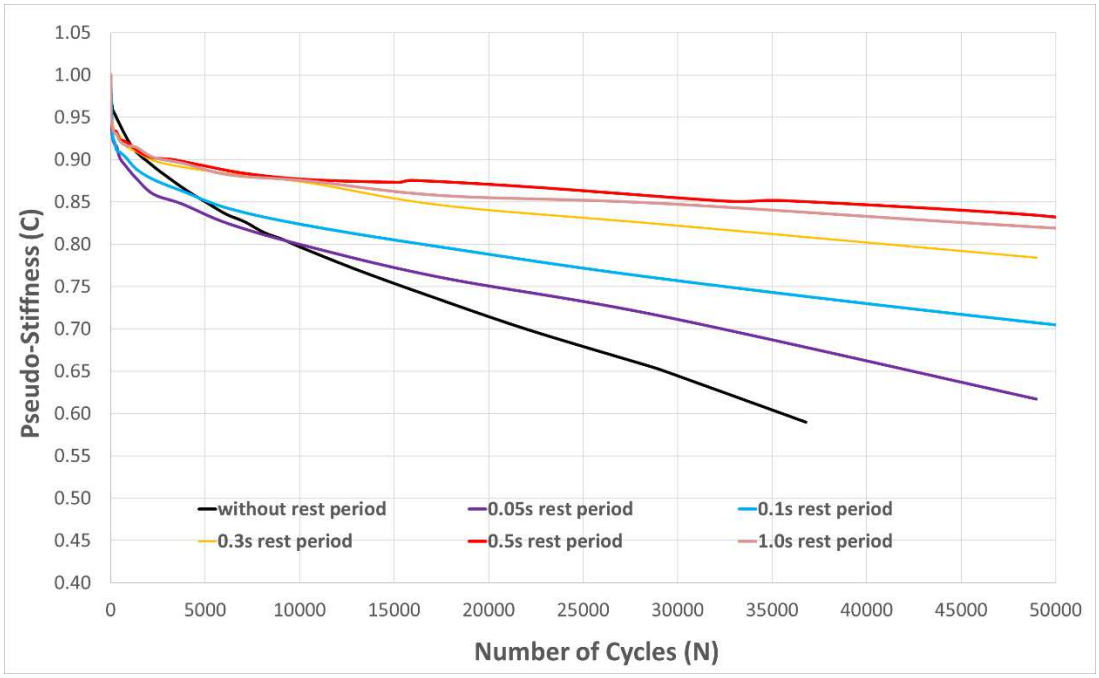

Figure 6-6: Pseudostiffness development with Number of Cycles at 12^{o}C, 200 cyclic microstrain (2nd Batch)

6.2.2. Study Healing Effect through Healing Ratio Method

It is evident from all 4 graphs (Figure 6-3 to Figure 6-6) that the improvement of rest period healing effect diminishes as the rest period goes higher. For instance, the gap between the curves of 0.1s and 0.3s rest period is relatively larger than the gap between curves of longer rest period, say between 0.3s and 0.5s curves, although the increase of rest period is the same as 0.2s. The same trend can be observed regardless of test temperature and mixture batches. In other words, the effect of rest period is to slow down the material deterioration by demonstrating less stiffness, while the healing rate per length of rest period decreases gradually with longer rest period. To clearly demonstrate this method with reference to Zeiada (2012)'s healing ratio method, the effect of rest period on the healing capacity are represented by the following equation:

$$HR = (C_x - C_0)/(1 - C_0) \tag{6.1}$$

in which C_x is the pseudostiffness at a designated x number of cycle for a test with certain length of rest period, C_0 is the pseudostiffness at the same number of cycle for a test with no rest period. Thus the healing ratio factor at certain cycle number for various rest periods is drawn in Figure 6-7, Figure 6-8, Figure 6-9 and Figure 6-10 corresponding to stiffness development curves from Figure 6-3 to Figure 6-6 respectively. Figure 6-7 and Figure 6-8 are for first batch mixtures with healing ratio calculated using C at 50,000 number of cycles (C_x=$C_{50,000}$). Regarding Figure 6-9 and Figure 6-10, they are for second batch of mixture, which is stiffer as demonstrated by representative stiffness gained from dynamic modulus tests (compare results between Table 5-1 and Table 5-2), so 25,000 cycles is selected for healing ratio calculation. Due to lack of test results at 200 microstrain for batch 2 mixture under 20^{o}C, the strain amplitude is 250 microstrain instead.

Also a concept of optimum rest period has been introduced to indicate a certain length of rest period, beyond which further rest period increase incurs little or no material healing (Zeiada, 2012). This parameter may not be directly shown from Figure 6-7 to Figure 6-10, however, it can be reasonably predicted by extrapolation as all four curves will finally be almost completely flat if rest period keeps

increasing. Zeiada (2012) conducted similar tests with various rest periods and obtained similar findings.

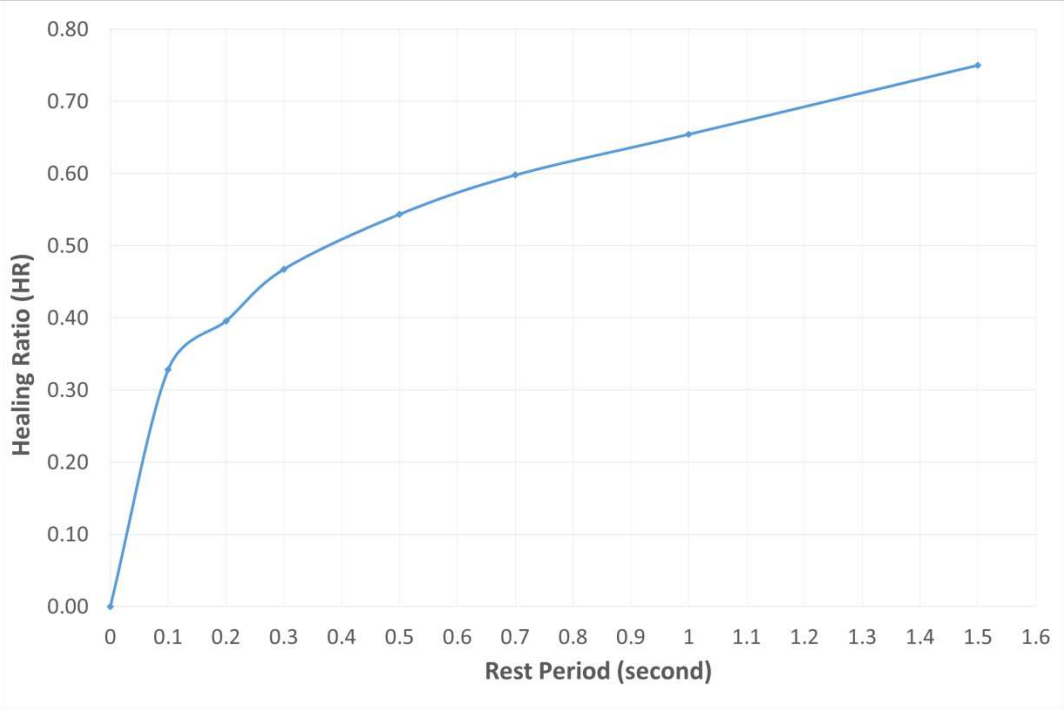

Figure 6-7: Healing ratio with rest period curve at 50,000 cycles under 200 microstrain tension-compression and 20^{o}C (Batch1 mixture)

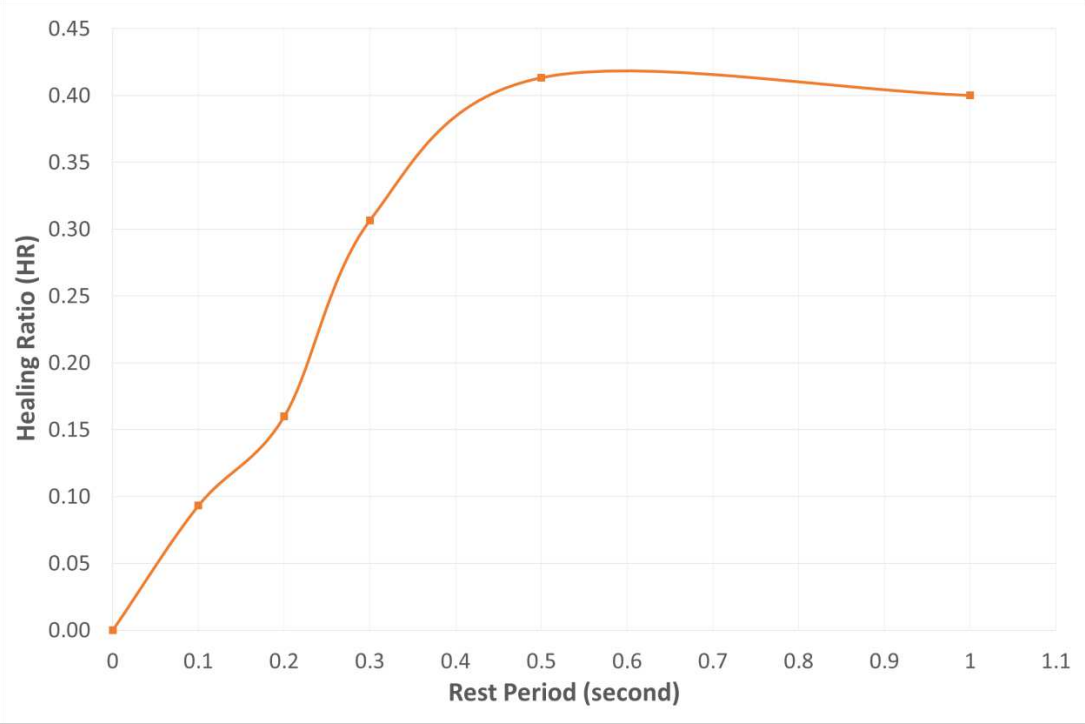

Figure 6-8: Healing ratio with rest period curve at 50,000 cycles under 200 microstrain tension-compression and 12^{o}C (Batch1 mixture)

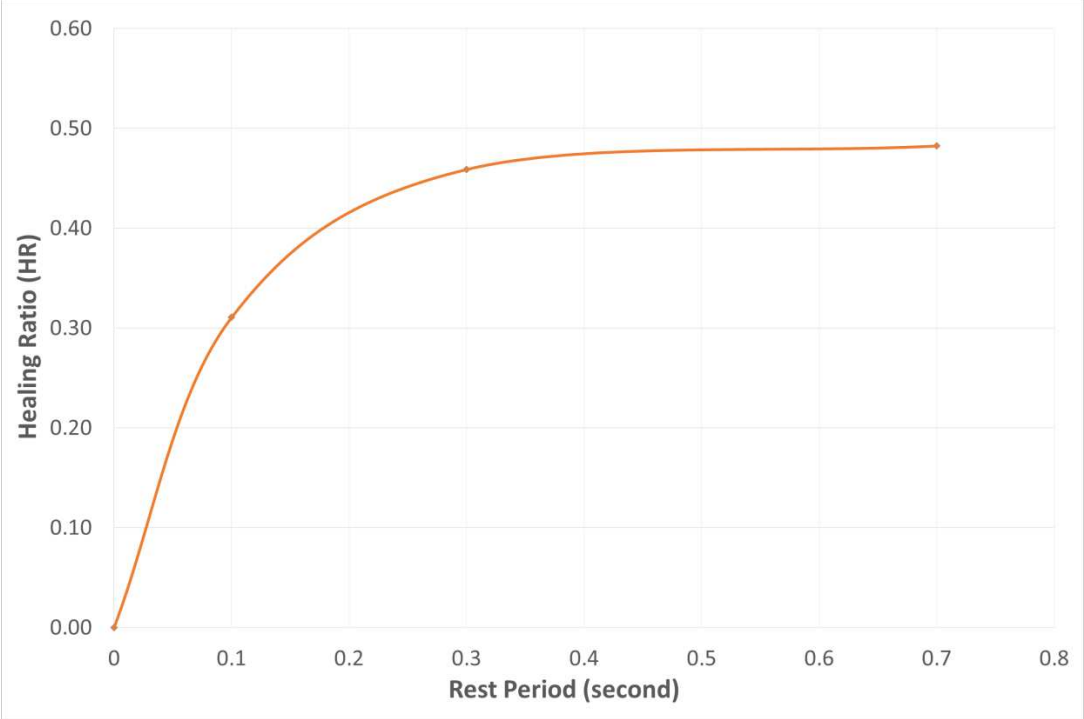

Figure 6-9: Healing ratio with rest period curve at 25,000 cycles under 250 microstrain tension-compression and 20^{o}C (Batch2 mixture)

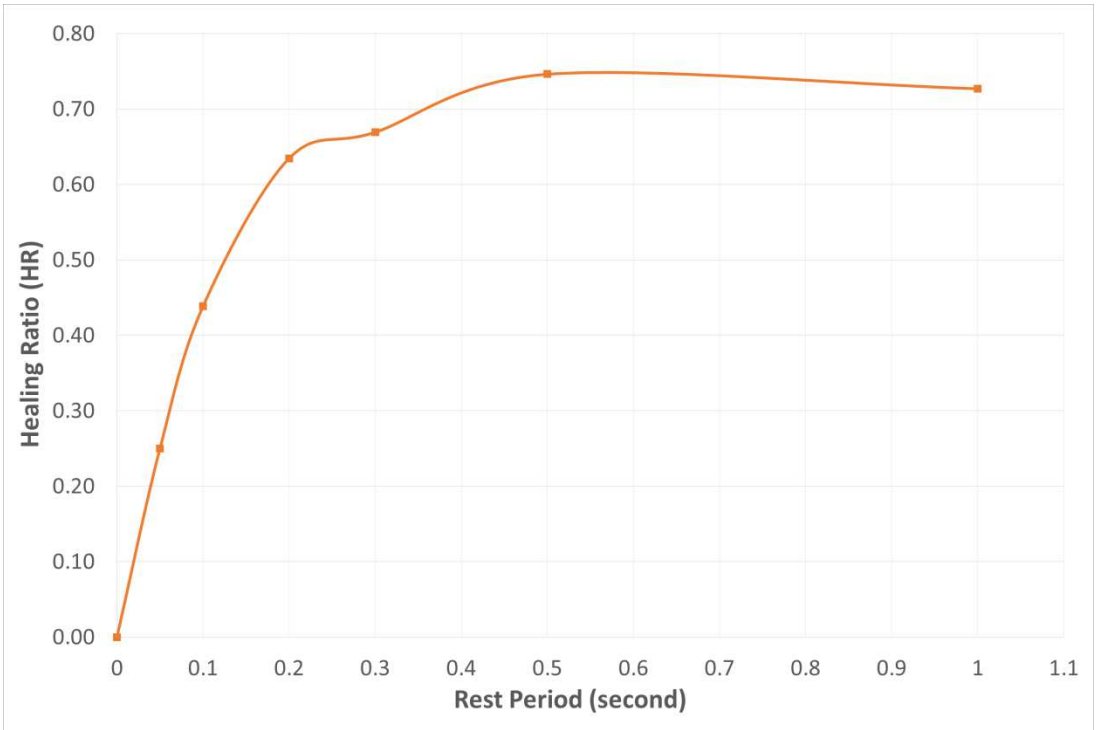

Figure 6-10: Healing ratio with rest period curve at 25,000 cycles under 200 microstrain tension-compression and 12^{o}C (Batch2 mixture)

6.2.3. Investigate Healing Ratio at Different Temperatures

Figure 6-11 puts together curves of batch 1 mixture in Figure 6-7 and Figure 6-8 since they are the same mixture tested under the same strain amplitude but at different temperatures of 20 and 12^{o}C respectively. It is evident that healing ratio at 20^{o}C is well above that of 12^{o}C, although the strain amplitude is the same. This is an indication that higher temperature improves asphalt healing, as proposed by most other relevant studies on rest period healing. Figure 6-12 summarizes Figure 6-9 and Figure 6-10 for batch 2 mixtures. Interestingly, 12^{o}C curve demonstrates higher healing ratio than that of 20^{o}C, and this is against batch 1 results in Figure 6-11 and wider findings that healing effect is smaller under lower temperature (Qiu et al., 2012a, Shen et al., 2010). One possible trigger of this effect may be a larger strain amplitude of 250 microstrain is applied on 20^{o}C results for batch 2 material, since increased strain amplitude means larger damage that somehow restricts healing effect. However, the 20^{o}C curve in Figure 6-12 is well below that of 12^{o}C, large strain level alone may not explain the scale of the difference while the validity of measuring healing ability through heal ratio factor only may be doubtful when there are different temperatures and strain amplitudes, so this phenomenon will be further investigated from results of damage curves and beam fatigue tests with rest periods.

Else, from both Figure 6-11 and Figure 6-12, all curves become flatter, or demonstrate decreasing tangent ratio, with longer rest period. This indicates the ratio of healing effect improvement per unit of rest period is decreasing with rest period, in other words, initial rest period obviously brings out stronger healing, while the later increase of rest period also causes more healing, much to a less extent. Else, Figure 6-11 and Figure 6-12 prove that lower temperature reduces optimum rest period, which is represented by a flat or nearly flat section of the curves. For instance, in Figure 6-11, the 12^{o}C curves become almost flat after a rest period of 0.5 seconds, which indicates that rest period larger than 0.5s has almost the same healing effect as that of 0.5s. On the contrary, the 20 ^{o}C curve in Figure 6-11 is still increasing after 0.5s, with 0.7s and 1.0s rest period still bringing out higher healing ratio. Although curves for batch 2 mixture in Figure 6-12 are from different strain amplitude, 12^{o}C curve still has a more obvious sign of reaching optimum rest period at around 0.3 – 0.5 seconds, while the 20^{o}C curve seems still increasing, although

very slightly. Besides, healing ratio is a reliable measurement for optimum rest period, since a flat section will always appear in such curve, which means same stiffness development curves (such as seen in Figure 6-3 and Figure 6-6) for rest periods above the optimum rest period.

To sum up, the following findings are made from investigation of stiffness development curves and healing ratio:

1. Longer rest period (before optimum rest period) always improves asphalt healing, and indicating larger healing ratio. However, there is always an optimum rest period that any larger rest period just keeps but not improve the healing capacity
2. the improvement of healing effect per second of rest period is not linear to the length of rest period. On the contrary, the ratio of healing improvement diminishes with longer rest period.
3. Compared to 12 ^{o}C, 20 ^{o}C has demonstrated higher optimum rest period for both batches of mixture, this also means the potential maximum rest period healing effect for 20 ^{o}C is higher than 12 ^{o}C

However, the above studies only refer to two temperatures and one typical asphalt mixture at the moment, more tests at higher or lower temperature and different mixtures are required to further verify and possibly quantify the temperature effect on rest period healing. Also, it is equally important to solve problems due to extreme temperatures as discussed in Section 3.9.1.

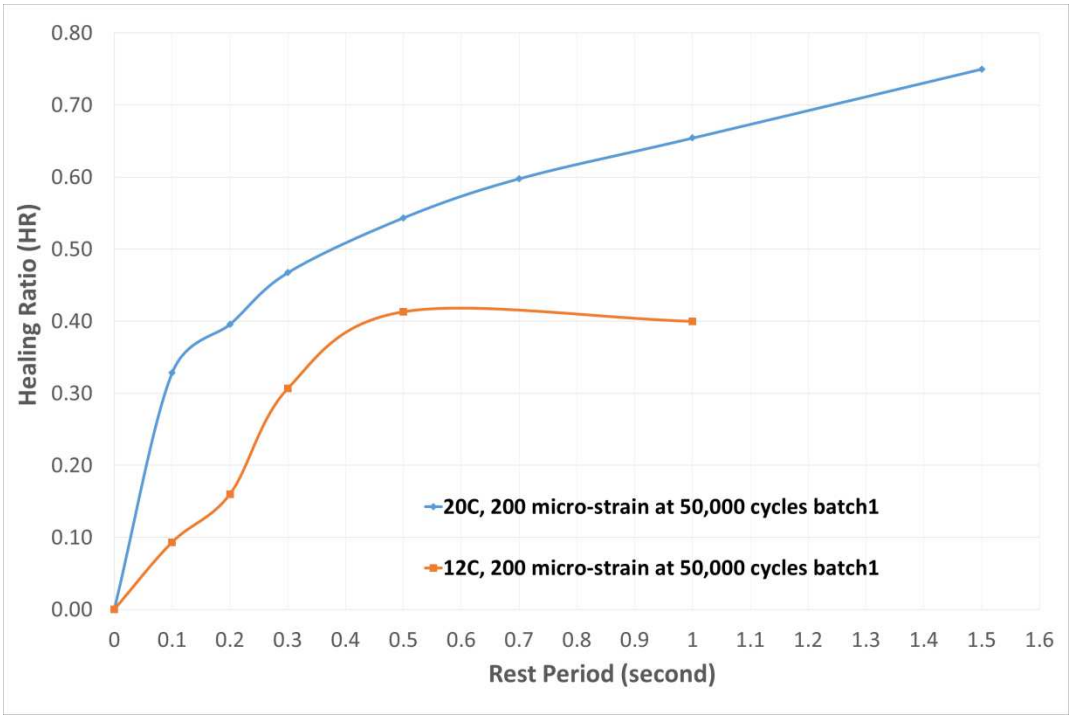

Figure 6-11: Batch 1 mixture healing ratio with rest period curves at 12 and 20°C, all under 200 microstrain

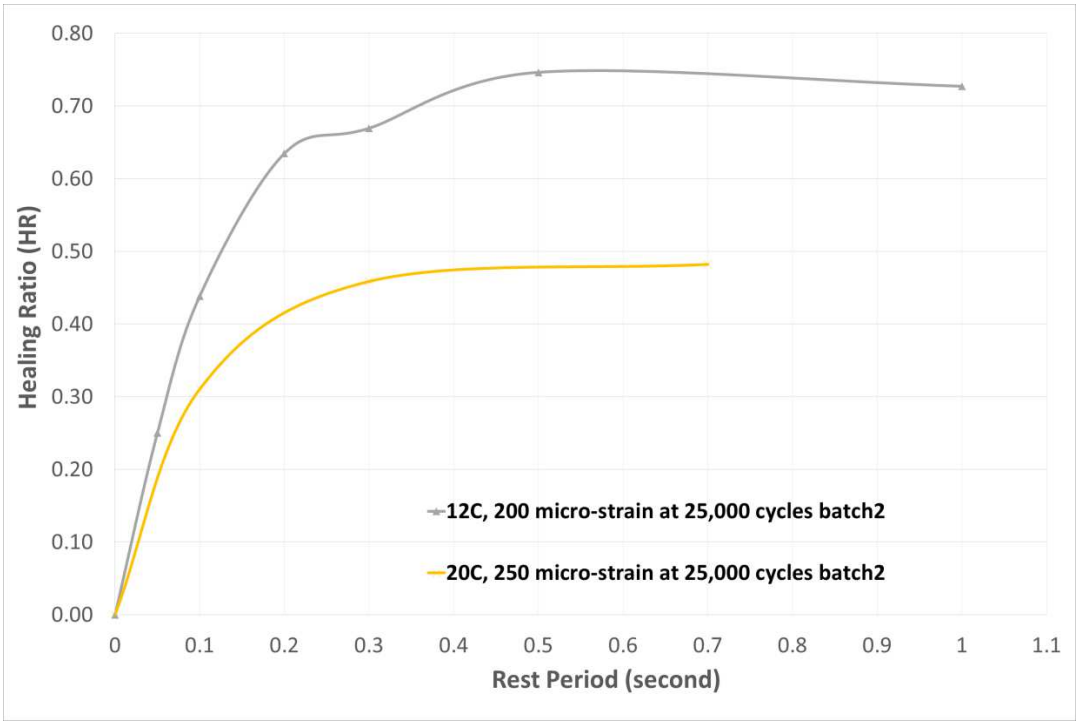

Figure 6-12: Batch 2 mixture healing ratio with rest period curves at 12 and 20°C, and strain level of 200 and 250 microstrain respectively

6.2.4. Statistical Results of Failure Stiffness

A stiffness reduction of 50% is widely regarded as an indication of asphalt fatigue failure for constant strain cyclic loading tests, but this only applies to 20°C. The failure stiffness also represents the formation of macro-cracks within asphalt mixture specimen. In a AMPT fatigue test, the fatigue failure is indicated by a sudden drop of material pseudostiffness value as demonstrated in Figure 6-13. It is necessary for crack to occur within the LVDT range (see Figure 3-10) to capture an accurate failure point. For all tests conducted in this research, the failure stiffness for 20°C is found to be close to the conventional 0.5 pseudostiffness, with variation between 0.5 to 0.6. However, at 12 °C, the failure stiffness shows a much larger fluctuation but normally higher than 0.5, ranging from 0.6 to 0.75. Figure 6-13 demonstrates two exemplary stiffness development curves at both temperatures. It is obvious that the failure stiffness for 12°C of around 0.71, is obviously higher than the failure stiffness at 20°C of 0.585 approximately.

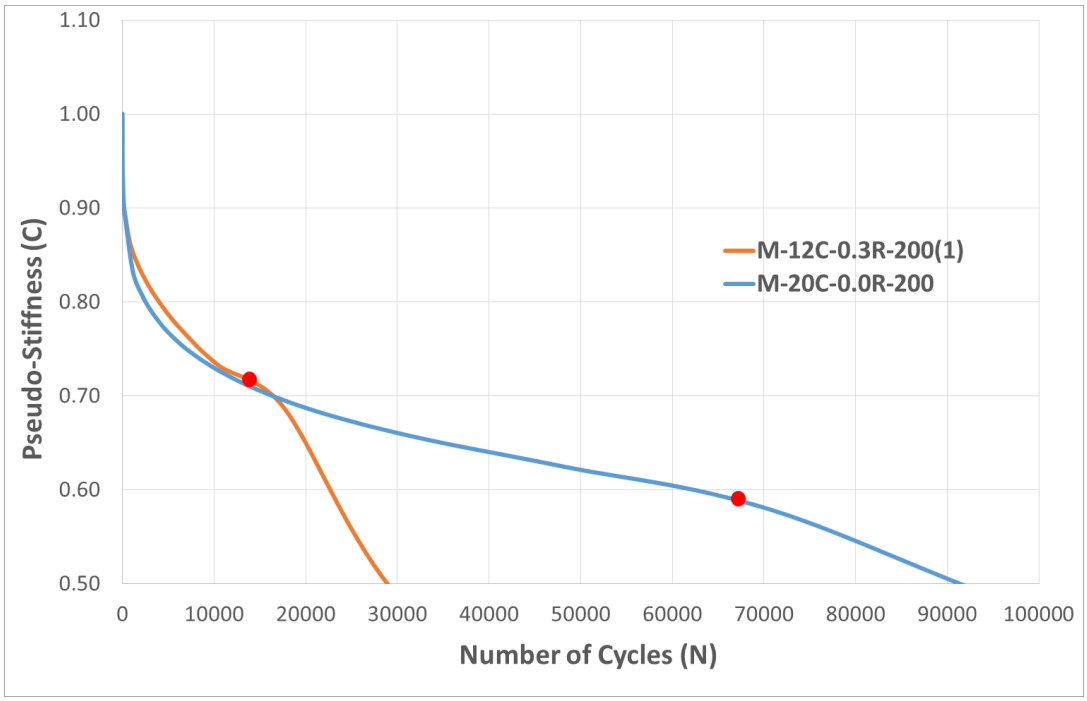

Figure 6-13: Example Stiffness Development Curves at both 12 and 20°C and their relative failure stiffness (red dots)

6.3. Damage Characteristic Curves from VECD Tests with Rest Period

Based on theories and calculations listed in Section 2.1, Section 5.2 and Section 5.3, damage parameter S is calculated and drawn against pseudostiffness C for each test, so damage characteristic curves are produced. The test temperatures, strain amplitudes and rest periods are set to be varying (as shown in Table 3-6) so their effects can be investigated with a focus on rest period healing effect. Damage characteristic curves under the same temperature are drawn together since temperature will change the healing effect of asphalt mixture. In other words, theoretically, damage curves with healing effect are different at different temperatures, so the healing effect caused by different rest period length can only be investigated under the same temperature.

It should be noted that it is inevitable to have certain degree of experimental fluctuation of tests results especially when rest period healing is present, thus it is necessary to run the tests under certain rest periods more than one time. Actually, the variation in VECD test results and the produced damage characteristic curves are common issue with current experimental practice (Kutay and Lanotte, 2018). In some cases, the test results that are not within acceptable range of accuracy are discarded, and this may be caused by reasons such as inevitable variation of mixture properties during the mixing and compaction procedures, or machine incidents such as gauging knots failure and glue failure.

6.3.1. Regression Coefficients for Damage Characteristic Curve

Firstly, an exemplary damage characteristic curve for specimen "L-20C-0.3R-300" at 20^{o}C and 0.3s rest period is shown in Figure 6-14. The damage characteristic curves produced from damage equation Eq.(5.11) using experimental data are marked as "TEST" after the specimen label, such as "L-20C-0.3R-300 TEST". Then curve fitting equation Eq. (5.13) is applied to produce a regression curve by solving for the regression parameters C1 and C2 using EXCEL's solver function. The purpose of EXCEL's solver function is to reach a minimum difference between pseudostiffness calculated based on tests output using Eq.(5.9) and pseudostiffness

calculated based on model equation Eq. (5.13). Specifically, the curve fitting tool such as EXCEL calculates the C1 and C2 values that yield the minimum sum of standard error between test and model C values. After trial and error, it is concluded that the "Non-Linear GRG" method provided by EXCEL plus Eq.(5.13) is the most effective approach for curve fitting of damage curves produced in this study. For instance, Figure 6-14 also indicates regression curve of the same specimen, marked as "MODEL" curve, which agrees perfectly with the "TEST" curve. As a convention in VECD research, the damage characteristic curves illustrated in this study are also regression curves only, unless specified otherwise.

Else, the damage curve produced in this study is based on simplified VECD procedures and methods listed in AASHTO TP107-14 as mentioned in Section 5.2 and Section 5.3, while no viscoplastic or post failure response is included. As a result, for typical test results such as Figure 6-13, damage curves are produced based on tests data excluding the section after the fatigue failure point.

Consequently, C1 and C2 values for each simplified VECD test are produced and listed in from Table 6-1 to Table 6-4. For the repeated tests under the same rest period, the average damage characteristic curves are produced by calculating average C1 and C2 values of repeated tests and then substitute them back into curve fitting equations of Eq. (5.13) to draw representative damage curves for each rest period under certain temperature. This method has been found to be an effective solution to deal with repeated VECD tests and capable of producing accurate and reasonable damage characteristic curves compared to curves produced by single test only, which subject to inevitable experimental fluctuation. However, certain curve fitting technique is required to produce correct average C1/C2 values and reasonable representative damage curve, rather than directly taking the values returned the software's solver function. As a result, representative damage characteristic curves at each rest period are produced and described in below sections.

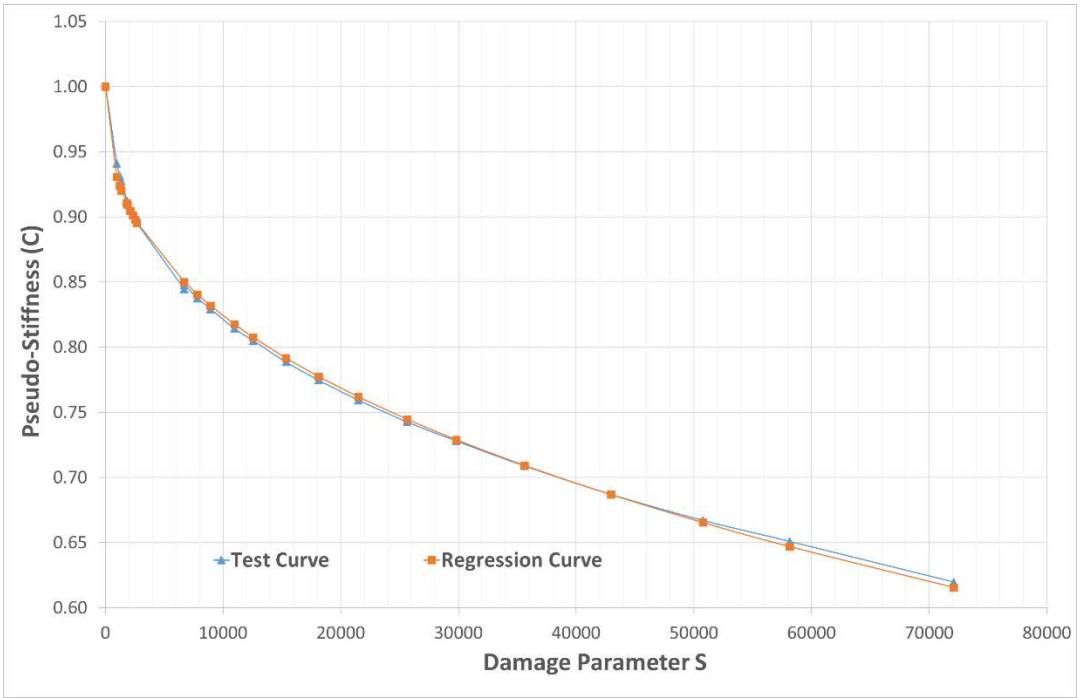

Figure 6-14: Example damage characteristic Curve from test data and curve fitting (20°C, 200 microstrain, 10Hz, 0.3s rest period or "L-20C-0.3R-300")

6.3.2. Batch 1 Mixture Tested under 20°C

For Batch 1 mixture, it is firstly tested under 20°C with a series of rest periods and Table 5-10 gives a full list of tests under this condition. To clearly illustrate each damage curve alongside with average curve for certain rest period, Figure 6-15 to Figure 6-21 present damage curves with rest periods of 0, 0.1, 0.2, 0.3, 0.5, 0.7 and 1 second respectively. From those figures, it is evident that using average C1 and C2 values (see Table 6-1), reasonable representative damage curve for a specific rest period has been produced, as they are at an average position of individual test curves. In addition, all average curves for each rest period are drawn together in Figure 6-22 to clarify the rest period healing effect.

Else, damage characteristic curves of individual tests under same rest period are mostly close to each other, although certain variation of test results exists since specimen can not be perfectly similar with each other and they vary in void ratio (but within 0.6%) as well as there is inevitable fluctuation with current simplified VECD tests. One exception of relatively large variation between individual curves is

the 1s rest period in Figure 6-21. This also indicates the need to produce a representative curve since individual test may give deviated results.

Table 6-1: C1 and C2 values for Batch 1 mixture tested under 20^{o}C

Rest Period (S)	Specimen Label	C1	C2	AVG C1	AVG C2
0	L-20C-0.0R-200 (1)	0.0013	0.5273	0.0011	0.5558
	M-20C-0.0R-200	0.0010	0.5713		
	L-20C-0.0R-200 (2)	0.0010	0.5689		
0.1	M-20C-0.1R-200	0.0032	0.4681	0.0030	0.4500
	L-20C-0.1R-200 (1)	0.0032	0.4400		
	L-20C-0.1R-200 (2)	0.0025	0.4700		
0.2	L-20C-0.2R-200 (1)	0.0038	0.4205	0.0034	0.4344
	L-20C-0.2R-200 (2)	0.0030	0.4482		
0.3	L-20C-0.3R-200 (1)	0.0039	0.4152	0.0038	0.4143
	L-20C-0.3R-200 (2)	0.0038	0.4149		
	L-20C-0.3R-400	0.0038	0.4129		
0.5	L-20C-0.5R-200	0.0047	0.3858	0.0044	0.3924
	L-20C-0.5R-300	0.0042	0.3991		
0.7	L-20C-0.7R-200 (1)	0.0042	0.3923	0.0042	0.3893
	L-20C-0.7R-200 (2)	0.0041	0.3862		
1	L-20C-1.0R-200 (2)	0.0044	0.3798	0.0049	0.3630
	L-20C-1.0R-200 (3)	0.0050	0.3738		
	L-20C-1.0R-200 (1)	0.0052	0.3355		
1.5	L-20C-1.5R-200	0.0048	0.3485	0.0048	0.3485

Table 6-2: C1 and C2 values for Batch 1 mixture tested under 12^{O}C

Rest Period (S)	Specimen Label	C1	C2	AVG C1	AVG C2
0	S-12C-0.0R-200	0.00045	0.63924	0.000375	0.652302
	M-12C-0.0R-200	0.00030	0.66536		
0.1	M-12C-0.1R-200 (1)	0.00110	0.55186	0.001148	0.541603
	M-12C-0.1R-200 (2)	0.00121	0.53144		
	L-12C-0.1R-200	0.00113	0.54151		
0.2	S-12C-0.2R-200	0.00103	0.54503	0.000948	0.556615
	L-12C-0.2R-200	0.00087	0.56820		
0.3	L-12C-0.3R-200	0.00143	0.49815	0.00142	0.507
	M-12C-0.3R-200 (1)	0.00088	0.57864		
	M-12C-0.3R-200 (2)	0.00098	0.54936		
0.5	M-12C-0.5R-200	0.00151	0.50176	0.00151	0.4878
	L-12C-0.5R-200	0.00150	0.47380		
1.0	M-12C-1.0R-200	0.00193	0.47883	0.0020436	0.456679
	L-12C-1.0R-200	0.00216	0.43453		

Table 6-3: C1 and C2 values for Batch 2 mixture tested under 20^{O}C

Rest Period (S)	Specimen Label	C1	C2	AVG C1	AVG C2
0	M-20C-0.0R-300	0.00047	0.62148	0.00066	0.5929
	M-20C-0.0R-250	0.00084	0.56432		
0.1	M-20C-0.1R-300	0.00213	0.47321	0.00221	0.47112
	M-20C-0.1R-250	0.00234	0.46372		
	M-20C-0.1R-200	0.00215	0.47641		
0.3	M-20C-0.3R-250	0.003	0.42827	0.00268	0.44522
	M-20C-0.3R-300	0.00236	0.46217		
0.7	M-20C-0.7R-250	0.00294	0.4264	0.00294	0.4264

According to Figure 6-22, it is evident that longer rest period yields higher lying damage characteristic curves and this agrees with longer rest period causing more healing so better damage performance. In the meanwhile, similar to pseudostiffness vs number of cycles curves discussed above in Section 6.2, the improvement of damage performance per unit increase of rest period diminishes with the increase of rest period. In other words, this effect can be illustrated by that from 0.1 to 0.3s rest period, the improvement of healing effect is much stronger than that from 0.3 to 0.5s rest period. These findings justify that it is available to use damage characteristic curves to interpret asphalt mixture's rest period healing effect.

Table 6-4: C1 and C2 values for Batch 2 mixture tested under 12^{O}C

Rest Period (S)	Specimen Label	C1	C2	AVG C1	AVG C2
0	M-12C-0.0R-200	0.0002	0.69903	0.00020	0.6990
0.05	M-12C-0.05R-200	0.0015	0.50505	0.00150	0.5050
0.1	M-12C-0.1R-200(1)	0.0023	0.45310	0.00209	0.4597
	M-12C-0.1R-200(2)	0.0019	0.46619		
0.2	M-12C-0.2R-200(1)	0.0020	0.46068	0.00197	0.46168
	M-12C-0.2R-200(2)	0.0020	0.46268		
0.3	M-12C-0.3R-200(1)	0.0026	0.42996	0.00231	0.44058
	M-12C-0.3R-200(2)	0.0020	0.45121		
0.5	M-12C-0.5R-200	0.0030	0.40549	0.00301	0.4055
1	M-12C-1.0R-200	0.0030	0.40414	0.00303	0.4041

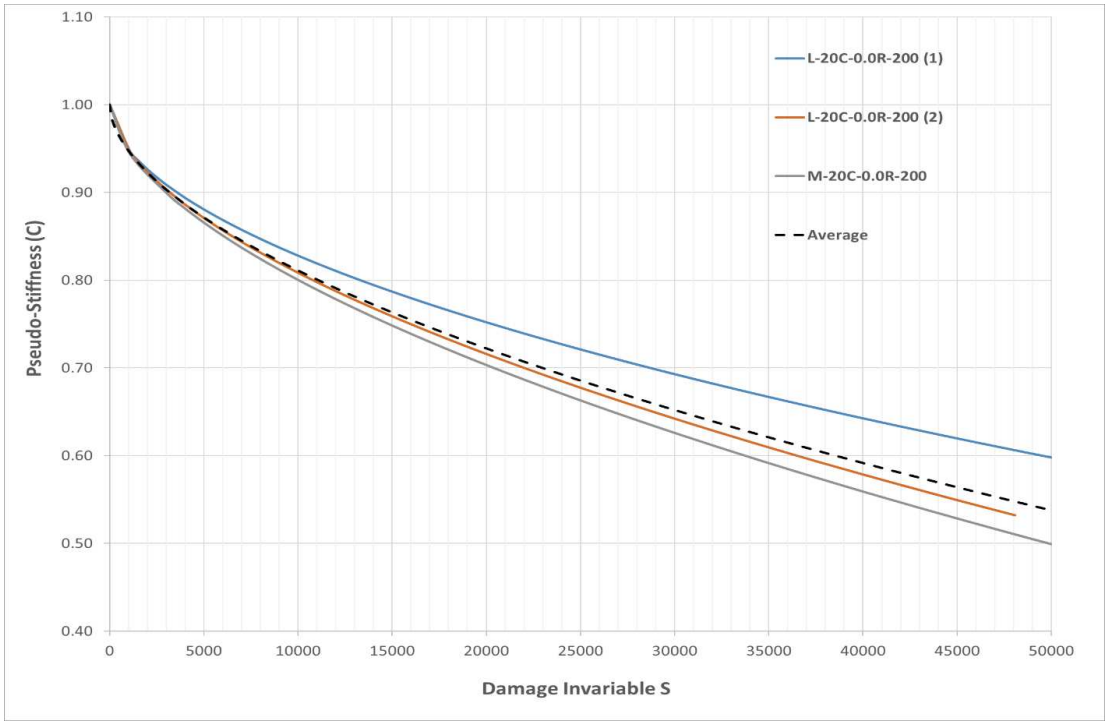

Figure 6-15: All damage curves and average representative curve for continuous loading at 20°C, Batch 1 mixture

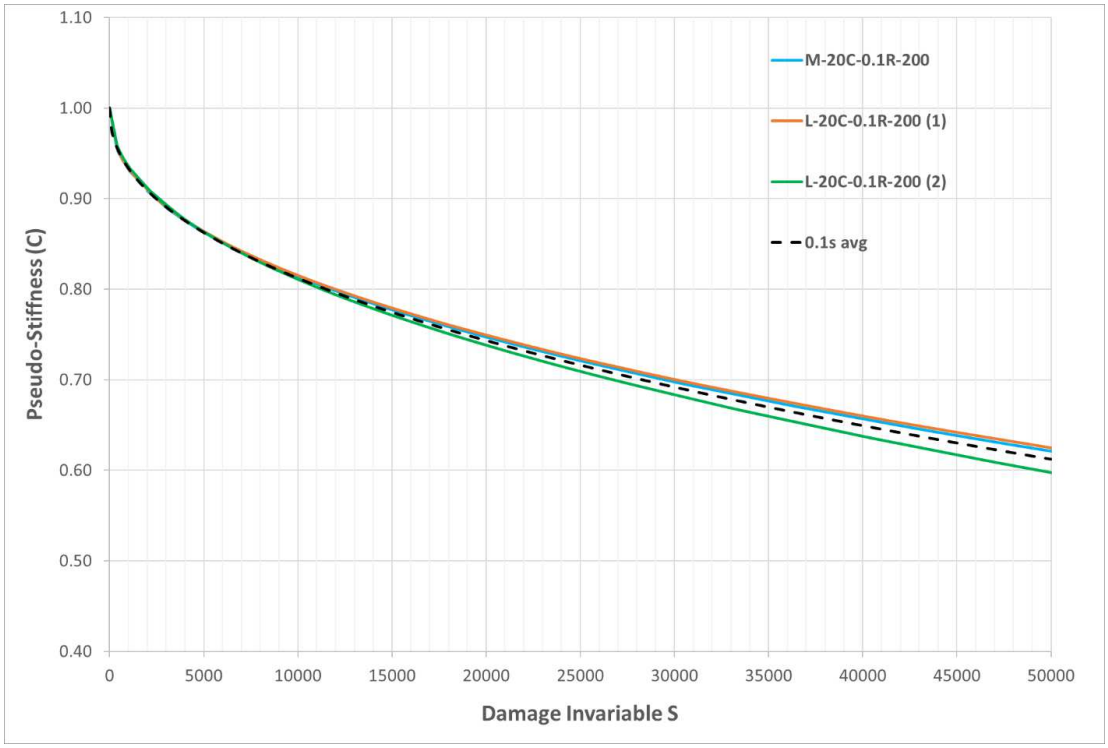

Figure 6-16: All damage curves and average representative curve for 0.1s rest period at 20°C, Batch 1 mixture

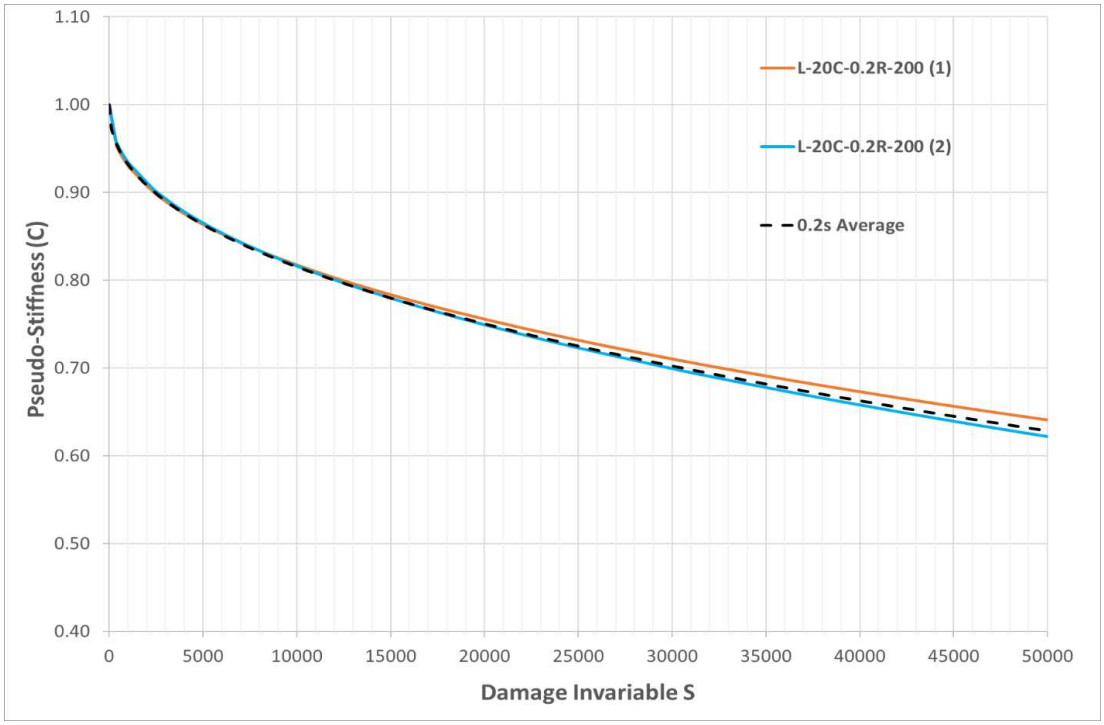

Figure 6-17: All damage curves and average representative curve with 0.2s rest period at 20°C, Batch 1 mixture

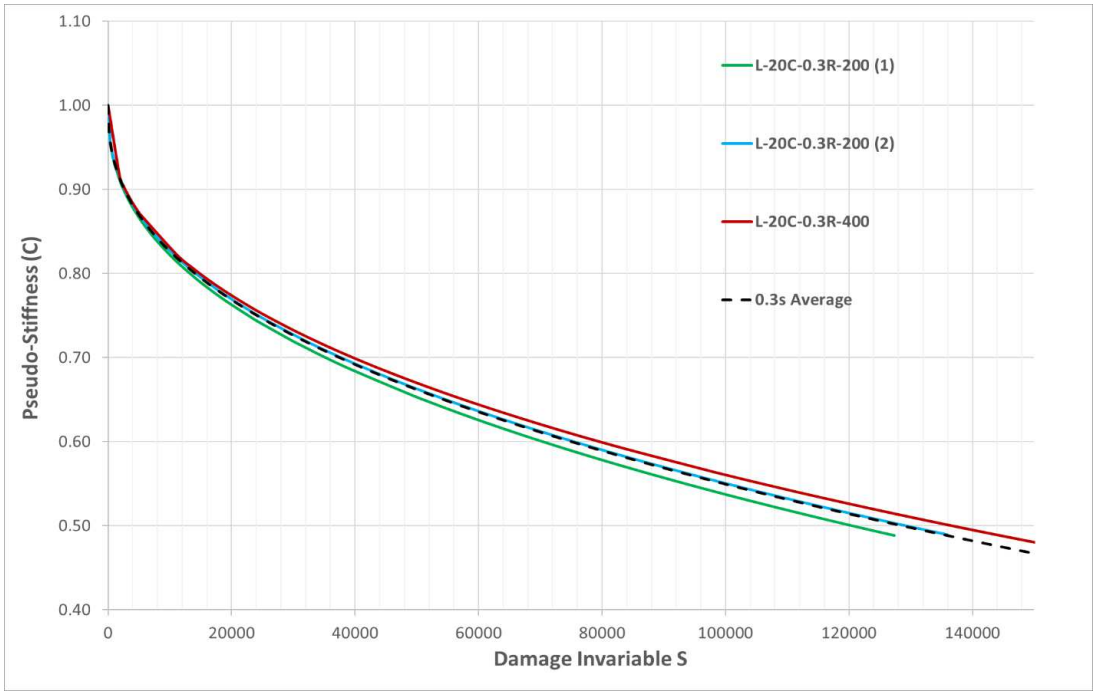

Figure 6-18: All damage curves and average representative curve with 0.3s rest period at 20°C, Batch 1 mixture

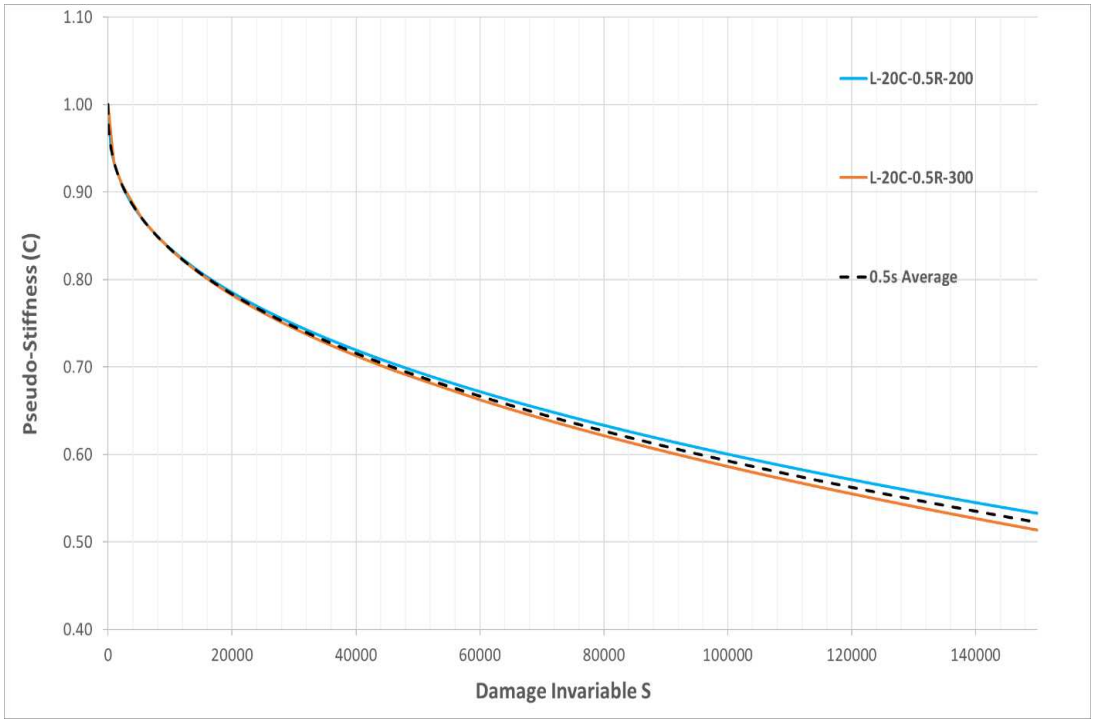

Figure 6-19: All damage curves and average representative curve with 0.5s rest period at 20°C, Batch 1 mixture

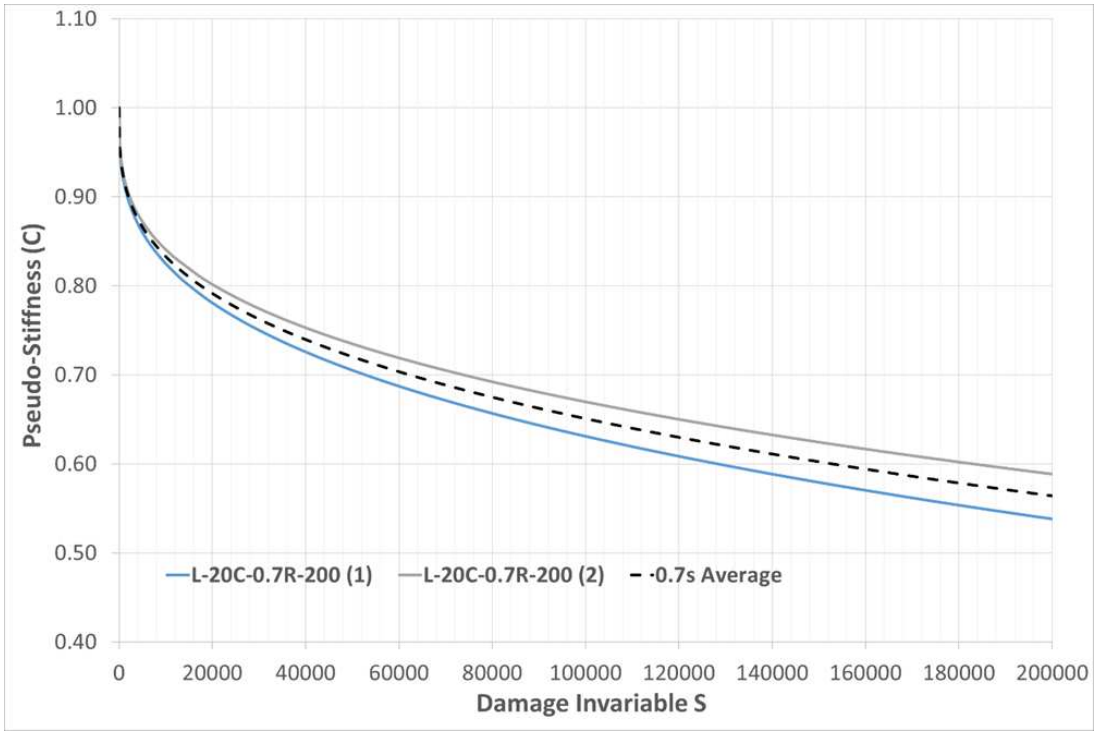

Figure 6-20: All damage curves and average representative curve with 0.7s rest period at 20°C, Batch 1 mixture

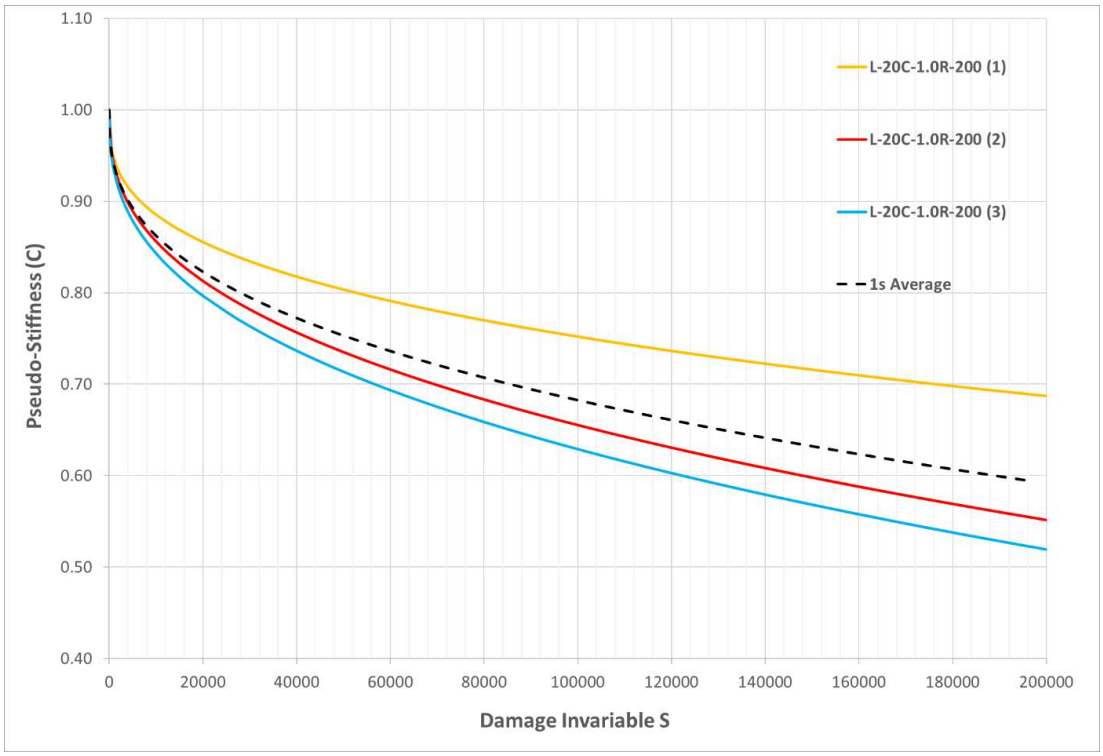

Figure 6-21: All damage curves and average representative curve with 1.0s rest period at 20^{o}c, batch 1 mixture

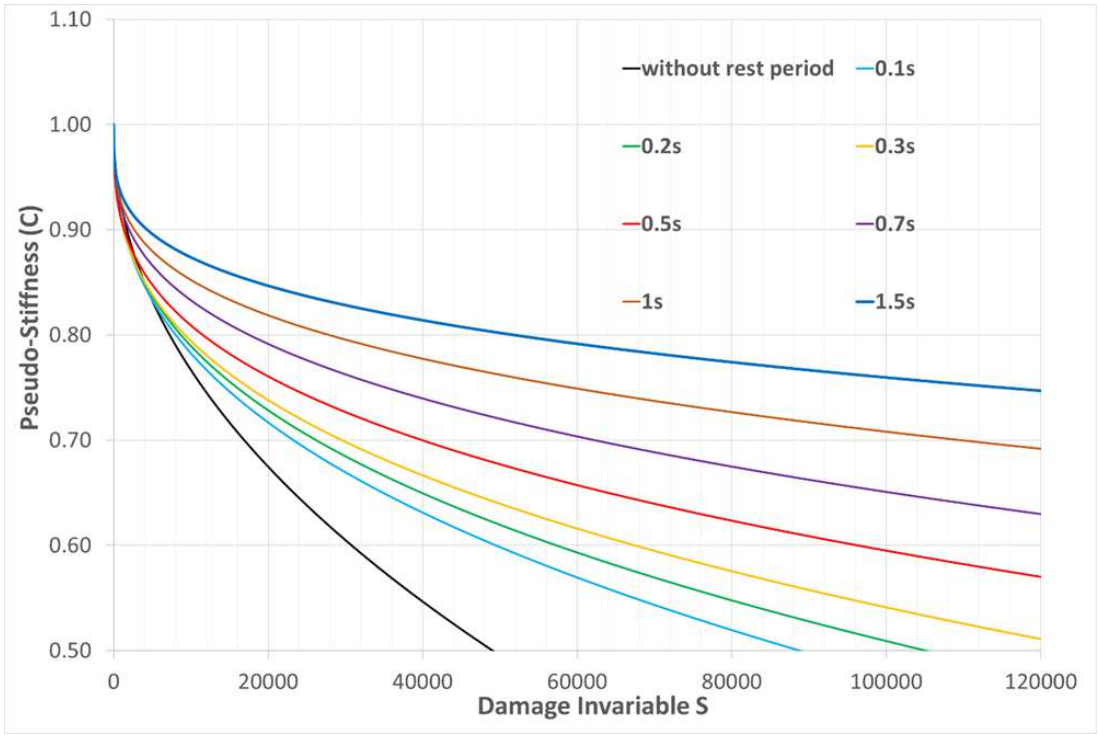

Figure 6-22: Damage characteristic curves under various rest periods at 20^{o}c, batch 1 mixture

6.3.3. Batch 1 mixture tested under 12 ^{o}C

As the temperature reduced to 12^{o}C, the mixture becomes stiffer than 20 ^{o}C, with Elve = 118056 Mpa at 12 ^{o}C compared to 7192 Mpa at 20 ^{o}C (see Table 5-1). While for Batch 1 mixture at 12^{o}C, damage characteristic curves at 0, 0.1, 0.2 0, 0.3, 0.5 and 1.0 second are demonstrated in from Figure 6-23 to Figure 6-28 respectively. Regarding individual tests with same rest period, it is evident that the produced curves show obviously larger variation when rest period becomes higher such as 0.5s and 1.0s. However, the representative curves eliminate individual variance by producing an averagely positioned damage curve for each rest period. Average damage characteristic curves at various rest period of 12 ^{o}C are summarized in Figure 6-29. Based on these figures, the effect of rest period healing is found to be similar to that of 20^{o}C described in last section. Although the general trend of rest period healing is reasonably illustrated as in Figure 6-29, the distance between 0.1 and 0.2s curves is too small compared to that of between 0.2 and 0.3s, this is probably caused by experimental fluctuation of data. In this case, it is difficult to directly identify which rest period may have subjected to too larger deviation from scientific average. Running more repeated tests under same rest period is a solution but this is highly time consuming. However, this problem will be further discussed with solution proposed in later Section 6.4 of this chapter.

Else, at 12^{o}C, the difference between curves of 0.5 and 1s rest period is very small and this indicates the optimum rest period is around 0.5s, so further increase of rest period has little improvement of healing effect. On the contrary, Figure 6-22 still demonstrates further healing effect from 1s to 1.5s rest period, which means optimum rest period is no less than 1.5s. A smaller optimum rest period compared to that of 20^{o}C agrees with findings made by stiffness development curves as shown in from Figure 6-4 and Figure 6-11.

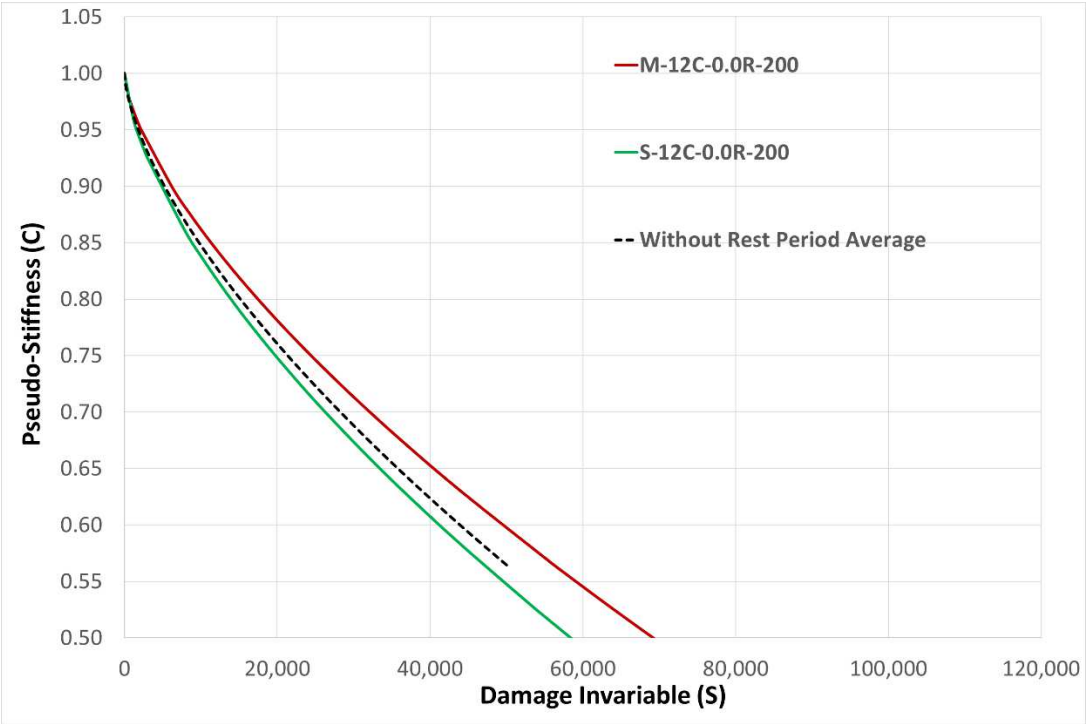

Figure 6-23: Damage characteristic curves without rest periods at 12^{o}c, batch 1 mixture

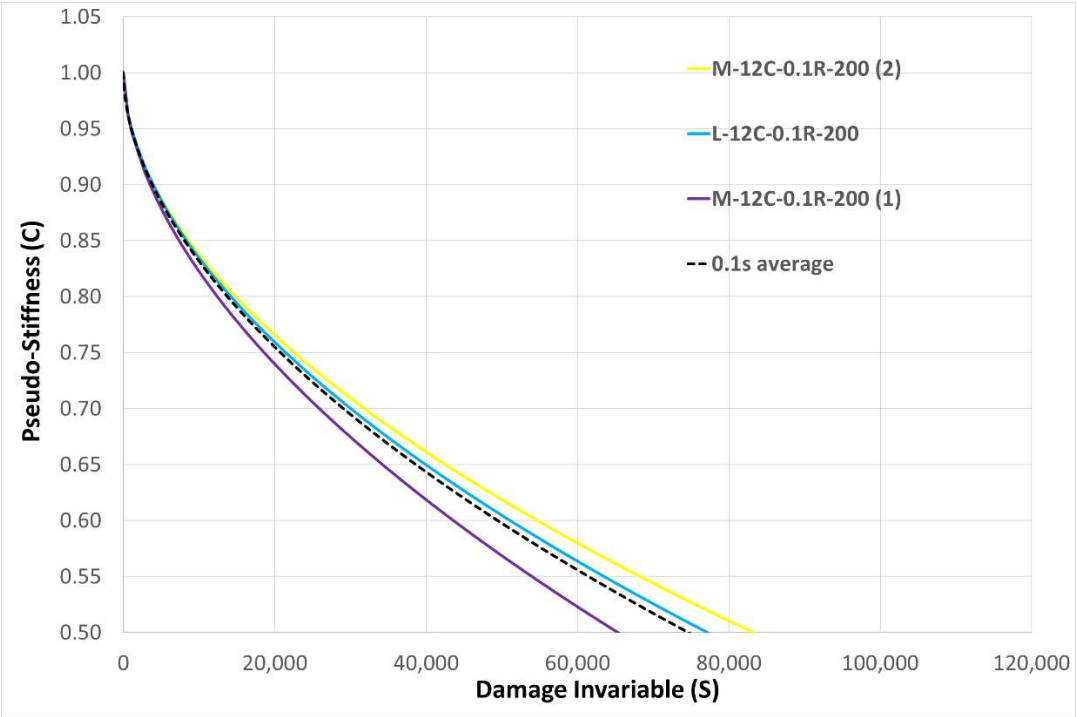

Figure 6-24: Damage characteristic curves under 0.1s rest periods at 12^{o}c, batch 1 mixture

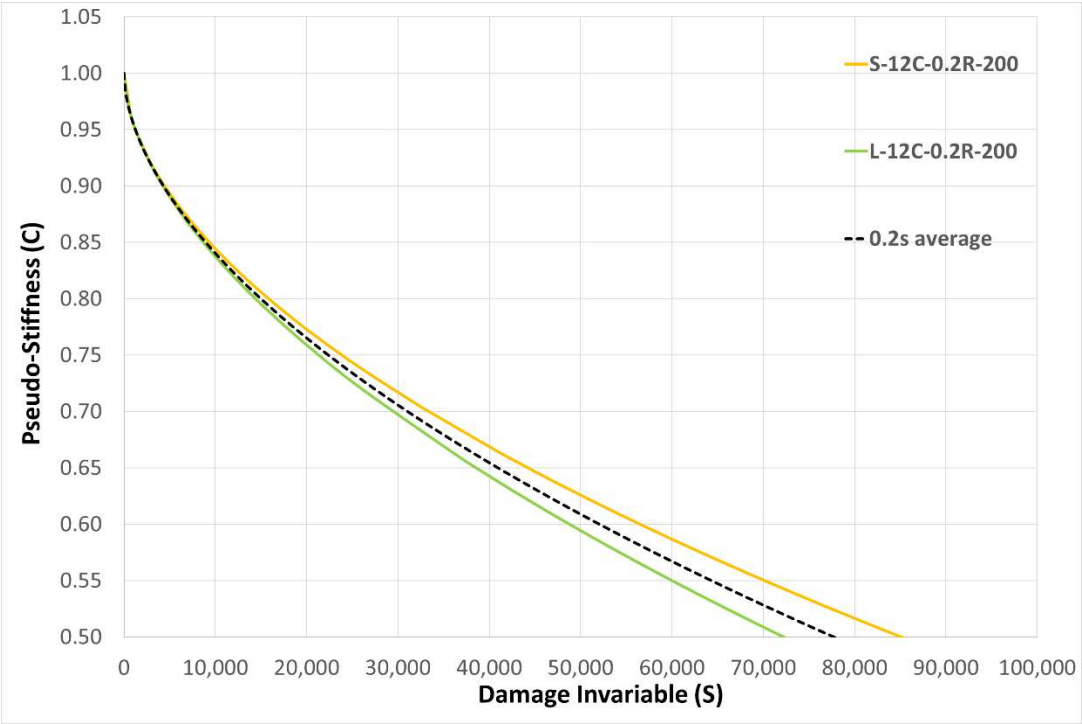

Figure 6-25: Damage characteristic curves under 0.2s rest periods at 12^{o}c, batch 1 mixture

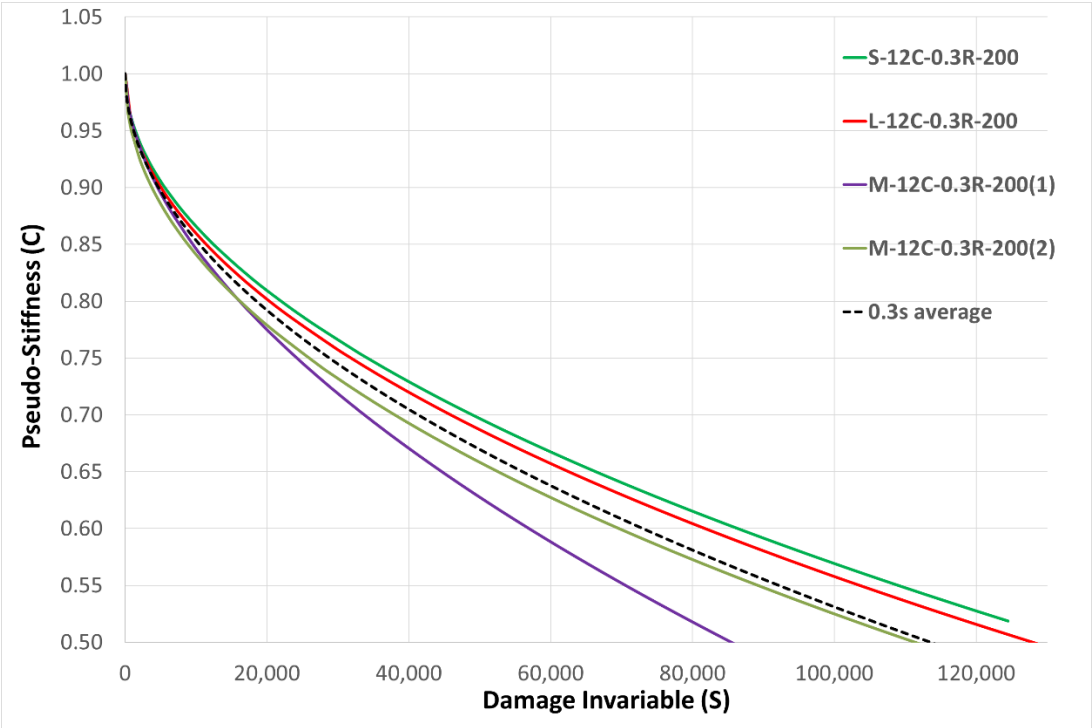

Figure 6-26: Damage characteristic curves under 0.3s rest periods at 12^{o}c, batch 1 mixture

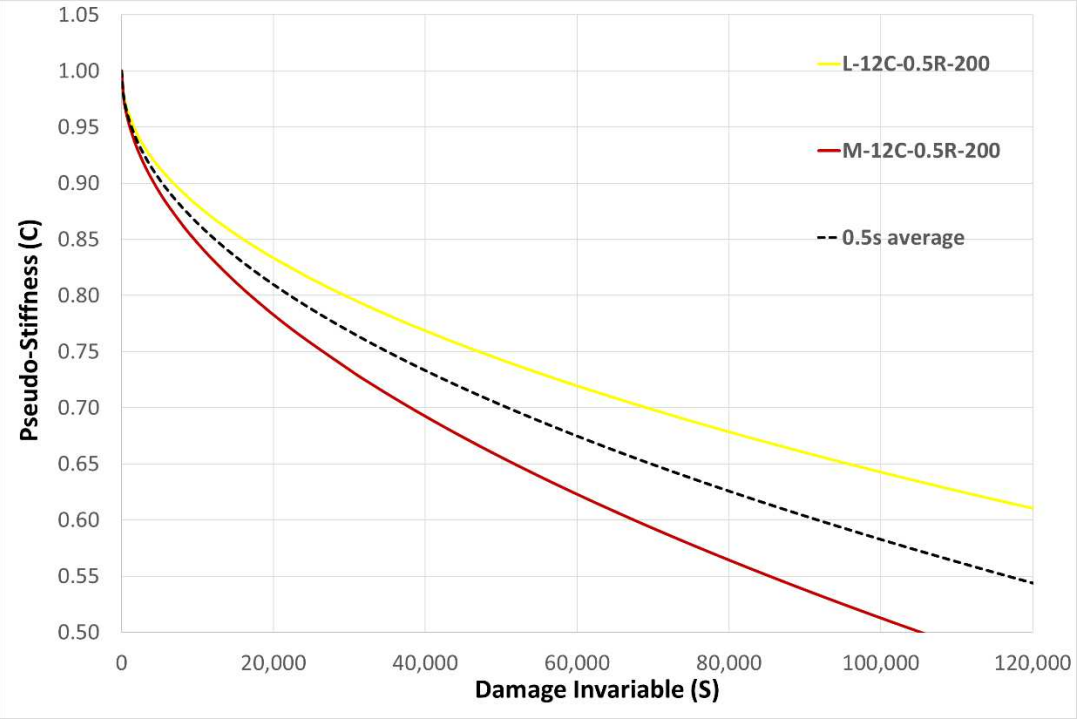

Figure 6-27: Damage characteristic curves under 0.5s rest periods at 12^{o}c, batch 1 mixture

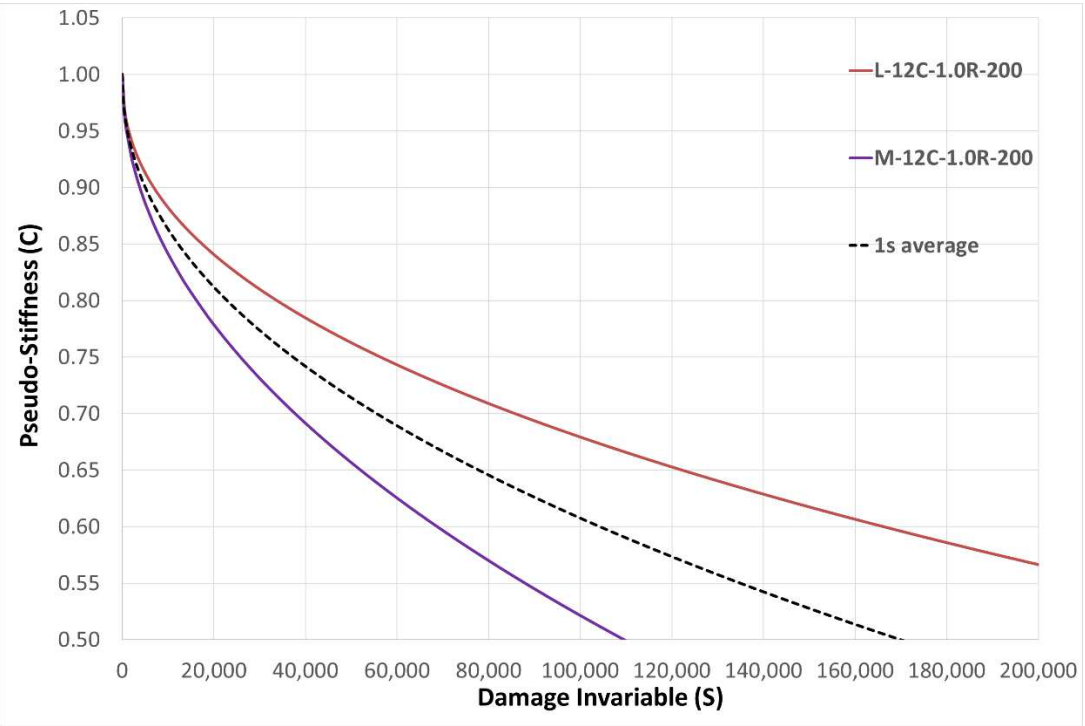

Figure 6-28: Damage characteristic curves under 1s rest periods at 12^{o}c, batch 1 mixture

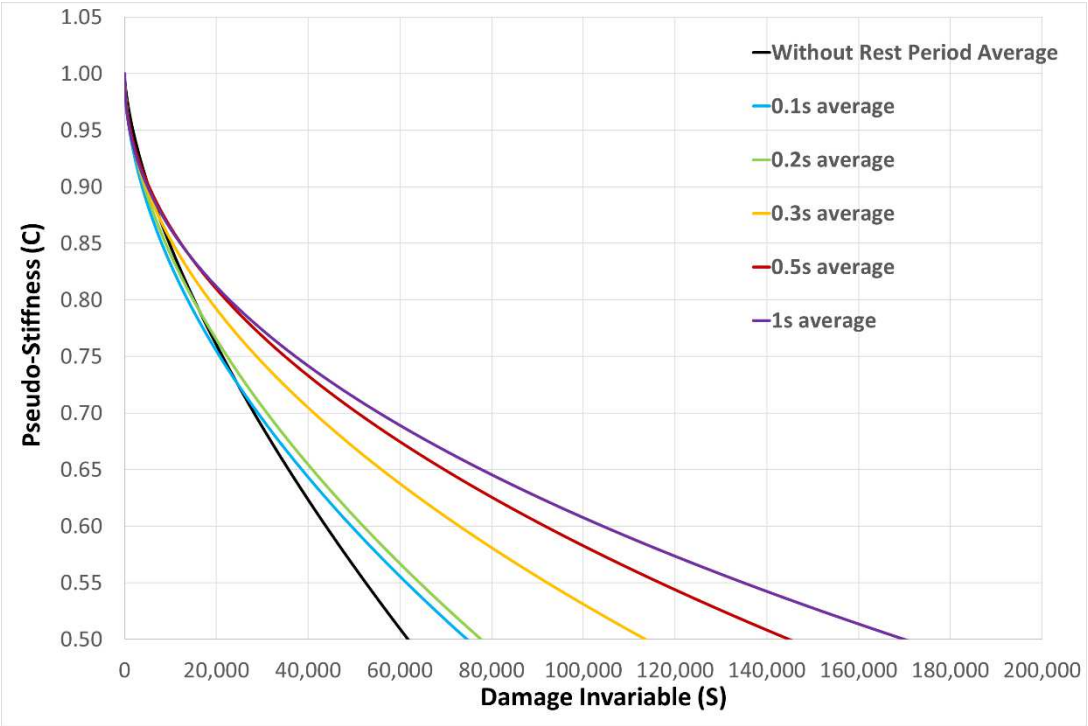

Figure 6-29: Damage characteristic curves under various rest periods at 12^{o}c, batch 1 mixture

6.3.4. Comparison of Damage Characteristic Curves with Rest Period at both Temperatures for batch 1 mixture

By some previous research (Shen et al., 2010, Qiu, 2012), it is discovered that the rest period healing effect is restrained at lower temperature compared to higher temperature. The microscopic explanation for this effect is that low temperature restricts the molecule activities and reduces the wetting and dispersion phenomena, which all contributes to asphalt healing. To investigate the temperature effect on healing, damage curves at both temperatures and under fixed rest period of 0, 0.2 and 0.5 second rest period are shown in Figure 6-30, while 0.1, 0.3 and 1 second rest period results are plotted in Figure 6-31. The rest periods results are separated into two figures to make graphs clear and distinguishable. Several noteworthy findings can be made.

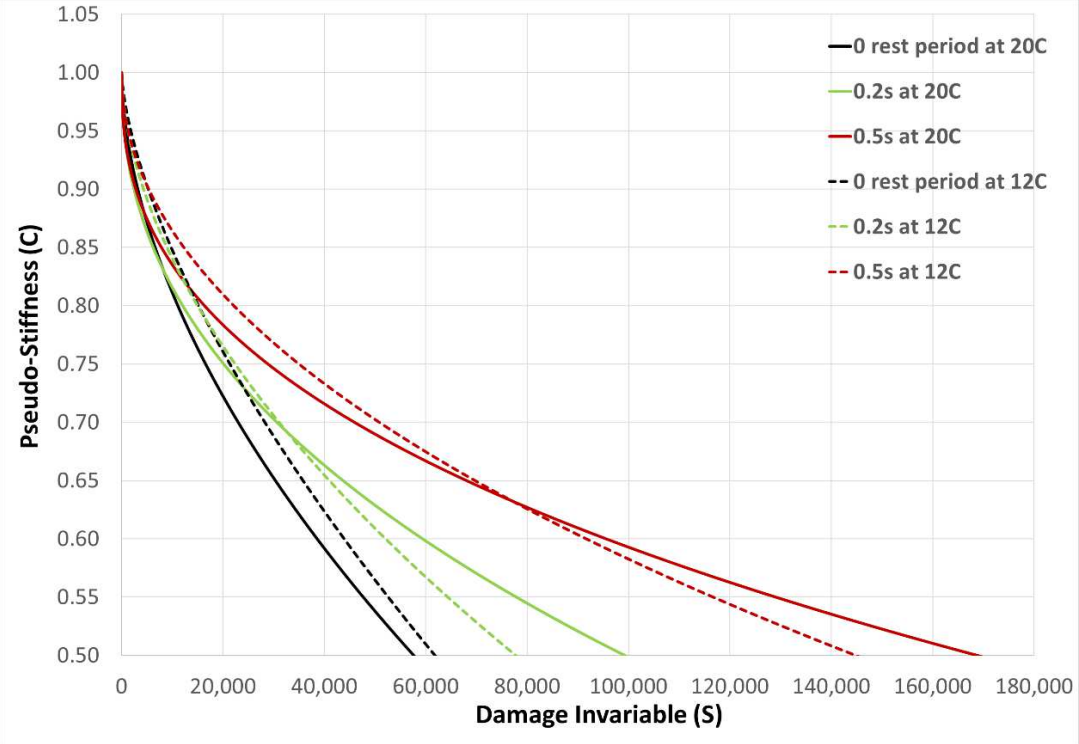

Figure 6-30: Comparison of damage characteristic curves under various rest periods between 12 and 20°c, batch 1 mixture (0,0.2 and 0.5 second rest period)

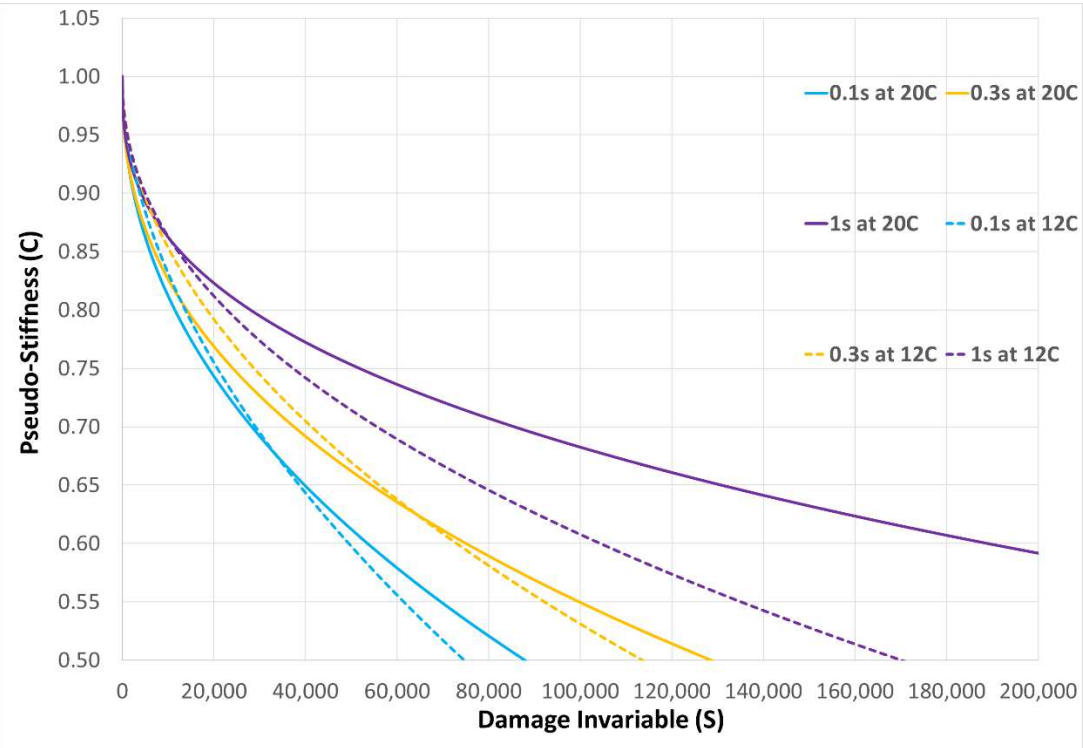

Figure 6-31: Comparison of damage characteristic curves under various rest periods between 12 and 20°c, batch 1 mixture (0.1, 0.3 and 1 second rest period)

At the beginning of each VECD test, the machine is trying to reach stability so the abnormalities at initial part of damage curves (sections with high C value and low S value) can be neglected. From Figure 6-30 and Figure 6-31, 20^{o}C curves are generally higher lying and become flatter with damage growth. Else, except at 0.5s rest period, the gap between two temperatures' damage curves becomes larger when the rest period gets longer. For instance, at 20^{o}C, the damage curve with 1 second rest period is significantly higher lying than the curve of same rest period at 12^{o}C. Theoretically, the damage curves at both temperature should be very close to each other under continuous loading after the application of time-temperature shift factor (Chehab, 2002), yet in Figure 6-30, the continuous loading curve of 12^{o}C is even slightly higher lying than that of 20^{o}C, but this is within the range of common experimental variation in results for current VECD method. The findings made here is also in line with previous investigation on healing ratio curve shown in Figure 6-11, which also demonstrates a stronger healing effect at higher temperature for batch 1mixture. However, it seems in damage curves, the temperature effect on healing is slight when rest period length is low, although this slight difference does not necessarily transfer to a slight degree of difference in stiffness development curves, which may be more evident depending on strain amplitude etc. The author suggests that healing ratio factor in Eq.(6.1) and Figure 6-11 is not a rigorous parameter to account for healing degree when initial stiffness is different between comparison targets, say damange curves at 12 and 20^{o}C, since the zero rest period stiffness development curve at two temperatures are different with each other. On the contrary, damage curve is a more rational indicator for the degree of healing since it is independent of temperature with continuous loading, so the extent of healing can be directly reflected how the damage curve with rest period change from original position (as in Figure 6-30 and Figure 6-31).

6.3.5. Batch 2 Mixture Tested under 20^{o}C

The Batch 2 mixture presents its summary results at 20^{o}C in Figure 6-32. The individual rest period results are similar to that of batch 1 mixture demonstrated earlier, they are not listed here for simplification reasons. The rest period healing effect shown in Figure 6-32 is similar to that of batch 1 mixture as described above. Relatively less rest period are tested for this condition.

6.3.6. Batch 2 mixture tested under 12 ^{o}C

Figure 6-33 presents damage characteristic curves for batch 2 mixture at 12^{o}C. Remarkably, a rest period of just 0.1s significantly improved the damage curve from 0s, so another rest period of 0.05s rest period was tested in this case and improvement is still obvious. As the failure pseudostiffness for batch 2 mixture is around 0.6 to 0.75, Figure 6-33 actually predicts pseudostiffness down to 0.5 since they are produced by curve fitting technique using Eq. (5.13).

6.3.7. Comparison of Damage Characteristic Curves with Rest Period at both Temperatures for batch 2 mixture

Similar to batch 1 mixture, damage curves for batch 2 mixture under 12 and 20 ^{o}C are drawn together and demonstrated in Figure 6-34. Surprisingly, damage curves at 12 ^{o}C lie well above those of 20 ^{o}C when rest period is the same. However, as mentioned above, the stiffness development curves of batch 2 mixture also show this stronger healing effect at 12 ^{o}C compared to that of 20 ^{o}C, which is already discussed in Section 6.2.3 and illustrated in Figure 6-12. Inevitable experimental fluctuation can not explain this phenomena here since both 0.1s and 0.3s rest period of 12 ^{o}C are evidently above curves of the same rest period under 20 ^{o}C.

To further investigate this "abnormality", both batch 1 and batch 2 results at 12 ^{o}C are drawn together in Figure 6-35. Still, the batch 2 curves are significantly higher lying compared to curves of batch 1 mixture, although batch 1 mixture should be softer with lower E_{lve} (see Table 5-1 and Table 5-2) and thus supposed to be higher lying under same rest period. Beam fatigue tests results presented in later Section 7.1 also verifies this effect. As a result, it is reasonable to conclude for batch 2 mixture, the healing effect has been changed due to change of bitumen supply, which has a higher healing effect at lower temperature for certain rest period. However, future detailed investigation is still needed to further verify and investigate this extraordinary phenomenon, especially tests results on bitumen from Dynamic Shear Rheometer (DSR) can shed lights of healing property and its relevance to temperature for various types of bitumen.

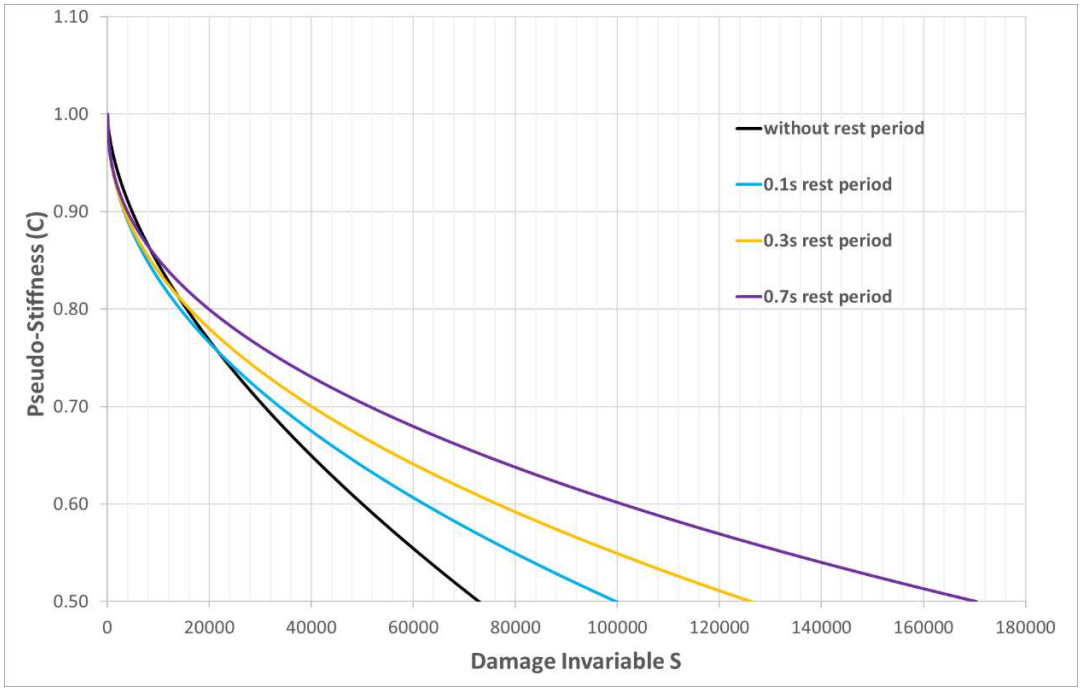

Figure 6-32: Damage characteristic curves under various rest periods under 20^{o}c, batch 2 mixture

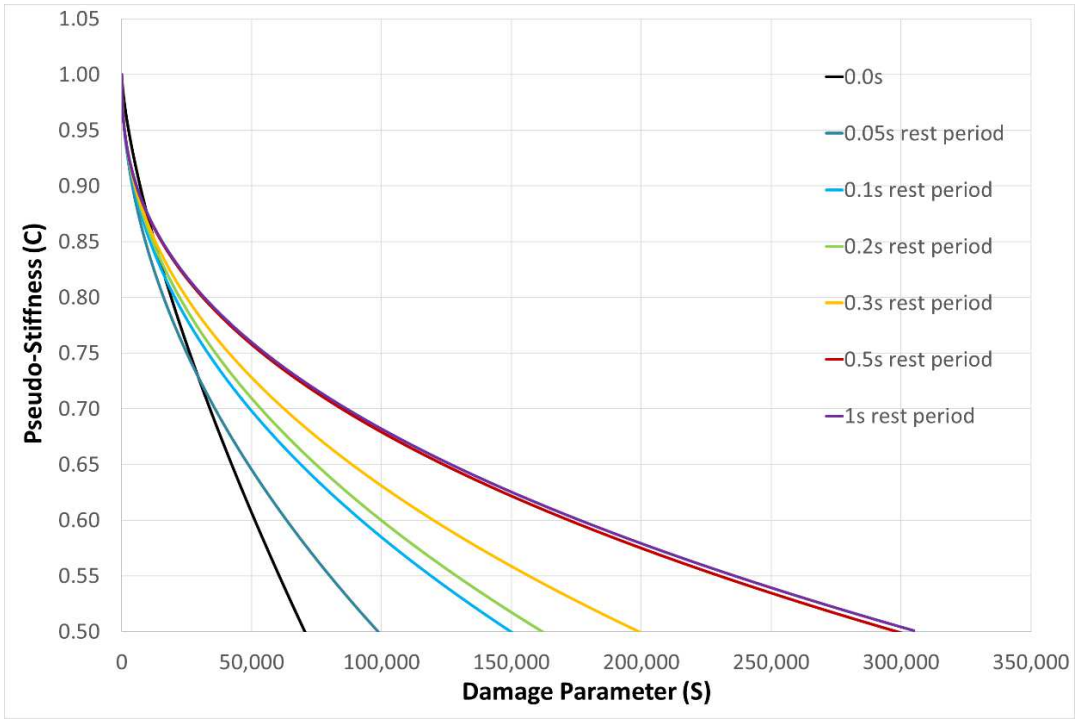

Figure 6-33: Damage characteristic curves with various rest periods under 12^{o}c, batch 2 mixture

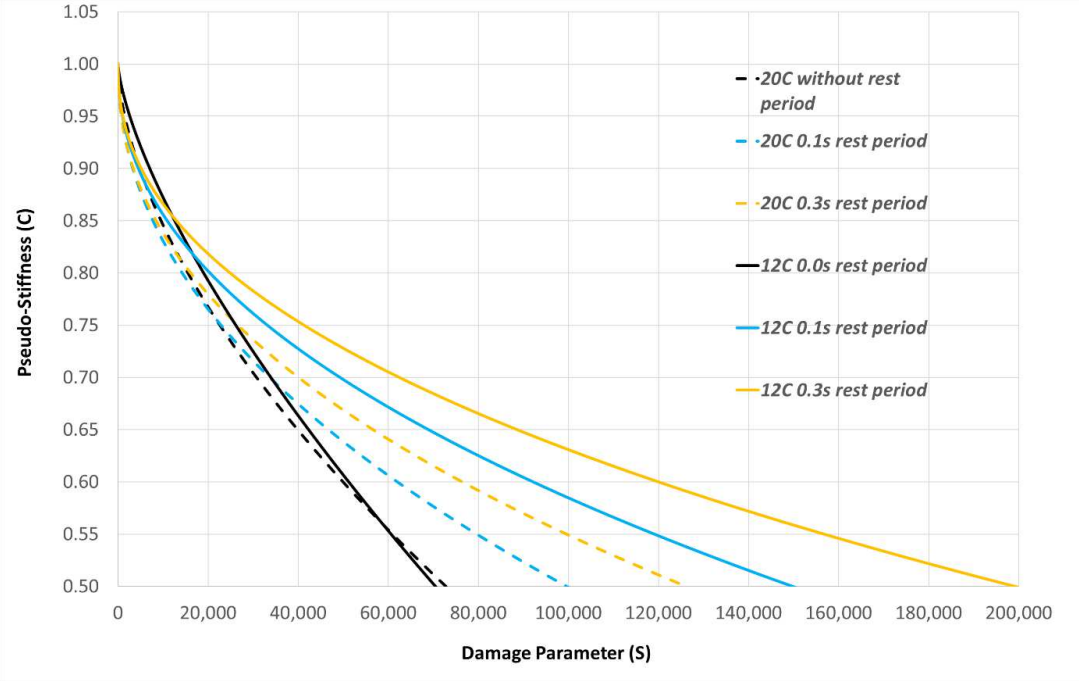

Figure 6-34: Comparison of damage characteristic curves under various rest periods between 12 and 20°c, batch 2 mixture (0, 0.1, 0.3 second rest period)

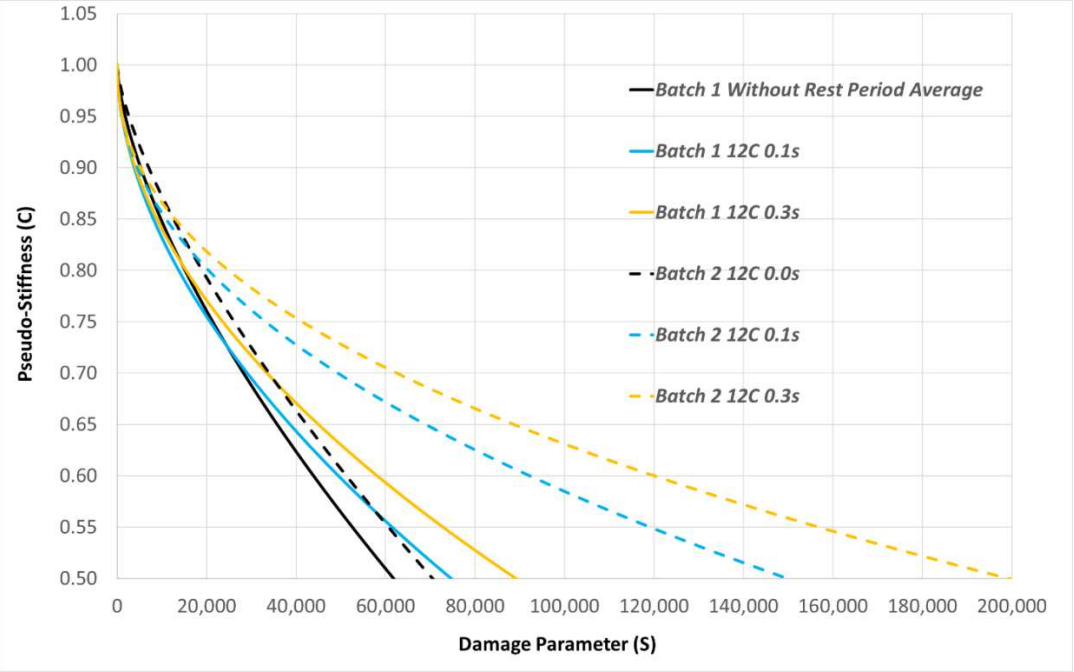

Figure 6-35: Comparison of damage characteristic curves under various rest periods between batch 1 and batch 2 mixture (0, 0.1, 0.3 second rest period) at 12 °c

6.4. Concept and Development of Novel Rest Period Damage Functions

As introduced in last section, individual test results may not yield a reasonable representative damage curve for a specific rest period. This section presents a novel regression fitting technique to accurately model damage characteristics with various rest period. Basically, it is an equational relationship between rest period length and the form of damage characteristic curves or its regression fitting equations. The novel functions are developed based on damage curve results under certain tested rest period, however, the equation can predict damage curves with any rest period length.

6.4.1. Damage Curve Fitting Parameters versus Length of Rest Period

Until now, damage characteristic curves have all been produced and presented, and the form of the curves is governed by Eq. (5.13) with C1 and C2 values (Table 6-1 to Table 6-4) corresponding to each rest period. Therefore, it becomes available to develop equational relationships between C1/C2 values and length of rest periods, and this can lead into a modified form of Eq.(5.13) that is able to produce damage characteristic curves with rest periods. For this purpose, C1 and C2 values tested under same temperature are drawn against length of rest periods, they are demonstrated in Figure 6-36 to Figure 6-43 for each condition.

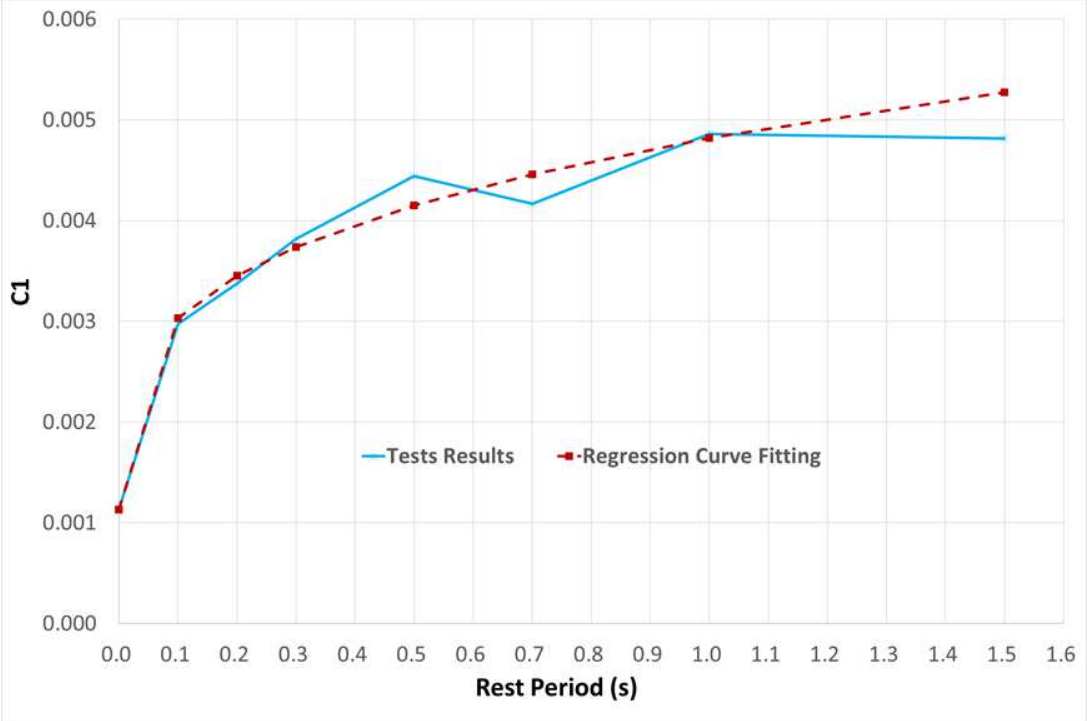

Figure 6-36: Relationship between C_1 and rest period at 20°C, Batch 1 mixture

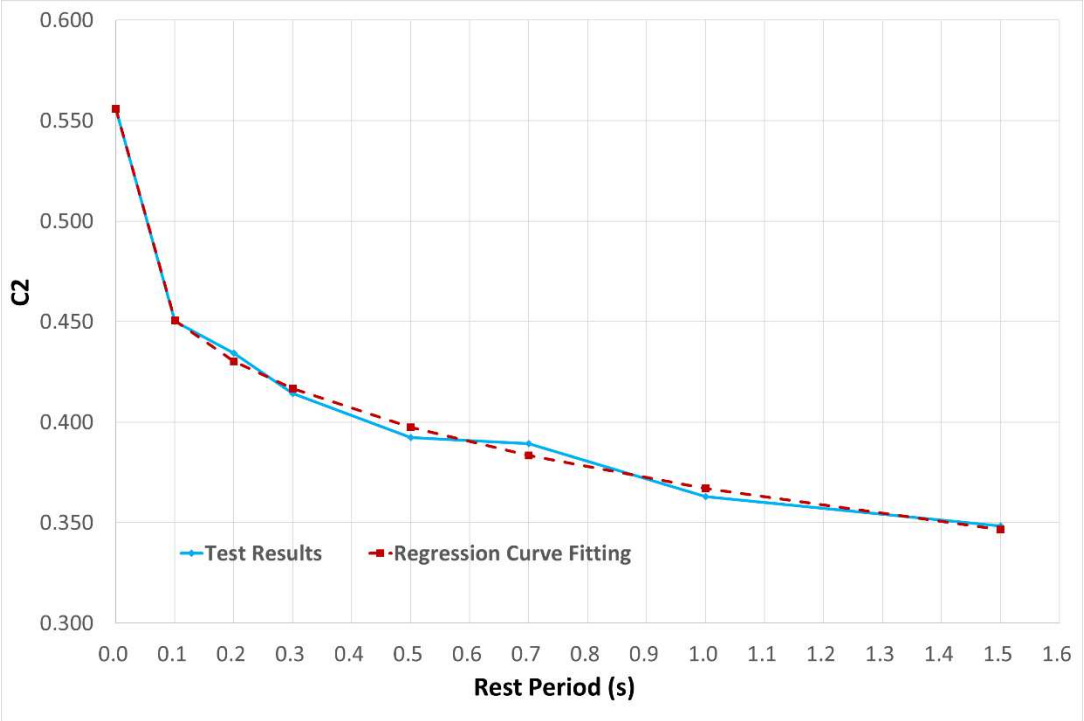

Figure 6-37: Relationship between C_2 and rest period at 20°C, Batch 1 mixture

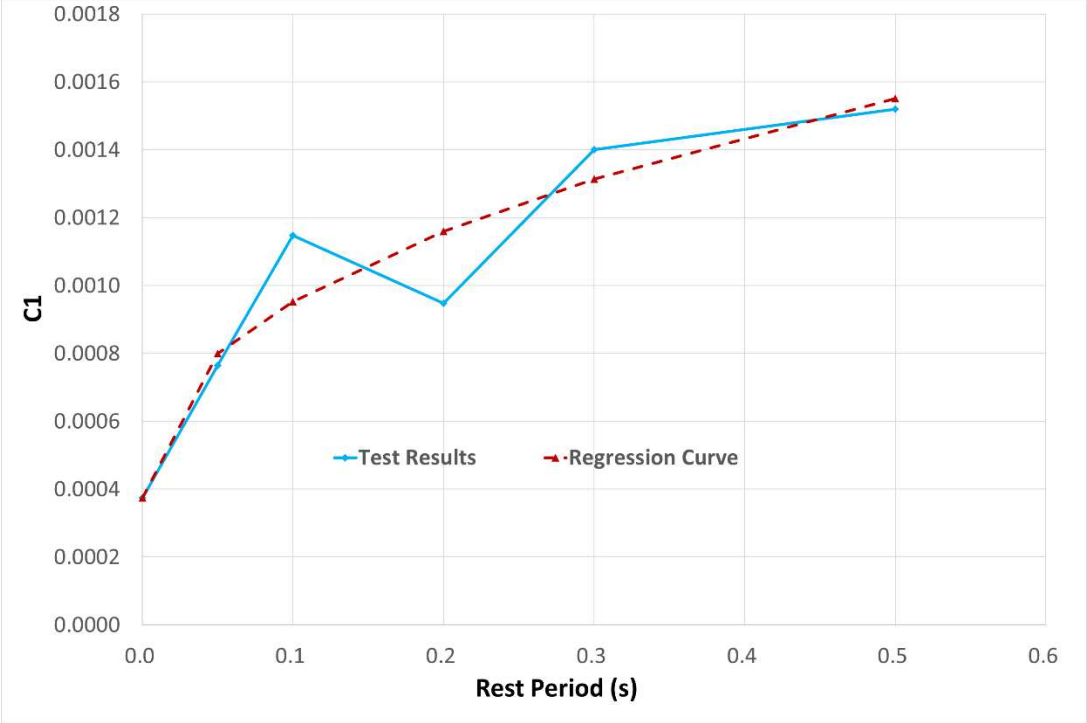

Figure 6-38: Relationship between C_1 and rest period at 12^{o}C, Batch 1 mixture

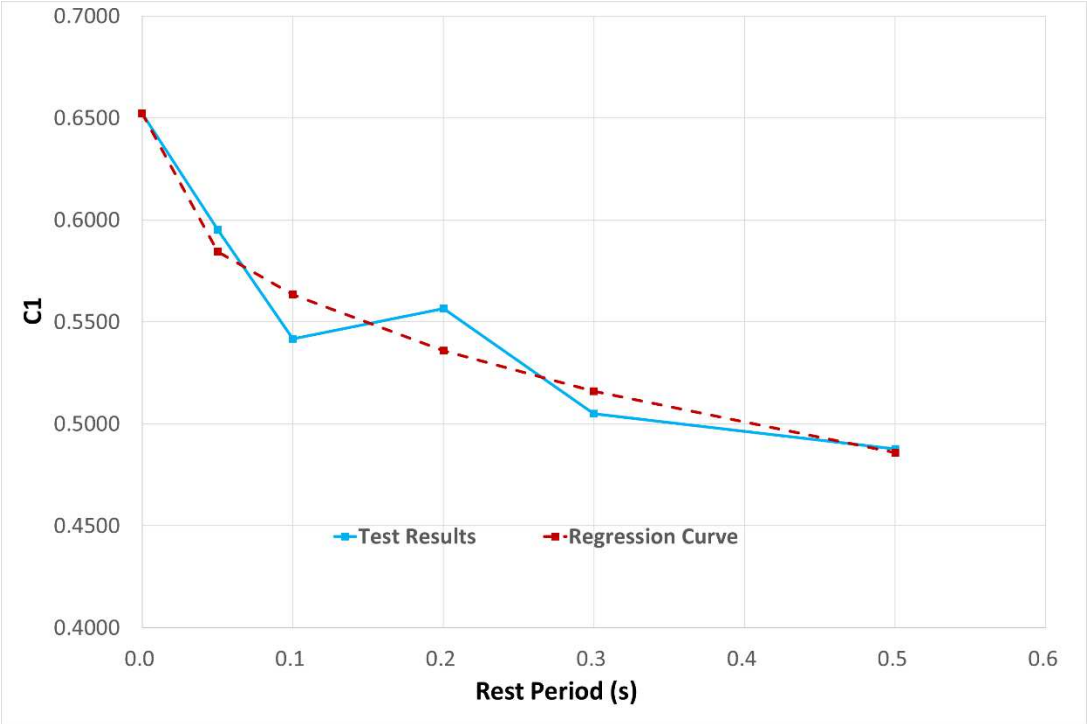

Figure 6-39: Relationship between C_2 and rest period at 12^{o}C, Batch 1 mixture

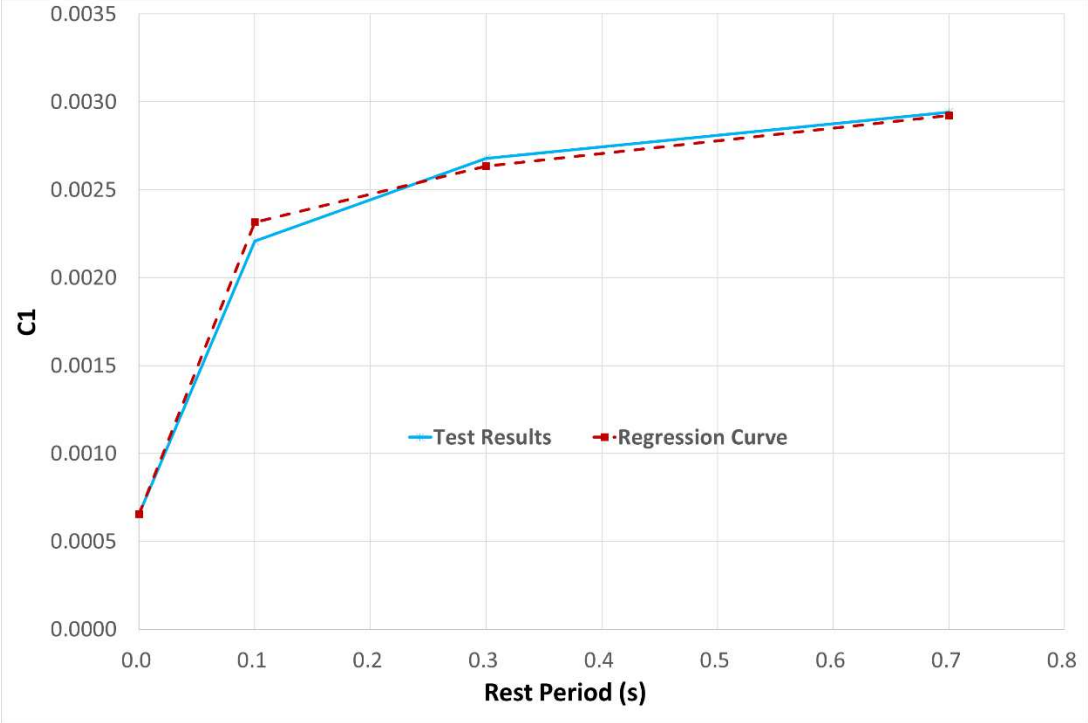

Figure 6-40: Relationship between C_1 and rest period at 20°C, Batch 2 mixture

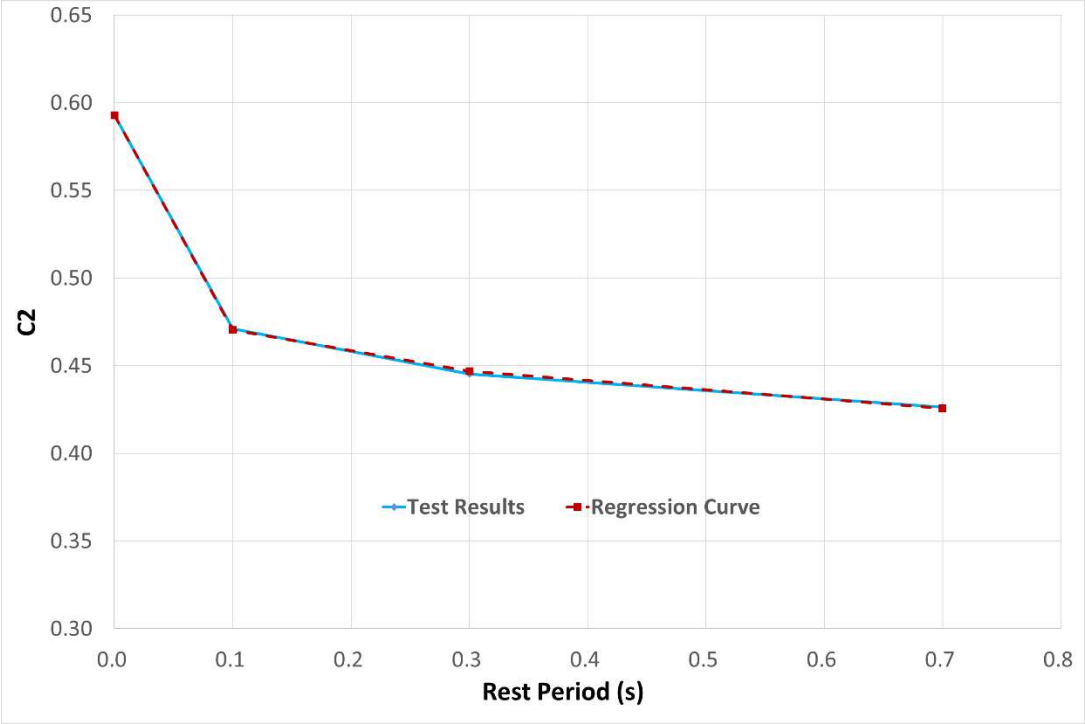

Figure 6-41: Relationship between C_2 and rest period at 20°C, Batch 2 mixture

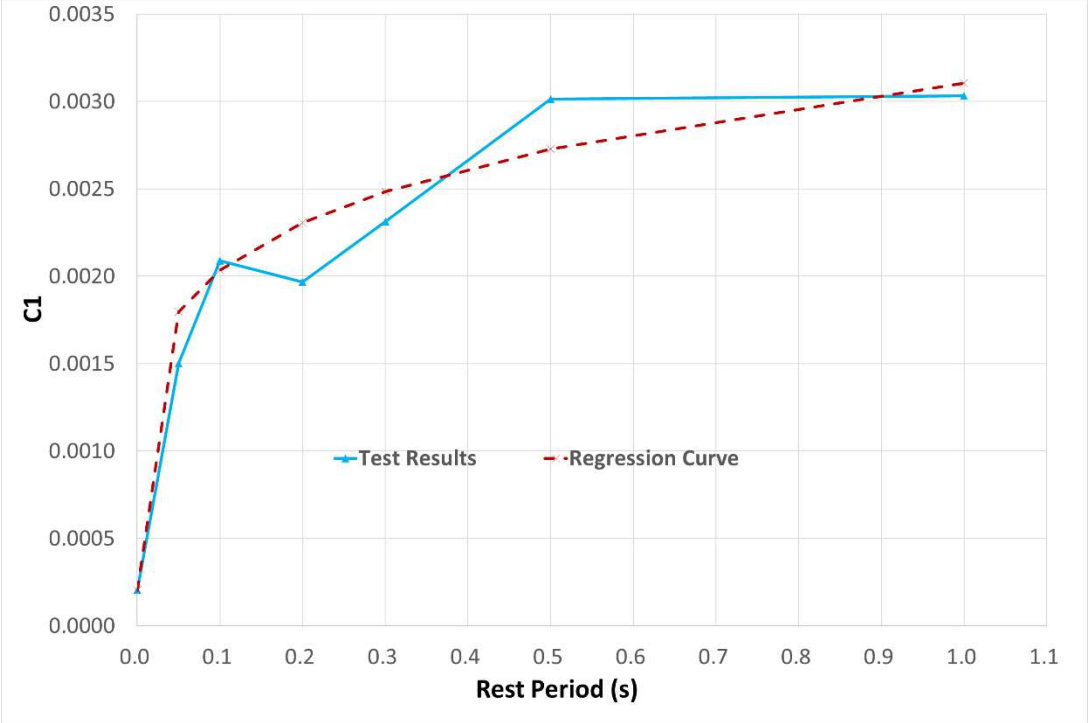

Figure 6-42: Relationship between C_1 and rest period at 12°C, Batch 2 mixture

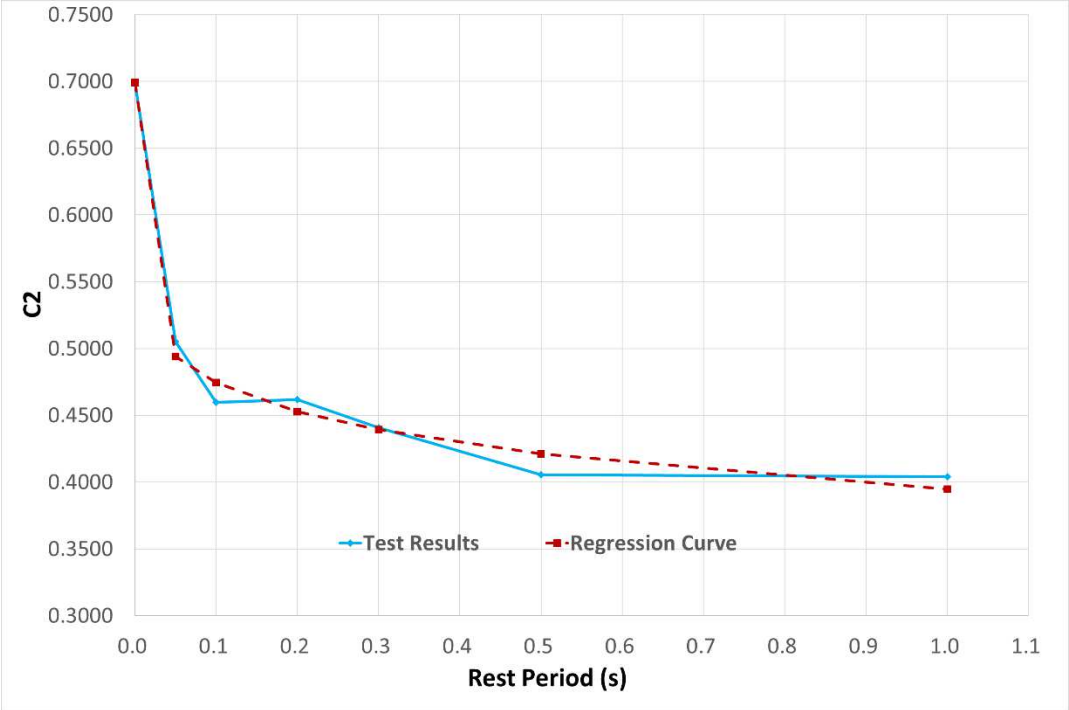

Figure 6-43: Relationship between C_2 and rest period at 12°C, Batch 2 mixture

6.4.2. Derivation of Rest Period Damage Functions

From those figures, C1 ("TESTED") is found to be increasing with the length of rest period, while C2("TESTED") is decreasing with rest period. Based on the trend of C1, C2 change with the length of rest period in from Figure 6-36 to Figure 6-43, it is found that they follow certain power functions, which lead into another set of curve fitting equations to sufficiently capture the trend. Since it is not possible or highly time consuming to test and obtain corresponding C1 and C2 values for each rest period, regression equations provide a much more convenient tool to predict C1 and C2 values for any desired rest period. Based on tested curves shown in Figure 6-36 through to Figure 6-41 (the "from Tested Damage Curves" of continuous lines), the adopted curve fitting equations for C1 and C2 values in relation to length of rest periods are listed below:

$$C_1 = C_{10} + a * (t_{rest})^b \tag{6.2}$$

$$C_2 = C_{20} - c * (\mathrm{t_{rest}})^{\mathrm{d}} \tag{6.3}$$

in which C_{10} and C_{20} are C1 and C2 values used in Eq.(5.13) at continuous loading conditions (t_{rest}=0). Substituting Eq. (6.2) and Eq. (6.3) into Eq. (5.13), an updated damage characteristic equation including rest period becomes:

$$C^* = 1 - [C_{10} + a * (t_{rest})^b]S^{[C_{20} - c*(t_{rest})^d]} \tag{6.4}$$

The fitting parameters a, b, c and d can be calculated using Excel's solver function to achieve least sum of standard error between tested and curve fitted values of C1 and C2:

$$\textit{Standard Error} = \sqrt{\sum_1^n (C_{test,n} - C_{model,n})^2} \tag{6.5}$$

in which n is the number of rest period length used to in the test, C_{test} and C_{model} can be either C1 or C2 for the nth rest period being tested. An example of regression parameters a, b, c and d are thus listed in Table 6-5, and this is for batch 1 mixture at 20 ^{o}C. The calculated a, b, c and d values for each batch under certain temperature are listed in Table 6-6. Eq.(6.4) is termed as "Rest Period Damage Functions" in this

study since it is fundamentally a damage characteristic curve fitting equation that includes additional parameter of rest period.

Table 6-5: Example calculation sheet for rest period regression parameters a, b, c and d (Batch 1 mixture at 20^{o}C)

a	0.0037	**c**	0.1888	**Sum of C1 standard error**	1.87E-07	
b	0.2877	**d**	0.2534	**Sum of C2 standard error**	0.00010	
Rest Period (s)	**C1**	**C2**	**fit C1**	**C1 error**	**fit C2**	**C2 error**
0	0.0011	0.5558	0.0011	0.00E+00	0.5558	0
0.1	0.0030	0.4501	0.0030	3.11E-09	0.4505	1.57E-07
0.2	0.0034	0.4344	0.0035	5.47E-09	0.4303	1.70E-05
0.3	0.0038	0.4143	0.0037	6.59E-09	0.4167	5.51E-06
0.5	0.0044	0.3924	0.0042	8.53E-08	0.3975	2.52E-05
0.7	0.0042	0.3893	0.0045	8.49E-08	0.3834	3.51E-05
1	0.0049	0.3630	0.0048	1.74E-09	0.3670	1.63E-05
1.5	0.0048	0.3485	0.0048	3.10E-12	0.3466	3.42E-06

Table 6-6: Fitting parameters for correlation equation between rest periods and damage characteristic curve parameters

Fitting parameters	**Batch 1 at 12^{o}C**	**Batch 1 at 20^{o}C**	**Batch 2 at 12^{o}C**	**Batch 2 at 20^{o}C**
a	0.0016	0.00369	0.0029	0.0024
b	0.442	0.288	0.2	0.16
c	0.218	0.189	0.3045	0.177
d	0.39	0.2534	0.132	0.16

Fundamentally, the values of curve fitting parameters a, b, c and d are determined by the material's damage and healing properties, thus different batches under different temperatures lead into varied curve fitting parameters. Since those parameters are related with mixture's healing effect, they are dependant on material's healing ability and thus on factors such as temperature and mixture type etc., which will change mixture's healing behaviour. Therefore, at this stage, each batch of mixture under certain temperature has a specific set of a, b, c and d, and their own rest period damage function as listed below:

Batch 1 at 20°C:

$$C^* = 1 - [0.00113 + 0.0037 * (t_{rest})^{0.29}]S^{[0.55583-0.189*(t_{rest})^{0.2534}]}$$
(6.6)

Batch 1 at 12°C:

$$C^* = 1 - [0.000375 + 0.0016 * (t_{rest})^{0.442}]S^{[0.652302-0.218*(t_{rest})^{0.39}]}$$
(6.7)

Batch 2 at 20°

$$C^* = 1 - [0.000655 + 0.0024 * (t_{rest})^{0.16}]S^{[0.5929-0.177*(t_{rest})^{0.16}]}$$
(6.8)

Batch 2 at 12°C

$$C^* = 1 - [0.0002 + 0.0029 * (t_{rest})^{0.2}]S^{[0.699-0.3045*(t_{rest})^{0.132}]}$$
(6.9)

Consequently, C1 and C2 values versus rest period regression curves can be produced by rest period damage functions, and they are drawn in Figure 6-36 to Figure 6-43 (the dotted "Regression Curve"). Also, the damage characteristic curves corresponding to C1 and C2 values calculated from rest period damage functions can be produced by inputting length of desired rest period as t_{rest} into rest period damage functions Eq.(6.4), forming Eq.(6.6) to Eq.(6.9). Therefore, the C1 and C2 values predicted by proposed rest period damage functions are listed in Table 6-7 and Table 6-8 for batch 1 and 2 respectively.

However, certain drifted points exist such as the C1 of 0.5s and 0.7s rest period in Figure 6-36, this is caused by fluctuation (experimental noise) of test results or inconsistent curve fitting coefficients. For instance, in Figure 6-38 and Figure 6-39, the 0.2s points are evidently swayed from the trend curve, and this corresponds to the 0.2s curve in Figure 6-29, which is not very accurate considering its position between 0.1 and 0.3s curve. However, it has now become possible to verify the damage curves generated by C1/C2 values on the "trend curve".

Rest period damage equations are used to produce damage characteristic curves under a series of rest period as demonstrated from Figure 6-44 to Figure 6-47. It is worth mentioning that curves from Figure 6-44 to Figure 6-47 are based on the prediction results from rest period damage functions as listed in Eq. (6.6) to Eq. (6.9), while Figure 6-22, Figure 6-29, Figure 6-32 and Figure 6-33 are obtained from tests results directly. It is evident that the rest period healing effect is clearly demonstrated from Figure 6-44 to Figure 6-47. The trend of rest period healing effect is even more reasonable compared to tested results, which may subject to sample specific variations or inevitable laboratory fluctuations. For instance, the 0.2s curve in Figure 6-47 is more reasonable than Figure 6-29, it indicates the regression curve C1 value of 0.2s rest period in Figure 6-42 has somehow corrected the error made by tested value. So the problem for divergence of laboratory data of tested C1/C2 values as mentioned in last paragraph has been overcome by application of rest period damage functions.

It is important to notice that the rest period damage function is not to be used beyond the optimum rest period, such as 0.5s rest period at 12 ^{o}C in Figure 6-47, in which no larger than 0.5s rest period results are shown since it is already close to optimum rest period as indicated in Figure 6-33. On this condition, the 0.7s or 1.0s rest period curve should be identical to 0.5s rest period curve and forcibly predicting it using rest period damage function will incur error. Thus, it is necessary to identify the optimum rest period for proper use of the proposed functions.

Table 6-7: C_1 and C_2 values for each rest period calculated using a, b, c and d values at both temperatures (Batch 1 Mixture)

Rest Period (s)	***12^{o}C***		***20^{o}C***	
	C1	***C2***	***C1***	***C2***
0	0.000374904	0.652301759	0.001129728	0.555833442
0.1	0.000952704	0.562882	0.003031464	0.450502105
0.2	0.001165133	0.538731514	0.003451164	0.430275349
0.3	0.001323965	0.521684115	0.003738393	0.416687734
0.5	0.001570277	0.496518145	0.004151379	0.397456923
0.7[(1)]	0.001570277	0.496518145	0.00445851	0.383359851
1	0.001570277	0.496518145	0.004818236	0.36704391

1: longer than 0.5s is identical to 0.5s due to its regarded as optimum rest period

Table 6-8: C_1 and C_2 values for each rest period calculated using a, b, c and d values at both temperatures (Batch 2 Mixture)

Rest Period (s)	12^oC		20^oC	
	C1	C2	C1	C2
0	0.000204192	0.699030061	0.00065502	0.592899185
0.1	0.002033968	0.474392358	0.002315414	0.470301642
0.2	0.002306053	0.452858239	0.002510157	0.455951816
0.3	0.002483601	0.439316918	0.002634498	0.446791195
0.5	0.002728788	0.421191511	0.00280308	0.434372886
0.7(1)	0.002728788	0.421191511	0.002921891	0.425621996
1	0.002728788	0.421191511	0.00305502	0.415817663

1: longer than 0.5s is identical to 0.5s due to its regarded as optimum rest period

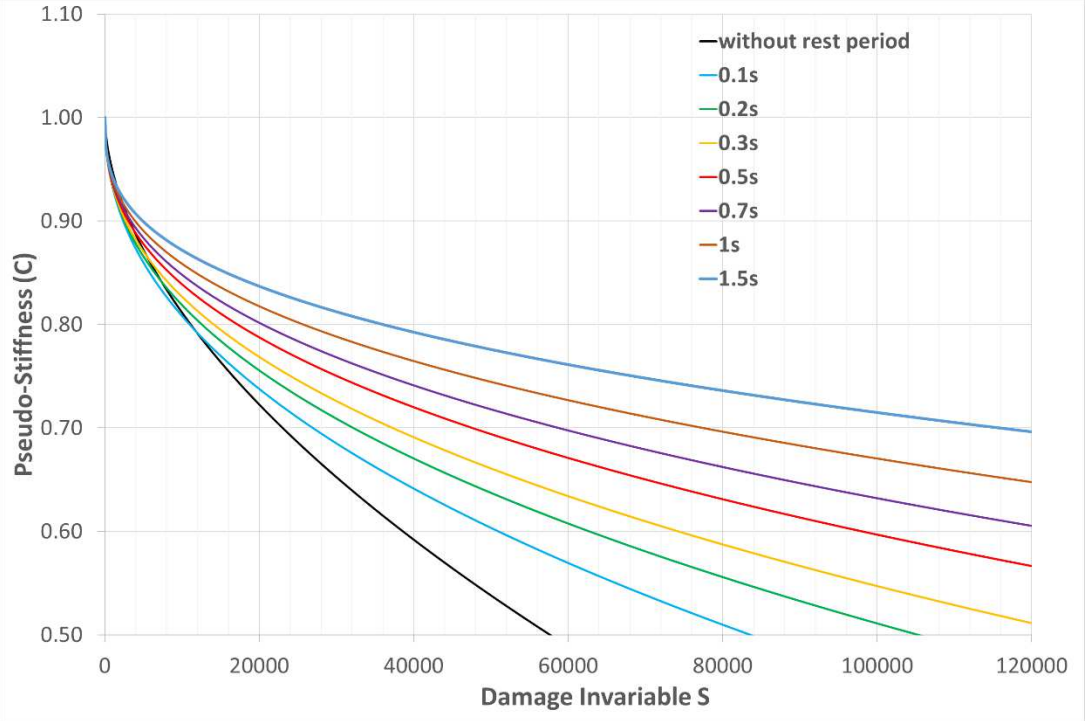

Figure 6-44: Damage Characteristic curves under various rest period produced by rest period damage functions (Batch 1 mixture at 20^oC)

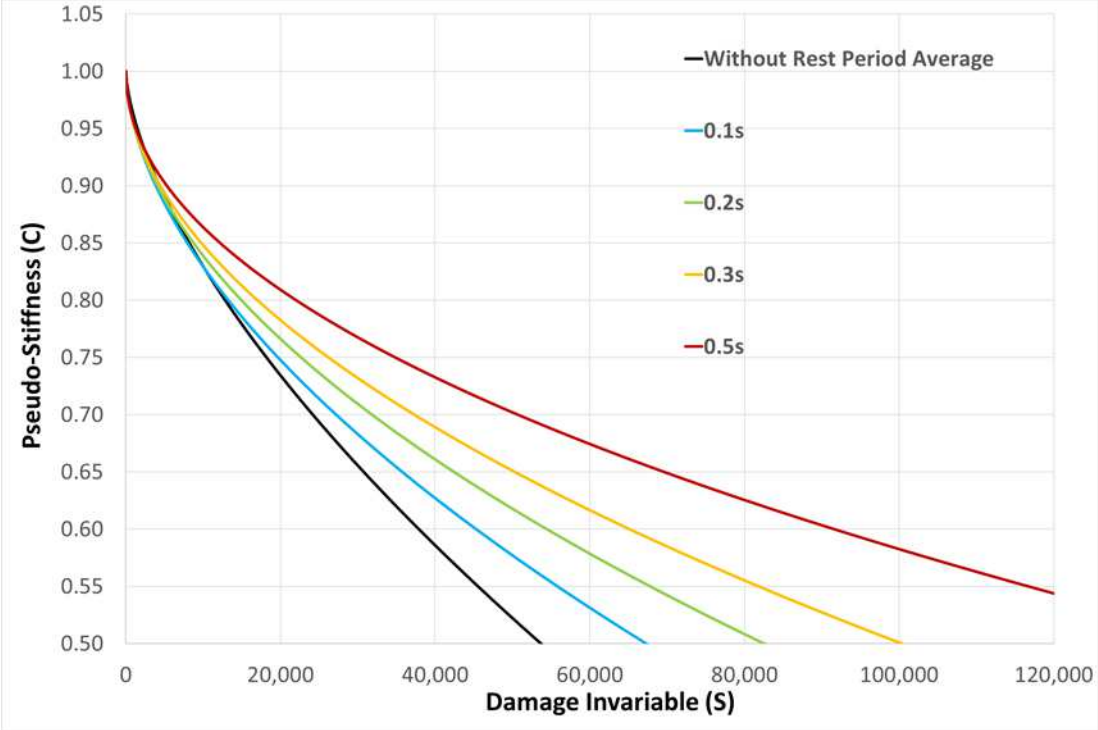

Figure 6-45: Damage Characteristic curves under various rest period produced by rest period damage functions (Batch 1 mixture at 12 ^{o}C)

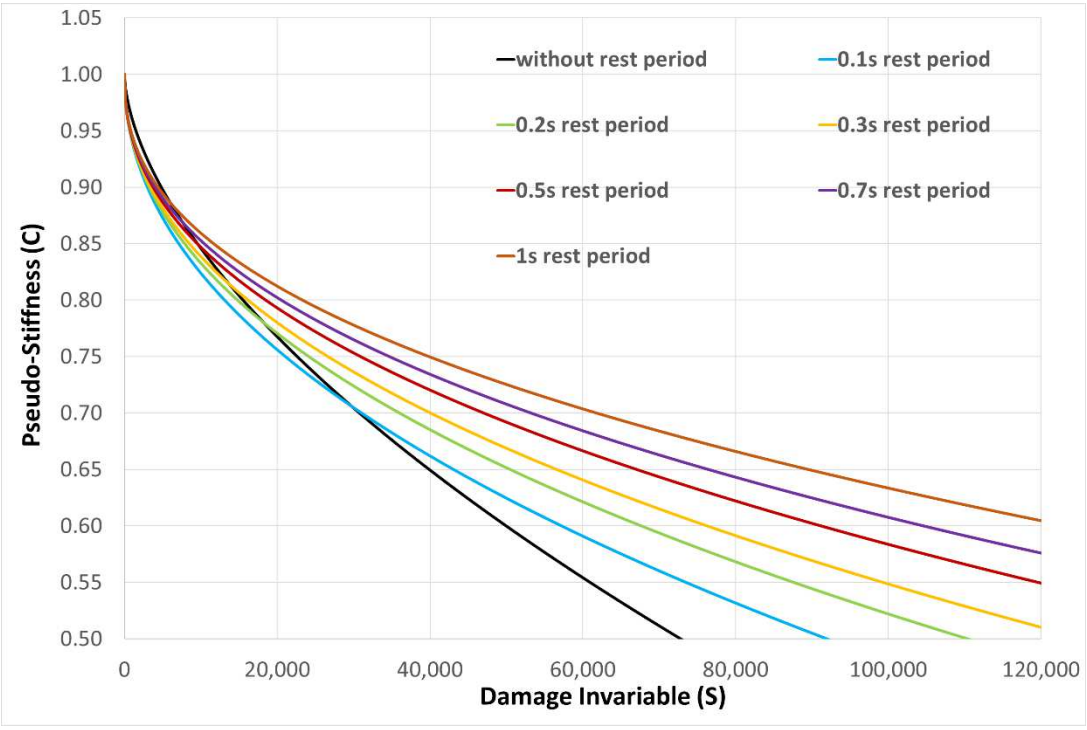

Figure 6-46: Damage Characteristic curves under various rest period produced by rest period damage functions (Batch 2 mixture at 20 ^{o}C)

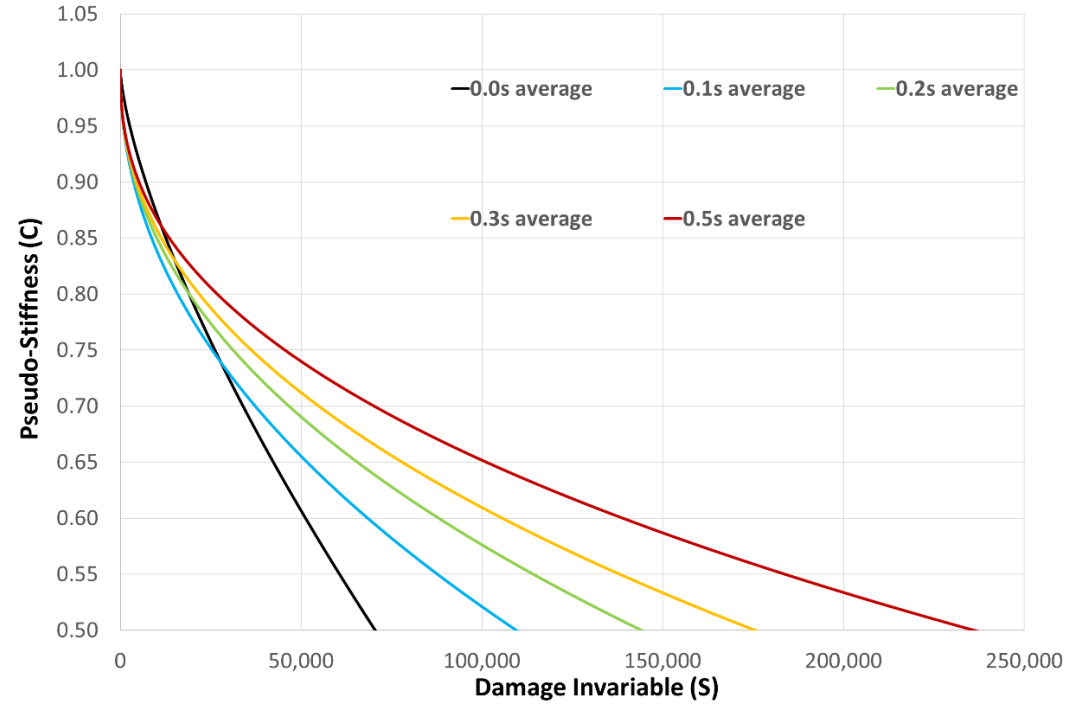

Figure 6-47: Damage Characteristic curves under various rest period produced by rest period damage functions (Batch 2 mixture at 12 ^{o}C)

Furthermore, taking Batch 2 mixture at 20^{o}C as an example (see Figure 6-46), although the tested rest periods are just 0, 0.1, 0.3 and 0.7s (see Table 6-3), the model curves are covering much more rest period such as 1s and 0.2s. This indicates that the trend of rest period healing predicted by just 4 tested are sufficient at predicting all other rest periods using rest period damage functions. As mentioned, the rest period damage functions have produced damage characteristic curves with more reasonable rest period healing effect compared to direct laboratory results. Since there is possibility of significant experimental variation of results between individual test curves with certain rest period. This could be caused by various reasons such as sample variation, inevitable variation of locational void ratio and laboratory noise etc.. What's more, significant time and laboratory labour can be saved by using rest period damage functions to produce damage characteristic curves.

Curve fitting equations are used twice from the original S-VECD tests results to the final derivation of rest period damage functions listed in Eq. (6.6) to Eq. (6.9), but they are for different parameters and purposes. To avoid confusion, it is helpful to clarify the logic and procedures involved in the production of rest period damage

functions. As a result, the below chart is listed to describe the logical procedures of developing rest period damage functions:

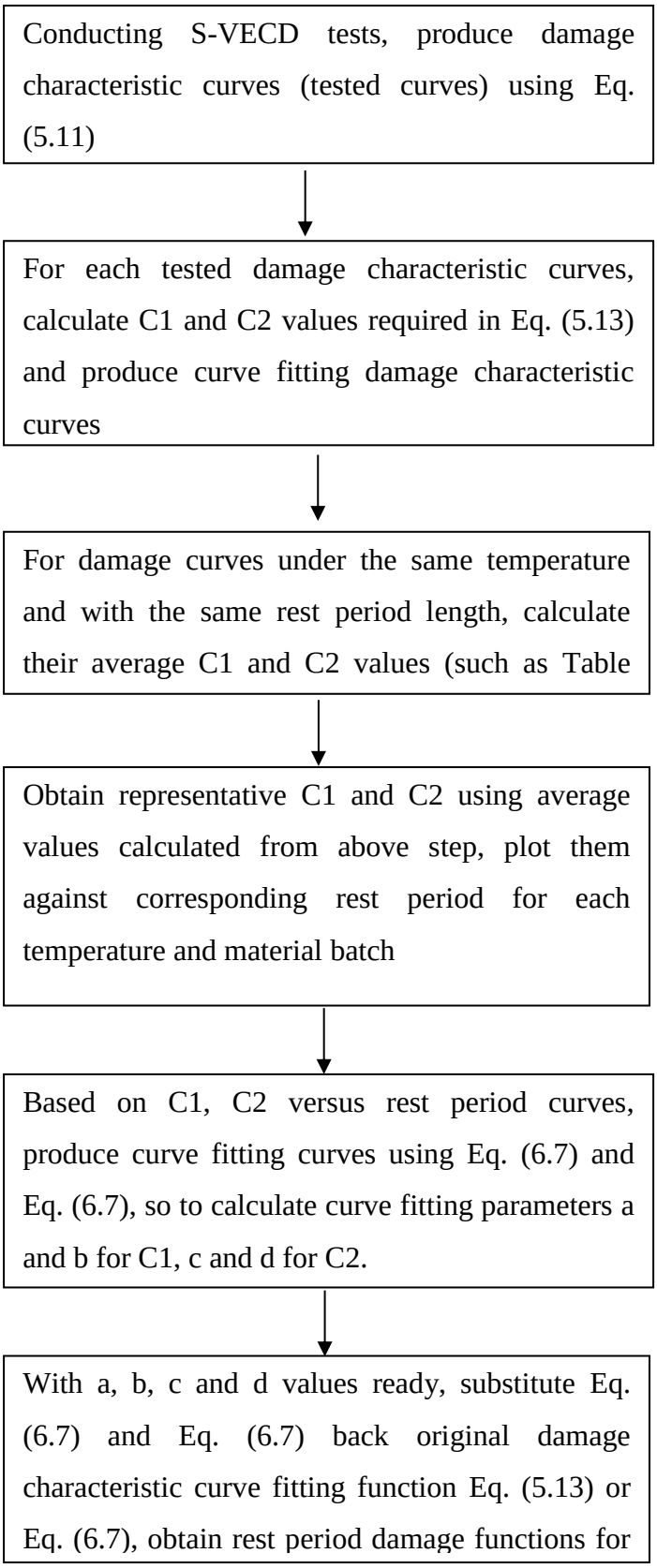

6.5. Proposed Procedures to Produce Rest Period Damage Function

For future application of rest period damage functions, the following suggestions are made for laboratory derivation of the equation:

1. For a new target mixture, firstly obtain its normal damage characteristic curve (without rest period) including prerequisite parameters from dynamic modulus tests
2. Select rest period length for VECD with rest period tests based on test conditions such as temperature and general knowledge about this mixture or bitumen's rest period healing effect. For normal gravel with bitumen mixtures, the suggested rest periods are: 2s, 1s, 0.6s, 0.3s and 0.1s (for lower than 20^{o}C the maximum rest period selected can be lowered)
3. Conduct VECD with rest period tests to produce representative damage characteristic curves under various rest periods. Obtain average C1 and C2 values for each rest period, and draw them together in a graph.
4. Based on C1 and C2 versus rest period graphs obtained above, use Excel or other curve fitting tools to calculate regression coefficients a, b, c and d used in damage with rest period function Eq. (6.4)
5. Substitute regression fitting parameters a, b, c and d back into Eq. (6.4), so the rest period damage function for that mixture and temperature can be produced

To increase efficiency and accuracy of acquiring rest period damage functions, the following points should be accentuated:

1. It is important to basically know the length of optimum rest period, and a test with rest period length close to or larger than optimum rest period is necessary. If not so, the rest period damage functions should better be avoided for rest period longer than the longest tested, since there may be significant error.
2. It is necessary for the damage characteristic curves without rest period to be accurate. The without rest period curve provides constant parameters used in rest period damage functions, which is not changed with length of rest period as shown in Eq.(6.4). It is also easier to achieve an accurate without rest period

damage curve since it is theoretical the same curve regardless of temperature level.

3. Larger tolerance of fluctuation is possible for curves with rest period, since it is inevitable to have experimental fluctuation of results while test with rest period is time consuming. These errors can be overcome by using the proposed rest period damage function, as long as the general trend of C1/C2 vs rest period is correctly captured.
4. The curve fitting procedure used for producing C values for each individual VECD test may require user experience and technique, such that the produced average C vs S curve for certain rest period should be lying in a correct position compared to individual curves at that rest period. Otherwise, sometimes the curve fitting software provides C values inconsistent between individual test under same rest period and not feasible to produce average C1/C2 values that can lead into representative curves.

The current procedures are based on tests results on certain Western Australia sourced mixture type. While more research and application may be needed to validate and improve the procedures for different mixtures. Else, current rest period damage functions are temperature dependent so future quantification of temperature effect on rest period healing may lead into one unified equation for various temperatures.

6.6. Investigation of Reduced Specimen Geometry for VECD tests with Rest Periods

As discussed in Section 2.4 , additional dynamic modulus and VECD with rest periods tests are conducted on reduced 54x110mm specimen using Batch 1 mixture.

Firstly, Table 6-9 presents the measured dynamic modulus and phase angle for each temperature and frequency used on 54x110mm specimen for dynamic modulus tests. The table also includes statistical measurement of reduced specimen results to standard size specimen. Then Mastersolver Version 2.2 developed by Bonaquist (2009) was used to produce the master curve as displayed in Figure 6-48. Also, the master curves of standard size specimen as shown in Figure 6-1 and obtained values

listed in Table 6-9 and standard 100x150mm specimen have produced quite closely matching master curves. While according to statistical measure of differences in Table 6-9, the difference only be increasing at higher temperature (both phase angle and dynamic modulus), which implies a condition of high temperature or low loading frequency. Same as Castorena et al. (2017), it is suggested that the reduced specimen geometry is able to produce adequate dynamic modulus master curve results at low to medium temperatures and frequencies, and slightly higher dynamic modulus at high temperature.

Table 6-9: Dynamic Modulus Master Curve results Data on 54X110mm Specimen

Small Specimen				
Temp (^{o}C)	**Frequency (Hz)**	**Measured Dynamic Modulus (Mpa)**	**Percent Difference in E* (%)**	**Percent Difference in Phase Angle (%)**
34	0.1	8790.0	0.53	0.33
34	1	12798.0	0.11	0.66
34	10	16900.0	0.25	0.72
12	0.1	4365.0	3.31	0.14
12	1	7598.0	2.32	0.05
12	10	11602.0	1.72	0.38
20	0.1	1824.0	0.15	0.10
20	1	3928.0	0.75	0.08
20	10	7092.0	1.39	0.18
38	0.1	190.3	16.25	1.89
38	1	530.5	7.70	0.78
38	10	1506.0	1.07	1.88

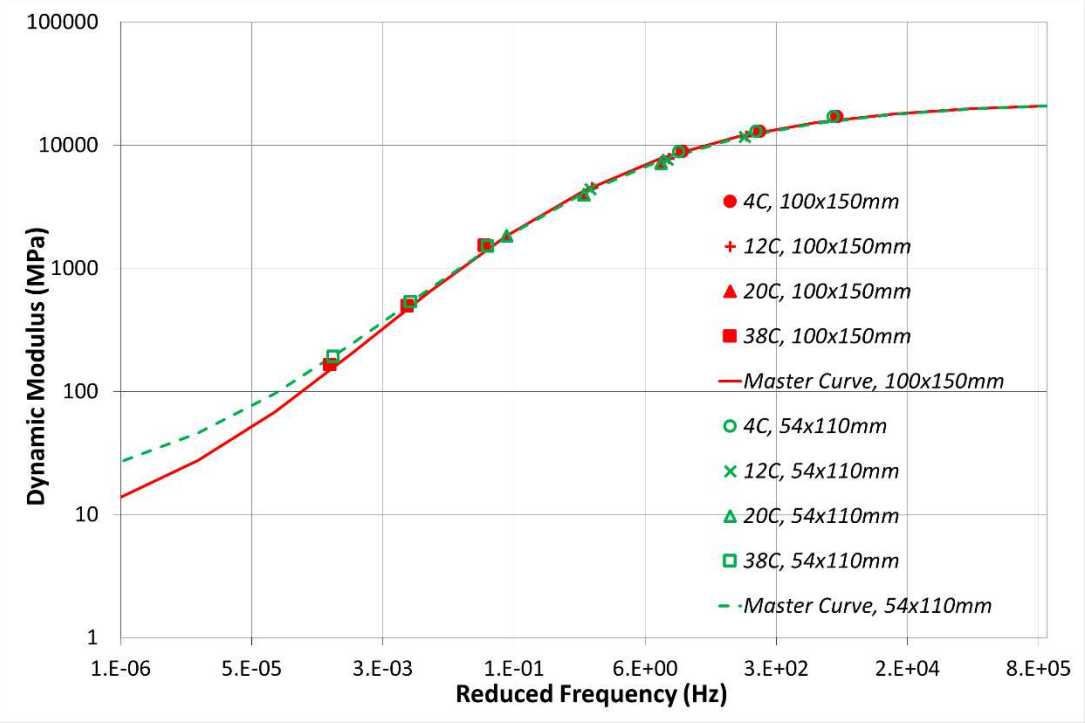

Figure 6-48: Dynamic Modulus Master Curve obtained using 54x110mm specimen, alongside with standard size results

6.6.1. Evaluation of Continuum Damage Power Parameter for Small Specimen

As mentioned above, before VECD tests, it is necessary to acquire continuum damage power parameter for use in simplified damage parameter calculation such as Eq.(5.11). Based on Appendix X1 in AASHTO TP107-14, long-term equilibrium modulus E_∞ and Modulus of prony term corresponding to each Relaxation Time of prony Term are displayed in Table 6-10, which is similar to Table 5-5 and Table 5-6 for standard size specimen. According to Appendix X3 in AASHTO TP107-14, the Relaxation Modulus Gaussian Distribution curve alongside damage power parameter for small specimen is demonstrated in Figure 6-49. To verify the accuracy of α obtained from dynamic modulus tests on 54 x 110mm geometry specimen, the acquired α is applied in simplified damage parameter equation Eq.(5.11) to calculate damage characteristic curves for exemplary specimen. Other than α, the representative stiffness modulus E_{lve} also varies between different specimen geometries. As a result, at 20°C, for small specimen $\alpha = 3.367$, Elve = 7092Mpa (Table 6-9) is used for production of damage characteristic curves; for standard

specimen $\alpha = 3.134$, Elve = 7192Mpa are used. While at 12 ^{o}C, for small specimen $\alpha = 3.367$, Elve = 11602Mpa; for standard specimen $\alpha = 3.16$, Elve = 11805Mpa. The results are then compared with the damage curves produced based on standard specimen, the results are as demonstrated in Figure 6-50 and Figure 6-51.

From Figure 6-50 and Figure 6-51, it is obvious that small specimen parameters produce quite close damage characteristic curves and relevant parameters to standard size specimen. What's more, for example, curves under both continuous loading and 0.3s rest period show close agreement, which demonstrates that VECD with rest period healing effect can be well tested by small sample parameters. Similarly, different strain levels do not reduce the capability of using small specimen parameters since the curves are still close regardless the strain amplitude. To conclude, although just one 54 x 110mm specimen has undergone dynamic modulus test, the produced parameter has shown sufficient capability for use in simplified VECD test with rest periods, since every produced damage curve is close to those produced by parameters from standard size specimen tests.

Table 6-10: Prony Coefficients obtained from Dynamic Modulus Tests Results on 54X110 mm specimen of Batch 1 mixture

E∞(kPa)	9509.26
Relaxation Time of Prony Term m: ρm	**Modulus of Prony Term m: E_m (kPa)**
200000000	3328.904555
20000000	1676.596094
2000000	4451.192479
200000	9002.216904
20000	21024.94957
2000	54933.96604
200	157894.4414
20	461404.2092
2	1207558.335
0.2	2506709.27
0.02	3884491.826
0.002	4540829.315
0.0002	4231904.728
0.00002	3358572.701
0.000002	2398029.962
0.0000002	1600044.338
0.00000002	1058593.93

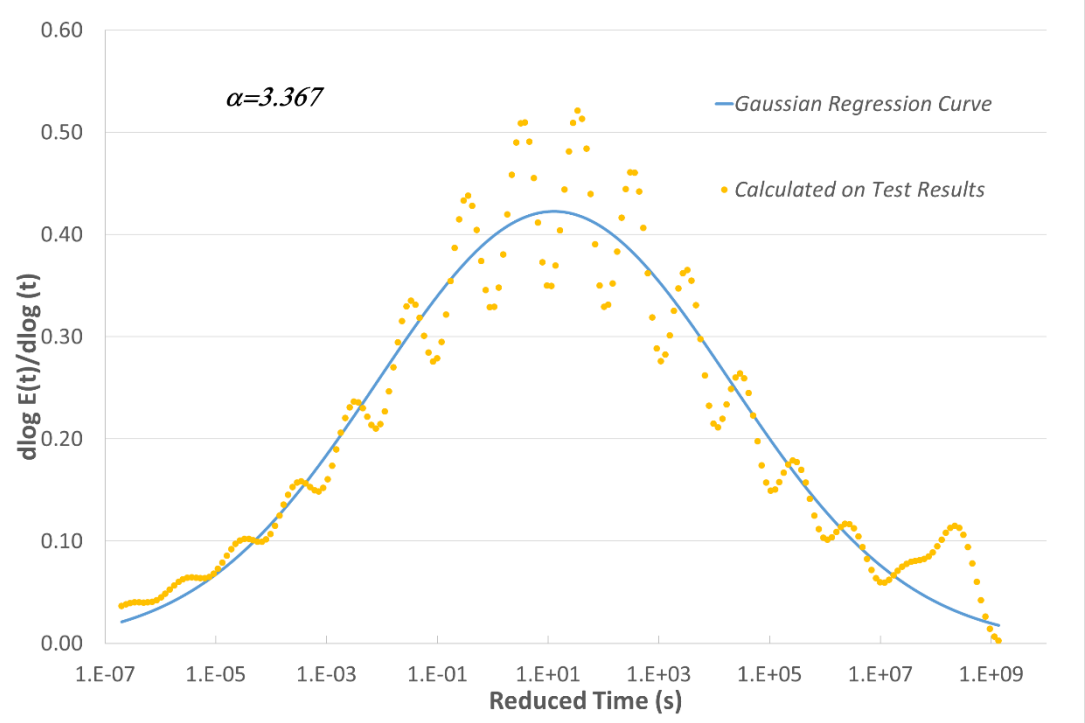

Figure 6-49: Plot of Relaxation Modulus versus Time and Gaussian Distribution Regression Curve obtained from 54 x 110 mm specimen

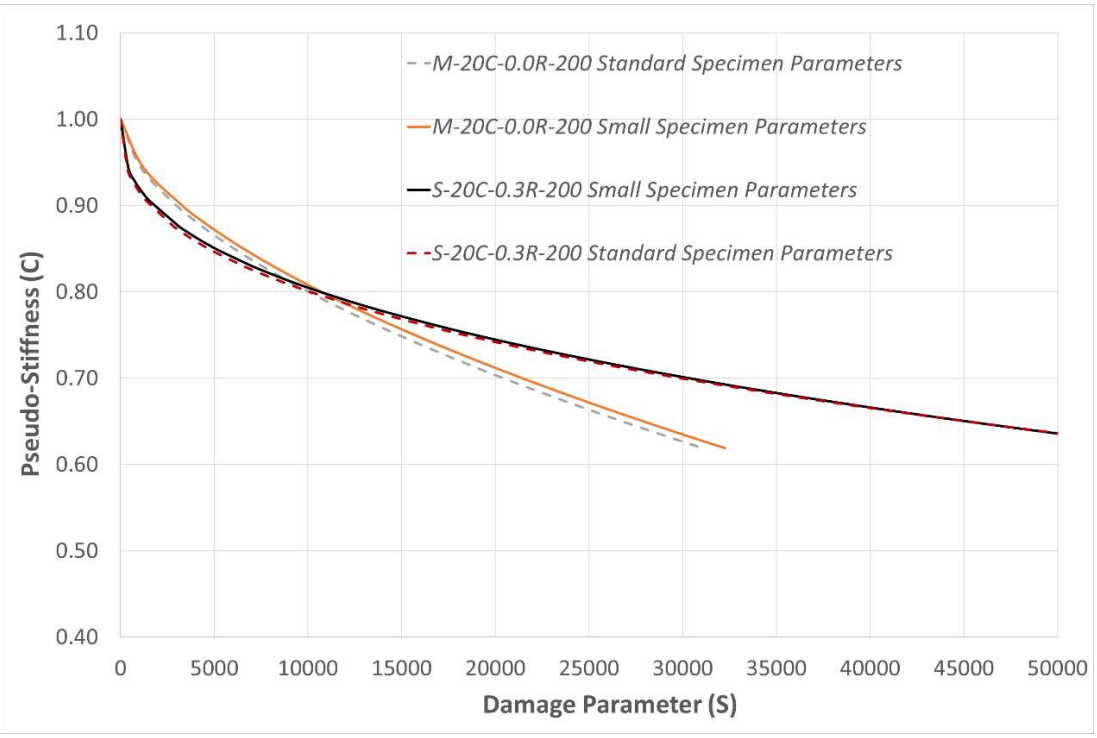

Figure 6-50: Damage Characteristic Curves using parameters of both specimen geometries at 20°C (Small Specimen Parameters: $\alpha = 3.367$, Elve = 7092Mpa; Large Specimen Parameters: $\alpha = 3.134$, Elve = 7192Mpa)

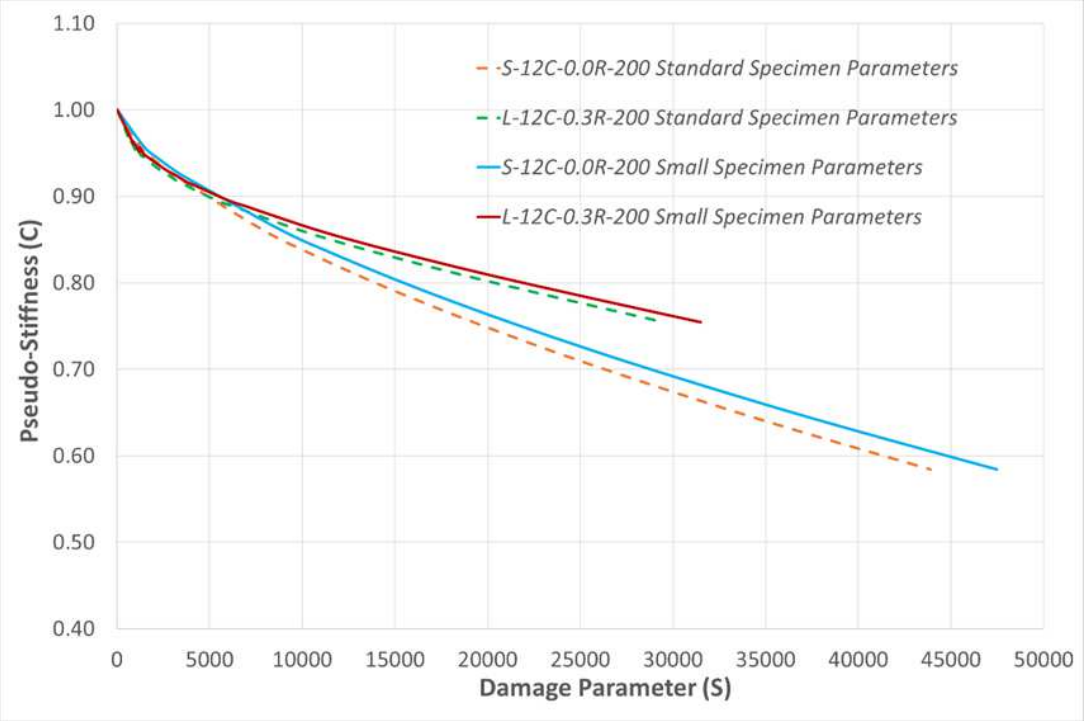

Figure 6-51: Damage Characteristic Curves using parameters of both specimen geometries at 12°C (Small Specimen Parameters: $\alpha = 3.367$, Elve = 11602Mpa; Large Specimen Parameters: $\alpha = 3.134$, Elve = 11805Mpa)

6.6.2. Evaluation of S-VECD Tests Results on Small Specimen

In addition, the damage characteristic curves of various specimen geometries under continuous loading and 0.3s rest period are shown in Figure 6-52 and Figure 6-53 for 12 and 20°C respectively, while the original damage characteristic curves under continuous loading are also presented for reference. Importantly, as mentioned earlier, the initial parts of the damage characteristic curves produced by S-VECD tests are influenced by unstable measurement at the beginning of the tests since the machine takes certain number of cycles trying to reach the required strain level and be stable. As a result, the beginning parts of damage curves may not be taken into account for conclusion of findings.

From Figure 6-52 at 12°C, damage curves produced by different geometries agree well with each other on both continuous loading and 0.3s rest period conditions, the deviation has no specific pattern and within common experimental variation. Based on Figure 6-53, all sizes of specimen produced close damage curves under continuous loading. However, when 0.3 second rest period is inserted, specimen of

different geometries show certain degree of deviation, although the general trend of damage curves are still similar. Specifically, "L-20C-0.3R-200 (2)" and "L-20C-0.3R-400" are showing highest lying and lowest lying curves under 0.3 seconds rest period. While the curve for small specimen "S-20C-0.3R-200" is lying in-between those two extremes and show no signs of deviation from larger size specimen.

In addition, Figure 6-52 and Figure 6-53 also demonstrate the common findings that the insertion of rest period after each load cycle improves the mixture's damage performance. Comparing different temperatures, it is found that the "shift up" of curves caused by the same 0.3s rest period is larger at 20^{o}C compared to that of 12^{o}C, this agrees with findings concluded by stiffness development curves and damage characteristic curves for batch 1 mixture.

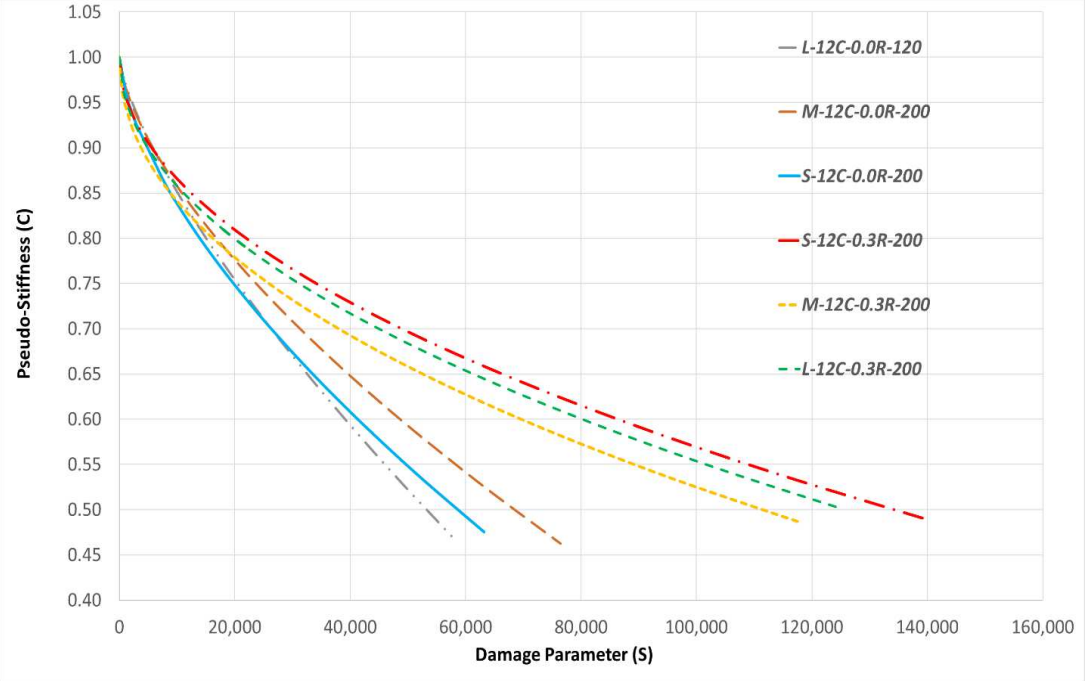

Figure 6-52: Damage Characteristic Curves results with 0.3s rest period at 12^{o}C and all under 200 microstrain

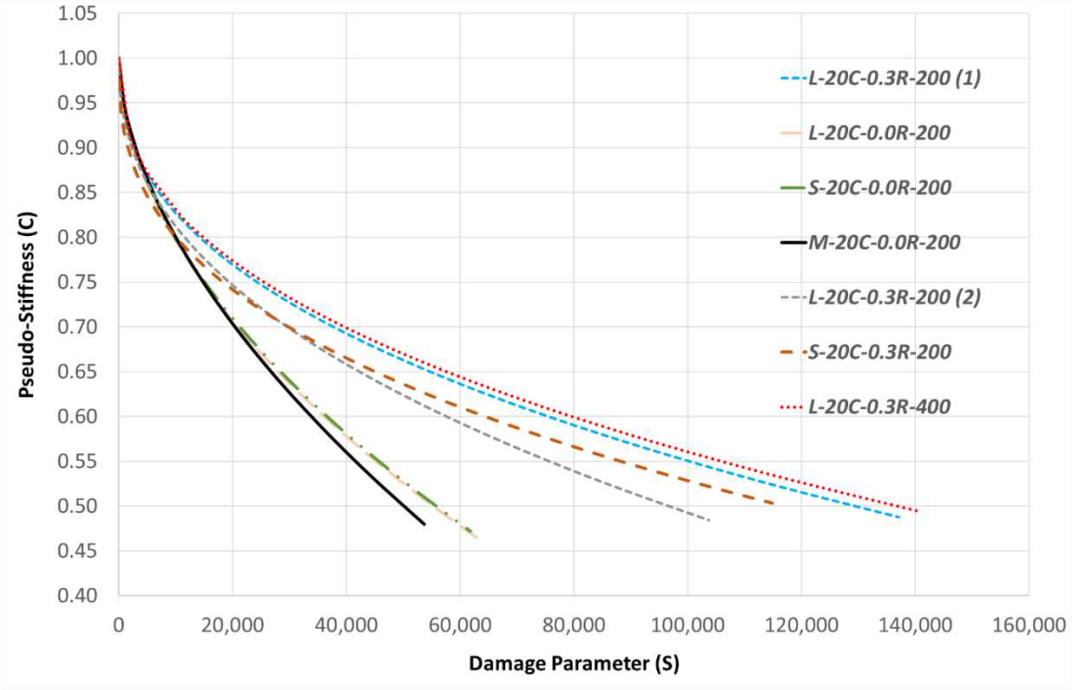

Figure 6-53: Damage Characteristic Curves results with 0.3s rest period at 20^{o}C under various specimen geometries

To sum up, the general observation from both figures is that closely matching curves are found between the results of different geometries. The effect of rest period healing are demonstrated by higher lying curves of 0.3s rest period, for specimen of Small, Medium and Large size, and at both 12 and 20 ^{o}C. Thus it is proven that 54x110mm specimen can produce damage characteristic curve and rest period healing effect similar to that of Large or Medium size (L or M) specimen.

What's more, there are a number of strain amplitudes being used to produce Figure 6-52 and Figure 6-53 as indicated in specimen label. From those curves, it seems the effect of strain amplitudes on damage curves and healing effect is not significant and follows no pattern, since larger strain curve lies slightly lower or higher but generally close to smaller strain curves. However, theoretically, healing effect will be changed according to the damage level at which the rest period occurs (Nascimento, 2015), although the reflection of this theory in S-VECD with rest period tests are due to be addressed by a larger number of tests and rigorous data process, which are out of the scope of current study due to time and resource limitations. Based on current damage curves, the strain amplitude is not influential

to the shape of damage curves with rest period healing effect present. However, the "strain amplitude" here refers to viscoelastic range only, on which the VECD theory is based.. As mentioned before, the strain level should not be too low to affect the proper production of damage curve, while not too large to incur plastic response that will lead into incorrect interpretation of damage property.

6.6.3. Failure Location Statistics

As mentioned in Section 3.4, for cyclic loading tests, it is important to have the failure location to be within LVDT range (refer to Figure 3-10) especially for fatigue life tests. For instance, Figure 6-13 demonstrates how a failure stiffness is identified for a destructive S-VECD test, while such failure point is only correct when the specimen subjects to middle failure. The location of failure is governed by locational void ratio distribution of the asphalt mixture, so a changed specimen geometry can alter the failure location due to changed air void distribution. Thus, it is significant to investigate the modified specimen geometry for its tendency of failure location.

Table 6-11 lists a statistical summary of laboratory obtained failure locations for S-VECD tests using large, medium and small specimen geometries. Those S-VECD tests are not limited to the specimen reported in this article but also from those failed due to various reasons but can still indicate failure location. It should also be noted that the factual results listed in Table 6-11 is based on Curtin University's geomechanical laboratory and relevant facilities/procedures (as listed in Section 3.10), different facilities and procedures adopted in other laboratories may alter the findings. Since the void ratio distribution along the specimen will be altered due to variations in the making procedures of the specimen.

Table 6-11: Possibility of Failure Locations for Various Specimen Geometries

Specimen Geometry	**100x150mm**	**100x130mm**	**54x110mm**
Possibility of Failure Location	Most likely end failure, very few middle failure	High chance of middle failure, occasional end failure	Highest chance of middle failure, low chance of end failure

Chapter 7. Beam Fatigue Tests Results

This chapter presents 4PB beam fatigue test results of flexural stiffness ratio versus number of loading cycles under various conditions.

After the data processing as listed in Section 5.4 and stiffness calculation in Eq.(4.1), Figure 7-1 to Figure 7-3 are beam fatigue test results represented by flexural stiffness ratio versus number of cycles curves. The advantage of presenting cyclic stiffness ratio rather than true stiffness is the availability to verify the healing effect by eliminating specimen to specimen variance.

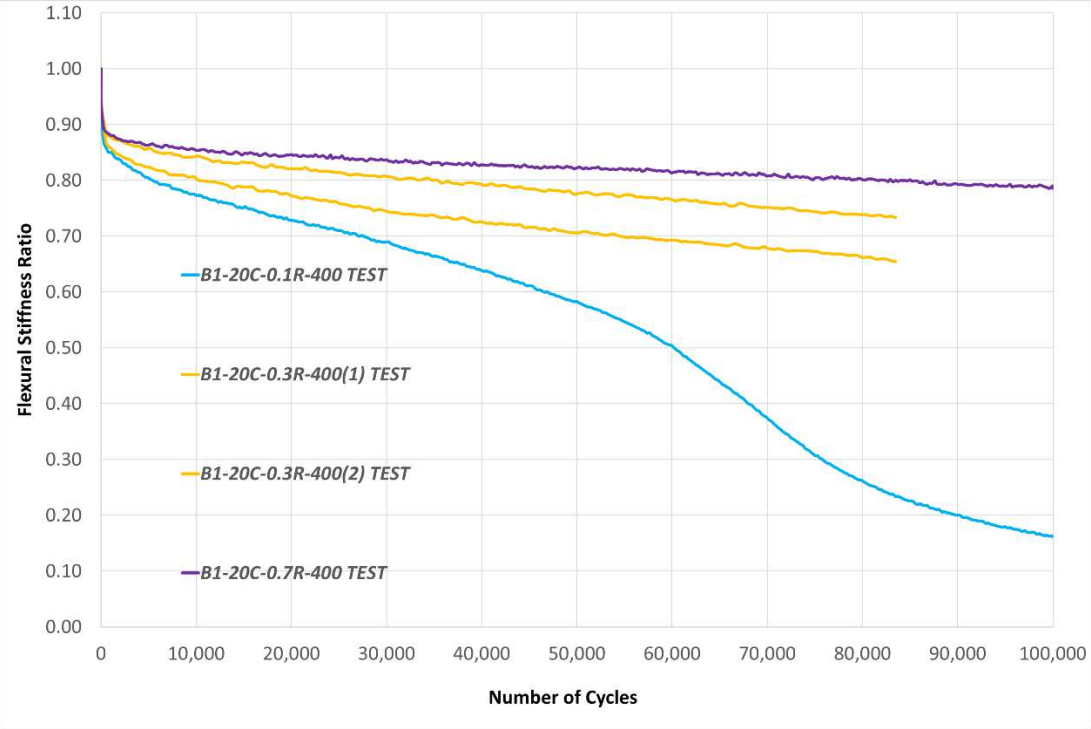

Figure 7-1: Beam Fatigue Test Results – Stiffness Ratio versus Number of Cycles at 20^{o}C, Batch 1 mixture

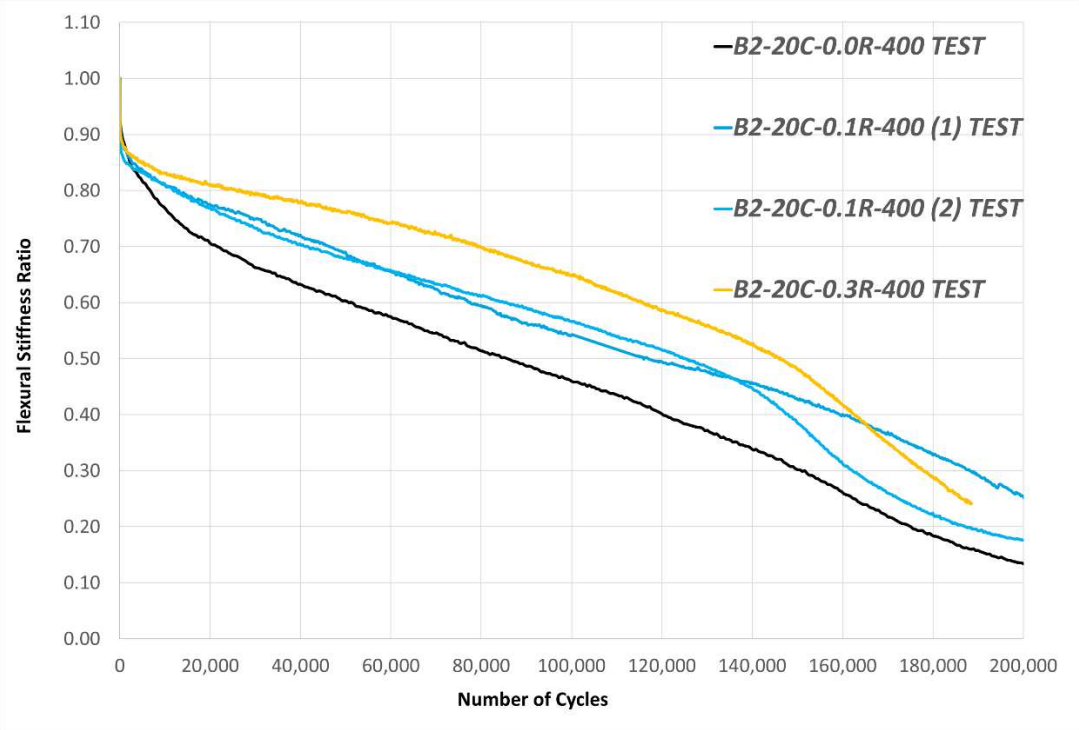

Figure 7-2: Beam Fatigue Test Results –Stiffness Ratio versus Number of Cycles at 20°C, Batch 2 mixture

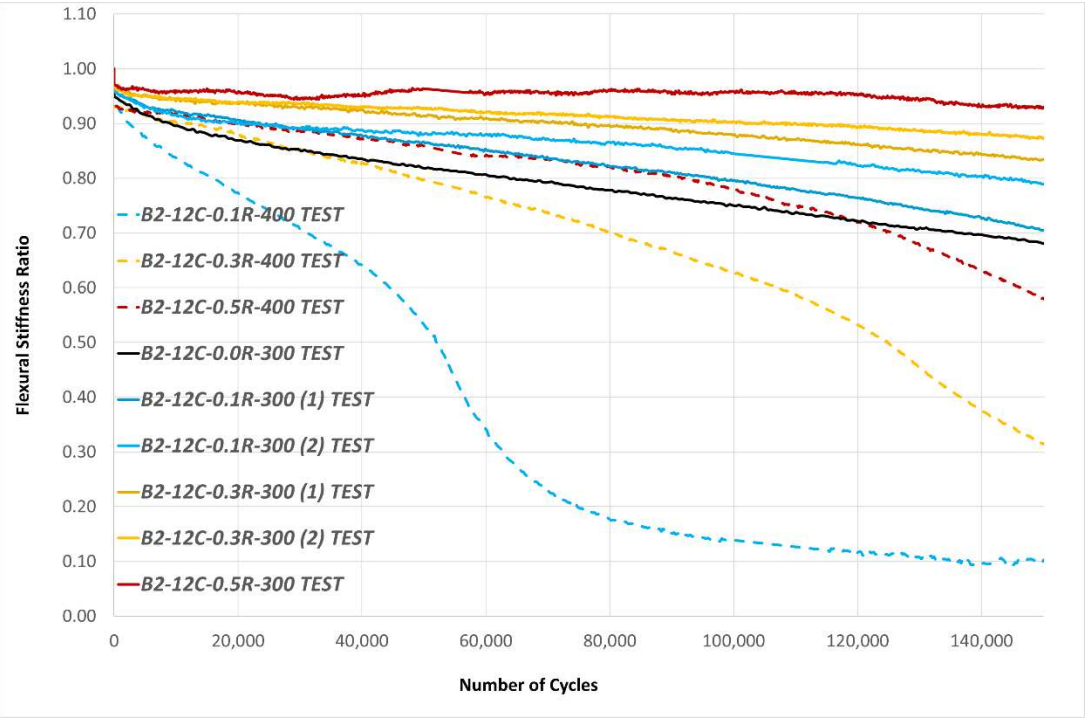

Figure 7-3: Beam Fatigue Test Results –Stiffness Ratio versus Number of Cycles at 12°C

7.1. Effect of Rest Period Healing from 4PB Beam Fatigue Test

From Figure 7-1 to Figure 7-3, the effect of rest period healing has been clearly demonstrated. Generally, for tests with same strain amplitude, longer rest period curves are always higher lying than curves with shorter rest period, this is consistent with AMPT tests findings.

As mentioned in stiffness development results (Section 6.2.3) as well as damage characteristic curve results (Section 6.3.7), batch 2 mixture showed an "unusually" improved healing effect at lower 12 ^{o}C than 20 ^{o}C. To further investigate and verify this interesting behaviour, beam fatigue tested stiffness development curves at both temperatures (12 and 20^{o}C) are drawn together in Figure 7-4 for batch 2 mixture. Remarkably, the curves demonstrated that 12^{o}C has a generally better healing performance at certain rest period. For instance, the 0.3s curve of 12^{o}C is well above that of 20^{o}C, while the 0.5s curve of 12^{o}C has almost been the same as the 0.7s curve of 20^{o}C. Thus, based on both AMPT (such as Figure 6-34) and beam fatigue test results (Figure 7-4), it is reasonable to deduce that improved healing effect at lower 12^{o}C from 20^{o}C is a true material feature for batch 2 of AC10 C320 asphalt mixture. While no such phenomenon is observed for batch 1 mixture, it also gives a clue that change of material supplies may significantly change the asphalt mixture's healing properties. The findings listed here trigger the need for further study on the temperature effect on asphalt mixture or bitumen's healing performance, especially tests like DSR on binder's rest period healing effect could lead into significant verification of findings described here.

To further study the effect of rest period healing, the same healing ratio equation as listed in Eq. (6.1) is utilized. For 20^{o}C, the number of cycles at which the healing ratio is calculated is 50,000. Regarding 12^{o}C, 50,000 cycle still works for those specimen tested under 300 microstrain. However, no healing ratio chart was produced for the microstrain of 400 at 12^{o}C, since the test without rest period at this condition is not done. Also, 400 microstrain is very aggressive test especially without rest period, so unable to obtain stiffness ratio at 50,000 cycles due to early fatigue failure.

Figure 7-5 and Figure 7-6 demonstrate the healing ratio versus length of rest period diagram for 12 and 20 ^{o}C respectively. Similar to AMPT tests results demonstrated from Figure 6-7 to Figure 6-10, the healing ratio increases with the length of rest period, however, the rate of healing ratio increase per second of rest period reduces with longer rest period as the curve becomes flat with longer rest period. Due to the healing ratio is calculated using flexural stiffness, it does not clearly demonstrate same optimum rest period to AMPT produced results (Figure 6-7 to Figure 6-10).

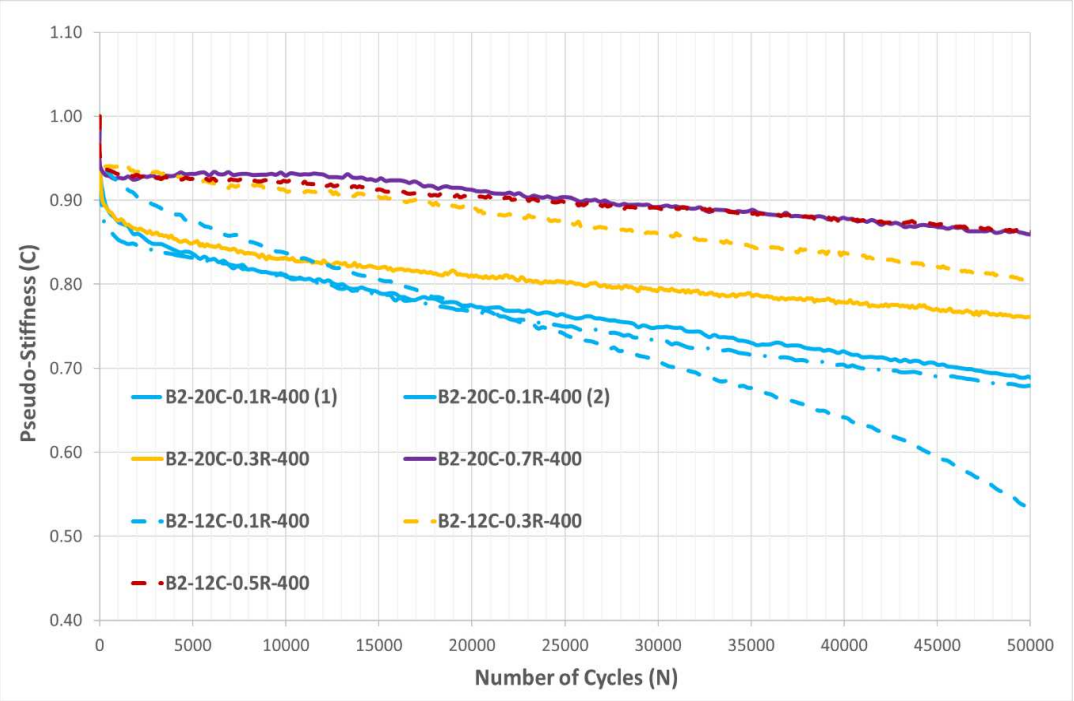

Figure 7-4: Collection of both 12 and 20 ^{o}C mixture tested under 400 microstrain (cyclic), batch 2 mixture

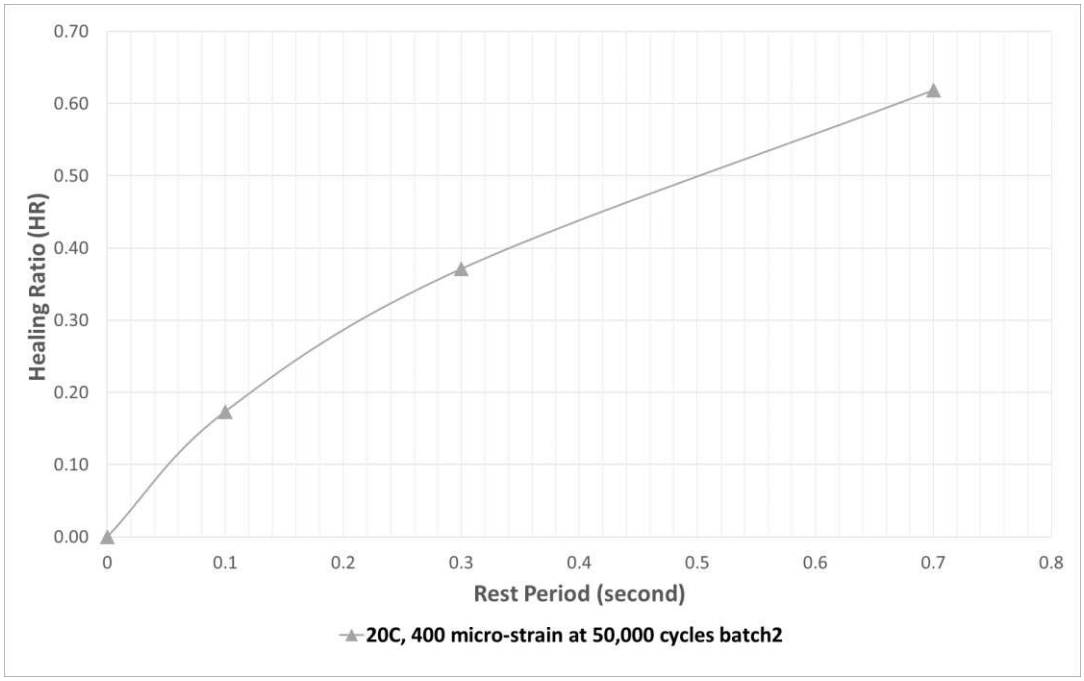

Figure 7-5: Healing ratio with rest period curve at 50,000 cycles under 400 microstrain tension-compression and 20^{o}C (Beam Fatigue Test, Batch 2 Mixture)

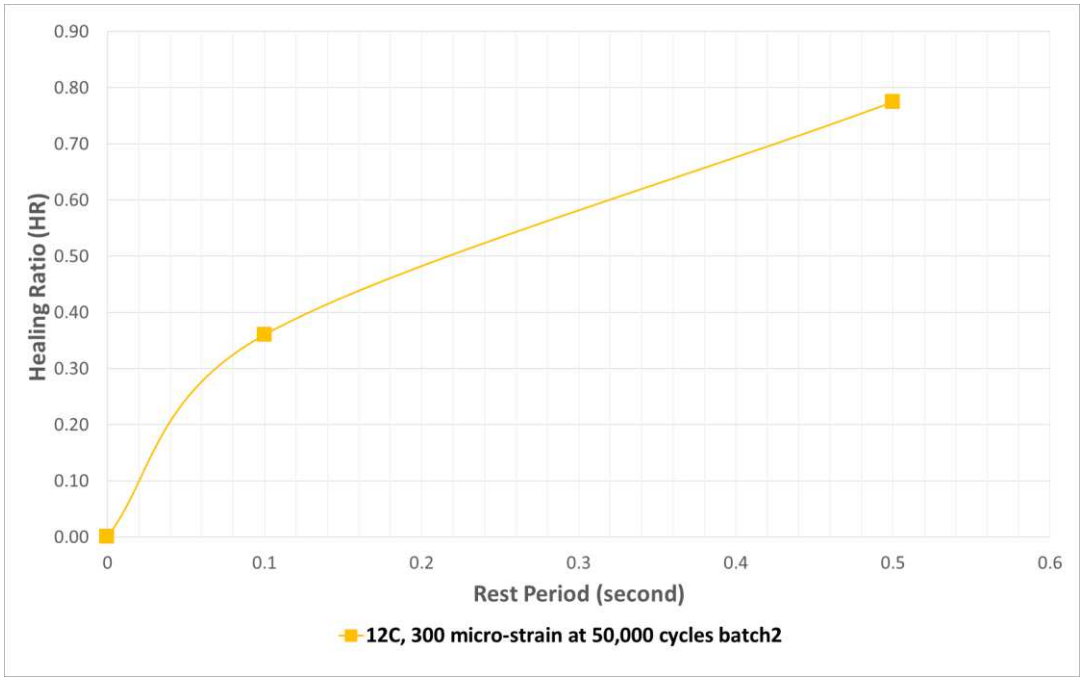

Figure 7-6: Healing ratio with rest period curve at 50,000 cycles under 300 microstrain tension-compression and 12^{o}C (Beam Fatigue Test, Batch 2 Mixture)

7.2. Failure Stiffness

From Figure 7-1 at 20^{o}C, it is evident that almost every specimen starts to drop stiffness much more quickly before the 0.5 stiffness ratio mark. For beam curves, there is always an extended section subjects to gradually increasing tangent ratio, similar to the yielding zone for steel. This is different to failure stiffness in AMPT test, which has much more drastic drop of stiffness ratio when failure occurs. The reason is that in beam fatigue test, the bottom section always subjects to larger strain amplitude so fails more quickly, while the flexural stiffness calculated by the controlling software and thus reflected in those figures is based on the assumption of constant stiffness for the whole cross section (see Section 5.4). As a result, the bottom stiffness ratio may have already declined to 0.5 and failed when the flexural stiffness ratio returned by the software is well above the 0.5 value. However, the testing software does not directly measure bottom stress so bottom layer stiffness can not be produced.

On the other hand, by observing the change of steepness for curves under both 12 and 20 ^{o}C, it is evident that at 12 ^{o}C, the curve starts to drop more quickly at a higher stiffness ratio. For instance, in Figure 7-3, B2-12C-0.5R-400 starts to decline more quickly at 0.8 stiffness ratio. However, most curves in Figure 7-1 and Figure 7-2, which subject to same strain of 200 tensile microstrain but at higher temperature of 20^{o}C, do not indicate more rapid decline until at least below 0.7. This is in line with the AMPT tests results that suggest the mixture has higher failure stiffness ratio at lower temperature.

Chapter 8. ABAQUS Modelling with Rest Period Damage Functions

The rest period damage functions are to be integrated into numerical software ABAQUS, which is used to build a 4PB beam fatigue test model. With procedures described in Roque et al. (2010b), the damage characteristic curve fitting equations and rest period damage functions are able to predict the pseudostiffness with number of cycle curves under specified conditions. The rest period damage functions, as demonstrated in Eq. (6.6) to Eq. (6.9), are written into a UMAT subroutine with a newly designed Fortran program to calculate pseudostiffness with number of cycles. The subroutine acts as a self-defined material constitutive stiffness in ABAQUS so it can produce the material response with output of pseudostiffness C and damage parameter S versus number of cycles under any rest period. The main purpose of building a numerical model with rest period damage functions as its constitutive model is to have a finite element tool that is able to predict damage status of any built model, and verify its capability in comparison to real 4PB beam fatigue test results. To achieve this, specific solutions are derived to compute equivalent flexural stiffness, as used in tests output, from modelling results of pseudostiffness based on a novel block method and beam bending theory.

8.1. Programming Rest Period Damage Functions into UMAT

Eq. (6.4) is the original equation of rest period damage function that needs to be programmed using Fortran language into the UMAT subroutine of ABAQUS. The principal of the program is to find a pseudostiffness that satisfies the C vs S relationship depicted in both Eq. (5.11) and Eq. (6.4), and this is realized by find a value of C that incurs least error between two equations. A Fortran program is thus designed to realize this purpose. The basic programming logic is described in the flow chart below:

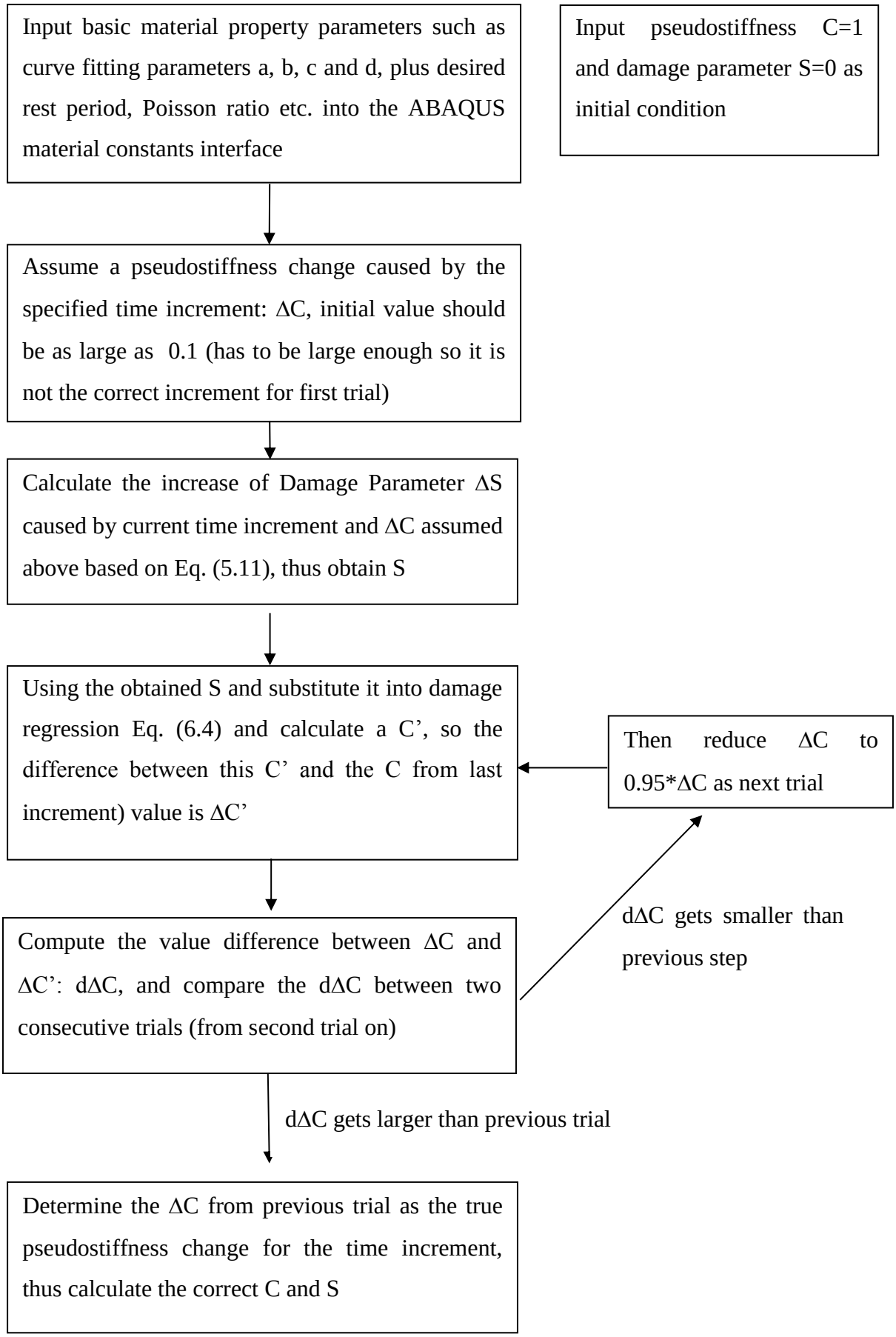
Input basic material property parameters such as curve fitting parameters a, b, c and d, plus desired rest period, Poisson ratio etc. into the ABAQUS material constants interface
Input pseudostiffness C=1 and damage parameter S=0 as initial condition
Assume a pseudostiffness change caused by the specified time increment: ΔC, initial value should be as large as 0.1 (has to be large enough so it is not the correct increment for first trial)
Calculate the increase of Damage Parameter ΔS caused by current time increment and ΔC assumed above based on Eq. (5.11), thus obtain S
Using the obtained S and substitute it into damage regression Eq. (6.4) and calculate a C', so the difference between this C' and the C from last increment) value is ΔC'
Then reduce ΔC to 0.95*ΔC as next trial
Compute the value difference between ΔC and ΔC': dΔC, and compare the dΔC between two consecutive trials (from second trial on)
dΔC gets smaller than previous step
dΔC gets larger than previous trial
Determine the ΔC from previous trial as the true pseudostiffness change for the time increment, thus calculate the correct C and S

The Fortran script of rest period damage function, produced in the aid of Microsoft Visual Studio 2012, is attached in Appendix A. The new constitutive model is capable of calculating the pseudostiffness C and damage parameter S for each loading cycle and it works for any geometrical shape of asphalt model as long as there are prescribed strain values. A list of important points regarding the current rest period damage model is presented below:

1. The model is based on cyclic values rather than time values, e.g. it gives the cyclic pseudostiffness for each cyclic loading time but not pseudostiffness for real time. The reason is that real time based model is highly time consuming to execute, since the time increment should be extremely small when complete VECD from of Eq.(2.8) is applied. What's more, simplified VECD tests itself is based on cyclic data, so is the 4PB beam fatigue result of flexural stiffness.
2. For now, the model produces only accurate pseudostiffness C and S but not the real stiffness and real stress. Since the real stiffness matrix for a beam under cyclic destructive loading is complex, such as only tensile stiffness of each node is changing with number of cycles. The current program does not calculate real stress and strain of the model as it is not necessary for a fatigue problem of beam.

As a result, for the purpose of this research project, this constitutive model is capable of modelling constant strain beam fatigue tests by producing damage S and pseudostiffness C with number of cycles. While a complete true stress strain model remains as a future topic.

8.2. ABAQUS Model Building

For a 4PB beam fatigue test, only the support span and loading span need to be modelled. The most critical section of a beam fatigue test is the bottom surface, where the tensile strain is the largest and is also the section that subjects to the input tensile strain. However, the whole height at centre section of the beam should be modelled due to different strain amplitude and damage status across the height. In this study, the beam is assumed to only bend as plane strain.

8.2.1. Beam Model

The beam is modelled as "2D Planner" of the longitudinal cross section of the supported span. Based on beam and set up dimension as listed in Table 4-5, the ABAQUS model of beam is built as shown in Figure 8-1, with two arrows at one third of the span each side representing the location of load cell. Since the beam test is strain controlled, two vertical strain displacements are applied at the arrow locations, and the magnitude of this boundary displacement is obtained by trial and error to achieve the desired tensile strain at the bottom of centre section. Also, the beam model is partitioned into two parts, thus the critical centre section can have nodes during meshing and this is easy for results interpretation.

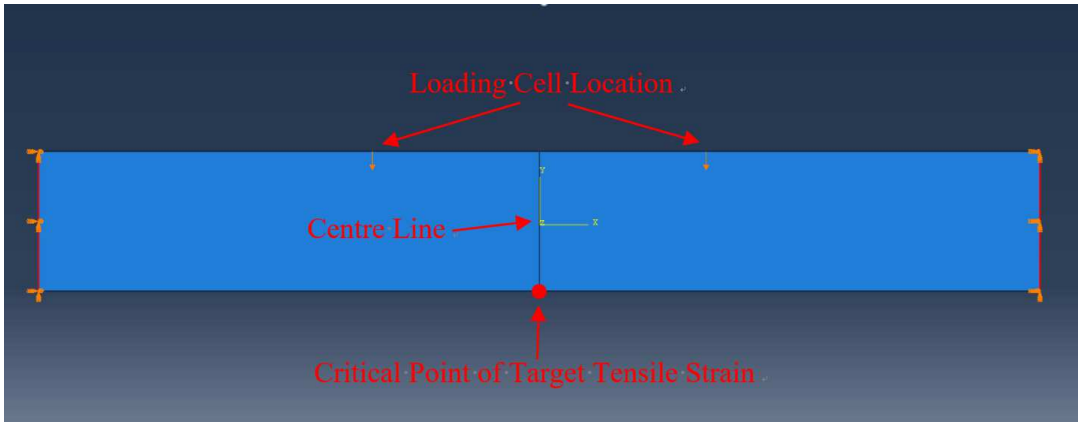

Figure 8-1: ABAQUS model of the Beam Bottom Section that subjects to prescribed tensile strain

8.2.2. Input Material Parameters

A total of 14 material constants are required into the "Material" section of ABAQUS. Those parameters correspond to certain mixture under certain temperature, and whenever the mixture type and temperature are changed, certain parameters need update. Table 8-1 gives a list of those 14 material constants with example values for batch 1 mixture at 12 and 20^{o}C. For each batch of mixture, they have relevant curve fitting parameters such as C10, C20, a, b, c and d, plus other material characteristic parameters used in Eq. (6.6) to Eq. (6.9). It also includes parameters like damage power term, finger print stiffness and representative stiffness. In a realistic model analysis, if a material's finger print stiffness (E_{finger}) and representative stiffness (E_{lve}) are ready, they can be input into the model.

However, for demonstration, finger print stiffness (E_{finger}) is set to be equivalent to representative stiffness (E_{lve}), which means the model uses the representative stiffness from dynamic modulus tests then adopt a E_{finger} of identical value. This makes the modelling results as a general average and more representative for certain rest period.

Table 8-1: ABAQUS Material's Constants Input, Definitions and Examples for Tested Mixture

Constants No.	**Definitions of Mechanical Constants**	**Example Values for Batch 1 Mixture at 12°C**	**Example Values for Batch 1 Mixture at 20°C**
1	Representative Stiffness (Elve) (Mpa)	11805.33	7192
2	Damage Power Term	3.13	3.13
3	K1 (see Eq.)	0.46	0.46
4	Time – Temperature Shift Factor	12.14	1
5	Rest Period	User Input	User Input
6	C10 (see Eq.)	0.000375	0.00113
7	C20 (see Eq.)	0.6523	0.5558
8	a (see Eq.)	0.0016	0.00369
9	b (see Eq.)	0.442	0.2877
10	c (see Eq.)	0.218	0.1888
11	d (see Eq.)	0.39	0.2534
12	Finger Print Modulus (Mpa)	11805.33	7192
13	Poison Ratio of Material	0.3	0.3
14	Loading Frequency	10	10

8.2.3. Time Increment

Since the model is based on simplified VECD (only calculate cyclic values) as stated in Eq. (5.11), the time increment should be chosen as the period of a loading cycle or its integer multiple. Since all beam fatigue and AMPT tests conducted are under standard 10Hz in this study, so the time increment should be 0.1(s) as minimum. However, a fixed 0.1s time increment makes the whole simulation highly time consuming, thus the integer multiples of 0.1s such as 10 and 100s are also used to speed up the simulation when the number of cycles get larger. The specific time

increment plan used in the ABAQUS model is listed in Table 8-2. The time increment is really a customized value and can be adjusted as long as the results are accurate, the philosophy here is to save modelling time while following considerations could also be important:

1. the initial cycles should better be true time increment as rapid damage and change of stiffness occur during the early stage of a fatigue test
2. as the stiffness develops with number of cycles, larger time increment of integer multiple of the original increment can be used proportional

This time increment plan (see Table 8-2) has already been verified for its accuracy. Compared to a time increment of 0.1s fixed throughout the whole cycles, gradually increasing time increments with number of cycles incurs little change on the modelling results.

Table 8-2: The time increment plan used in ABAQUS modelling

Number of Cycles	Input Time Increment (second)
0-100	0.1
100-1100	1
1100-11100	10
11100-211100	50

8.2.4. Boundary Conditions

Both ends of the model are modelled as fixed end using "Encastrate" in ABAQUS to simulate the sections of the real beam fixed by clamps. As shown in Figure 8-1, the model is separated into two parts with its centre line to mark out the critical central section. Two boundary conditions are added at the top surface to simulate the locations of loading cells of the real beam sitting in test facility. They are given vertical displacement of the same magnitude so to bring out a tensile strain at the bottom of centre line as the target tensile strain.

8.2.5. Model Mesh

Since the VECD with rest period constitutive model calculates the damage performance based on element strain, and the calculation results are governed by the

user defined constitutive model with user input material parameters. The centre line of the model has strain values varying across the whole height and thus requires finer mesh, while both ends of the model can be sparsely meshed for computational simplicity, as only centre line results are necessary at this stage. As a result, a simple mesh scheme is applied as shown in Figure 8-2. The mesh scheme also accommodates the need of block method introduced in below section.

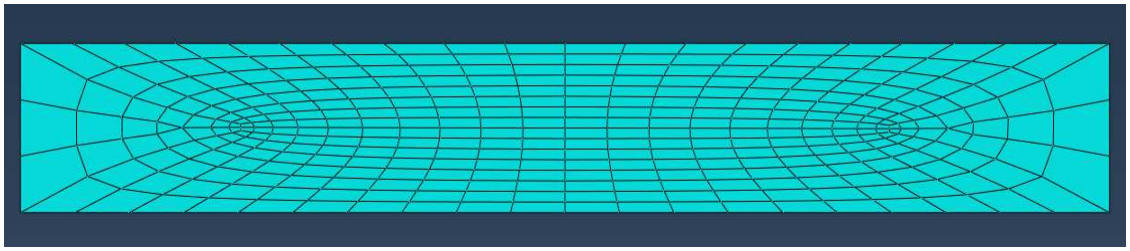

Figure 8-2: Meshed ABAQUS Model

8.3. Equation Derivation for Flexural Stiffness using Block Methods

It is important to realize that the flexural stiffness returned by beam test control software is programed in a way to calculate the stiffness of the critical bottom section as shown in Eq.(5.16) and Eq.(5.17). However, flexural stiffness is equivalent to bottom stiffness only when the stiffness value is assumed to be unchanged throughout the beam's cross section. In reality, the bottom section of the cross section subjects to the largest strain so quicker stiffness reduction, thus the flexural stiffness has no physical meaning in such case but just a mathematical indication that is proportional to the general damage status of the cross section. Figure 8-3 demonstrates the strain amplitude and stiffness condition for the critical cross section of the beam.

On the other hand, the modelling results return a stiffness profile across the critical section, for which only the tensile section below neutral axis is of interest for fatigue problems. Therefore, the simulation results of pseudostiffness need to be converted into flexural stiffness that test software produced from damaged cross section. The purpose is to re-calculate the equivalent flexural stiffness based on ABAQUS output, in a way same as 4PB beam test software has used to produce the flexural stiffness. In beam tests, the flexural stiffness is calculated as:

$$E_{flexural} = \frac{\sigma_{tensile}}{\varepsilon_{tensile}} \tag{8.1}$$

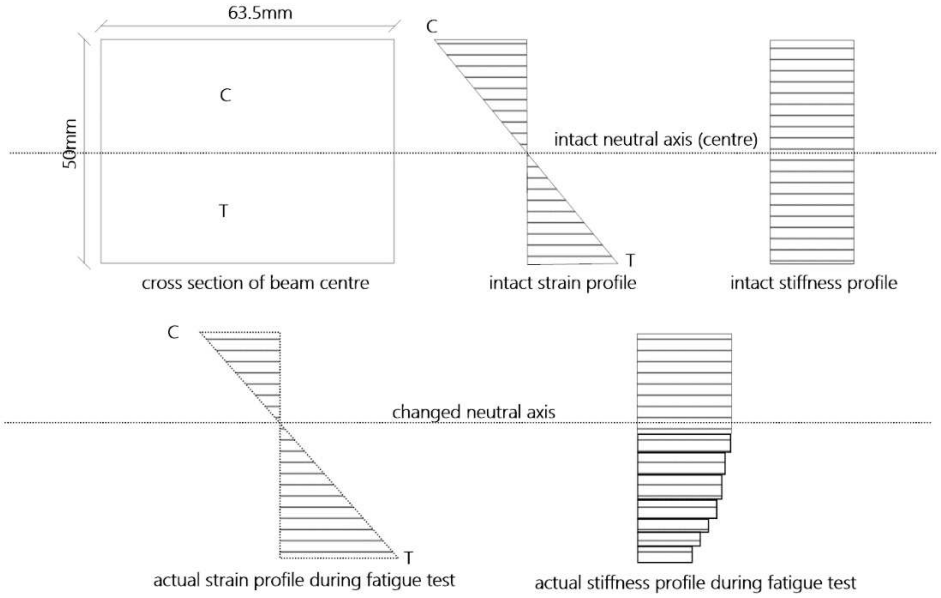

Figure 8-3: Illustration of strain and stiffness profiles for the centre cross section of beam (T=tension, C=compression)

in which $E_{flexural}$ is the flexural stiffness that returned by beam fatigue test; $\varepsilon_{b,tensile}$ is the tensile strain at the bottom of the beam (input constant strain value); $\sigma_{tensile}$ is the tensile stress calculated based on the moment on the cross section exerted by the loading cell (under the assumption of constant stiffness on the whole cross section):

$$\sigma_{tensile} = \frac{d*M}{2I} = \frac{L_{support}*\sigma_{cyc}*1000000}{b*H^2} \tag{8.2}$$

in which d is the height of the beam, M is the bending moment exerted on the centre section of the beam and is calculated by the machine based on loading cell readings (also the largest bending moment inside the beam), I is the second moment of inertia for the beam cross section. Importantly, as mentioned, Eq.(8.2) is an expanded form of Eq.(5.16) and is thus based on assumption of constant cross section stiffness. For beam fatigue test, the $\sigma_{tensile}$ computed here is not the true tensile stress at the bottom of the beam, since the real stiffness there is actually reduced with number of cycles due to damage.

As a result, for the longitudinal cross section modelled by ABAQUS, only the M value on the central cross section (see Figure 8-1) should be calculated so the corresponding flexural stiffness for beam model can be obtained through Eq.(8.2). However, the current model in ABAQUS does not directly produce M as the proposed constitutive model is about pseudostiffness and damage status at each node and element for each load cycle, rather than true stiffness and stress at a real time. This is also previously discussed in Section 8.1. Consequently, special methods need to be developed to calculate bending moment M at the central cross section thus flexural stiffness based on simulation results of pseudostiffness.

The ABAQUS simulation provides pseudostiffness along each element node of the centre line, while strain amplitude is constant and linearly distributed (see Figure 8-3) along the transverse cross section throughout the whole simulated load cycles. The method adopted in this study to calculate bending moment M in critical cross section is to divide the cross section by 9 nodes into 9 blocks, this method is similar to the approaches proposed by Christensen and Bonaquist (2005). However, the current block method remain true length of each block, instead of the equivalent length used by Christensen and Bonaquist (2005), since ABAQUS is able to calculate the psuedostiffness thus real stiffness at each node as shown in Figure 8-6.

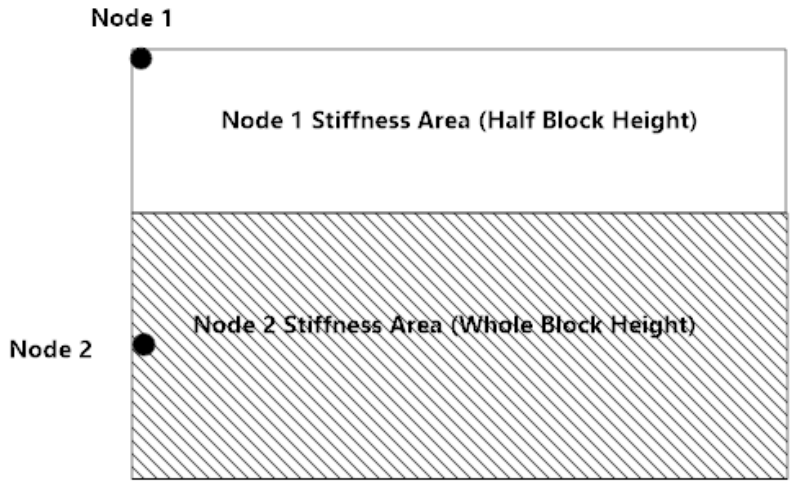

Figure 8-4: Illustration of ABAQUS nodes and the relevant element block area for stiffness assignment

The division scheme for the block method is illustrated in Figure 8-4 (top two blocks). The illustrated blocks are two representative blocks generated, in real model, there are actually two end blocks plus 7 middle blocks. The end node (node 1) are nodes located at the bottom and neutral axis of the cross section area. The strain and stiffness of each element (block) for the tensile section (lower half of the model) are represented by the strain and stiffness at the node locations marked in Figure 8-4, in which the elements are separated into two categories: end elements (2 of them) and middle elements (7 of them). From simulation, each node produces a pseudostiffness value at certain number of cycles throughout the whole fatigue test modelling. The pseudostiffness at each block is assigned by corresponding node stiffness at the centre of the block for 7 middle blocks, with two end blocks having pseudostiffness of the nodes at the corner.

The strain at each representative block is calculated as:

$$\mathcal{E}_n = \frac{2*\varepsilon_{b,tensile}*y_n}{d} \tag{8.3}$$

Then, the bending moment on the tensile part of the cross section can be calculated as:

$$M_{tensile\ section} = \sum_1^N (E_n * \varepsilon_n * b * y_n * H_n) \tag{8.4}$$

in which E_n is the representative stiffness at the nth block, y_n is the vertical distance to neutral axis of each block, b is the breadth of each block (same as the whole cross section), H_n is the height of each block.

Since the beam subjects to damage, the stiffness reduces along the cross section and this will lead into change of neutral axis away from centre height location. Once the stiffness of each block is calculated based on ABAQUS output of pseudostiffness value, the change of neutral axis by distance Δy can be computed according to force equilibrium on the cross section, so the following equation is derived:

$$\Delta y = \frac{\zeta - 1}{\zeta + 1} * \frac{d}{2} \tag{8.5}$$

$$\zeta = \sqrt{\frac{0.5*\varepsilon_{b,tensile}*E'}{\sum_1^N E_n*\varepsilon_{t,n}*\frac{2*H_n}{d'}}} \tag{8.6}$$

in which d' is the height of tensile cross section based on the updated neutral axis. $\frac{2*H_n}{d'}$ actually accounts for the height (or area) ratio of the height of each divided block to the height of the whole tension area of beam's cross section, so it actually remains unchanged no matter how d' changes. $\varepsilon_{t,n}$ is the representative tensile strain of each block, which is assumed to be unchanged during the whole cycle, although it actually slightly increase as neutral axis moves upwards with more tensile damage (the influence is assumed to be little). It should be noted that Eq. (8.5) and Eq. (8.6) do not give exactly accurate change of neutral axis since the force based on blocks is just an approximation, however, the accuracy can be improved by generating more blocks. The total moment at cross section can then be computed as:

$$M_{model} = \sum_1^N (E_n * \varepsilon_n * b * y_n * H_n) + \varepsilon_{t,comp} * E' * \frac{bd'^2}{12} \tag{8.7}$$

in which the second term is derived from common beam theories to calculate the contribution of bending moment from the compressive section by assuming intact compressive stiffness of E' = finger print stiffness. $\varepsilon_{t,comp}$ is the compressive strain at the top of the beam and can be calculated from the movement of neutral axis. The strain ε_n is fixed based on Eq.(8.3), but it actually increases slightly with the changing neutral axis caused by damage, but this effect of changing tensile strain on the calculated moment in Eq.(8.7) is neglected as the effected is countered by more damage also caused by larger strain. Since larger damage brings out lower stiffness E_n that reduces total moment in Eq.(8.7), while increased ε_n raises the moment in Eq.(8.7).

In fact, the beam's cross section subjects to both tension and compression, and the compression stiffness can be assumed as constant of intact material stiffness (fingerprint stiffness). Substitute Eq. (8.7) into Eq. (8.2), after processing, the following equation is obtained for calculating flexural stiffness from ABAQUS output:

$$E_{flexural} = \frac{6*\sum_1^n (E_n*\varepsilon_n*y_n*H_n)}{d^2*\varepsilon_{target}} + \frac{\varepsilon_{t,comp}}{\varepsilon_{target}} * \frac{1}{2} * E' \quad (8.8)$$

E_n can be represented using pseudostiffness C as:

$$E_n = E' * C \quad (8.9)$$

in which E' is the intact stiffness of the material and can be taken as equal to finger print stiffness. Substitute Eq. (8.9) into Eq. (8.8) the equation becomes:

$$E_{flexural} = \frac{6*\sum_1^n (E'*C_n*\varepsilon_n*y_n*H_n)}{d^2*\varepsilon_{target}} + \frac{\varepsilon_{t,comp}}{\varepsilon_{target}} * \frac{1}{2} * E' \quad (8.10)$$

in which C_n is the representative pseudostiffness for each block, equal to the node pseudostiffness at corresponding locations (see Figure 8-4). It is important to notice that the flexural stiffnes $E_{flexural}$ calculated from above equation derivation stands for equivalent flexural stiffness output by software only. The testing control software assumes no-damage on cross section to calculate its flexural stiffness as demonstrated in Eq.(8.2), so it does not directly measure the bottom tensile stress so impossible to produce true stiffness at the bottom surface directly. However, the true flexural stiffness at bottom node due to each damage status can be directly obtained from ABAQUS simulation.

In addition, it is necessary to identify the fatigue endurance limit strain level, and make the pseudostiffness constant as 1 for block sections that subject to a strain amplitude exceeds endurance limit level (no damage). Since otherwise, forcibly using damage equations, when there is actually no accumulated damage, incurs wrong results. The fatigue endurance limit can be obtained by conducting the 4PB beam fatigue tests at a very low strain level and increase it until there is evident drop of stiffness values with number of cycles. Alternatively, it can be estimated from AMPT tests in a similar way.

8.4. Modelling Results Presentation

ABAQUS runs simulation of 4PB beam fatigue tests with user subroutine UMAT, which integrates the proposed rest period damage functions as constitutive model.

Firstly, necessary displacement and geometry factors for each block are presented. It is followed simulation results of flexural stiffness ratio versus number of cycles at each temperature for each batch of mixture. Such results are presented alongside real tests results, this enables a comparison study to evaluate the accuracy and capability of the proposed rest period damage functions.

8.4.1. Acquire parameters for each block

After simulation, the deformed model is illustrated in Figure 8-5. The nodes subject to tensile strain along the centre line are marked in red (including the top red point that can be regarded as at neutral axis position) in Figure 8-6, while the node at the bottom subjects to largest tensile strain, which is also input tensile strain magnitude. Since this research uses two strain magnitudes of 300 and 400 microstrain (cyclic strain), so the tensile strain magnitude applied at the bottom red point is 150 and 200 tensile microstrain respectively. Among the nine red nodes in tensile, the top nodal strain is known as zero and the bottom strain is equal to the input strain amplitude for the test. The strain for nodes in between follows the linear extrapolation since the beam can be assumed as plane strain in such case. ABAQUS model has fixed strain at each node. But for actual bending beam, the tensile strain across the beam height, excluding bottom surface, will slightly increase with more number of cycles due to rising of neutral axis. This means the actual bending moment and flexural stiffness on the cross section is slightly larger than calculated in Eq.(8.10). However, slightly larger strain also means larger damage, which reduces the obtained flexural stiffness values, thus the strain increase with load cycles can be reasonably neglected. As a result, according to the scheme indicated in Figure 8-4, the representative tensile strain amplitude (ε_n), the block height (H_n) and arm of moment calculation (y_n) for each block are demonstrated in Table 8-3. It is noteworthy that for strain at each node, both ABAQUS output and linear extrapolation lead into quite close values so using either value is eligible. Consequently, with the ABAQUS output of pseudostiffness (C_n), all parameters are now available so Eq. (8.5) to Eq. (8.10) can be activated to calculate the final modelling results of flexural stiffness.

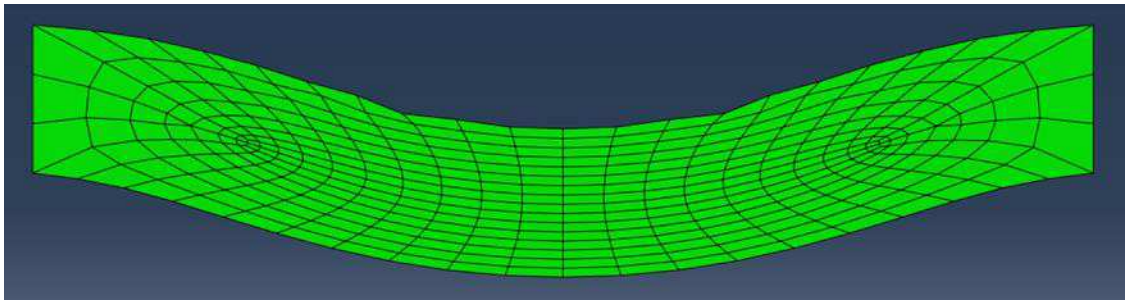

Figure 8-5: Deformed ABAQUS model after simulation (scaled up)

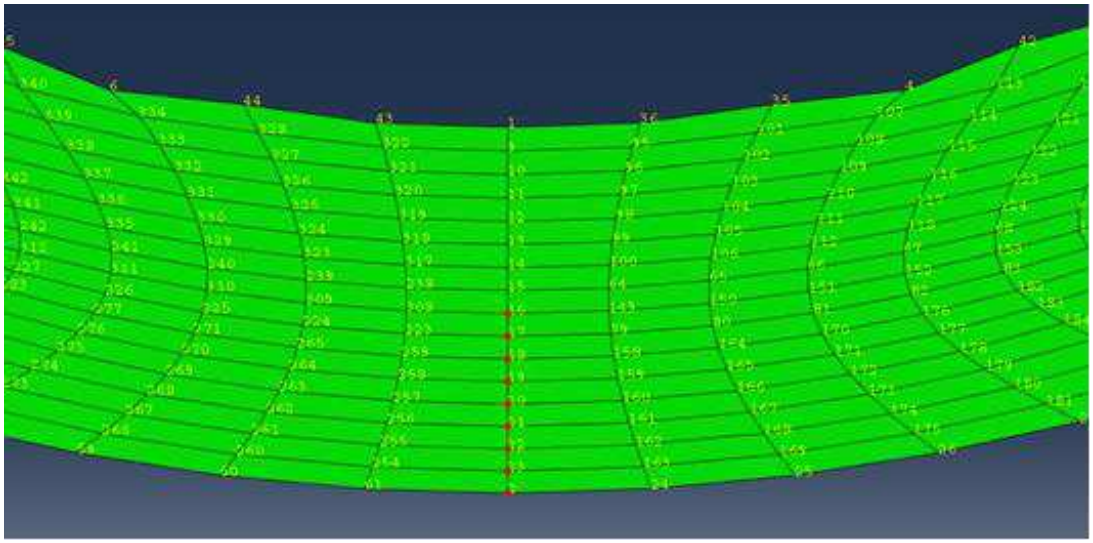

Figure 8-6: A close view of deformed model -- Nodes along the centre line marked in red

Table 8-3: Representative strain, height and moment arm of each block of beam's cross section under two used tensile strain amplitudes

Strain Amplitude = 200 microstrain								
ε1	**ε2**	**ε3**	**ε4**	**ε5**	**ε6**	**ε7**	**ε8**	**ε9**
5.23E-06	2.09E-05	4.60E-05	7.13E-05	9.70E-05	1.23E-04	1.49E-04	1.74E-04	1.94E-04
H1	**H2**	**H3**	**H4**	**H5**	**H6**	**H7**	**H8**	**H9**
1.5625	3.125	3.125	3.125	3.125	3.125	3.125	3.125	1.5625
y1	**y2**	**y3**	**y4**	**y5**	**y6**	**y7**	**y8**	**y9**
0.78125	3.125	6.25	9.375	12.5	15.625	18.75	21.875	24.21875
Strain Amplitude = 150 microstrain								
ε1	**ε2**	**ε3**	**ε4**	**ε5**	**ε6**	**ε7**	**ε8**	**ε9**
3.93E-06	1.57E-05	3.45E-05	5.36E-05	7.28E-05	9.22E-05	1.12E-04	1.31E-04	1.45E-04
H1	**H2**	**H3**	**H4**	**H5**	**H6**	**H7**	**H8**	**H9**
1.5625	3.125	3.125	3.125	3.125	3.125	3.125	3.125	1.5625
y1	**y2**	**y3**	**y4**	**y5**	**y6**	**y7**	**y8**	**y9**
0.78125	3.125	6.25	9.375	12.5	15.625	18.75	21.875	24.21875

8.4.2. Batch 1 mixture at 20°C

The beam fatigue tests of batch1 mixture at 20°C are conducted with 0.1, 0.3 and 0.7 seconds rest periods and under single magnitude of 400 cyclic tension compression microstrain (so 200 tensile microstrain). As mentioned, to take into account the fatigue endurance limit effect, any block section subjects to lower than 75 (for batch 1 mixture only) tensile micro strain is given an intact pseudostiffness of 1. The tests and simulation results under this condition are plotted together in Figure 8-7.

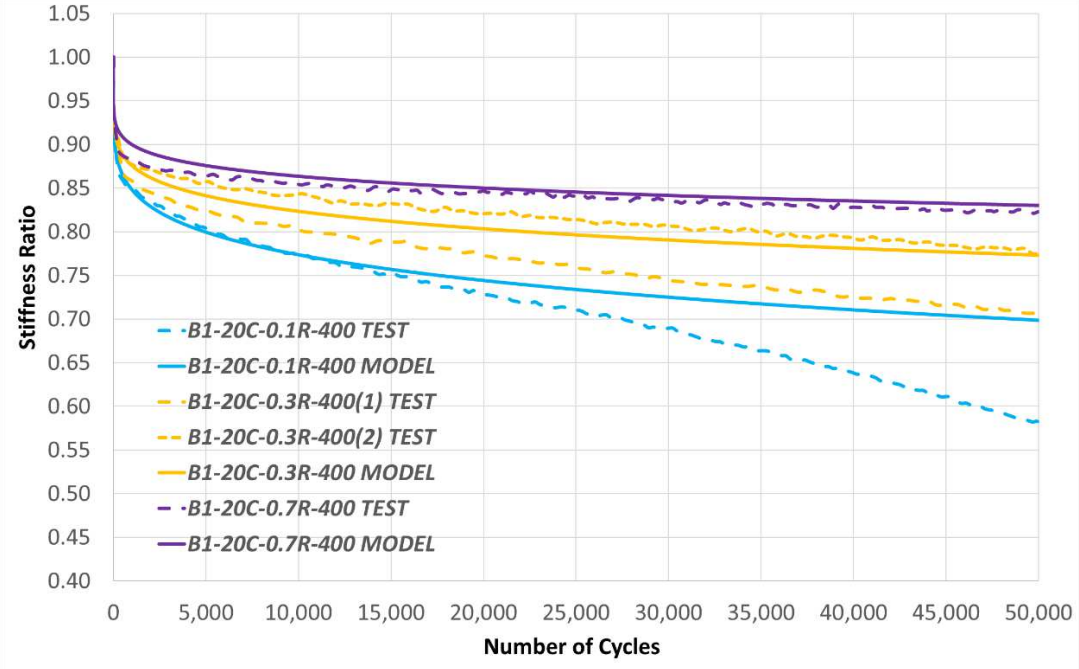

Figure 8-7: Model and Tests Results comparison at 20°C, 200 tensile microstrain of batch 1 mixture

Since there are two sets of 0.3 second rest period tests as shown in Table 4-1, the simulation results of 0.3s rest period curve lie close to an average position of two tests results. From the figure, there is good agreement between modelling and tests results within the viscoelastic range. The viscoelastic range means when the whole cross section is still governed by viscoelastic continuum damage without fatigue failure (macro-cracks). Obviously, the ABAQUS simulation is based on rest period damage functions of VECD method, it only produces results of viscoelastic behaviour. However, for real beam fatigue test indicated in Figure 8-3, the bottom block of the beam has reached failure already while the total flexural stiffness is a reflection of all blocks on the cross section. Outside of viscoelastic range, the

stiffness starts to decrease more quickly for beam fatigue test results due to viscoplastic response at certain part of the cross section, e.g. the "B1-20C-0.1R-400 TEST" curve declines more quickly than "B1-20C-0.1R-400 TEST" after certain point. With the beam subject to more loading cycles, more blocks have reached the limit of viscoelasticity so the stiffness declines more and more drastically.

To prove this effect, the stiffness development curves for the bottom node (see Figure 8-6) produced by ABAQUS is drawn in Figure 8-8. A failure stiffness ratio of 0.5-0.6 is common failure criteria as proven by VECD tests results, so it is indicated clearly in the figure that less rest period leads into quicker failure for bottom section. For instance, for 0.1s the bottom section may subjects to failure between 10,000 to 30,000 cycles (see Figure 8-8), that is also the number of cycles that the test results start to drop more quickly in Figure 8-7. Lastly, the 0.7s curve in Figure 8-8 does not exceed the 0.6 stiffness ratio mark, so in Figure 8-7, tests and simulation results of 0.7s are well in line for the whole loading cycle demonstrated, since the real beam is within viscoelastic response.

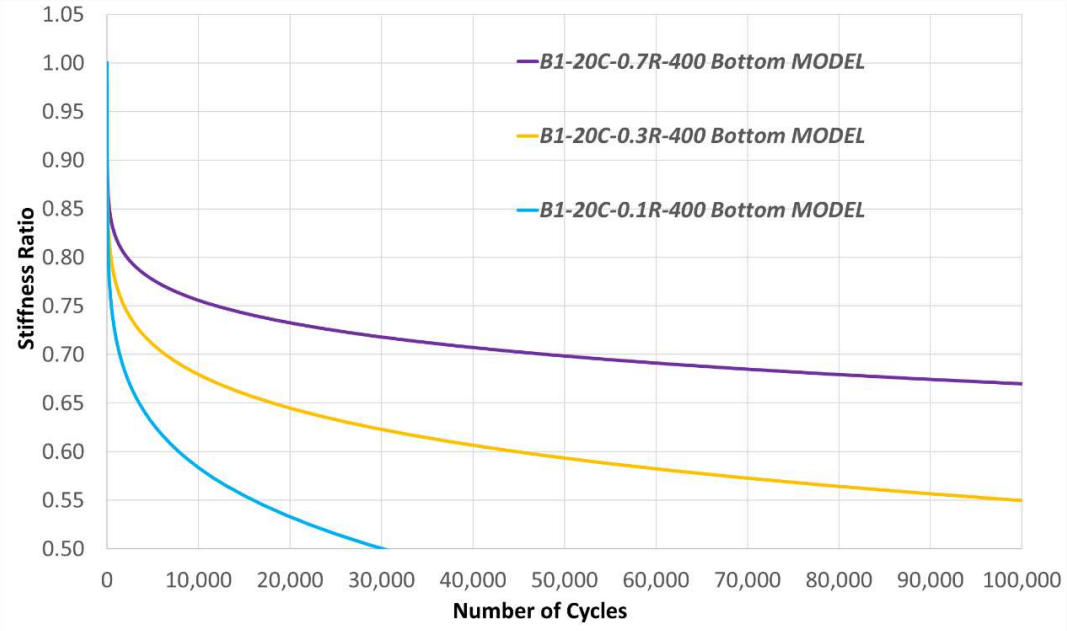

Figure 8-8: Stiffness development curve for bottom node under 200 tensile microstrain and at 20 ^{o}C, batch 1 mixture

8.4.3. Batch 1 mixture at 12^{o}C

Unfortunately, due to change of material supply, there is no beam fatigue tests conducted on batch 1 mixture at 12 ^{o}C. However, many tests are done on batch 2 mixtures as discussed below.

8.4.4. Batch 2 mixture at 20^{o}C

For batch 2 mixture, all conducted beam fatigue tests are listed in Table 4-2, and the endurance limit strain amplitude is found to be around 100 tensile microstrain. Consequently, ABAQUS simulated the beam tests with 0, 0.1 and 0.3 second of rest period and under 400 cyclic microstrain. The flexural stiffness ratio results are presented in Figure 8-9, and the stiffness development at bottom node is shown in Figure 8-10. Again, the stiffness development curve predicted by ABAQUS model seems to match well with beam fatigue tests results for the viscoelastic range. In addition, the bottom section reaches representative 0.5-0.6 failure stiffness ratio (see Figure 8-10) at certain number of cycles that see rapid decline of tested flexural stiffness ratio curve in Figure 8-9. For instance, for 0.1s rest period, the bottom section reaches failure between 10,000 and 20,000 cycles as shown in Figure 8-10, while in Figure 8-9, this is also approximately the number of cycle where the tested results start to decline more drastically from the model results due to fatigue failure at bottom surface.

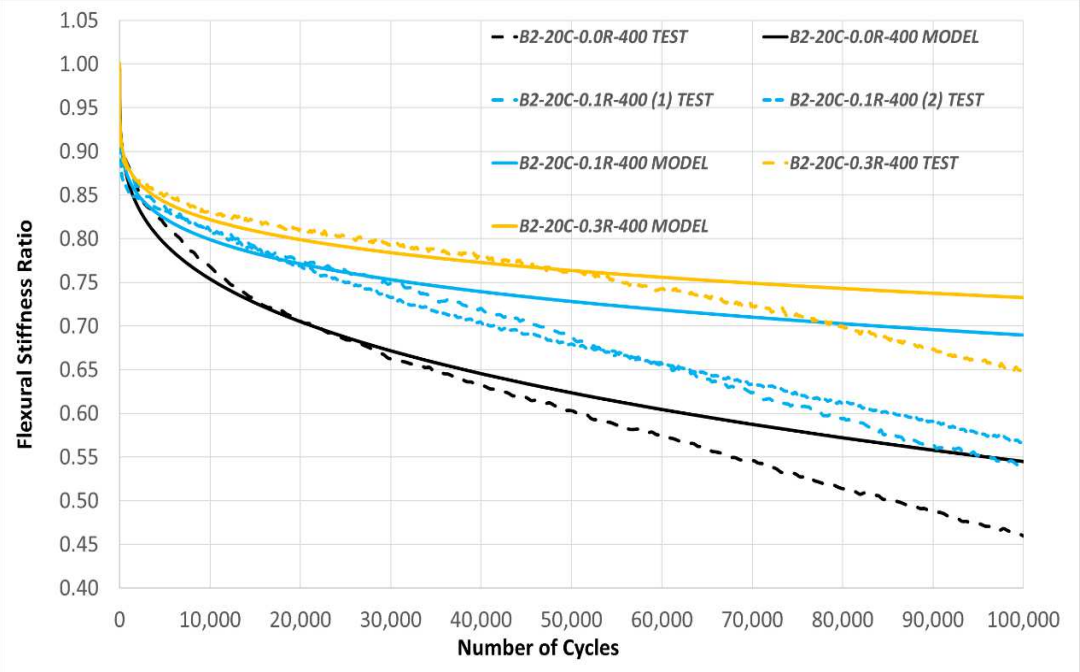

Figure 8-9: Model and Tests Results comparison at 20^{o}C, 200 tensile microstrain of batch 2 mixture

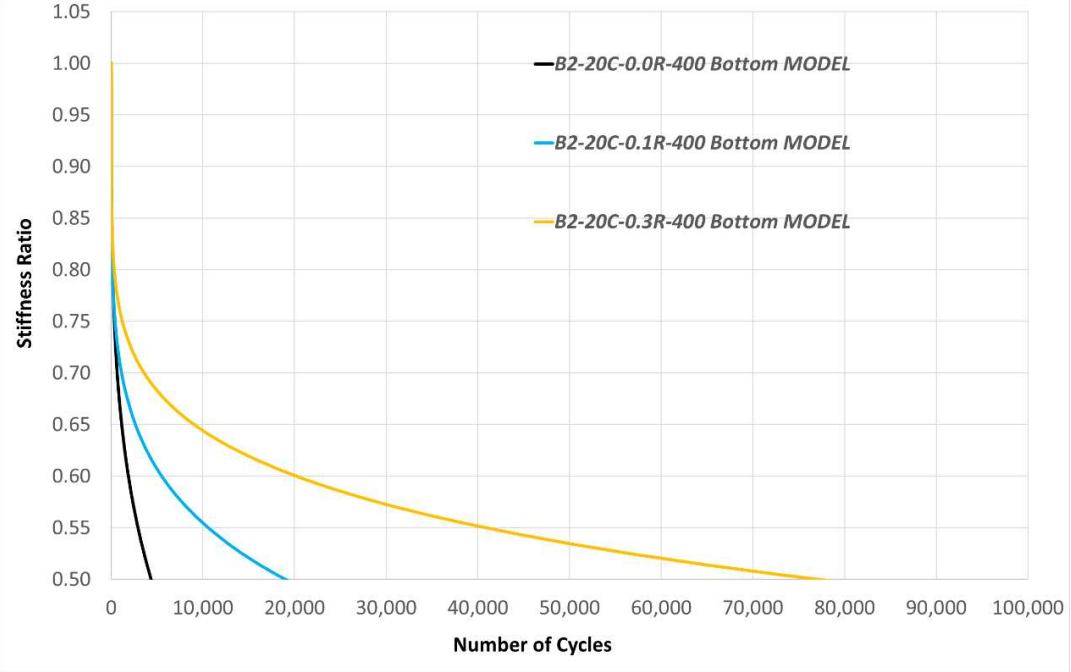

Figure 8-10: Stiffness development curve for bottom node under 200 tensile microstrain and at 20^{o}C, batch 2 mixture

8.4.5. Batch 2 mixture at 12°C

At 12°C, the beam fatigue tests are conducted under two cyclic strains of 300 and 400 microstrains respectively. At the beginning, the strain level of 250 cyclic microstrain was tried, but there is no stiffness reduction even with large number of cycles (no damage). Thus, for this condition, any section that subjects to strain level below 125 tensile micro strain is considered as reaching fatigue endurance limit.

The modelling results compared with tests results of batch 2 mixture under 300 microstrain is demonstrated in Figure 8-11, and the bottom stiffness is illustrated in Figure 8-12. Similar to previous conditions, simulation results are consistent with 4PB beam fatigue tests results under all rest period. Although certain variation between numerical and experimental results exist such as the 0.5s curves, it is because the 0.5s rest period has a strong healing effect so the specimen may have larger threshold of endurance limit (larger strain). This also points out the endurance limit strain amplitude could be larger than 125 microstrain under strong rest period healing effect.

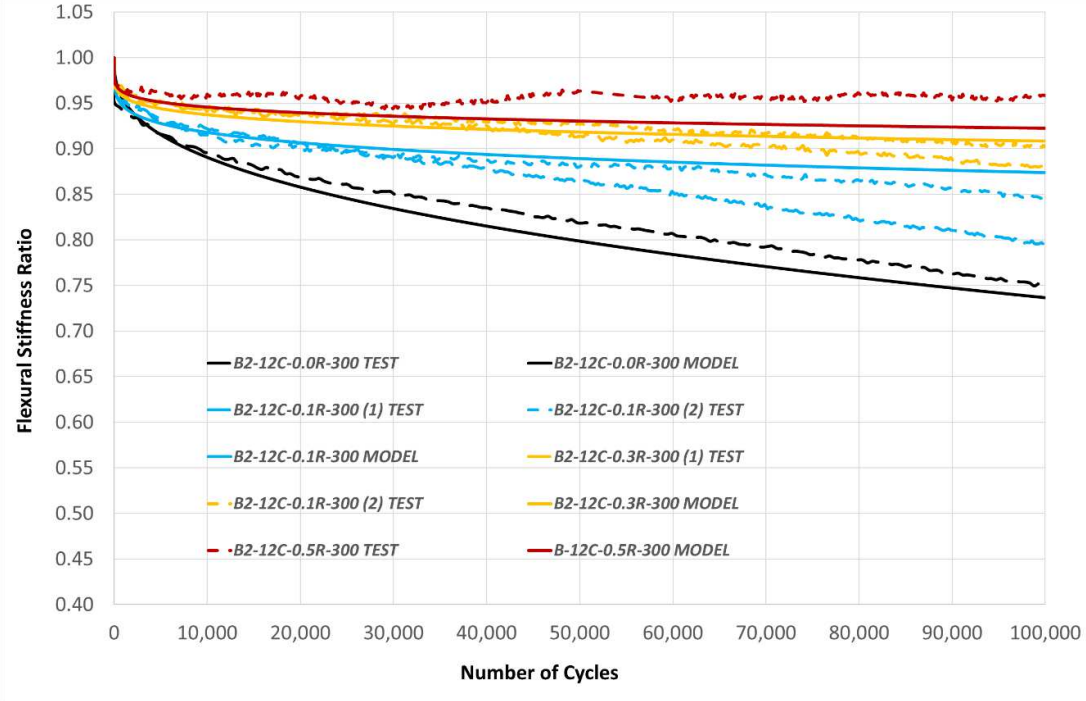

Figure 8-11: Model and Tests Results comparison at 12°C, 150 tensile microstrain of batch 2 mixture

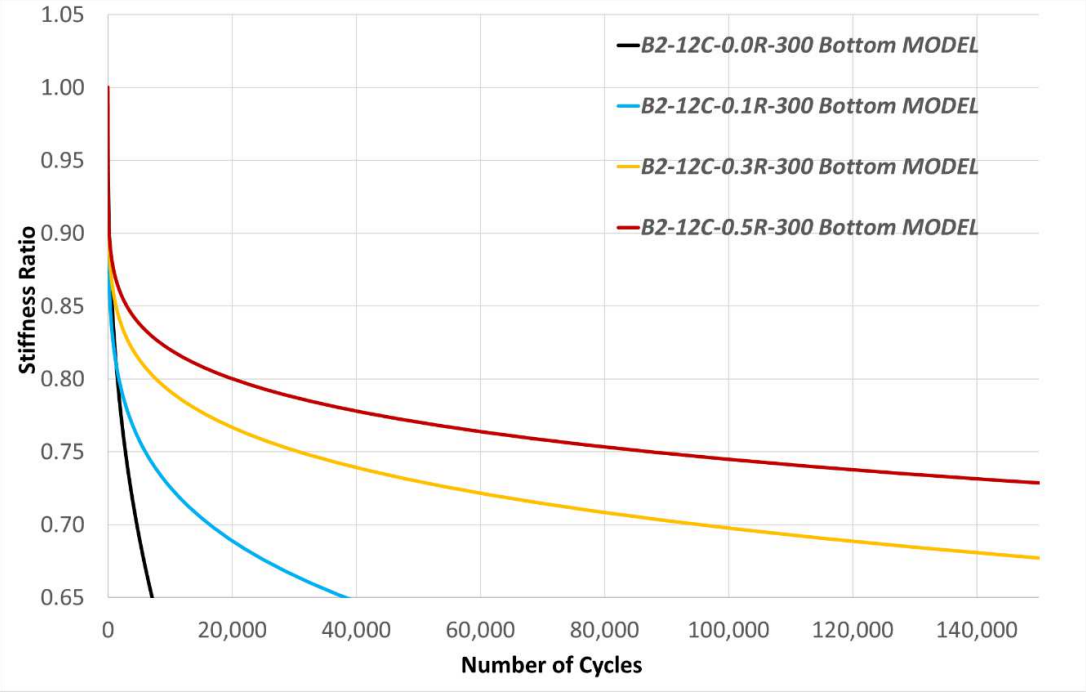

Figure 8-12: Stiffness development curve for bottom node under 150 tensile microstrain and at 12 ^{o}C, batch 2 mixture

Based on VECD test results, the failure stiffness ratio at 12^{o}C falls in a range of 0.6-0.75, so the minimum stiffness ratio indicated in Figure 8-12 is 0.6. The stiffness at bottom node in Figure 8-12 can still reasonably predict bottom surface failure, thus the number of cycles for viscoelasticity response in Figure 8-11. For instance, 0.5s curve in Figure 8-12 does not reach failure criteria for the number of cycles shown, so is the 0.5s curve in Figure 8-11 does not show drastic decline. The 0.3s curve may reach a failure at around 60,000 cycles, which is also where the test curves start to deviate from simulation curve of 0.3s in Figure 8-11.

The results of batch 2 mixture under 400 cyclic microstrain are demonstrated in Figure 8-13, and the stiffness development at the bottom node is listed in Figure 8-14. The 400 micro strain at 12 ^{o}C is a very aggressive test so it is common to see the tested curves droping dramatically even at a very early stage due to early failure at bottom node. The bottom section might have failed at a pseudostiffness of around 0.7, and it is similar to the point when the curve in Figure 8-14 starts to decline much more quickly. Since longer rest period prolongs fatigue life, so curves between model and test results with longer rest period almost always start to depart at a higher number of cycles.

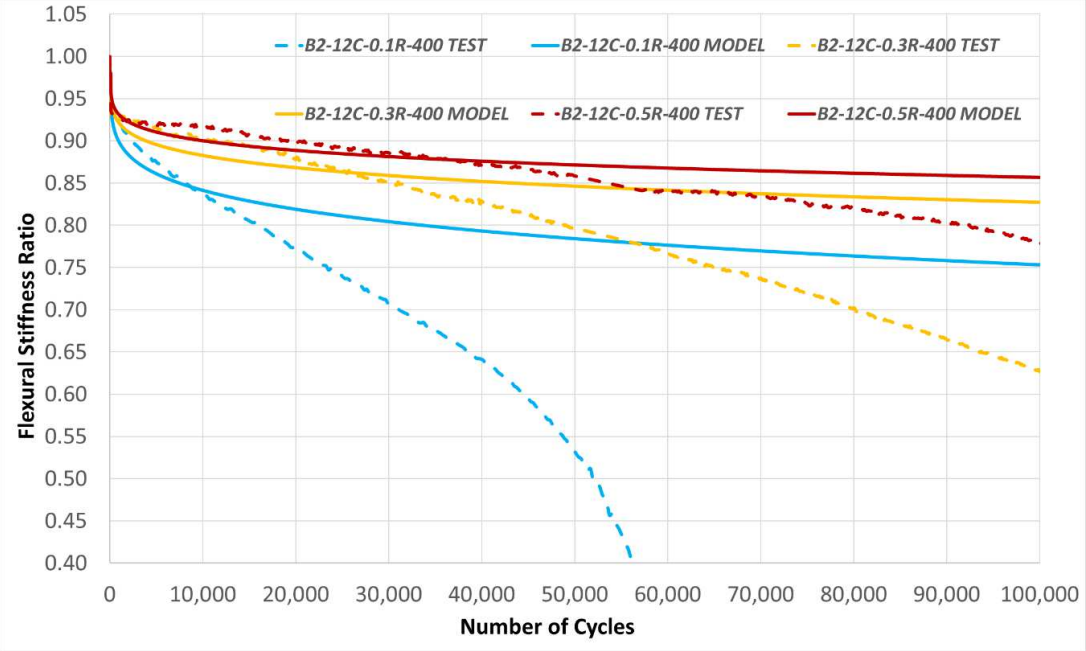

Figure 8-13: Model and Tests Results comparison at 12^{o}C, 200 tensile microstrain of batch 2 mixture

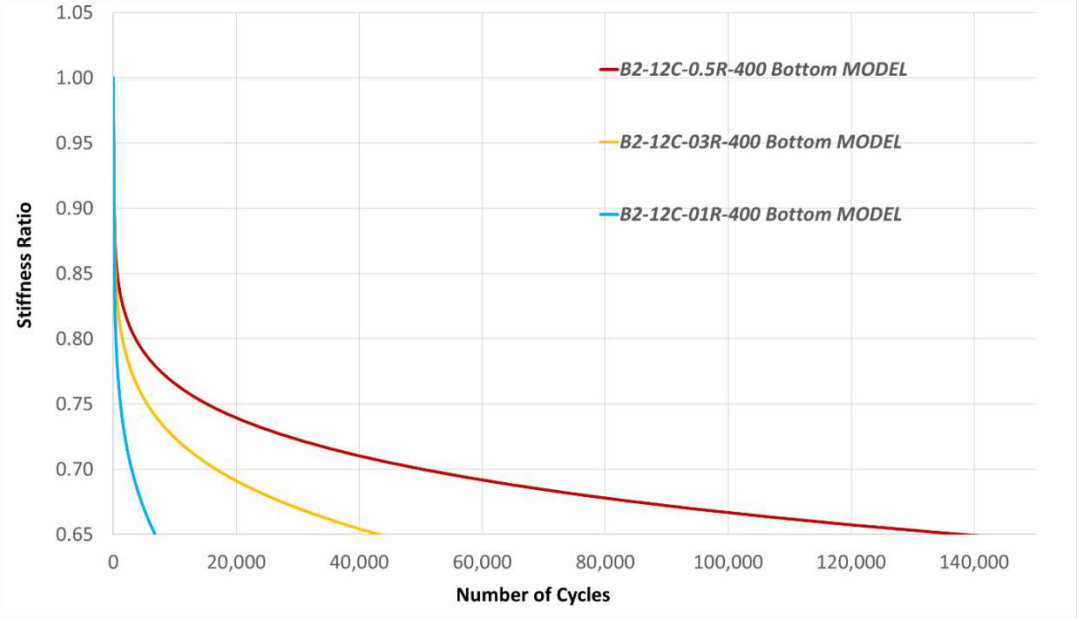

Figure 8-14: Stiffness development curve for bottom node under 200 tensile microstrain and at 12 ^{o}C, batch 2 mixture

8.4.6. Summary of Simulation Results

ABAQUS simulation with user subroutine to integrate the newly proposed rest period damage functions has been implemented to model 4PB beam fatigue tests with various length of rest period at two temperature levels. The simulation results of equivalent flexural stiffness development curves have been produced, as well as the stiffness ratio versus number of cycle curves for the critical bottom section.

From comparison study, simulation and tests results agree well with each other within viscoelasticity range, and they start to deviate once the bottom section reaches an approximate failure stiffness. The longer rest period always has a higher number of cycle as a deviation point between tested and simulated curves, consistent with the fact that higher rest period increases fatigue life.

Based on simulation results of both batches of mixtures under various conditions, it is verified that the present numerical model, with the novel rest period damage function as constitutive model, has the capability at predicting the beam fatigue tests results within viscoelastic range. Also, the current model can provide the true stiffness development of the bottom section, thus to indicate fatigue failure at bottom surface. This is proved by successfully prediction of the depart point between test and simulation results by bottom section failure. This is also an indication of end of viscoelastic behaviour for the cross section.

It is worth mentioning that although the beam fatigue test is a dynamically loaded test, the consideration of dynamic influence on the oscillating beam is not included in current model. In addition, deviation of results could also occur since the real beam may not have consistent air void ratio along the cross section, however, the ABAQUS model is based on homogeneous material properties. Consequently, a 3D model of the beam with consideration of both real stiffness matrix as constitutive model and dynamic effect remains as a subject for future research.

Chapter 9. Conclusion

In general, this research develops a new approach to quantify the healing effect on asphalt mixture's damage characteristic curves caused by rest period after each loading cycle, based on phenomenological interpretation of simplified VECD experimental data. The proposed methods are verified by building a new constitutive model inside UMAT subroutine of ABAQUS, which simulates 4PB beam fatigue tests then compare the modelling results with laboratory tests results of real 4PB beam. This research project contains systematic VECD with rest period tests to investigate the damage characteristic coupled with rest period healing effect for certain asphalt mixture made of commonly encountered Western Australia gravels and bitumen. The damage characteristic curves with various rest periods after each load cycle are drawn under two temperature levels (12 and 20^{o}C), different strain amplitudes and two batches of material supply. The behaviour of asphalt mixture's rest period healing effect on stiffness development curves and damage characteristic curves has undergone qualitative and quantitative investigation.

In addition, a series of beam fatigue tests are conducted also with various length of rest period, and under two temperatures (12 and 20^{o}C). The flexural stiffness ratio with number of cycle curves are produced so observation of the effect of rest period healing can be made, which is similar to the findings listed in AMPT results.

Listed below are main findings from experimental results:

1. The effect of rest period healing on asphalt mixture is indicated by both stiffness development curves and damage characteristic curves. In addition, such effect is further verified by beam fatigue tests results of flexural stiffness ratio development curve with number of cycles
2. Based on the utilized calculation method for S, different rest period length yields different curves, all damage characteristic curves and stiffness development curves demonstrate improved healing effect with longer rest period
3. Although the rest period is improving the material's damage performance, this healing effect is not linearly proportional to the length of rest period, instead,

the degree of improvement is diminishing with increasing rest period until reaching an approximate optimum rest period

4. The damage characteristic curves at different temperatures do not collapse into a single curve when rest period is present. With same rest period, batch 1 mixture has better healing effect at 20 ^{o}C compared to 12 ^{o}C. However, for batch 2 mixture, the healing effect is improved at lower temperature of 12^{o}C compared to 20 ^{o}C at certain rest period, this phenomenon is proved by both AMPT (10 tested samples with repetitions at 0.1, 0.2 and 0.3s rest period) and 4PB beam fatigue tests

5. For both batches of mixture, 20 ^{o}C always has a longer optimum rest period compared to 12 ^{o}C, which means a greater maximum healing effect at higher temperature

6. By analysing damage characteristic curves with various rest period, a novel equational relationship is established to interpret damage characteristics curves with any length of rest period, and it is termed "rest period damage functions". The accuracy of predicted damage curves is evaluated and initially verified

7. A reduced size specimen of 54mm (diameter) x 110mm (height) is verified to be able to produce reasonably accurate results from both dynamic modulus tests (at low and medium temperature) and VECD tests with rest period; in addition, small specimen size has the benefits of material/labour save as well as high tendency towards middle failure

With the derived rest period damage function, a novel constitutive model for asphalt mixture material is developed using Fortran programming language on the platform of UMAT subroutine in ABAQUS. Using ABAQUS, a 4PB beam fatigue model is built incorporating the rest period damage function based constitutive model. Below lists methods development and findings summary from modelling study and comparison of simulation and laboratory results:

1. Based on block method, a series of equations are derived to calculate the equivalent flexural stiffness based on simulation output of pseudostiffness. Thus, the tests results of flexural stiffness ratio can be directly compared with simulation results to evaluate the proposed quantification method for rest period healing effect on damage.

2. Within the viscoelastic range, the model has shown good capability of predicting accurate 4PB beam fatigue test results including rest period healing effect, thus verify the ability of the proposed rest period damage functions to be applied as a material constitutive model in numerical modelling of asphalt mixture's fatigue damage performance
3. The model is able to directly produce true stiffness and damage status for the critical bottom surface. The accuracy of such prediction is verified by correctly predicting the viscoelastic range.

The proposed rest period damage function is fundamentally a combination of mechanical and phenomenological methods to interpret the rest period healing effect through the damage characteristics of asphalt mixture, based on simplified VECD theory and test results. A number of future research can expand the experimental findings as well as improve the numerical tools presented in this study, prospective future directions on this topic are listed below.

1. It is statistically meaningful to verify the applicability range of this study, covering topics such as viscoplasticity, various mixture types, higher than 20^{o}C temperature etc.
2. As current VECD healing effect is dependent on temperature, the quantification of temperature effect in rest period healing could reduce the number of rest period damage functions.
3. It is valuable to analyse the data obtained from VECD and 4PB tests using other methods such as energy approach and fracture mechanics
4. It is meaningful to acquire real asphalt pavement fatigue/crack data, and build a real road model with rest period damage functions as constitutive model. Thus, the capability of the functions can be further verified against field data.
5. Smeared continuum damage approach is used to produce damage characteristic curves with pulse-rest loading; and current solution is based on certain simplification and assumptions. The damage characteristic curves production can be amended when such method was further developed to interpret the damage and pseudostiffness change during pulse-rest period.
6. Since the healing methods developed in this study is based on regression fitting of experimental data, alternative analysis methods based on fundamental healing

mechanism can be used to further evaluate current or future test data, this could possibly contribute to a physically rigorous solution for predicting asphalt mixture's damage characteristics with rest period healing.

To conclude, there was a scarcity of experimental phenomenological approach to interpret the rest period healing effect using VECD model with pulse-rest loading mode. The results presented in this paper further shed light on the rest period healing effect on the damage and fatigue behaviour of asphalt mixture under various conditions, especially the interaction between temperature, rest period length and VECD behaviour. The experimental results lead into the establishment of a new method to interpret the rest period healing effect using VECD model. Also, the experimental data obtained in this study built a platform for future reference and investigations in rest period effect, asphalt damage and cyclic fatigue. The research outcome provides a first quantification tool for VECD model under pulse-rest loading. It is valuable that the rest period damage function is established, so damage characteristic curve can be predicted with any length of rest period after each load cycle. The new function also has evident and verified benefit of saving time and improving the accuracy of VECD with rest period (pulse-rest type) test, while provides a framework to capture the relationship between rest period length and fatigue damage behaviour. Else, the numerical method developed in this study provides a new tool to model the bending beam behaviour of asphalt using damage characteristic functions obtained from VECD tests. The proposed beam test prediction method takes into account important realistic physical response of the bending beam and provides a solution that can be conveniently realized using spreadsheet. The numerical modelling part contained an ABAQUS self-defined constitutive model based on VECD damage curve function, and this is computationally cheap and able to produce damage and stiffness results of any geometry under repetitive loading and with any rest period. The numerical simulation results successfully verified the proposed rest period damage function based on real beam fatigue tests results. Combined with the rest period damage function, it facilitates the testing and modelling of various loading modes such as direction tension, beam bending and wheel loading, for future research and engineering of asphalt pavement.

Reference

ASHOURI, M. 2014. Modeling Microdamage Healing in Asphalt Pavements Using Viscoelastic Continuum Damage Theory. *PhD Thesis, North Carolina State University*.

BAEK, C. 2010. *Investigation of Top-Down Cracking Mechanisms Using the Viscoelastic Continuum Damage Finite Element Program.* Doctor of Philosophy, North Carolina State University.

BHASIN, A., LITTLE, D. N., BOMMAVARAM, R. & VASCONCELOS, K. 2008. A Framework to Quantify the Effect of Healing in Bituminous Materials using Material Properties. *Road Materials and Pavement Design,* 9**,** 219-242.

BONAQUIST, R. 2008a. NCHRP Report 614: Refining the Simple Performance Tester for Use in Routine Practice. Washington, DC: Transportation Research Board.

BONAQUIST, R. 2008b. NCHRP Report 629: Ruggedness Testing of the Dynamic Modulus and Flow Number Tests with the Simple Performance Tester. Washington, DC: Transportation Research Board.

BONAQUIST, R. 2009. Mastersolver Version 2.2.

BONAQUIST, R. 2011. NCHRP Report 702: Precision of the Dynamic Modulus and Flow Number Tests Conducted with the Asphalt Mixture Performance Tester. Washington, DC: Transportation Research Board.

BONAQUIST, R. F., CHRISTENSEN, D. W. & WILLIAM STUMP, I. 2003. NCHRP Report 513: Simple Performance Tester for Superpave Mix Design: First-Article Development and Evaluation. Washington, D.C.: Transportation Research Board.

CASTORENA, C., KIM, Y. R., PAPE, S. & LEE, K. 2017. NCHRP IDEA Project N-181: Development of Small Specimen Geometry for Asphalt Mixture

Performance Testing. Transportation Research Board: North Carolina State University.

CASTRO, M. & SÁNCHEZ, J. A. 2006. Fatigue and Healing of Asphalt Mixtures: Discriminate Analysis of Fatigue Curves. *Journal of Transportation Engineering,* 132**,** 168-174.

CHEHAB, G. R. 2002. Characterization of Asphalt Concrete in Tension Using a ViscoElastoPlastic Model. *PhD Thesis, North Carolina State University*.

CHRISTENSEN, J., D. W. & BONAQUIST, R. 2005. Practical Application of Continuum Damage Theory to Fatigue Phenomena in Asphalt Concrete Mixtures *Journal of the Association of Asphalt Paving Technologists,* 74**,** 963-1002.

CHRISTENSEN, J., D. W. & BONAQUIST, R. 2009. Analysis of HMA Fatigue Data Using the Concepts of Reduced Loading Cycles and Endurance Limit. *Journal of the Association of Asphalt Paving Technologists*, 78**,** 377-416.

DANIEL, J. S. & KIM, Y. R. 2001. Laboratory Evaluation of Fatigue Damage and Healing of Asphalt Mixtures. *Journal of Materials in Civil Engineering,* 13**,** 434-440.

DANIEL, J. S. & Y.R.KIM 2002. Development of a Simplified Fatigue Test and Analysis Procedure Using a Viscoelastic Continuum Damage Model. *Journal of the Association of Asphalt Paving Technologists,* 71**,** 619-650.

ESLAMINIA, M., THIRUNAVUKKARASU, S., GUDDATI, M. N. & KIM, Y. R. Accelerated Pavement Performance Modeling Using Layered Viscoelastic Analysis. *In:* SCARPAS, A., KRINGOS, N., AL-QADI, I. & A, L., eds. 7th RILEM International Conference on Cracking in Pavements, 2012 Dordrecht. Springer Netherlands, 497-506.

H.HUANG, Y. 2004. *Pavement Analysis and Design*, Upper Saddle River, New Jersey, Pearson Education.

HADDADI, F., AMERI, M., MIRABIMOGHADAM, M. H. & HOSSEINI, H. R. A. 2015. Validation of a simplified method in viscoelastic continuum damage (VECD) model developed for flexural mode of loading. *Construction and Building Materials,* 95**,** 892-897.

HOU, T., UNDERWOOD, B. S. & KIM, Y. R. 2010. Fatigue Performance Prediction of North Carolina Mixtures Using the Simplified Viscoelastic Continuum Damage Model. *Journal of the Association of Asphalt Paving Technologists (AAPT),* 79**,** 35-73.

HUBNER, D. & ALDERSON, A. 2008. Testing Asphalt in Accordance with the Austroads Mix Design Procedures. Sydney NSW: Austroads Incorporated.

ISSAC, D. 2014. Mix Design. *In:* DESIGN, A.-B. A.-C. M. (ed.).

KIM, Y.-R., LITTLE, D. N. & LYTTON, R. L. 2003. Fatigue and Healing Characterization of Asphalt Mixtures. *Journal of Materials in Civil Engineering,* 15**,** 75-83.

KIM, Y. R., GUDDATI, M. N., UNDERWOOD, B. S., YUN, T. Y., SUBRAMANIAN, V. & SAVADATTI, S. 2009. Development of A Multiaxial Viscoelastoplastic Continuum Damage Model for Asphalt Mixtures. *FHWA-HRT-08-073.* U.S. Department of Transportation.

KIM, Y. R. & LITTLE, D. N. 1988. Evaluation of Healing and Constitutive modeling of Asphalt Concrete by Means of the Theory of Nonlinear Viscoelasticity and Damage Mechanics. *Final Report.* National Science Foundation: National Science Foundation.

KIM, Y. R. & LITTLE, D. N. 1990. One-Dimensional Constitutive Modeling of Asphalt Concrete. *Journal of Engineering Mechanics,* 116**,** 751-772.

KUTAY, M. E., GIBSON, N. & YOUTCHEFF, J. Conventional and viscoelastic continuum damage (VECD) - based fatigue analysis of polymer modified asphalt pavements. 2008 Annual Meeting of the Association of Asphalt Paving Technologists, AAPT, 2008 Philadelphia, PA. 395-433.

KUTAY, M. E. & LANOTTE, M. 2018. Viscoelastic continuum damage (VECD) models for cracking problems in asphalt mixtures. *International Journal of Pavement Engineering,* 19**,** 231-242.

LEE, H.-J., DANIEL, J. S. & KIM, Y. R. 2000. Continuum Damage Mechanics-Based Fatigue Model of Asphalt Concrete. *Journal of Materials in Civil Engineering,* 12**,** 105-112.

LEE, H.-J. & KIM, Y. R. 1998a. Viscoelastic Constitutive Model for Asphalt Concrete under Cyclic Loading. *Journal of Engineering Mechanics,* 124**,** 32-40.

LEE, H.-J. & KIM, Y. R. 1998b. Viscoelastic Continuum Damage Model of Asphalt Concrete with Healing. *Journal of Engineering Mechanics,* 124**,** 1224-1232.

LEE, J., NOROUZI, A. & KIM, Y. 2017a. Determining Specimen Geometry of Cylindrical Specimens for Direct Tension Fatigue Testing of Asphalt Concrete. *Journal of Testing and Evaluation,* 45**,** 613-623.

LEE, K., PAPE, S., CASTORENA, C. & KIM, Y. R. 2017b. Evaluation of Small Specimen Geometries for Asphalt Mixture Performance Testing and Pavement Performance Prediction. *Transportation Research Record: Journal of the Transportation Research Board,* 2631**,** 74-82.

LU, X., SOENEN, H. & REDELIUS, P. 2003. Fatigue and healing characteristics of bitumens studied using dynamic shear rheometer. *In:* PARTL, M. N. (ed.) *Sixth International RILEM Symposium on Performance Testing and Evaluation of Bituminous* RILEM Publications SARL.

LUO, X., LUO, R. & LYTTON, R. L. 2015. Mechanistic modeling of healing in asphalt mixtures using internal stress. *International Journal of Solids and Structures,* 60-61**,** 35-47.

MUN, S., GUDDATI, M. N. & KIM, Y. R. 2005. Continuum damage finite element modeling of asphalt concrete. *KSCE Journal of Civil Engineering,* 9**,** 205-211.

NASCIMENTO, L. A. H. D. 2015. Implementation and Validation of the Viscoelastic Continuum Damage Theory for Asphalt Mixture and Pavement Analysis in Brazil. *PhD Thesis, North Carolina State University*.

PHILIPS, M. C. Multi-step Models for Fatigue and Healing, and Binder Properties Involved in Healing. Proceedings of Eurobitume Workshop on Performance Related Properties for Bituminous Binders, 1998.

PRAMESTI, F. P., MOLENAAR, A. A. A. & VAN DE VEN, M. F. C. 2013. The Prediction of Fatigue Life based on Four Point Bending Test. *Procedia Engineering*, 54**,** 851-862.

QIU, J. 2012. *Self Healing of Asphalt Mixtures: Towards a Better Understanding of the Mechanism* Docter of Philosophy, Technische Universiteit Delft.

QIU, J., MOLENAAR, A. A. A., VAN DE VEN, M. F. C., WU, S. & YU, J. 2012a. Investigation of self healing behaviour of asphalt mixes using beam on elastic foundation setup. *Materials and Structures*, 45**,** 777-791.

QIU, J., VAN DE VEN, M. C., SCHLANGEN, E., WU, S. & MOLENAAR, A. A. Cracking and Healing Modelling of Asphalt Mixtures. *In:* SCARPAS, A., KRINGOS, N., AL-QADI, I. & A, L., eds. 7th RILEM International Conference on Cracking in Pavements, 2012/01/01 2012b. Springer Netherlands, 1135-1144.

ROQUE, R., ZOU, J., KIM, Y. R., BAEK, C., THIRUNAVUKKARASU, S., UNDERWOOD, B. S. & GUDDATI, M. N. 2010a. NCHRP Report 01-42A: Top-Down Cracking of Hot-Mix Asphalt Layers: Models for Initiation and Propagation. Washington, D.C.: Transportation Research Board.

ROQUE, R., ZOU, J., KIM, Y. R., BAEK, C., THIRUNAVUKKARASU, S., UNDERWOOD, B. S. & GUDDATI, M. N. 2010b. Top-Down Cracking of Hot-Mix Asphalt Layers: Models for Initiation and Propagation. *National Cooperative Highway Research Program (NCHRP) Report 01-42A*.

SCHAPERY, R. A. 1984. Correspondence Principles and a Generalized J Integral for Large Deformation and Fracture Analysis of Viscoelastic Media. *International Journal of Fracture,* 25**,** 195-223.

SCHAPERY, R. A. 1990. A Theory of Mechanical Behavior of Elastic Media with Growing Damage and Other Changes in Structure. *Journal of the Mechanics and Physics of Solids,* 38**,** 215-253.

SHEN, S., CHIU, H.-M. & HUANG, H. 2010. Characterization of Fatigue and Healing in Asphalt Binders. *Journal of Materials in Civil Engineering,* 22**,** 846-852.

UNDERWOOD, B. S., KIM, Y. R. & GUDDATI, M. N. 2010. Improved Calculation Method of Damage Parameter in Viscoelastic Continuum Damage Model. *International Journal of Pavement Engineering,* 11**,** 459-476.

UNDERWOOD, B. S. & ZEIADA, W. 2014. Characterization of Microdamage Healing in Asphalt Concrete with a Smeared Continuum Damage Approach. *Transportation Research Record: Journal of the Transportation Research Board,* 2447**,** 126-135.

UNDERWOOD, S., KIM, Y. R., GUDDATI, M., PELLINEN, T., RONGZONG, W., KING, G., KLUTTZ, R. & GIBSON, N. 2006. Characterization and performance prediction of ALF mixtures using a viscoelastoplastic continuum damage model. *Asphalt Paving Technology: Association of Asphalt Paving Technologists-Proceedings of the Technical Sessions* 75**,** 577-636.

VAN DEN BERGH, W. & VAN DE VEN, M. F. C. 2012. The Influence of Ageing on the Fatigue and Healing Properties of Bituminous Mortars. *Procedia - Social and Behavioral Sciences,* 53**,** 256-265.

WITZCAK, M. W., KALOUSH, K., PELLINEN, T., EL-BASYOUNY, M. & VON QUINTUS, H. 2002. NCHRP Report 465: Simple Performance Tester for Superpave Mix Design. Washington, D.C.: Transportation Research Board.

WOOL, R. P. & O'CONNOR, K. M. 1981. A theory crack healing in polymers. *Journal of Applied Physics,* 52**,** 5953-5963.

ZEIADA, W. 2012. Endurance Limit for HMA Based on Healing Phenomenon Using Viscoelastic Continuum Damage Analysis. *PhD Thesis, Arizona State University*.

NOTE: *Every reasonable effort has been made to acknowledge the owners of copyright material. I would be pleased to hear from any copyright owner who has been omitted or incorrectly acknowledged.*

Appendix A: Fortran Program for Applying Rest Period Damage Functions into UMAT Subroutine

```
      SUBROUTINE UMAT(STRESS, STATEV, DDSDDE, SSE, SPD, SCD, RPL,
     1 DDSDDT, DRPLDE, DRPLDT, STRAN, DSTRAN, TIME, DTIME, TEMP,
     DTEMP,
     2 PREDEF, DPRED, CMNAME, NDI, NSHR, NTENS, NSTATV, PROPS,
     NPROPS,
     3 COORDS, DROT, PNEWDT, CELENT, DFGRD0, DFGRD1, NOEL, NPT,
     LAYER,
     4 KSPT, KSTEP, KINC)
C
      INCLUDE 'ABA_PARAM.INC'
C
      CHARACTER*80 CMNAME
      DIMENSION STRESS(NTENS),STATEV(NSTATV),
     1 DDSDDE(NTENS,NTENS),DDSDDT(NTENS),DRPLDE(NTENS),
     2 STRAN(NTENS),DSTRAN(NTENS),TIME(2),PREDEF(1),DPRED(1),
     3 PROPS(NPROPS),COORDS(3),DROT(3,3),DFGRD0(3,3),DFGRD1(3,3)


C
C PROPS(1)=Elve (representative stiffness)
```

```
C PROPS(2)=alpha (power damage parameter)
C PROPS(3)=K1
C PROPS(4)=at (time-temperature shift factor)
C PROPS(5)=trest  (length of desired rest period)
C PROPS(6)=C10    (C1 value when rest period is 0)
C PROPS(7)=C20    (C2 value when rest period is 0)
C PROPS(8)=a (rest period fitting parameter)
C PROPS(9)=b (rest period fitting parameter)
C PROPS(10)=c (rest period fitting parameter)
C PROPS(11)=d (rest period fitting parameter)
C PROPS(12)=Efp (finger print stiffness)
C PROPS(13)=v  (poisson ratio)
C PRPOS(14)=loading frequency
C
C EVALUATE NEW STIFFNESS
C
      DMR=PROPS(12)/PROPS(1)
      IF (STRAN(1)>0) THEN
        ETR=STRAN(1)*PROPS(1)
      ELSE
```

```
      ETR=0
      END IF
      DTR=DTIME/PROPS(4)
      C1=PROPS(6)+PROPS(8)*PROPS(5)**PROPS(9)
      C2=PROPS(7)-PROPS(10)*PROPS(5)**PROPS(11)
C
C     CALCULATE DAMAGE PARAMETER
C
      DC=0.1
      DDC=1
      IF (ETR==0) THEN
        SPRE=STATEV(1)
        DC2PRE=0
        GO TO 11
      ELSE
        GO TO 10
      END IF
   10 CONTINUE
      TERM1=DC*0.5*DMR*ETR**2
      TERM2=TERM1**(PROPS(2)/(PROPS(2)+1))
```

```
      DS=TERM2*(PROPS(3)*DTR)**(1/(PROPS(2)+1))
      S=STATEV(1)+DS
      DC2=STATEV(2)-1+C1*S**C2
      ! Execute iteration until difference between C is larger than previous step
      IF (ABS(DC2-DC)<DDC) THEN
        DDC=ABS(DC2-DC)
        DC=0.95*DC
        SPRE=S
        DC2PRE=DC2
        GO TO 10
      ELSE
        GO TO 11
      END IF
   11 CONTINUE
      STATEV(1)=SPRE
      STATEV(2)=STATEV(2)-DC2PRE
      E=PROPS(12)
C
C     EVALUATE NEW STRESS TENSOR
C
```

```
      TERM1=E*(1-PROPS(13))/(1+PROPS(13))/(1-2*PROPS(13))
      TERM2=E*PROPS(13)/(1+PROPS(13))/(1-2*PROPS(13))
      TERM3=E*(1-2*PROPS(13))/(1+PROPS(13))/(1-2*PROPS(13))
      DO K1=1,NTENS
        DO K2=1,NTENS
          DDSDDE(K2,K1)=0
        END DO
      END DO
C
      DO K1=1,NDI
        DDSDDE(K1,K1)=TERM1
      END DO
C
      DO K1=2,NDI
        N1=K1-1
        DO K2=1,N1
          DDSDDE(K2,K1)=TERM2
          DDSDDE(K1,K2)=TERM2
        END DO
      END DO
```

```
C
      I1=NDI
      DO K1=1,NSHR
        I1=I1+1
        DDSDDE(I1,I1)=TERM3
      END DO
C
      DO K1=1,NTENS
        STRESS(K1)=0
        DO I1=1,NTENS
          STRESS(K1)=STRESS(K1)+DDSDDE(K1,I1)*STRAN(I1)
        END DO
      END DO
      RETURN
      END
```

Appendix B: Spreadsheet Data for Calculation of Relaxation Modulus Prony Coefficients

Batch 1 Mixture

b	k	d	g	a1	a2	Sum of log	log Fit	wc
3.052187	4.146621	0.801191	0.638485	0.000497	-0.15138	0.031684	10132926	925.5641

Frequency	Dynamic Modulus (MPa)	Phase Angle (Degrees)	Temperature (°C)	at	wr	Storage Modulus E' (kPa or psi)	Storage Modulus E'fit (log) (kPa or psi)	OFlog
0.1	8836.667	18.13	4	170.2375	106.9634	8397952	7326251	0.003515
1	12811.67	13.17667	4	170.2375	1069.634	12474359	10300640	0.006915
10	16942.67	9.74	4	170.2375	10696.34	16698448	12522935	0.015618
0.1	4514.333	27.03333	12	12.1405	7.628101	4021107	3781879	0.00071
1	7778.667	20.37	12	12.1405	76.28101	7292223	6854348	0.000723
10	11805.33	14.97667	12	12.1405	762.8101	11404320	9903890	0.003753
0.1	1826.667	34.76667	20	1	0.628319	1500572	1469757	8.12E-05
1	3957.667	29.00333	20	1	6.283185	3461342	3553658	0.000131
10	7192	22.23	20	1	62.83185	6657437	6582874	2.39E-05
0.1	163.7	35.62333	38	0.005811	0.003651	133065.8	132560.4	2.73E-06
1	492.5667	40.07667	38	0.005811	0.036514	376904	383533.6	5.73E-05
10	1522.333	38.75	38	0.005811	0.365144	1187244	1153719	0.000155

E8 (kpa)	14015.91163	
wr	***E'***	***E'norm***
100000000	15507613.36	15493597.45
10000000	15247494.79	15233478.88
1000000	14770114.36	14756098.45
100000	13917645.24	13903629.33
10000	12469970.94	12455955.03
1000	10222990.62	10208974.7
100	7232525.84	7218509.928
10	4111712.085	4097696.173
1	1791965.709	1777949.797
0.1	626028.2155	612012.3039
0.01	207190.6506	193174.739
0.001	79569.42131	65553.50968
0.0001	39576.01745	25560.10582
0.00001	25265.50026	11249.58863
0.000001	19378.9812	5363.069573
0.0000001	16694.81135	2678.899723
0.00000001	15389.05747	1373.145844

Bmi	**wi**																
ρm	1.00E+08	1.00E+07	1.00E+06	1.00E+05	1.00E+04	1.00E+03	1.00E+02	1.00E+01	1.00E+00	1.00E-01	1.00E-02	1.00E-03	1.00E-04	1.00E-05	1.00E-06	1.00E-07	1.00E-08
2.00E+08	1.00E+00	1.00E+00	1.00E+00	1.00E+00	1.00E+00	1.00E+00	1.00E+00	1.00E+00	1.00E+00	1.00E+00	1.00E+00	1.00E+00	1.00E+00	1.00E+00	1.00E+00	9.98E-01	8.00E-01
2.00E+07	1.00E+00	1.00E+00	1.00E+00	1.00E+00	1.00E+00	1.00E+00	1.00E+00	1.00E+00	1.00E+00	1.00E+00	1.00E+00	1.00E+00	1.00E+00	1.00E+00	9.98E-01	8.00E-01	3.85E-02
2.00E+06	1.00E+00	1.00E+00	1.00E+00	1.00E+00	1.00E+00	1.00E+00	1.00E+00	1.00E+00	1.00E+00	1.00E+00	1.00E+00	1.00E+00	1.00E+00	9.98E-01	8.00E-01	3.85E-02	4.00E-04
2.00E+05	1.00E+00	1.00E+00	1.00E+00	1.00E+00	1.00E+00	1.00E+00	1.00E+00	1.00E+00	1.00E+00	1.00E+00	1.00E+00	1.00E+00	9.98E-01	8.00E-01	3.85E-02	4.00E-04	4.00E-06
2.00E+04	1.00E+00	1.00E+00	1.00E+00	1.00E+00	1.00E+00	1.00E+00	1.00E+00	1.00E+00	1.00E+00	1.00E+00	1.00E+00	9.98E-01	8.00E-01	3.85E-02	4.00E-04	4.00E-06	4.00E-08
2.00E+03	1.00E+00	1.00E+00	1.00E+00	1.00E+00	1.00E+00	1.00E+00	1.00E+00	1.00E+00	1.00E+00	1.00E+00	9.98E-01	8.00E-01	3.85E-02	4.00E-04	4.00E-06	4.00E-08	4.00E-10
2.00E+02	1.00E+00	1.00E+00	1.00E+00	1.00E+00	1.00E+00	1.00E+00	1.00E+00	1.00E+00	1.00E+00	9.98E-01	8.00E-01	3.85E-02	4.00E-04	4.00E-06	4.00E-08	4.00E-10	4.00E-12
2.00E+01	1.00E+00	1.00E+00	1.00E+00	1.00E+00	1.00E+00	1.00E+00	1.00E+00	1.00E+00	9.98E-01	8.00E-01	3.85E-02	4.00E-04	4.00E-06	4.00E-08	4.00E-10	4.00E-12	4.00E-14
2.00E+00	1.00E+00	1.00E+00	1.00E+00	1.00E+00	1.00E+00	1.00E+00	1.00E+00	9.98E-01	8.00E-01	3.85E-02	4.00E-04	4.00E-06	4.00E-08	4.00E-10	4.00E-12	4.00E-14	4.00E-16
2.00E-01	1.00E+00	1.00E+00	1.00E+00	1.00E+00	1.00E+00	1.00E+00	9.98E-01	8.00E-01	3.85E-02	4.00E-04	4.00E-06	4.00E-08	4.00E-10	4.00E-12	4.00E-14	4.00E-16	4.00E-18
2.00E-02	1.00E+00	1.00E+00	1.00E+00	1.00E+00	1.00E+00	9.98E-01	8.00E-01	3.85E-02	4.00E-04	4.00E-06	4.00E-08	4.00E-10	4.00E-12	4.00E-14	4.00E-16	4.00E-18	4.00E-20
2.00E-03	1.00E+00	1.00E+00	1.00E+00	1.00E+00	9.98E-01	8.00E-01	3.85E-02	4.00E-04	4.00E-06	4.00E-08	4.00E-10	4.00E-12	4.00E-14	4.00E-16	4.00E-18	4.00E-20	4.00E-22
2.00E-04	1.00E+00	1.00E+00	1.00E+00	9.98E-01	8.00E-01	3.85E-02	4.00E-04	4.00E-06	4.00E-08	4.00E-10	4.00E-12	4.00E-14	4.00E-16	4.00E-18	4.00E-20	4.00E-22	4.00E-24
2.00E-05	1.00E+00	1.00E+00	9.98E-01	8.00E-01	3.85E-02	4.00E-04	4.00E-06	4.00E-08	4.00E-10	4.00E-12	4.00E-14	4.00E-16	4.00E-18	4.00E-20	4.00E-22	4.00E-24	4.00E-26
2.00E-06	1.00E+00	9.98E-01	8.00E-01	3.85E-02	4.00E-04	4.00E-06	4.00E-08	4.00E-10	4.00E-12	4.00E-14	4.00E-16	4.00E-18	4.00E-20	4.00E-22	4.00E-24	4.00E-26	4.00E-28
2.00E-07	9.98E-01	8.00E-01	3.85E-02	4.00E-04	4.00E-06	4.00E-08	4.00E-10	4.00E-12	4.00E-14	4.00E-16	4.00E-18	4.00E-20	4.00E-22	4.00E-24	4.00E-26	4.00E-28	4.00E-30
2.00E-08	8.00E-01	3.85E-02	4.00E-04	4.00E-06	4.00E-08	4.00E-10	4.00E-12	4.00E-14	4.00E-16	4.00E-18	4.00E-20	4.00E-22	4.00E-24	4.00E-26	4.00E-28	4.00E-30	4.00E-32

Bmi -1	wi																
ρm	1.00E+08	1.00E+07	1.00E+06	1.00E+05	1.00E+04	1.00E+03	1.00E+02	1.00E+01	1.00E+00	1.00E-01	1.00E-02	1.00E-03	1.00E-04	1.00E-05	1.00E-06	1.00E-07	1.00E-08
2.00E+08	-2.22E-16	-2.22E-16	-5.55E-17	-1.53E-16	3.12E-16	-8.12E-16	1.79E-14	-4.41E-13	1.10E-11	-2.76E-10	6.90E-09	-1.72E-07	4.31E-06	-1.08E-04	2.69E-03	-6.72E-02	1.33E+00
2.00E+07	-2.92E-16	5.83E-16	7.29E-17	1.09E-16	-6.38E-16	1.89E-14	-4.64E-13	1.16E-11	-2.90E-10	7.25E-09	-1.81E-07	4.53E-06	-1.13E-04	2.83E-03	-7.06E-02	1.42E+00	-1.68E+00
2.00E+06	2.95E-16	-2.95E-16	-2.22E-16	-4.80E-16	1.80E-14	-4.64E-13	1.16E-11	-2.90E-10	7.25E-09	-1.81E-07	4.53E-06	-1.13E-04	2.83E-03	-7.06E-02	1.42E+00	-1.70E+00	4.37E-01
2.00E+05	0.00E+00	2.95E-16	-2.95E-16	1.80E-14	-4.63E-13	1.16E-11	-2.90E-10	7.25E-09	-1.81E-07	4.53E-06	-1.13E-04	2.83E-03	-7.06E-02	1.42E+00	-1.70E+00	4.42E-01	-1.09E-01
2.00E+04	2.95E-16	-1.18E-15	1.83E-14	-4.63E-13	1.16E-11	-2.90E-10	7.25E-09	-1.81E-07	4.53E-06	-1.13E-04	2.83E-03	-7.06E-02	1.42E+00	-1.70E+00	4.42E-01	-1.11E-01	2.73E-02
2.00E+03	-1.18E-15	1.89E-14	-4.64E-13	1.16E-11	-2.90E-10	7.25E-09	-1.81E-07	4.53E-06	-1.13E-04	2.83E-03	-7.06E-02	1.42E+00	-1.70E+00	4.42E-01	-1.11E-01	2.77E-02	-6.83E-03
2.00E+02	1.77E-14	-4.64E-13	1.16E-11	-2.90E-10	7.25E-09	-1.81E-07	4.53E-06	-1.13E-04	2.83E-03	-7.06E-02	1.42E+00	-1.70E+00	4.42E-01	-1.11E-01	2.77E-02	-6.91E-03	1.71E-03
2.00E+01	-4.41E-13	1.16E-11	-2.90E-10	7.25E-09	-1.81E-07	4.53E-06	-1.13E-04	2.83E-03	-7.06E-02	1.42E+00	-1.70E+00	4.42E-01	-1.11E-01	2.77E-02	-6.92E-03	1.73E-03	-4.27E-04
2.00E+00	1.10E-11	-2.90E-10	7.25E-09	-1.81E-07	4.53E-06	-1.13E-04	2.83E-03	-7.06E-02	1.42E+00	-1.70E+00	4.42E-01	-1.11E-01	2.77E-02	-6.92E-03	1.73E-03	-4.32E-04	1.07E-04
2.00E-01	-2.76E-10	7.25E-09	-1.81E-07	4.53E-06	-1.13E-04	2.83E-03	-7.06E-02	1.42E+00	-1.70E+00	4.42E-01	-1.11E-01	2.77E-02	-6.92E-03	1.73E-03	-4.32E-04	1.08E-04	-2.67E-05
2.00E-02	6.90E-09	-1.81E-07	4.53E-06	-1.13E-04	2.83E-03	-7.06E-02	1.42E+00	-1.70E+00	4.42E-01	-1.11E-01	2.77E-02	-6.92E-03	1.73E-03	-4.32E-04	1.08E-04	-2.70E-05	6.67E-06
2.00E-03	-1.72E-07	4.53E-06	-1.13E-04	2.83E-03	-7.06E-02	1.42E+00	-1.70E+00	4.42E-01	-1.11E-01	2.77E-02	-6.92E-03	1.73E-03	-4.32E-04	1.08E-04	-2.70E-05	6.75E-06	-1.67E-06
2.00E-04	4.31E-06	-1.13E-04	2.83E-03	-7.06E-02	1.42E+00	-1.70E+00	4.42E-01	-1.11E-01	2.77E-02	-6.92E-03	1.73E-03	-4.32E-04	1.08E-04	-2.70E-05	6.75E-06	-1.69E-06	4.17E-07
2.00E-05	-1.08E-04	2.83E-03	-7.06E-02	1.42E+00	-1.70E+00	4.42E-01	-1.11E-01	2.77E-02	-6.92E-03	1.73E-03	-4.32E-04	1.08E-04	-2.70E-05	6.75E-06	-1.69E-06	4.22E-07	-1.04E-07
2.00E-06	2.69E-03	-7.06E-02	1.42E+00	-1.70E+00	4.42E-01	-1.11E-01	2.77E-02	-6.92E-03	1.73E-03	-4.32E-04	1.08E-04	-2.70E-05	6.75E-06	-1.69E-06	4.22E-07	-1.06E-07	2.60E-08
2.00E-07	-6.72E-02	1.42E+00	-1.70E+00	4.42E-01	-1.11E-01	2.77E-02	-6.91E-03	1.73E-03	-4.32E-04	1.08E-04	-2.70E-05	6.75E-06	-1.69E-06	4.22E-07	-1.06E-07	2.64E-08	-6.51E-09
2.00E-08	1.33E+00	-1.68E+00	4.37E-01	-1.09E-01	2.73E-02	-6.83E-03	1.71E-03	-4.27E-04	1.07E-04	-2.67E-05	6.67E-06	-1.67E-06	4.17E-07	-1.04E-07	2.60E-08	-6.51E-09	1.61E-09

Batch 2 Mixture

b	k	d	g	a1	a2	Sum Oflog	log Fit	wc
3.356497116	3.940159007	0.855454665	0.599256725	0.000497473	-0.151380416	0.00069529	11793451.72	925.5641367

requency	Dynamic Modulus (MPa)	Phase Angle (Degrees)	Temperature (°C)	at	wr	Storage Modulus E' (kPa or psi)	Storage Modulus E'fit (log) (kPa or psi)	OFlog
0.1	8578.666667	18.12333333	4	160.4603763	100.8202279	8153071.566	8239514.441	2.09797E-05
1	12022.33333	12.68666667	4	160.4603763	1008.202279	11728816.22	11919789.58	4.92019E-05
10	15422.66667	9.1	4	160.4603763	10082.02279	15228554	14856724.49	0.000115253
0.1	4933.333333	27.64333333	12	11.79649746	7.41195795	4370207.791	4170863.277	0.000411122
1	8124.333333	20.04666667	12	11.79649746	74.1195795	7632110.347	7727254.573	2.89506E-05
10	11673.33333	14.09	12	11.79649746	741.195795	11322135.49	11460308.59	2.77514E-05
0.1	1993.666667	36.22	20	1	0.628318531	1608398.763	1616077.301	4.27828E-06
1	4504.666667	29.75	20	1	6.283185307	3910946.26	3950970.29	1.95533E-05
10	8047.666667	21.98666667	20	1	62.83185307	7462367.953	7453171.482	2.86809E-07
0.1	166.6	34.18333333	38	0.006166317	0.003874411	137818.8575	137193.7597	3.89781E-06
1	547.2333333	39.95	38	0.006166317	0.038744114	419511.8584	422978.5219	1.2774E-05
10	1710.333333	40.69666667	38	0.006166317	0.387441141	1296727.31	1300058.134	1.24125E-06

E8 (kpa)	8712.825	
wr	***E'***	***E'norm***
1E+08	19270155	19261442
10000000	18848881	18840168
1000000	18111217	18102504
100000	16859238	16850525
10000	14847984	14839271
1000	11907769	11899056
100	8225899	8217186
10	4585077	4576364
1	1974454	1965741
0.1	679549.7	670836.9
0.01	215441.3	206728.5
0.001	76108.14	67395.31
0.0001	34035.52	25322.69
0.00001	19644.16	10931.33
0.000001	13922.82	5209.997
1E-07	11352.86	2640.034
1E-08	10099.03	1386.204

Bmi	wi																
ρm	100000000	10000000	1000000	100000	10000	1000	100	10	1	0.1	0.01	0.001	0.0001	0.00001	0.000001	0.0000001	0.00000001
200000000	1.00E+00	1.00E+00	1.00E+00	1.00E+00	1.00E+00	1.00E+00	1.00E+00	1.00E+00	1.00E+00	1.00E+00	1.00E+00	1.00E+00	1.00E+00	1.00E+00	1.00E+00	9.98E-01	8.00E-01
20000000	1.00E+00	1.00E+00	1.00E+00	1.00E+00	1.00E+00	1.00E+00	1.00E+00	1.00E+00	1.00E+00	1.00E+00	1.00E+00	1.00E+00	1.00E+00	1.00E+00	9.98E-01	8.00E-01	3.85E-02
2000000	1.00E+00	1.00E+00	1.00E+00	1.00E+00	1.00E+00	1.00E+00	1.00E+00	1.00E+00	1.00E+00	1.00E+00	1.00E+00	1.00E+00	1.00E+00	9.98E-01	8.00E-01	3.85E-02	4.00E-04
200000	1.00E+00	1.00E+00	1.00E+00	1.00E+00	1.00E+00	1.00E+00	1.00E+00	1.00E+00	1.00E+00	1.00E+00	1.00E+00	1.00E+00	9.98E-01	8.00E-01	3.85E-02	4.00E-04	4.00E-06
20000	1.00E+00	1.00E+00	1.00E+00	1.00E+00	1.00E+00	1.00E+00	1.00E+00	1.00E+00	1.00E+00	1.00E+00	1.00E+00	9.98E-01	8.00E-01	3.85E-02	4.00E-04	4.00E-06	4.00E-08
2000	1.00E+00	1.00E+00	1.00E+00	1.00E+00	1.00E+00	1.00E+00	1.00E+00	1.00E+00	1.00E+00	1.00E+00	9.98E-01	8.00E-01	3.85E-02	4.00E-04	4.00E-06	4.00E-08	4.00E-10
200	1.00E+00	1.00E+00	1.00E+00	1.00E+00	1.00E+00	1.00E+00	1.00E+00	1.00E+00	1.00E+00	9.98E-01	8.00E-01	3.85E-02	4.00E-04	4.00E-06	4.00E-08	4.00E-10	4.00E-12
20	1.00E+00	1.00E+00	1.00E+00	1.00E+00	1.00E+00	1.00E+00	1.00E+00	1.00E+00	9.98E-01	8.00E-01	3.85E-02	4.00E-04	4.00E-06	4.00E-08	4.00E-10	4.00E-12	4.00E-14
2	1.00E+00	1.00E+00	1.00E+00	1.00E+00	1.00E+00	1.00E+00	1.00E+00	9.98E-01	8.00E-01	3.85E-02	4.00E-04	4.00E-06	4.00E-08	4.00E-10	4.00E-12	4.00E-14	4.00E-16
0.2	1.00E+00	1.00E+00	1.00E+00	1.00E+00	1.00E+00	1.00E+00	9.98E-01	8.00E-01	3.85E-02	4.00E-04	4.00E-06	4.00E-08	4.00E-10	4.00E-12	4.00E-14	4.00E-16	4.00E-18
0.02	1.00E+00	1.00E+00	1.00E+00	1.00E+00	1.00E+00	9.98E-01	8.00E-01	3.85E-02	4.00E-04	4.00E-06	4.00E-08	4.00E-10	4.00E-12	4.00E-14	4.00E-16	4.00E-18	4.00E-20
0.002	1.00E+00	1.00E+00	1.00E+00	1.00E+00	9.98E-01	8.00E-01	3.85E-02	4.00E-04	4.00E-06	4.00E-08	4.00E-10	4.00E-12	4.00E-14	4.00E-16	4.00E-18	4.00E-20	4.00E-22
0.0002	1.00E+00	1.00E+00	1.00E+00	9.98E-01	8.00E-01	3.85E-02	4.00E-04	4.00E-06	4.00E-08	4.00E-10	4.00E-12	4.00E-14	4.00E-16	4.00E-18	4.00E-20	4.00E-22	4.00E-24
0.00002	1.00E+00	1.00E+00	9.98E-01	8.00E-01	3.85E-02	4.00E-04	4.00E-06	4.00E-08	4.00E-10	4.00E-12	4.00E-14	4.00E-16	4.00E-18	4.00E-20	4.00E-22	4.00E-24	4.00E-26
0.000002	1.00E+00	9.98E-01	8.00E-01	3.85E-02	4.00E-04	4.00E-06	4.00E-08	4.00E-10	4.00E-12	4.00E-14	4.00E-16	4.00E-18	4.00E-20	4.00E-22	4.00E-24	4.00E-26	4.00E-28
0.0000002	9.98E-01	8.00E-01	3.85E-02	4.00E-04	4.00E-06	4.00E-08	4.00E-10	4.00E-12	4.00E-14	4.00E-16	4.00E-18	4.00E-20	4.00E-22	4.00E-24	4.00E-26	4.00E-28	4.00E-30
0.00000002	8.00E-01	3.85E-02	4.00E-04	4.00E-06	4.00E-08	4.00E-10	4.00E-12	4.00E-14	4.00E-16	4.00E-18	4.00E-20	4.00E-22	4.00E-24	4.00E-26	4.00E-28	4.00E-30	4.00E-32

Bmi -1	wi																
ρm	100000000	10000000	1000000	100000	10000	1000	100	10	1	0.1	0.01	0.001	0.0001	0.00001	0.000001	0.0000001	0.00000001
200000000	-2.22E-16	-2.22E-16	-5.55E-17	-1.53E-16	3.12E-16	-8.12E-16	1.79E-14	-4.41E-13	1.10E-11	-2.76E-10	6.90E-09	-1.72E-07	4.31E-06	-1.08E-04	2.69E-03	-6.72E-02	1.33E+00
20000000	-2.92E-16	5.83E-16	7.29E-17	1.09E-16	-6.38E-16	1.89E-14	-4.64E-13	1.16E-11	-2.90E-10	7.25E-09	-1.81E-07	4.53E-06	-1.13E-04	2.83E-03	-7.06E-02	1.42E+00	-1.68E+00
2000000	2.95E-16	-2.95E-16	-2.22E-16	-4.80E-16	1.80E-14	-4.64E-13	1.16E-11	-2.90E-10	7.25E-09	-1.81E-07	4.53E-06	-1.13E-04	2.83E-03	-7.06E-02	1.42E+00	-1.70E+00	4.37E-01
200000	0.00E+00	2.95E-16	-2.95E-16	1.80E-14	-4.63E-13	1.16E-11	-2.90E-10	7.25E-09	-1.81E-07	4.53E-06	-1.13E-04	2.83E-03	-7.06E-02	1.42E+00	-1.70E+00	4.42E-01	-1.09E-01
20000	2.95E-16	-1.18E-15	1.83E-14	-4.63E-13	1.16E-11	-2.90E-10	7.25E-09	-1.81E-07	4.53E-06	-1.13E-04	2.83E-03	-7.06E-02	1.42E+00	-1.70E+00	4.42E-01	-1.11E-01	2.73E-02
2000	-1.18E-15	1.89E-14	-4.64E-13	1.16E-11	-2.90E-10	7.25E-09	-1.81E-07	4.53E-06	-1.13E-04	2.83E-03	-7.06E-02	1.42E+00	-1.70E+00	4.42E-01	-1.11E-01	2.77E-02	-6.83E-03
200	1.77E-14	-4.64E-13	1.16E-11	-2.90E-10	7.25E-09	-1.81E-07	4.53E-06	-1.13E-04	2.83E-03	-7.06E-02	1.42E+00	-1.70E+00	4.42E-01	-1.11E-01	2.77E-02	-6.91E-03	1.71E-03
20	-4.41E-13	1.16E-11	-2.90E-10	7.25E-09	-1.81E-07	4.53E-06	-1.13E-04	2.83E-03	-7.06E-02	1.42E+00	-1.70E+00	4.42E-01	-1.11E-01	2.77E-02	-6.92E-03	1.73E-03	-4.27E-04
2	1.10E-11	-2.90E-10	7.25E-09	-1.81E-07	4.53E-06	-1.13E-04	2.83E-03	-7.06E-02	1.42E+00	-1.70E+00	4.42E-01	-1.11E-01	2.77E-02	-6.92E-03	1.73E-03	-4.32E-04	1.07E-04
0.2	-2.76E-10	7.25E-09	-1.81E-07	4.53E-06	-1.13E-04	2.83E-03	-7.06E-02	1.42E+00	-1.70E+00	4.42E-01	-1.11E-01	2.77E-02	-6.92E-03	1.73E-03	-4.32E-04	1.08E-04	-2.67E-05
0.02	6.90E-09	-1.81E-07	4.53E-06	-1.13E-04	2.83E-03	-7.06E-02	1.42E+00	-1.70E+00	4.42E-01	-1.11E-01	2.77E-02	-6.92E-03	1.73E-03	-4.32E-04	1.08E-04	-2.70E-05	6.67E-06
0.002	-1.72E-07	4.53E-06	-1.13E-04	2.83E-03	-7.06E-02	1.42E+00	-1.70E+00	4.42E-01	-1.11E-01	2.77E-02	-6.92E-03	1.73E-03	-4.32E-04	1.08E-04	-2.70E-05	6.75E-06	-1.67E-06
0.0002	4.31E-06	-1.13E-04	2.83E-03	-7.06E-02	1.42E+00	-1.70E+00	4.42E-01	-1.11E-01	2.77E-02	-6.92E-03	1.73E-03	-4.32E-04	1.08E-04	-2.70E-05	6.75E-06	-1.69E-06	4.17E-07
0.00002	-1.08E-04	2.83E-03	-7.06E-02	1.42E+00	-1.70E+00	4.42E-01	-1.11E-01	2.77E-02	-6.92E-03	1.73E-03	-4.32E-04	1.08E-04	-2.70E-05	6.75E-06	-1.69E-06	4.22E-07	-1.04E-07
0.000002	2.69E-03	-7.06E-02	1.42E+00	-1.70E+00	4.42E-01	-1.11E-01	2.77E-02	-6.92E-03	1.73E-03	-4.32E-04	1.08E-04	-2.70E-05	6.75E-06	-1.69E-06	4.22E-07	-1.06E-07	2.60E-08
0.0000002	-6.72E-02	1.42E+00	-1.70E+00	4.42E-01	-1.11E-01	2.77E-02	-6.91E-03	1.73E-03	-4.32E-04	1.08E-04	-2.70E-05	6.75E-06	-1.69E-06	4.22E-07	-1.06E-07	2.64E-08	-6.51E-09
0.00000002	1.33E+00	-1.68E+00	4.37E-01	-1.09E-01	2.73E-02	-6.83E-03	1.71E-03	-4.27E-04	1.07E-04	-2.67E-05	6.67E-06	-1.67E-06	4.17E-07	-1.04E-07	2.60E-08	-6.51E-09	1.61E-09

54mm x 110mm Mixture

b	k	d	g	a1	a2	Sum of log	log Fit	wc
3.45516014	3.978147	0.654734	0.509175	0.000497	-0.15138	0.001935	11958840	925.5641

Frequency	Dynamic Modulus (MPa)	Phase Angle (Degrees)	Temperature (°C)	at	wr	Storage Modulus E' (kPa or psi)	Storage Modulus E'fit (log) (kPa or psi)	OFlog
0.1	8790	18.26	4	172.3233	108.2739	8347375	7859178	0.000685
1	12798	13.23	4	172.3233	1082.739	12458331	12263158	4.7E-05
10	16900	9.74	4	172.3233	10827.39	16656397	16502658	1.62E-05
0.1	4365	27.35	12	12.21256	7.673378	3877066	3748627	0.000214
1	7598	20.68	12	12.21256	76.73378	7108441	7242395	6.57E-05
10	11602	15.2	12	12.21256	767.3378	11196121	11594291	0.00023
0.1	1824	34.36	20	1	0.628319	1505726	1481723	4.87E-05
1	3928	28.86	20	1	6.283185	3440149	3507668	7.13E-05
10	7092	22.4	20	1	62.83185	6556880	6893346	0.000472
0.1	190.3	30.59	38	0.005741	0.003607	163816.1	162589.9	1.06E-05
1	530.5	36.8	38	0.005741	0.036072	424788	433239.5	7.32E-05
10	1506	38.56	38	0.005741	0.360716	1177625	1177392	7.42E-09

E8 (kpa)	9509.259737	
wr	***E'***	***E'norm***
100000000	25294190.42	25284681.16
10000000	24166007.34	24156498.08
1000000	22425196.88	22415687.62
100000	19863785.41	19854276.16
10000	16367057.91	16357548.65
1000	12109016.75	12099507.49
100	7715158.249	7705648.99
10	4084364.745	4074855.485
1	1786101.213	1776591.954
0.1	678012.3192	668503.0595
0.01	248344.4482	238835.1884
0.001	99149.91778	89640.65805
0.0001	46943.4406	37434.18087
0.00001	26987.85064	17478.59091
0.000001	18426.32208	8917.062343
0.0000001	14346.02518	4836.765442
0.00000001	12238.68448	2729.424747

Bmi	wi																
ρm	1.00E+08	1.00E+07	1.00E+06	1.00E+05	1.00E+04	1.00E+03	1.00E+02	1.00E+01	1.00E+00	1.00E-01	1.00E-02	1.00E-03	1.00E-04	1.00E-05	1.00E-06	1.00E-07	1.00E-08
2.00E+08	1.00E+00	1.00E+00	1.00E+00	1.00E+00	1.00E+00	1.00E+00	1.00E+00	1.00E+00	1.00E+00	1.00E+00	1.00E+00	1.00E+00	1.00E+00	1.00E+00	1.00E+00	9.98E-01	8.00E-01
2.00E+07	1.00E+00	1.00E+00	1.00E+00	1.00E+00	1.00E+00	1.00E+00	1.00E+00	1.00E+00	1.00E+00	1.00E+00	1.00E+00	1.00E+00	1.00E+00	1.00E+00	9.98E-01	8.00E-01	3.85E-02
2.00E+06	1.00E+00	1.00E+00	1.00E+00	1.00E+00	1.00E+00	1.00E+00	1.00E+00	1.00E+00	1.00E+00	1.00E+00	1.00E+00	1.00E+00	1.00E+00	9.98E-01	8.00E-01	3.85E-02	4.00E-04
2.00E+05	1.00E+00	1.00E+00	1.00E+00	1.00E+00	1.00E+00	1.00E+00	1.00E+00	1.00E+00	1.00E+00	1.00E+00	1.00E+00	1.00E+00	9.98E-01	8.00E-01	3.85E-02	4.00E-04	4.00E-06
2.00E+04	1.00E+00	1.00E+00	1.00E+00	1.00E+00	1.00E+00	1.00E+00	1.00E+00	1.00E+00	1.00E+00	1.00E+00	1.00E+00	9.98E-01	8.00E-01	3.85E-02	4.00E-04	4.00E-06	4.00E-08
2.00E+03	1.00E+00	1.00E+00	1.00E+00	1.00E+00	1.00E+00	1.00E+00	1.00E+00	1.00E+00	1.00E+00	1.00E+00	9.98E-01	8.00E-01	3.85E-02	4.00E-04	4.00E-06	4.00E-08	4.00E-10
2.00E+02	1.00E+00	1.00E+00	1.00E+00	1.00E+00	1.00E+00	1.00E+00	1.00E+00	1.00E+00	1.00E+00	9.98E-01	8.00E-01	3.85E-02	4.00E-04	4.00E-06	4.00E-08	4.00E-10	4.00E-12
2.00E+01	1.00E+00	1.00E+00	1.00E+00	1.00E+00	1.00E+00	1.00E+00	1.00E+00	1.00E+00	9.98E-01	8.00E-01	3.85E-02	4.00E-04	4.00E-06	4.00E-08	4.00E-10	4.00E-12	4.00E-14
2.00E+00	1.00E+00	1.00E+00	1.00E+00	1.00E+00	1.00E+00	1.00E+00	1.00E+00	9.98E-01	8.00E-01	3.85E-02	4.00E-04	4.00E-06	4.00E-08	4.00E-10	4.00E-12	4.00E-14	4.00E-16
2.00E-01	1.00E+00	1.00E+00	1.00E+00	1.00E+00	1.00E+00	1.00E+00	9.98E-01	8.00E-01	3.85E-02	4.00E-04	4.00E-06	4.00E-08	4.00E-10	4.00E-12	4.00E-14	4.00E-16	4.00E-18
2.00E-02	1.00E+00	1.00E+00	1.00E+00	1.00E+00	1.00E+00	9.98E-01	8.00E-01	3.85E-02	4.00E-04	4.00E-06	4.00E-08	4.00E-10	4.00E-12	4.00E-14	4.00E-16	4.00E-18	4.00E-20
2.00E-03	1.00E+00	1.00E+00	1.00E+00	1.00E+00	9.98E-01	8.00E-01	3.85E-02	4.00E-04	4.00E-06	4.00E-08	4.00E-10	4.00E-12	4.00E-14	4.00E-16	4.00E-18	4.00E-20	4.00E-22
2.00E-04	1.00E+00	1.00E+00	1.00E+00	9.98E-01	8.00E-01	3.85E-02	4.00E-04	4.00E-06	4.00E-08	4.00E-10	4.00E-12	4.00E-14	4.00E-16	4.00E-18	4.00E-20	4.00E-22	4.00E-24
2.00E-05	1.00E+00	1.00E+00	9.98E-01	8.00E-01	3.85E-02	4.00E-04	4.00E-06	4.00E-08	4.00E-10	4.00E-12	4.00E-14	4.00E-16	4.00E-18	4.00E-20	4.00E-22	4.00E-24	4.00E-26
2.00E-06	1.00E+00	9.98E-01	8.00E-01	3.85E-02	4.00E-04	4.00E-06	4.00E-08	4.00E-10	4.00E-12	4.00E-14	4.00E-16	4.00E-18	4.00E-20	4.00E-22	4.00E-24	4.00E-26	4.00E-28
2.00E-07	9.98E-01	8.00E-01	3.85E-02	4.00E-04	4.00E-06	4.00E-08	4.00E-10	4.00E-12	4.00E-14	4.00E-16	4.00E-18	4.00E-20	4.00E-22	4.00E-24	4.00E-26	4.00E-28	4.00E-30
2.00E-08	8.00E-01	3.85E-02	4.00E-04	4.00E-06	4.00E-08	4.00E-10	4.00E-12	4.00E-14	4.00E-16	4.00E-18	4.00E-20	4.00E-22	4.00E-24	4.00E-26	4.00E-28	4.00E-30	4.00E-32

Bmi -1	wi																
ρm	1.00E+08	1.00E+07	1.00E+06	1.00E+05	1.00E+04	1.00E+03	1.00E+02	1.00E+01	1.00E+00	1.00E-01	1.00E-02	1.00E-03	1.00E-04	1.00E-05	1.00E-06	1.00E-07	1.00E-08
2.00E+08	-2.22E-16	-2.22E-16	-5.55E-17	-1.53E-16	3.12E-16	-8.12E-16	1.79E-14	-4.41E-13	1.10E-11	-2.76E-10	6.90E-09	-1.72E-07	4.31E-06	-1.08E-04	2.69E-03	-6.72E-02	1.33E+00
2.00E+07	-2.92E-16	5.83E-16	7.29E-17	1.09E-16	-6.38E-16	1.89E-14	-4.64E-13	1.16E-11	-2.90E-10	7.25E-09	-1.81E-07	4.53E-06	-1.13E-04	2.83E-03	-7.06E-02	1.42E+00	-1.68E+00
2.00E+06	2.95E-16	-2.95E-16	-2.22E-16	-4.80E-16	1.80E-14	-4.64E-13	1.16E-11	-2.90E-10	7.25E-09	-1.81E-07	4.53E-06	-1.13E-04	2.83E-03	-7.06E-02	1.42E+00	-1.70E+00	4.37E-01
2.00E+05	0.00E+00	2.95E-16	-2.95E-16	1.80E-14	-4.63E-13	1.16E-11	-2.90E-10	7.25E-09	-1.81E-07	4.53E-06	-1.13E-04	2.83E-03	-7.06E-02	1.42E+00	-1.70E+00	4.42E-01	-1.09E-01
2.00E+04	2.95E-16	-1.18E-15	1.83E-14	-4.63E-13	1.16E-11	-2.90E-10	7.25E-09	-1.81E-07	4.53E-06	-1.13E-04	2.83E-03	-7.06E-02	1.42E+00	-1.70E+00	4.42E-01	-1.11E-01	2.73E-02
2.00E+03	-1.18E-15	1.89E-14	-4.64E-13	1.16E-11	-2.90E-10	7.25E-09	-1.81E-07	4.53E-06	-1.13E-04	2.83E-03	-7.06E-02	1.42E+00	-1.70E+00	4.42E-01	-1.11E-01	2.77E-02	-6.83E-03
2.00E+02	1.77E-14	-4.64E-13	1.16E-11	-2.90E-10	7.25E-09	-1.81E-07	4.53E-06	-1.13E-04	2.83E-03	-7.06E-02	1.42E+00	-1.70E+00	4.42E-01	-1.11E-01	2.77E-02	-6.91E-03	1.71E-03
2.00E+01	-4.41E-13	1.16E-11	-2.90E-10	7.25E-09	-1.81E-07	4.53E-06	-1.13E-04	2.83E-03	-7.06E-02	1.42E+00	-1.70E+00	4.42E-01	-1.11E-01	2.77E-02	-6.92E-03	1.73E-03	-4.27E-04
2.00E+00	1.10E-11	-2.90E-10	7.25E-09	-1.81E-07	4.53E-06	-1.13E-04	2.83E-03	-7.06E-02	1.42E+00	-1.70E+00	4.42E-01	-1.11E-01	2.77E-02	-6.92E-03	1.73E-03	-4.32E-04	1.07E-04
2.00E-01	-2.76E-10	7.25E-09	-1.81E-07	4.53E-06	-1.13E-04	2.83E-03	-7.06E-02	1.42E+00	-1.70E+00	4.42E-01	-1.11E-01	2.77E-02	-6.92E-03	1.73E-03	-4.32E-04	1.08E-04	-2.67E-05
2.00E-02	6.90E-09	-1.81E-07	4.53E-06	-1.13E-04	2.83E-03	-7.06E-02	1.42E+00	-1.70E+00	4.42E-01	-1.11E-01	2.77E-02	-6.92E-03	1.73E-03	-4.32E-04	1.08E-04	-2.70E-05	6.67E-06
2.00E-03	-1.72E-07	4.53E-06	-1.13E-04	2.83E-03	-7.06E-02	1.42E+00	-1.70E+00	4.42E-01	-1.11E-01	2.77E-02	-6.92E-03	1.73E-03	-4.32E-04	1.08E-04	-2.70E-05	6.75E-06	-1.67E-06
2.00E-04	4.31E-06	-1.13E-04	2.83E-03	-7.06E-02	1.42E+00	-1.70E+00	4.42E-01	-1.11E-01	2.77E-02	-6.92E-03	1.73E-03	-4.32E-04	1.08E-04	-2.70E-05	6.75E-06	-1.69E-06	4.17E-07
2.00E-05	-1.08E-04	2.83E-03	-7.06E-02	1.42E+00	-1.70E+00	4.42E-01	-1.11E-01	2.77E-02	-6.92E-03	1.73E-03	-4.32E-04	1.08E-04	-2.70E-05	6.75E-06	-1.69E-06	4.22E-07	-1.04E-07
2.00E-06	2.69E-03	-7.06E-02	1.42E+00	-1.70E+00	4.42E-01	-1.11E-01	2.77E-02	-6.92E-03	1.73E-03	-4.32E-04	1.08E-04	-2.70E-05	6.75E-06	-1.69E-06	4.22E-07	-1.06E-07	2.60E-08
2.00E-07	-6.72E-02	1.42E+00	-1.70E+00	4.42E-01	-1.11E-01	2.77E-02	-6.91E-03	1.73E-03	-4.32E-04	1.08E-04	-2.70E-05	6.75E-06	-1.69E-06	4.22E-07	-1.06E-07	2.64E-08	-6.51E-09
2.00E-08	1.33E+00	-1.68E+00	4.37E-01	-1.09E-01	2.73E-02	-6.83E-03	1.71E-03	-4.27E-04	1.07E-04	-2.67E-05	6.67E-06	-1.67E-06	4.17E-07	-1.04E-07	2.60E-08	-6.51E-09	1.61E-09

Appendix C: Example S-VECD Tests Data Sheet (with Heavy Filtration scheme and Selected Parameters)

Specimen Label: B1-L-20C-1.0R-200 (1)												
Diameter (mm)	**Height (mm)**	**Elve**	**Efinger**	**DMR**	**Damage Power Term**	**Rest Period**	**αt**	**C1**	**C2**			
102.6	149.1	7.19E+06	6822	9.49E-01	3.133848	1	1	0.005212	0.335455			
Cycle	**Dynamic Modulus (Mpa)**	**P2P strain ε_{pp} (microstrain)**	**P2P Reduced Pseudostrain ε_r (microstrain)**	**Form Factor (b)**	**Tensile Reduced Pseudostrain ε_{rt} (microstrain)**	**Max Tensilie Stress (kPa)**	**Pseudostiffness C**	**K1**	**Reduced Time Increment Δt_r**	**ΔS**	**S**	**C from Damage Function**
1	6620.6	160.871	1.16E+09	0.068158	6.18E+02	568.83	9.70E-01	0.464087	0.095	314.9347	314.9347	0.964101
2	6603.3	161.017	1.16E+09	0.059781	6.14E+02	563.4	9.68E-01	0.462154	0.1	49.15343	364.0882	0.962311
3	6549.2	171.407	1.23E+09	0.102972	6.80E+02	619.091	9.60E-01	0.472184	0.1	136.4989	500.587	0.958063
4	6565.5	183.541	1.32E+09	0.086177	7.17E+02	654.446	9.62E-01	0.468264	0.1	0	500.587	0.958063
5	6502.9	195.167	1.40E+09	0.080295	7.58E+02	685.533	9.53E-01	0.466898	0.1	179.5743	680.1613	0.953521
6	6528	198.364	1.43E+09	0.071551	7.64E+02	693.79	9.57E-01	0.464871	0.1	0	680.1613	0.953521
7	6470.8	201.925	1.45E+09	0.066288	7.74E+02	696.616	9.49E-01	0.463655	0.1	172.8889	853.0502	0.949852
8	6485.4	200.907	1.44E+09	0.062221	7.67E+02	692.017	9.51E-01	0.462717	0.1	0	853.0502	0.949852
9	6488.3	200.399	1.44E+09	0.068957	7.70E+02	694.954	9.51E-01	0.464272	0.1	0	853.0502	0.949852
10	6488.9	200.108	1.44E+09	0.068027	7.69E+02	693.402	9.51E-01	0.464057	0.1	0	853.0502	0.949852
110	6400.2	199.236	1.43E+09	0.064013	7.62E+02	678.385	9.38E-01	0.46313	10	716.992	1570.042	0.938464
210	6341	200.326	1.44E+09	0.062601	7.65E+02	674.894	9.29E-01	0.462804	10	530.721	2100.763	0.932149
310	6318	200.108	1.44E+09	0.064037	7.66E+02	672.622	9.26E-01	0.463135	10	259.4509	2360.214	0.929446
488	6283.5	200.544	1.44E+09	0.057872	7.63E+02	666.526	9.21E-01	0.461715	17.8	402.772	2762.986	0.925617
815	6291.7	200.399	1.44E+09	0.063333	7.66E+02	670.35	9.22E-01	0.462973	32.7	0	2762.986	0.925617
1359	6251.5	199.817	1.44E+09	0.062018	7.63E+02	663.312	9.16E-01	0.46267	54.4	593.5431	3356.529	0.920599
2267	6236.9	200.471	1.44E+09	0.060852	7.65E+02	663.201	9.14E-01	0.462401	90.8	312.5804	3669.11	0.918192
3792	6238.3	200.035	1.44E+09	0.062658	7.64E+02	663.035	9.14E-01	0.462817	152.5	0	3669.11	0.918192
6309	6221.6	199.164	1.43E+09	0.06006	7.59E+02	656.773	9.12E-01	0.462219	251.7	437.9205	4107.03	0.915038
10551	6211.3	199.164	1.43E+09	0.062624	7.61E+02	657.272	9.10E-01	0.462809	424.2	345.9254	4452.955	0.912702
17579	6164.3	199.309	1.43E+09	0.058048	7.58E+02	649.957	9.04E-01	0.461755	702.8	1229.75	5682.706	0.90526
29286	6174.9	200.035	1.44E+09	0.060117	7.63E+02	654.723	9.05E-01	0.462232	1170.7	0	5682.706	0.90526
48977	6162	200.253	1.44E+09	0.06305	7.66E+02	655.886	9.03E-01	0.462908	1969.1	597.412	6280.118	0.90203
81595	6120.1	199.454	1.43E+09	0.059652	7.60E+02	646.743	8.97E-01	0.462124	3261.8	1641.171	7921.288	0.894095
135241	6079.3	200.181	1.44E+09	0.06343	7.66E+02	647.075	8.91E-01	0.462995	5364.6	1830.938	9752.226	0.886443
225597	6009	200.108	1.44E+09	0.062814	7.65E+02	638.985	8.81E-01	0.462853	9035.6	3135.351	12887.58	0.875312

Specimen Label: B1-L-20C-0.1R-200 (1)												
Diameter (mm)	**Height (mm)**	**Elve**	**Efinger**	**DMR**	Damage Power Term	**Rest Period**	**αt**	**C1**	**C2**			
100.4	150.3	7.19E+06	6753	9.39E-01	3.133848	0.1	1	0.00321	0.440065			
Cycle	**Dynamic Modulus (Mpa)**	**P2P strain ε_{pp} (microstrain)**	**P2P Reduced Pseudostrain ε_r (microstrain)**	**Form Factor (b)**	**Tensile Reduced Pseudostrain ε_{rt} (microstrain)**	**Max Tensilie Stress (kPa)**	**Pseudostiffness C**	**K1**	**Reduced Time Increment Δt_r**	**ΔS**	**S**	**C from Damage Function**
1	6467.5	160.072	1.15E+09	0.089072	6.27E+02	563.736	9.58E-01	0.468938	0.095	420.5161	420.5161	0.954177
2	6457.2	161.017	1.16E+09	0.062294	6.15E+02	552.238	9.56E-01	0.462734	0.1	33.28887	453.8049	0.952615
3	6371.5	170.971	1.23E+09	0.100987	6.77E+02	599.674	9.44E-01	0.471719	0.1	192.2574	646.0623	0.944646
4	6397.3	189.79	1.36E+09	0.059865	7.23E+02	643.412	9.47E-01	0.462174	0.1	0	646.0623	0.944646
5	6363.7	194.441	1.40E+09	0.056687	7.39E+02	653.754	9.42E-01	0.461442	0.1	107.3692	753.4315	0.940771
6	6347.1	198.873	1.43E+09	0.05598	7.55E+02	666.465	9.40E-01	0.461279	0.1	65.06265	818.4941	0.938572
7	6325.6	200.544	1.44E+09	0.047004	7.55E+02	664.096	9.37E-01	0.459217	0.1	79.01996	897.5141	0.93603
8	6352.4	200.399	1.44E+09	0.044796	7.53E+02	665.02	9.41E-01	0.458711	0.1	0	897.5141	0.93603
9	6300.2	201.343	1.45E+09	0.0486	7.59E+02	665.078	9.33E-01	0.459583	0.1	156.119	1053.633	0.931352
10	6298.9	201.707	1.45E+09	0.045476	7.58E+02	664.154	9.33E-01	0.458867	0.1	9.731136	1063.364	0.931074
110	6084.2	201.416	1.45E+09	0.049599	7.60E+02	643.123	9.01E-01	0.459813	10	1392.948	2456.312	0.900369
210	6021.6	200.326	1.44E+09	0.048185	7.55E+02	632.203	8.92E-01	0.459488	10	541.9465	2998.258	0.891233
310	5958.1	200.617	1.44E+09	0.047274	7.56E+02	625.905	8.82E-01	0.459279	10	547.6525	3545.911	0.8829
488	5940.8	199.091	1.43E+09	0.047238	7.50E+02	619.318	8.80E-01	0.459271	17.8	232.3817	3778.293	0.879582
815	5852.9	199.309	1.43E+09	0.048638	7.52E+02	611.634	8.67E-01	0.459592	32.7	927.0546	4705.347	0.867375
1359	5731	200.544	1.44E+09	0.048562	7.56E+02	602.563	8.49E-01	0.459575	54.4	1355.291	6060.638	0.851748
2267	5676.3	199.963	1.44E+09	0.051667	7.56E+02	596.843	8.41E-01	0.460288	90.8	836.2259	6896.864	0.843071
3792	5577.7	200.181	1.44E+09	0.046209	7.53E+02	584.074	8.26E-01	0.459035	152.5	1470.617	8367.481	0.829138
6309	5480.3	200.471	1.44E+09	0.046542	7.54E+02	574.887	8.12E-01	0.459111	251.7	1650.159	10017.64	0.815054
10551	5391.5	199.091	1.43E+09	0.050382	7.52E+02	563.736	7.98E-01	0.459992	424.2	1738.033	11755.67	0.801564
17579	5273.2	200.181	1.44E+09	0.046087	7.53E+02	552.123	7.81E-01	0.459007	702.8	2443.296	14198.97	0.784369
29286	5172.2	200.762	1.44E+09	0.047741	7.56E+02	543.976	7.66E-01	0.459386	1170.7	2470.395	16669.36	0.768598
48977	5095.6	199.164	1.43E+09	0.047423	7.50E+02	531.496	7.55E-01	0.459313	1969.1	2242.148	18911.51	0.755384
81595	4972.5	200.689	1.44E+09	0.045276	7.54E+02	521.559	7.36E-01	0.458821	3261.8	3660.175	22571.69	0.735577
135241	4864.4	199.745	1.44E+09	0.04668	7.52E+02	508.501	7.20E-01	0.459143	5364.6	3723.475	26295.16	0.717199
225597	4698.2	199.963	1.44E+09	0.048585	7.54E+02	492.554	6.96E-01	0.45958	9035.6	5880.307	32175.47	0.690934
376318	4455.6	200.399	1.44E+09	0.044519	7.53E+02	466.323	6.60E-01	0.458647	15072.1	8836.117	41011.59	0.656104
511550	4218.1	199.817	1.44E+09	0.046202	7.52E+02	440.901	6.25E-01	0.459033	13523.2	8452.813	49464.4	0.626542

Specimen Label: B1-L-12C-0.2R-200												
Diameter (mm)	**Height (mm)**	**Elve**	**Efinger**	**DMR**	**Damage Power Term**	**Rest Period**	**αt**	**C1**	**C2**			
100.4	149.1	1.18E+07	10968	9.29E-01	3.134	0.3	12.14	0.000868	0.568198			
Cycle	**Dynamic Modulus (Mpa)**	**P2P strain ε_{pp} (microstrain)**	**P2P Reduced Pseudostrain ε_r (microstrain)**	**Form Factor (b)**	**Tensile Reduced Pseudostrain ε_{rt} (microstrain)**	**Max Tensilie Stress (kPa)**	**Pseudostiffness C**	**K1**	**Reduced Time Increment Δt_r**	**ΔS**	**S**	**C from Damage Function**
1	10733.9	156.366	1.85E+09	0.037188	9.57E+02	870.42	9.79E-01	0.456959	0.078254	447.5929	447.5929	0.972164
2	10562.9	159.127	1.88E+09	0.030526	9.68E+02	866.081	9.63E-01	0.455438	0.008237	207.9275	655.5205	0.965425
3	10511	167.992	1.98E+09	0.076691	1.07E+03	950.595	9.58E-01	0.466052	0.008237	98.28049	753.801	0.962569
4	10535.3	179.981	2.12E+09	0.061045	1.13E+03	1005.954	9.61E-01	0.462435	0.008237	0	753.801	0.962569
5	10500.8	193.569	2.29E+09	0.037566	1.19E+03	1054.488	9.57E-01	0.457046	0.008237	84.24294	838.0439	0.960247
6	10477.9	196.475	2.32E+09	0.042711	1.21E+03	1073.288	9.55E-01	0.458223	0.008237	63.40262	901.4465	0.958565
7	10463.2	198.582	2.34E+09	0.040563	1.22E+03	1081.039	9.54E-01	0.457731	0.008237	46.13583	947.5824	0.957373
8	10439.2	199.963	2.36E+09	0.039517	1.23E+03	1084.973	9.52E-01	0.457492	0.008237	67.19575	1014.778	0.955681
9	10443.5	200.181	2.36E+09	0.036801	1.23E+03	1083.758	9.52E-01	0.456871	0.008237	0	1014.778	0.955681
10	10411.2	200.835	2.37E+09	0.037238	1.23E+03	1084.394	9.49E-01	0.456971	0.008237	84.51816	1099.296	0.95362
110	10197.5	199.745	2.36E+09	0.039021	1.23E+03	1058.19	9.30E-01	0.457378	0.823723	1073.105	2172.402	0.9317
210	9986.9	200.98	2.37E+09	0.038677	1.23E+03	1042.398	9.11E-01	0.4573	0.823723	1070.804	3243.205	0.914235
310	9957.8	200.399	2.37E+09	0.039801	1.23E+03	1037.481	9.08E-01	0.457557	0.823723	237.9733	3481.179	0.910714
488	9907.7	199.382	2.35E+09	0.039445	1.22E+03	1026.663	9.03E-01	0.457475	1.466227	410.4538	3891.633	0.904877
815	9764.6	200.471	2.37E+09	0.037529	1.23E+03	1015.499	8.90E-01	0.457037	2.693575	1057.324	4948.957	0.890958
1359	9581.8	199.745	2.36E+09	0.039231	1.23E+03	994.501	8.74E-01	0.457427	4.481054	1437.043	6386	0.873962
2267	9443.1	200.762	2.37E+09	0.040185	1.23E+03	985.997	8.61E-01	0.457645	7.479407	1331.498	7717.498	0.859643
3792	9232.2	199.89	2.36E+09	0.041126	1.23E+03	960.66	8.42E-01	0.45786	12.56178	2062.747	9780.245	0.839421
6309	9013.9	200.835	2.37E+09	0.039016	1.23E+03	940.472	8.22E-01	0.457377	20.73311	2399.403	12179.65	0.818102
10551	8745.7	198.873	2.35E+09	0.038281	1.22E+03	902.929	7.97E-01	0.457209	34.94234	3132.355	15312	0.79284
17579	8390	200.181	2.36E+09	0.039333	1.23E+03	872.791	7.65E-01	0.45745	57.89127	4433.936	19745.94	0.760635
29286	7918.4	200.108	2.36E+09	0.038041	1.23E+03	822.407	7.22E-01	0.457154	96.43328	6196.886	25942.82	0.720479
48977	7083.1	200.326	2.36E+09	0.038445	1.23E+03	736.736	6.46E-01	0.457247	162.1993	10864.81	36807.64	0.659015

Specimen Label: B1-M-12C-0.5R-200												
Diameter (mm)	**Height (mm)**	**Elve**	**Efinger**	**DMR**	**Damage Power Term**	**Rest Period**	**αt**	**C1**	**C2**			
100.5	130.7	1.18E+07	11554	9.79E-01	3.134	0.5	12.1439	0.00151	0.501764			
Cycle	**Dynamic Modulus (Mpa)**	**P2P strain ε_{pp} (microstrain)**	**P2P Reduced Pseudostrain ε_r (microstrain)**	**Form Factor (b)**	**Tensile Reduced Pseudostrain ε_{rt} (microstrain)**	**Max Tensilie Stress (kPa)**	**Pseudostiffness C**	**K1**	**Reduced Time Increment Δt_r**	**ΔS**	**S**	**C from Damage Function**
1	11260.5	156.148	1.84E+09	763.0236	1.84E-02	895.32	9.75E-01	0	0.452674	0.008235	298.4581	298.4581
2	11177.9	157.747	1.86E+09	763.0236	9.50E-03	890.008	9.67E-01	0	0.450655	0.008235	114.3321	412.7901
3	11131	166.611	1.97E+09	763.0236	5.63E-02	979.506	9.63E-01	0	0.461348	0.008235	86.90133	499.6915
4	11080.7	187.102	2.21E+09	763.0236	1.51E-02	1052.258	9.59E-01	0	0.451926	0.008235	102.6617	602.3532
5	11079.5	189.79	2.24E+09	763.0236	2.57E-02	1078.415	9.59E-01	0	0.454338	0.008235	6.134399	608.4876
6	11061.4	193.932	2.29E+09	763.0236	2.18E-02	1095.968	9.57E-01	0	0.45345	0.008235	50.4365	658.9241
7	11002.2	198.655	2.35E+09	763.0236	1.38E-02	1107.92	9.52E-01	0	0.451635	0.008235	126.8583	785.7824
8	10992.4	199.599	2.36E+09	763.0236	1.49E-02	1113.405	9.51E-01	0	0.451886	0.008235	32.73743	818.5198
9	10950.6	200.471	2.37E+09	763.0236	1.49E-02	1114.04	9.48E-01	0	0.45189	0.008235	98.86393	917.3838
10	10900.5	201.271	2.38E+09	763.0236	1.56E-02	1114.04	9.43E-01	0	0.45203	0.008235	114.3326	1031.716
110	10779	200.326	2.36E+09	763.0236	2.01E-02	1101.337	9.33E-01	0	0.453059	0.823459	681.6986	1713.415
210	10708.2	199.963	2.36E+09	763.0236	2.15E-02	1093.6	9.27E-01	0	0.453373	0.823459	452.4551	2165.87
310	10633.2	200.253	2.36E+09	763.0236	2.18E-02	1087.884	9.20E-01	0	0.45345	0.823459	473.4153	2639.285
488	10578.2	200.035	2.36E+09	763.0236	2.38E-02	1083.207	9.16E-01	0	0.45391	1.465757	431.8782	3071.164
815	10500.8	199.745	2.36E+09	763.0236	2.57E-02	1075.701	9.09E-01	0	0.45434	2.69271	648.2004	3719.364
1359	10377.7	200.399	2.37E+09	763.0236	2.64E-02	1067.328	8.98E-01	0	0.454504	4.479616	1047.653	4767.017
2267	10250.2	200.617	2.37E+09	763.0236	2.56E-02	1054.452	8.87E-01	0	0.454304	7.477006	1219.206	5986.223
3792	10044	200.326	2.36E+09	763.0236	2.66E-02	1032.8	8.69E-01	0	0.454543	12.55775	1988.053	7974.277
6309	9940.4	199.672	2.36E+09	763.0236	2.56E-02	1017.787	8.60E-01	0	0.454308	20.72646	1323.119	9297.396
10551	9705.7	199.599	2.36E+09	763.0236	2.75E-02	995.269	8.40E-01	0	0.45475	34.93112	2797.956	12095.35
17579	9327.5	200.326	2.36E+09	763.0236	2.65E-02	959.066	8.07E-01	0	0.45453	57.87269	4556.745	16652.1
29286	8854.5	200.326	2.36E+09	763.0236	2.52E-02	909.236	7.66E-01	0	0.454223	96.40233	6094.636	22746.73
48977	8290.2	199.745	2.36E+09	763.0236	2.81E-02	851.207	7.18E-01	0	0.454877	162.1473	7901.951	30648.68

Specimen Label: B2-M-20C-0.3R-250												
Diameter (mm)	**Height (mm)**	**Elve**	**Efinger**	**DMR**	**Damage Power Term**	**Rest Period**	**αt**	**C1**	**C2**			
100.5	131.4	8.05E+06	8227	1.02E+00	3.067	0.3	1	0.003	0.428274			
Cycle	**Dynamic Modulus (Mpa)**	**P2P strain ε_{pp} (microstrain)**	**P2P Reduced Pseudostrain ε_r (microstrain)**	**Form Factor (b)**	**Tensile Reduced Pseudostrain ε_{rt} (microstrain)**	**Max Tensilie Stress (kPa)**	**Pseudostiffness C**	**K1**	**Reduced Time Increment Δt_r**	**ΔS**	**S**	**C from Damage Function**
1	7794.8	195.458	1.57E+09	0.063239	8.36E+02	809.956	9.47E-01	0.467445	0.1	786.524	786.524	0.947847
2	7796.4	196.257	1.58E+09	0.050323	8.29E+02	803.544	9.48E-01	0.464451	0.1	0	786.524	0.947847
3	7776.5	204.395	1.64E+09	0.079914	8.88E+02	858.246	9.45E-01	0.47133	0.1	84.69059	871.2146	0.945512
4	7714.9	229.536	1.85E+09	0.082624	1.00E+03	958.581	9.38E-01	0.471964	0.1	237.4749	1108.689	0.939587
5	7677.3	245.594	1.98E+09	0.047669	1.04E+03	987.694	9.33E-01	0.463838	0.1	171.7009	1280.39	0.935744
6	7658.2	248.282	2.00E+09	0.045964	1.04E+03	994.394	9.31E-01	0.463444	0.1	104.6986	1385.089	0.933544
7	7636.9	249.881	2.01E+09	0.045071	1.05E+03	997.167	9.28E-01	0.463237	0.1	114.2785	1499.367	0.931249
8	7628.5	250.68	2.02E+09	0.042409	1.05E+03	996.705	9.27E-01	0.462623	0.1	56.9693	1556.337	0.930142
9	7587.1	251.988	2.03E+09	0.042964	1.06E+03	996.994	9.22E-01	0.462751	0.1	190.758	1747.095	0.926596
10	7592.6	251.697	2.03E+09	0.042619	1.06E+03	996.243	9.23E-01	0.462671	0.1	0	1747.095	0.926596
110	7350.6	249.154	2.01E+09	0.035388	1.04E+03	948.126	8.93E-01	0.461005	10	2175.983	3923.078	0.896205
210	7284.3	249.736	2.01E+09	0.034452	1.04E+03	940.905	8.85E-01	0.460789	10	822.2687	4745.347	0.887392
310	7235.9	248.355	2.00E+09	0.035904	1.04E+03	930.797	8.80E-01	0.461124	10	643.3115	5388.658	0.881091
488	7124	250.389	2.02E+09	0.034099	1.04E+03	922.306	8.66E-01	0.460708	17.8	1408.671	6797.329	0.868656
815	7068.9	249.59	2.01E+09	0.034704	1.04E+03	912.775	8.59E-01	0.460847	32.7	956.6302	7753.959	0.861036
1359	6978.2	250.026	2.01E+09	0.03506	1.04E+03	902.955	8.48E-01	0.460929	54.4	1581.299	9335.259	0.84954
2267	6868.4	249.59	2.01E+09	0.03511	1.04E+03	887.243	8.35E-01	0.460941	90.8	2066.929	11402.19	0.836084
3792	6745.3	249.736	2.01E+09	0.037616	1.04E+03	873.958	8.20E-01	0.461518	152.5	2572.67	13974.86	0.82116
6309	6655.4	248.718	2.00E+09	0.034721	1.04E+03	856.398	8.09E-01	0.460851	251.7	2271.197	16246.05	0.809246
10551	6538.5	249.808	2.01E+09	0.036108	1.04E+03	846.174	7.95E-01	0.461171	424.2	3175.433	19421.49	0.794089
17579	6385.7	249.808	2.01E+09	0.035704	1.04E+03	826.072	7.76E-01	0.461077	702.8	4397.611	23819.1	0.77528
29286	6244.7	250.099	2.01E+09	0.037576	1.04E+03	810.245	7.59E-01	0.461509	1170.7	4711.604	28530.7	0.757219
48977	6076.6	250.462	2.02E+09	0.037725	1.05E+03	789.681	7.39E-01	0.461543	1969.1	6132.829	34663.53	0.736106
81595	5898.3	249.953	2.01E+09	0.04063	1.05E+03	767.096	7.17E-01	0.462213	3261.8	7266.136	41929.67	0.713698
135241	5634.8	249.227	2.01E+09	0.038253	1.04E+03	729.03	6.85E-01	0.461665	5364.6	10935.67	52865.34	0.683823

Specimen Label: B2-M-20C-0.7R-250												
Diameter (mm)	**Height (mm)**	**Elve**	**Efinger**	**DMR**	**Damage Power Term**	**Rest Period**	**αt**	**C1**	**C2**			
100.5	130.3	8.05E+06	8380	1.04E+00	3.067	0.3	1	0.002941	0.426396			
Cycle	**Dynamic Modulus (Mpa)**	**P2P strain ε_{pp} (microstrain)**	**P2P Reduced Pseudostrain ε_r (microstrain)**	**Form Factor (b)**	**Tensile Reduced Pseudostrain ε_{rt} (microstrain)**	**Max Tensilie Stress (kPa)**	**Pseudostiffness C**	**K1**	**Reduced Time Increment Δt_r**	**ΔS**	**S**	**C from Damage Function**
1	8027.3	195.24	1.57E+09	0.040492	8.17E+02	815.353	9.58E-01	0.462181	0.1	650.2553	650.2553	0.953439
2	7971.7	197.274	1.59E+09	0.035401	8.22E+02	814.141	9.51E-01	0.461008	0.1	162.605	812.8603	0.948791
3	7936.3	215.948	1.74E+09	0.047901	9.11E+02	897.967	9.47E-01	0.463891	0.1	135.1428	948.0032	0.94532
4	7839.6	227.865	1.83E+09	0.065108	9.77E+02	951.332	9.36E-01	0.46788	0.1	321.7046	1269.708	0.938065
5	7838.3	238.691	1.92E+09	0.054024	1.01E+03	986.004	9.35E-01	0.465308	0.1	12.68246	1282.39	0.937802
6	7808.8	246.102	1.98E+09	0.04506	1.03E+03	1004.177	9.32E-01	0.463235	0.1	143.008	1425.398	0.934934
7	7801.3	249.082	2.00E+09	0.039606	1.04E+03	1010.062	9.31E-01	0.461977	0.1	51.34568	1476.744	0.933944
8	7780.3	251.043	2.02E+09	0.037689	1.05E+03	1013.408	9.28E-01	0.461535	0.1	112.5014	1589.245	0.931844
9	7767.1	251.479	2.02E+09	0.03754	1.05E+03	1013.292	9.27E-01	0.461501	0.1	79.87165	1669.117	0.930404
10	7778.4	250.607	2.02E+09	0.037616	1.05E+03	1011.331	9.28E-01	0.461518	0.1	0	1669.117	0.930404
110	7550.2	250.535	2.02E+09	0.038978	1.05E+03	982.658	9.01E-01	0.461832	10	2111.718	3780.835	0.901372
210	7484.9	250.317	2.01E+09	0.039352	1.05E+03	973.658	8.93E-01	0.461918	10	821.4413	4602.276	0.892747
310	7436.9	249.518	2.01E+09	0.037401	1.04E+03	962.524	8.87E-01	0.461468	10	645.3247	5247.601	0.886575
488	7357.6	249.808	2.01E+09	0.037885	1.04E+03	953.812	8.78E-01	0.46158	17.8	1089.681	6337.282	0.877073
815	7276.2	249.953	2.01E+09	0.034734	1.04E+03	940.947	8.68E-01	0.460854	32.7	1284.821	7622.102	0.867006
1359	7193.7	249.445	2.01E+09	0.03678	1.04E+03	930.217	8.58E-01	0.461325	54.4	1472.344	9094.447	0.856604
2267	7092.2	249.518	2.01E+09	0.03547	1.04E+03	916.198	8.46E-01	0.461024	90.8	1948.937	11043.38	0.844226
3792	6957.3	250.317	2.01E+09	0.035545	1.04E+03	901.717	8.30E-01	0.461041	152.5	2756.381	13799.76	0.8287
6309	6866.5	249.082	2.00E+09	0.03589	1.04E+03	885.852	8.19E-01	0.461121	251.7	2297.579	16097.34	0.817074
10551	6721.1	250.171	2.01E+09	0.033385	1.04E+03	868.775	8.02E-01	0.460544	424.2	3735.752	19833.1	0.80005
17579	6601.2	248.718	2.00E+09	0.035314	1.04E+03	849.91	7.88E-01	0.460988	702.8	3634.662	23467.76	0.785176
29286	6347	250.68	2.02E+09	0.049567	1.06E+03	834.968	7.57E-01	0.464276	1170.7	7516.777	30984.53	0.758155
48977	6076.5	250.825	2.02E+09	0.042053	1.05E+03	794.122	7.25E-01	0.462541	1969.1	8854.794	39839.33	0.730793

Specimen Label: B2-M-12C-0.05R-200												
Diameter (mm)	**Height (mm)**	**Elve**	**Efinger**	**DMR**	**Damage Power Term**	**Rest Period**	**αt**	**C1**	**C2**			
100.4	129.2	1.17E+07	13738	1.18E+00	3.061273	0.2	11.8	0.001502	0.505053			
Cycle	**Dynamic Modulus (Mpa)**	**P2P strain ε_{pp} (microstrain)**	**P2P Reduced Pseudostrain ε_r (microstrain)**	**Form Factor (b)**	**Tensile Reduced Pseudostrain ε_{rt} (microstrain)**	**Max Tensilie Stress (kPa)**	**Pseudostiffness C**	**K1**	**Reduced Time Increment Δt_r**	**ΔS**	**S**	**C from Damage Function**
1	13348.9	151.062	1.76E+09	0.034309	9.12E+02	1042.845	9.72E-01	0.461143	0.004237	285.0589	285.0589	0.97391
2	13274.7	153.169	1.79E+09	0.01299	9.06E+02	1029.84	9.66E-01	0.456249	0.008475	95.68819	380.7471	0.969803
3	13271.5	158.837	1.85E+09	0.041676	9.66E+02	1097.926	9.66E-01	0.462841	0.008475	9.887033	390.6341	0.969409
4	13199.4	176.711	2.06E+09	0.046685	1.08E+03	1220.689	9.61E-01	0.463998	0.008475	122.4454	513.0795	0.964893
5	13175.7	188.482	2.20E+09	0.016548	1.12E+03	1262.245	9.59E-01	0.457064	0.008475	55.61221	568.6917	0.96302
6	13169.9	192.261	2.24E+09	0.020338	1.14E+03	1291.78	9.59E-01	0.457932	0.008475	20.10784	588.7996	0.962365
7	13060.4	197.856	2.31E+09	0.017647	1.18E+03	1314.841	9.51E-01	0.457316	0.008475	190.1744	778.974	0.956651
8	13087.5	199.527	2.33E+09	0.013059	1.18E+03	1322.702	9.53E-01	0.456265	0.008475	0	778.974	0.956651
9	13071.9	199.817	2.33E+09	0.010002	1.18E+03	1319.06	9.52E-01	0.455565	0.008475	43.72796	822.7019	0.955439
10	13043.2	200.399	2.34E+09	0.00942	1.18E+03	1319.234	9.49E-01	0.455432	0.008475	69.78186	892.4838	0.953568
110	12700.3	200.762	2.34E+09	0.016117	1.19E+03	1295.421	9.24E-01	0.456965	0.847458	1424.603	2317.087	0.924824
210	12614.5	199.672	2.33E+09	0.020078	1.19E+03	1284.671	9.18E-01	0.457873	0.847458	500.579	2817.666	0.917018
310	12578.8	199.527	2.33E+09	0.021693	1.19E+03	1282.128	9.16E-01	0.458243	0.847458	259.0049	3076.671	0.913249
488	12388.4	200.181	2.34E+09	0.02291	1.20E+03	1268.372	9.02E-01	0.458522	1.508475	1060.658	4137.329	0.89925
815	12252.4	200.544	2.34E+09	0.025757	1.20E+03	1260.222	8.92E-01	0.459176	2.771186	963.0165	5100.346	0.88802
1359	12056.4	201.053	2.35E+09	0.030353	1.21E+03	1248.778	8.78E-01	0.460233	4.610169	1454.222	6554.568	0.872894
2267	11801.6	201.343	2.35E+09	0.032643	1.21E+03	1226.873	8.59E-01	0.460759	7.694915	2021.74	8576.308	0.85441
3792	11641.6	199.672	2.33E+09	0.035308	1.21E+03	1203.292	8.47E-01	0.461373	12.92373	1604.304	10180.61	0.841238
6309	11314.9	199.309	2.33E+09	0.035471	1.20E+03	1167.573	8.24E-01	0.461411	21.33051	3101.355	13281.97	0.818418
10551	10944.1	199.745	2.33E+09	0.035323	1.21E+03	1131.622	7.97E-01	0.461377	35.94915	3890.727	17172.69	0.793259
17579	10444.7	200.762	2.34E+09	0.035226	1.21E+03	1085.384	7.60E-01	0.461354	59.55932	5555.882	22728.58	0.761819
29286	9814.3	199.817	2.33E+09	0.032125	1.20E+03	1012.039	7.14E-01	0.46064	99.21186	7419.158	30147.73	0.725294

Specimen Label: B2-M-12C-0.5R-200												
Diameter (mm)	**Height (mm)**	**Elve**	**Efinger**	**DMR**	**Damage Power Term**	**Rest Period**	**αt**	**C1**	**C2**			
100.4	150.5	1.17E+07	13798	1.18E+00	3.061273	0.2	11.8	0.003013	0.405486			
Cycle	**Dynamic Modulus (Mpa)**	**P2P strain ε_{pp} (microstrain)**	**P2P Reduced Pseudostrain ε_r (microstrain)**	**Form Factor (b)**	**Tensile Reduced Pseudostrain ε_{rt} (microstrain)**	**Max Tensilie Stress (kPa)**	**Pseudostiffness C**	**K1**	**Reduced Time Increment Δt_r**	**ΔS**	**S**	**C from Damage Function**
1	13365.3	150.989	1.76E+09	0.055724	9.30E+02	1065.232	9.69E-01	0.466091	0.004237	319.0956	319.0956	0.96879
2	13365.3	152.515	1.78E+09	0.036088	9.22E+02	1055.986	9.69E-01	0.461553	0.008475	0	319.0956	0.96879
3	13270.3	162.76	1.90E+09	0.088744	1.03E+03	1175.777	9.62E-01	0.473791	0.008475	142.1468	461.2424	0.963761
4	13220.7	182.524	2.13E+09	0.047726	1.12E+03	1264.132	9.58E-01	0.464239	0.008475	97.23536	558.4777	0.960838
5	13155.8	186.521	2.18E+09	0.060569	1.15E+03	1301.231	9.53E-01	0.467216	0.008475	125.4694	683.9471	0.957484
6	13154.7	191.316	2.23E+09	0.05924	1.18E+03	1332.898	9.53E-01	0.466907	0.008475	6.033583	689.9807	0.957332
7	13132.7	195.821	2.29E+09	0.053142	1.20E+03	1354.163	9.52E-01	0.465493	0.008475	59.05185	749.0325	0.955888
8	13122.2	196.911	2.30E+09	0.055842	1.21E+03	1364.102	9.51E-01	0.466119	0.008475	34.21161	783.2441	0.955082
9	13094.8	198.074	2.31E+09	0.054205	1.22E+03	1367.165	9.49E-01	0.465739	0.008475	71.11748	854.3616	0.95347
10	13092.3	199.091	2.32E+09	0.053938	1.22E+03	1373.579	9.49E-01	0.465677	0.008475	11.62101	865.9826	0.953215
110	12903.2	199.599	2.33E+09	0.053333	1.23E+03	1356.417	9.35E-01	0.465537	0.847458	956.2949	1822.278	0.936741
210	12886.5	199.817	2.33E+09	0.053905	1.23E+03	1356.879	9.34E-01	0.46567	0.847458	153.8096	1976.087	0.934628
310	12868.7	199.672	2.33E+09	0.057032	1.23E+03	1358.035	9.33E-01	0.466395	0.847458	162.3891	2138.476	0.9325
410	12787	200.108	2.34E+09	0.058492	1.24E+03	1354.221	9.27E-01	0.466733	0.847458	514.3636	2652.84	0.926336
510	12733.8	200.399	2.34E+09	0.057971	1.24E+03	1349.887	9.23E-01	0.466613	0.847458	372.4143	3025.254	0.922305
707	12722.6	200.108	2.34E+09	0.059264	1.24E+03	1348.384	9.22E-01	0.466913	1.669492	136.2492	3161.503	0.920905
1039	12661.5	199.599	2.33E+09	0.061051	1.24E+03	1340.757	9.18E-01	0.467328	2.813559	554.8039	3716.307	0.915546
1525	12540.1	200.181	2.34E+09	0.06236	1.24E+03	1333.418	9.09E-01	0.467632	4.118644	1029.374	4745.681	0.906744
2238	12447.5	200.835	2.34E+09	0.064007	1.25E+03	1329.951	9.02E-01	0.468015	6.042373	929.5592	5675.24	0.899728
3285	12417.3	199.309	2.33E+09	0.065938	1.24E+03	1319.029	9.00E-01	0.468464	8.872881	435.6583	6110.899	0.896676
4823	12324.2	199.89	2.33E+09	0.064906	1.24E+03	1311.69	8.93E-01	0.468223	13.0339	1120.614	7231.513	0.889375
7079	12194.1	200.108	2.34E+09	0.065148	1.24E+03	1299.555	8.84E-01	0.46828	19.11864	1588.641	8820.154	0.880098
10351	12093.6	201.489	2.35E+09	0.068488	1.26E+03	1301.809	8.76E-01	0.469057	27.72881	1455.517	10275.67	0.872437
15193	12047.6	200.326	2.34E+09	0.068454	1.25E+03	1289.327	8.73E-01	0.469049	41.0339	882.2204	11157.89	0.868105
22301	11969.8	199.672	2.33E+09	0.06794	1.24E+03	1276.209	8.68E-01	0.46893	60.23729	1431.138	12589.03	0.86149
32734	11737.4	199.672	2.33E+09	0.066499	1.24E+03	1249.743	8.51E-01	0.468594	88.41525	3582.469	16171.5	0.846687
48047	11531.9	200.544	2.34E+09	0.06639	1.25E+03	1233.101	8.36E-01	0.468569	129.7712	3611.688	19783.19	0.833629
57543	11272	202.288	2.36E+09	0.066221	1.26E+03	1215.592	8.17E-01	0.468529	80.47458	3882.942	23666.13	0.821089
70523	11126.8	199.527	2.33E+09	0.070721	1.25E+03	1188.548	8.06E-01	0.469577	110	2666.671	26332.8	0.813173
77923	11028.9	198.946	2.32E+09	0.228496	1.43E+03	1347.749	7.99E-01	0.507582	62.71186	2154.162	28486.96	0.80712